# Advanced Signal Processing Techniques for MIMO Communication Systems

*A dissertation submitted for the degree of Doctor of Philosophy*

Inaki Berenguer, Trinity Hall

December 2004

Laboratory for Communication Engineering
Department of Engineering
University of Cambridge

***To my father .....***

... for being the pillar of strength in my life.

# Abstract

Rapid growth in mobile computing and other wireless multimedia services is inspiring many research and development activities concerning high-speed wireless communication systems. The main challenges in this area include the development of efficient coding and modulation techniques to improve the quality and spectral efficiency of wireless systems. Multiple-input multiple-output (MIMO) techniques for wireless communication have recently emerged and offer a powerful paradigm for meeting these challenges. In particular, MIMO systems constitute a unified way of modeling a wide range of different communication channels, which can be handled with a compact vector-matrix notation. This thesis proposes new signal processing techniques for two representative cases of MIMO systems: (a) systems employing multiple transmit and receive antennas, and (b) systems with multiple users transmitting simultaneously and overlapping in both time and frequency. Owing to the common MIMO system model notation, similar signal processing techniques are applicable to both scenarios as will be demonstrated in the thesis.

Chapter 2 gives an overview of the recent development in space-time coding and signal processing techniques for MIMO communication systems having multiple antennas. We first review the information theoretic results on the capacities of wireless systems employing multiple transmit and receive antennas. We then describe two representative categories of space-time systems, namely, the BLAST systems and systems employing space-time block coding. The extension of MIMO techniques to frequency-selective channels is also addressed. Finally, alternative coding and signal processing techniques for wireless systems employing multiple transmit and receive antennas are also briefly touched upon.

The most costly element of a multiple antenna device is usually the RF chains (amplifiers, filters, digital-to-analog converters, etc.). A promising approach for reducing the cost and complexity while retaining a reasonably large fraction of the high potential data rate of a MIMO system is to employ a reduced number of

RF chains at the receiver (or transmitter) and attempt to optimally allocate each chain to one of a larger number of receive (transmit) antennas. In this way, only the *best* set of antennas is used, while the remaining antennas are not employed, thus reducing the number of RF chains required. Different approaches to selecting the *best* antennas are proposed in Chapter 3. In particular, we consider a new framework for antenna subset selection in noisy environments and also fast antenna selection algorithms.

Wireless communication using multiple antennas can increase the multiplexing gain (i.e., throughput) and diversity gain (i.e., robustness) of a communication system in fading channels. It has been shown that for any given number of antennas there is a fundamental tradeoff between these two gains. Pioneering works on space-time architectures had focused on maximizing either the diversity gain or the multiplexing gain. However, recent works have proposed space-time architectures that simultaneously achieve good diversity and multiplexing performance. In Chapter 4 of this thesis a family of lattice space-time (LAST) codes is presented that can achieve the optimum diversity-multiplexing tradeoff in delay-limited MIMO channels. In Chapter 4, using stochastic optimization techniques we design LAST codes that can further optimize the error rate. The design of minimum error rate LAST codes is later extended to scenarios in which multiple transmitting terminals cooperate by sharing their antennas.

In the final part of the thesis we consider MIMO systems with multiple users instead of multiple antennas. In particular, we address the downlink of time domain duplex code division multiple access (TDD-CDMA) systems. First we obtain and compare the capacity results of a downlink CDMA system with either multiuser detection (i.e., receiver processing) or precoding (i.e., transmitter processing). It is demonstrated that the two schemes exhibit similar capacity regions, which motivates the development of efficient transmitter precoding techniques to reduce the receiver complexity at the mobile units without degrading the system performance. We then compare two classes of linear interference suppression techniques for downlink TDD-CDMA systems over multipath fading channels, namely, linear multiuser detection methods and linear precoding methods. We later develop non-linear multiuser precoding methods, to remove multiuser interference, interchip interference and inter-symbol interference. Efficient algorithms for multiuser power loading and cancellation ordering are also developed.

In summary, a range of signal processing tools appropriate for use in MIMO communication systems have been developed in the work presented in this thesis.

# Declaration

Except where noted in the text, this dissertation is the result of my own work during my PhD study.

I hereby declare that this dissertation is not substantially the same as any that I have submitted for a degree or diploma or other qualification at any other University. I further state that no part of my dissertation has already been or is being concurrently submitted for any such degree, diploma or qualification.

This dissertation does not exceed sixty thousand words, including footnotes and bibliography.

Ignacio (Inaki) Berenguer
December 2004

# Acknowledgements

I am very grateful to my thesis advisor, Professor Xiaodong Wang at Columbia University, whose advice, support, and guidance have been invaluable throughout this project. Thanks are also due to my thesis supervisor, Dr Ian J. Wassell who allowed me the freedom to pursue my interests.

My most sincere appreciation is extended to the Fulbright Commission, The British Council, La Caixa, the Cambridge-MIT Institute (the CMI and the CII), and Banco Santander Central Hispano (SCH), for sponsoring my research and thus giving me an opportunity to study with probably the best people and at the best places in the world.

I am specially indebted to a number of people that have helped me along the path to this completed thesis. In particular, thanks to my dad, Paco Aura, Walter Heylen, Maria J. Fraile, Raju Hormis, David Ruiz-Alonso, and Alberto Lopez-Toledo.

Finally, I would like to thank all the collaborators and friends that have made my PhD more enjoyable. Thanks to Chuxiang Li, Kuo-ching, Kai Li, Angelica, Ramon Verastegui, Avinash, Borja, Maria Figueroa, and Raul Rodriguez at Columbia University; Eli Katsiri, Pablo Vidales, Evans Mella, Kam, and Diego Lopez de Ipina at the LCE; Aimin Sang, Mohammad Madihian, Jibing Wang, and Guosen Yue at NEC Laboratories America; Professor V. Krishnamurthy from the University of British Columbia, Daniel P. Palomar from Princeton University, and Professor A. Host-Madsen from the University of Hawaii; and the rest of my friends in New York and Cambridge.

# Publications

Some of the work discussed in this dissertation has been presented in the following publications;

1. Inaki Berenguer, Xiaodong Wang, Jibing Wang, and Mohammad Madihian, "On the design of lattice space-time codes," submitted to *IEEE Transactions on Communications,* Jan. 2005.

2. Inaki Berenguer, Anders Host-Madsen, Manuel Donaire, Daryl Reynolds, and Xiaodong Wang, "Linear precoding and user scheduling for downlink TDD-CDMA," submitted to *IEEE Journal on Selected Areas in Communications,* Sep. 2004.

3. Inaki Berenguer and Xiaodong Wang, "Multiuser TH-Precoding for CDMA over multipath channels," submitted to *IEEE Transactions on Communications,* April 2004 (under review).

4. Inaki Berenguer, Xiaodong Wang, and Vikram Krishnamurthy, "Adaptive MIMO antenna selection via discrete stochastic approximation," submitted to *IEEE Transactions on Signal Processing*, June 2003, revised Nov. 2003 (accepted for publication).

5. Inaki Berenguer and Xiaodong Wang, "MIMO antenna selection with lattice-reduction-aided linear receivers," *IEEE Transactions on Vehicular Technology* , 53(5), pp. 1289-1302, Sep. 2004.

6. Inaki Berenguer, Xiaodong Wang, and Ian J. Wassell, "Transmit antenna selection in linear receivers: geometrical approach," *IEE Electronics Letters*, 4(5), pp. 292-293, Mar. 2004.

7. Inaki Berenguer and Xiaodong Wang, “Space-time coding and signal processing form MIMO communications,” *Journal of Computer Science and Technology,* 18(6), pp. 689-702, Nov. 2003.

8. Inaki Berenguer, Xiaodong Wang, Jibing Wang, and Mohammad Madihian, “Design of LAST codes via stochastic optimization and gradient estimation,” submitted to *IEEE Globecom,* St. Louis, MO, Nov. 2005.

9. Inaki Berenguer, Xiaodong Wang, Daryl Reynolds, and Anders Host-Madsen, “Linear MUD versus linear precoding in the downlink of multiuser CDMA systems,” submitted to *6th IEEE Workshop on Signal Processing Advances in Wireless Communications (SPAWC),* New York, NY, June 2005.

10. Inaki Berenguer, Ian J. Wassell, and Xiaodong Wang, “Opportunistic User Scheduling and Antenna Selection in the Downlink of Multiuser MISO Systems,” *61st IEEE Vehicular Technology Conference (VTC 2005),* Stockholm, Sweden, June 2005.

11. Inaki Berenguer, Xiaodong Wang, and Ian J. Wassell, “Tomlinson-Harashima precoding techniques in multipath fading CDMA,” *7th Wireless Personal Multimedia Communications (WPMC04),* Padova, Italy, Sep. 2004.

12. Jaime Adeane, Miguel Rodrigues, Inaki Berenguer, and Ian J. Wassell, “Improved detection methods for MIMO-OFDM-CDM in fading channels,” *60th IEEE Vehicular Technology Conference (VTC 2004),* Los Angeles, CA, Sep. 2004.

13. Inaki Berenguer, Jaime Adeane, Ian J. Wassell, and Xiaodong Wang, “Lattice-reduction-aided receivers for MIMO-OFDM in spatial multiplexing systems,” *15th Personal Indoor Multimedia and Radio Communications (PIMRC04),* Barcelona, Spain, Sep. 2004.

14. Inaki Berenguer, Xiaodong Wang, and Anders Host-Madsen, “Non-linear multiuser precoding for CDMA over multipath channels,” *2nd International Workshop for Wireless Communications (SPWC04),* London, UK, June 2004.

15. Inaki Berenguer, Xiaodong Wang, and Vikram Krishnamurthy, “Adaptive MIMO antenna selection,” *37th Asilomar Conference on Signals, Systems, and Computers,* Pacific Grove, CA, Nov. 2003.

16. Inaki Berenguer, Michele Palazzi, Oscar Bastidas, Loic Bonizec, and Yves Rasse "Efficient VLSI design of a pulse shaping filter and DAC interface for W-CDMA transmission," *16th IEEE International ASIC/SoC Conference*, Portland, Oregon, Sep. 2003.

17. Inaki Berenguer and Ian J. Wassell "Efficient FMT equalization in outdoor broadband wireless systems," *IEEE International Symposium on Advances in Wireless Communications (ISWC'02)*, Victoria, Canada, Sep. 2002.

18. Inaki Berenguer and Ian J. Wassell, "FMT modulation: receiver filter bank definition for the derivation of an efficient implementation," *IEEE 7th International OFDM Workshop*, Hamburg, Germany, Sep. 2002.

19. Inaki Berenguer, Filtered Multitone (FMT) Modulation for Broadband Fixed Wireless Systems, MPhil Thesis, University of Cambridge, August 2002.

# Contents

# List of Figures

# Glossary

**AWGN** Additive White Gaussian Noise

**BER** Bit Error Rate

**BLAST** Bell-Labs Layered Space Time

**CIR** Channel Impulse Response

**CDMA** Code Division Multiple Access

**CP** Cyclic Prefix

**CSI** Channel State Information

**DFE** Decision Feedback Equaliser

**DFT** Discrete Fourier Transform

**DSL** Digital Subscriber Line

**DMT** Digital Multitone

**FB** Feedback

**FF** Feedforward

**FFT** Fast Fourier Transform

**FIR** Finite Impulse Response

**FMT** Filtered Multitone

**ICI** Inter Carrier Interference

**ICI** Inter Chip Interference

**IEEE** Institute of Electrical and Electronic Engineers

**IFFT** Inverse Fast Frequency Transform

**ISI** Inter Symbol Interference

**LAST** LAttice Space-Time

**LRA** Lattice Reduction Aided

**LMS** Least Mean Square

**LOS** Line of Sight

**MAI** Multiple Access Interference

**MIMO** Multiple-Input Multiple-Output

**MISO** Multiple-Input Single-Output

**ML** Maximum Likelihood

**MLSE** Maximum Likelihood Sequence Estimator

**MMSE** Minimum Mean Squared Error

**MUD** Multiuser Detection

**OFDM** Orthogonal Frequency Division Multiplexing

**PAM** Pulse Amplitude Modulation

**pdf** Probability Density Function

**QAM** Quadrature Amplitude Modulation

**QoS** Quality of Service

**QPSK** Quaternary Phase Shift Keying

**RC** Raised Cosine

**RLS** Recursive Least Square

**RF** Radio Frequency

**R-M** Robbins-Monro

**SER** Symbol Error Rate

**SINR** Signal-to-Interference-plus-Noise Ratio

**SISO** Single-Input Single-Output

**SNR** Signal-to-Noise Ratio

**STBC** Space Time Block Codes

**STC** Space Time Codes

**STTC** Space Time Trellis Codes

**SVD** Singular Value Decomposition

**TDD** Time Division Duplex

**THP** Tomlinson Harashima Precoding

**ZF** Zero Forcing

# Chapter 1

# Introduction

Rapid growth in mobile computing and other wireless multimedia services is inspiring many research and development activities concerning high-speed wireless communication systems. The main challenges in this area include the development of efficient coding and modulation techniques to improve the quality and spectral efficiency of wireless systems. Multiple-input multiple-output (MIMO) techniques for wireless communication have recently emerged and offer a powerful paradigm for meeting these challenges. In particular, MIMO systems constitute a unified way of modeling a wide range of different communication channels, which can be handled with a compact vector-matrix notation. In this thesis, we propose new signal processing techniques for two representative cases of MIMO systems: (a) systems employing multiple transmit and receive antennas, and (b) systems with multiple users simultaneously transmitting and overlapping in both time and frequency. Owing to the common MIMO system model notation, similar signal processing techniques are applicable to both scenarios as will be demonstrated in the thesis.

The main motivation of this research is to propose powerful signal processing techniques to improve the performance of MIMO communication systems.

## 1.1 Outline of the thesis and main contributions

**Chapter 2** provides an overview on the recent developments in space-time coding and signal processing techniques appropriate for MIMO communication systems having multiple antennas. We first review the information theoretic results on the capacities of wireless systems employing multiple transmit and receive antennas. We then describe two representative categories of space-time systems, namely, the

Bell-Labs Layered Space Time (BLAST) systems and systems employing space-time block coding. Signal processing techniques for channel estimation and decoding in space-time systems are also discussed and compared. The extension of MIMO techniques to frequency-selective channels is also addressed. Finally, some other useful signal processing techniques for wireless systems employing multiple transmit and receive antennas are also briefly touched upon.

Previously published work has shown that it is possible to improve the performance of MIMO systems by employing a larger number of antennas than is actually used at any instant, where the optimal subset of antennas is selected based on the channel state information. Existing antenna selection algorithms assume perfect channel knowledge and optimize criteria such as Shannon capacity or various bounds on error rate. **Chapter 3** begins by examining MIMO antenna selection algorithms where the set of possible solutions is large and only a noisy estimate of the channel is available. Using an approach similar to that employed by traditional adaptive filtering algorithms, we propose a new framework based on simulation based discrete stochastic optimization algorithms to adaptively select a better antenna subset using criteria such as maximum mutual information, bounds on error rate, etc. These discrete stochastic approximation algorithms are ideally suited to minimize the error rate since computing a closed form expression for the error rate is intractable. We also consider time-varying channels for which the antenna selection algorithms can track the time-varying optimal antenna configuration. We present several numerical examples to show the convergence of these algorithms under various performance criteria, and also demonstrate their tracking capabilities. We later propose various new antenna selection criteria and also fast antenna selection algorithms.

Wireless communications using multiple antennas can increase the multiplexing gain (i.e., throughput) and diversity gain (i.e., robustness) of communication systems in fading channels. It has been shown that for any given number of antennas there is a fundamental tradeoff between these two gains. Pioneering works on space-time architectures focused on maximizing either the diversity gain or the multiplexing gain. However, recent works have proposed space-time architectures that simultaneously achieve good diversity and multiplexing performance. In **Chapter 4** of this thesis we consider a family of lattice space-time (LAST) codes that can achieve the optimum diversity-multiplexing tradeoff in delay-limited MIMO channels. Unfortunately, the diversity-multiplexing tradeoff analysis does not say anything about the coding gain or error rate at signal-to-noise (SNR) ratios of interest (also note that the tradeoff analysis gives asymptotic results). That is, two space-time codes belonging to the family of LAST codes can obtain different error rate performance at the signal to noise ratios of interest. Therefore, in Chapter 4 we design spherical LAST codes subject to the minimum error-rate criterion by employing a stochastic approximation technique based on the well known Robbins-Monro algorithm together with unbiased gradient estimation. The design of minimum error rate LAST codes is later extended to scenarios in which multiple transmitting terminals cooperate by sharing their antennas.

In **Chapter 5** we consider MIMO systems with multiple users instead of multiple antennas. In particular, we address the downlink of time division duplex code division multiple access (TDD-CDMA) systems. First we obtain and compare the capacity results of a downlink CDMA system with either mulituser detection (i.e., receiver processing) or precoding (i.e., transmitter processing). It is seen that the two schemes exhibit similar capacity regions for both sum-rate and maximum equal rate, which motivates the development of efficient nonlinear transmitter precoding techniques to reduce the receiver complexity at the mobile units without degrading the system performance. We then compare two classes of linear interference suppression techniques for downlink TDD-CDMA systems over multipath fading channels, namely, linear multiuser detection methods and linear precoding methods. For the linear precoding schemes, we assume that the channel state information (CSI) is available only at the transmitter but not at the receiver. We propose several precoding techniques and the corresponding power control algorithms. The performance metric used in the comparisons is the total power required at the transmitter to achieve a certain Quality of Service (QoS) at the receiver (e.g., minimum signal to noise ratio). Our results reveal that in general multiuser detection and precoding offer similar performance; but in certain scenarios, precoding can bring a substantial performance improvement. These results motivate the use of precoding techniques to reduce the complexity of the mobile terminals (only a matched-filter to its *own* spreading sequence is required and CSI is not required). We later develop both bit-wise and chip-wise Tomlinson-Harashima (TH) multiuser precoding methods for downlink CDMA with multipath, to remove multi-user interference, inter-chip interference and inter-symbol interference. Efficient algorithms for multiuser power loading and ordering are also developed. Implementation of the proposed TH-precoding schemes in time-varying channels based on channel prediction is also addressed. Simulations results are provided to demonstrate the effectiveness of the proposed techniques in suppressing interference in the CDMA downlink. It should be noted that CSI at the transmitter can facilitate efficient user scheduling. We therefore further develop low-complexity user allocation algorithms based on the proposed linear precoding techniques.

**Chapter 6** concludes the dissertation summarizing the main results and enumerating future lines of work.

# Chapter 2

# Overview of MIMO Systems

## 2.1 Introduction

Multiple-input multiple-output (MIMO) communication technology has received significant recent attention due to the rapid development of high-speed broadband wireless communication systems employing multiple transmit and receive antennas. Information theoretic results show that MIMO systems can offer significant capacity gains over traditional single-input single-output channels [40, 119]. This increase in capacity is enabled by the fact that in rich scattering wireless environments, the signals from each individual transmitter appear highly uncorrelated at each of the receive antennas. When conveyed through uncorrelated channels between the transmitter and the receiver, the signals corresponding to each of the individual transmit antennas have attained different spatial signatures. The receiver can exploit these differences in spatial signatures to separate the signals originating from different transmit antennas.

Many MIMO techniques have been proposed and are usually targeted at different scenarios in wireless communications. The Bell-Labs Layered Space Time (BLAST) system [42, 131] is a layered space-time architecture originally proposed by Bell-Labs to achieve high data rate wireless transmission. In this scheme, different symbol streams are simultaneously transmitted from all transmit antennas (i.e., they overlap both in frequency and in time). The receive antennas yield the superposition of all the transmitted symbol streams and recover them via proper signal processing. On the other hand, in Space-Time Coding (STC) systems [3, 114, 115, 118], the same information symbol stream is transmitted from different transmit antennas in an appropriate manner in order to obtain transmit diversity. Hence, in

STC systems the MIMO channel is exploited to provide more reliable communications, whereas in the BLAST system the MIMO channel is used to provide higher rate communications. Note that by employing higher level signal constellations, STC systems can also achieve higher throughput. In this chapter, we give a general overview of the capacity results for MIMO systems as well as for BLAST and STC techniques.

The remainder of this chapter is organized as follows. In Section 2.2 we summarize the capacity results for MIMO systems and discuss the impact of antenna correlation on capacity. In Section 2.3, we describe the BLAST system and related decoding and channel estimation techniques. In Section 2.4, we discuss space-time coding techniques and in particular the space-time block codes. Performance comparisons between the BLAST system and the space-time block coding system are also made. In Section 2.5 we consider MIMO systems in frequency selective channels. Finally, in Section 2.6, we briefly touch upon some other useful space-time coding and signal processing techniques.

## 2.2 Capacity of MIMO Systems

In this section, we summarize the information theoretic results on the capacities of MIMO channels, developed in the late 1990s [40, 119]. These results show the significant potential gains in channel capacity by employing multiple antennas at both the transmitter and receiver ends; and inspired an enormous surge of world-wide research activities to develop space-time coding and signal processing techniques that can approach the MIMO channel capacity.

### 2.2.1 Capacity Results

Consider a MIMO system with $n_T$ transmit antennas and $n_R$ receive antennas signaling through flat fading channels, as shown in Figure 2.1. The input-output relationship of this system is given by

$$\boldsymbol{y} = \boldsymbol{H}\boldsymbol{x} + \boldsymbol{v}, \tag{2.1}$$

where $\boldsymbol{x} = [x_1, x_2, ..., x_{n_T}]^T$ is the ($n_T \times$ 1) transmitted signal vector, $\boldsymbol{y} = [y_1, y_2, ..., y_{n_R}]^T$ is the ($n_R \times$ 1) received signal vector, $\boldsymbol{v} = [v_1, v_2, ..., v_{n_R}]^T$ is the received noise

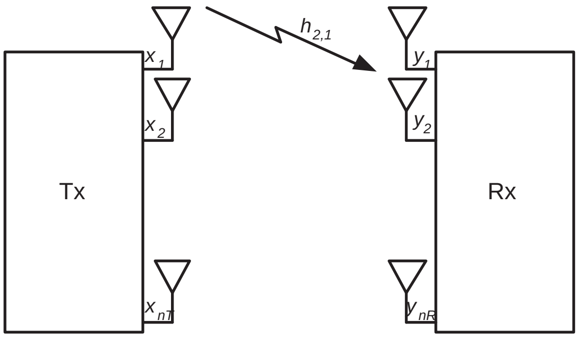


Figure 2.1: Schematic representation of a MIMO system.

vector and

$$\boldsymbol{H} = \begin{bmatrix} h_{11} & h_{21} & \cdots & h_{1,n_T} \\ h_{21} & h_{22} & \cdots & h_{2,n_T} \\ \vdots & & \ddots & \vdots \\ h_{n_R,1} & h_{n_R,1} & \cdots & h_{n_R,n_T} \end{bmatrix} \tag{2.2}$$

is the $(n_R \times n_T)$ MIMO channel matrix with $h_{ij}$ representing the complex gain of the channel between the *j*th transmit antenna and the *i*th receive antenna.

It is assumed that the noise sample $v_i$, $i = 1, 2, ..., n_R$, is a circularly symmetric complex Gaussian random variable with zero mean and variance $\sigma^2$, denoted as $v_i \sim \mathcal{N}_c(0, \sigma^2)$. That is, $\Re\{v_i\} \sim \mathcal{N}(0, \frac{\sigma^2}{2})$, $\Im\{v_i\} \sim \mathcal{N}(0, \frac{\sigma^2}{2})$, and that they are independent. It is assumed that the complex channel gains $h_{ij} \sim \mathcal{N}_c(0, 1)$. Note that in general, the channel gains may be correlated.

Assuming that the channel matrix $\boldsymbol{H}$ is known at the receiver, but not at the transmitter, the ergodic (mean) capacity of the MIMO channel with an average total transmit power $P$ (i.e., $\mathrm{tr}\Big(E\left\{\boldsymbol{x}\boldsymbol{x}^H\right\}\Big) \leq P$) is given by [119, 40]

$$\begin{aligned} C &= E\left\{\log\det\left(\boldsymbol{I}_{n_R} + \frac{1}{n_T}\frac{P}{\sigma^2}\boldsymbol{H}\boldsymbol{H}^H\right)\right\} \\ &= E\left\{\log\det\left(\boldsymbol{I}_{n_T} + \frac{1}{n_T}\frac{P}{\sigma^2}\boldsymbol{H}^H\boldsymbol{H}\right)\right\} \quad \text{bits/s/Hz}, \end{aligned} \tag{2.3}$$

where the expectation is taken with respect to the distribution of the random channel matrix $\boldsymbol{H}$.

To gain some insight on the capacity expression in (2.3), denote $\rho = P/\sigma^2$ which permits the capacity to be expressed as

$$C = \sum_{k=1}^{p} E\{\log(1+\frac{\rho}{n_T}\lambda_k)\}, \tag{2.4}$$

where $p = \min\{n_T, n_R\}$ and $\lambda_1, ..., \lambda_p$ are the eigenvalues of the matrix $\boldsymbol{H}\boldsymbol{H}^H$ or $\boldsymbol{H}^H\boldsymbol{H}$. Note that the matrices $\boldsymbol{H}\boldsymbol{H}^H$ and $\boldsymbol{H}^H\boldsymbol{H}$ have the same eigenvalues which are all real and non-negative. If we compare (2.4) with the capacity of a single-input single-output (SISO) channel [25], we observe that the capacity of a MIMO system is equivalent to the sum of $p$ parallel SISO channels, each one with an equivalent signal-to-noise ratio equal to $\lambda_i$.

Furthermore, it can be shown that when both $n_T$ and $n_R$ increase, the capacity increases *linearly* with respect to min$\{n_T, n_R\}$. On the other hand, if $n_R$ is fixed and $n_T$ increases, then the capacity saturates at some fixed value; whereas if $n_T$ is fixed and $n_R$ increases, the capacity increases logarithmically with $n_R$. These asymptotic behaviors of the ergodic capacity are shown in Figure 2.2.

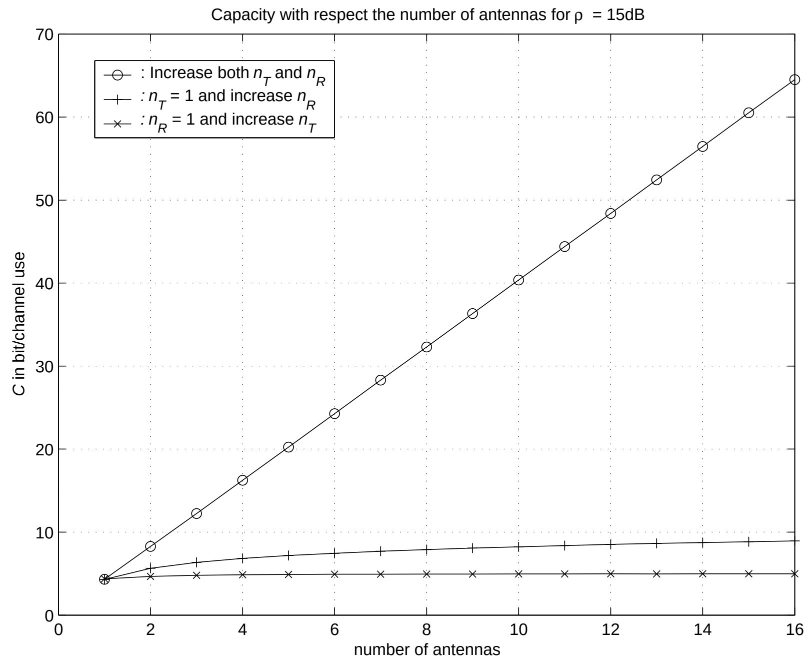


Figure 2.2: Ergodic capacities of uncorrelated MIMO channels. The channel is assumed to be known at the receiver but not at the transmitter.

Another notion that is frequently used in practice is the outage capacity. The instantaneous capacity is defined as

$$\phi\left(\boldsymbol{H},\rho\right)=\log\det\left(\boldsymbol{I}_{n_R}+\frac{\rho}{n_T}\boldsymbol{H}\boldsymbol{H}^H\right). \tag{2.5}$$

Obviously $\phi(\boldsymbol{H},\rho)$ is a random variable since $\boldsymbol{H}$ is random. Given a certain outage probability $P_{out}$, the corresponding outage capacity $C_{out}$ is defined through the following equation,

$$P\left\{\phi(\boldsymbol{H},\rho)\leq C_{out}\right\}=P_{out}. \tag{2.6}$$

So far we have assumed that the channel matrix $\boldsymbol{H}$ is known at the receiver but not at the transmitter. Another scenario is that the channel is known at both the transmitter and receiver. This is the case, for example, when the system employs time-division duplex (TDD) so that the uplink and downlink channels are reciprocal to each other. In this case, the instantaneous capacity is given by the following "water-filling" equation [112]

$$\psi(\boldsymbol{H},\rho)=\sum_{i=1}^{n_T}\left[\log\left(\upsilon\lambda_i\right)\right]^{+}\quad \text{bits/s/Hz}, \tag{2.7}$$

where $\lambda_1,...,\lambda_{n_T}$ are the eigenvalues of the matrix $\boldsymbol{H}^H\boldsymbol{H}$, $\upsilon$ is chosen such that $\rho=\sum\limits_{i=1}^{n_T}\left[\upsilon-\frac{1}{\lambda_i}\right]^{+}$ and the operator $(\cdot)^{+}$ is specified as

$$(x)^{+}=\begin{cases} x & \text{if} \quad x>0,\\ 0 & \text{if} \quad x\leq 0.\end{cases} \tag{2.8}$$

The ergodic capacity is then given by $C=E\{\psi(\boldsymbol{H},\rho)\}$. Moreover, the outage capacity in this case is specified by

$$P\left\{\psi(\boldsymbol{H},\rho)\leq C_{out}\right\}=P_{out}. \tag{2.9}$$

Figure 2.3 shows the 10% outage capacity of uncorrelated MIMO channels with and without water-filling. It is seen that by knowing the channel at the transmitter, some capacity gain can be obtained at low signal-to-noise ratios.

### 2.2.2 Effects of Antenna Correlations

It has been observed that antennas placed with large enough separations will receive essentially uncorrelated signals [83]. However, in handsets or small termi-

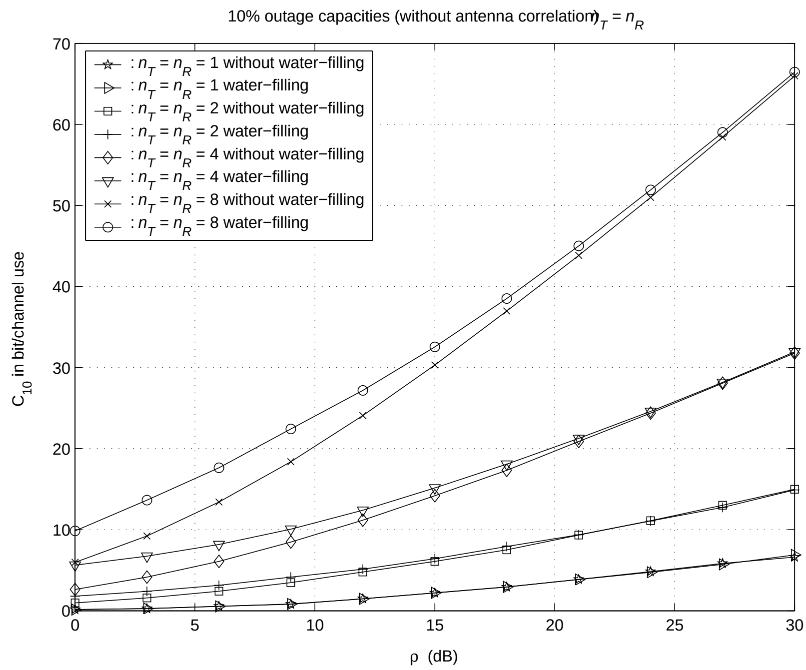


Figure 2.3: 10% outage capacities of uncorrelated MIMO channels with and without employing water-filling.

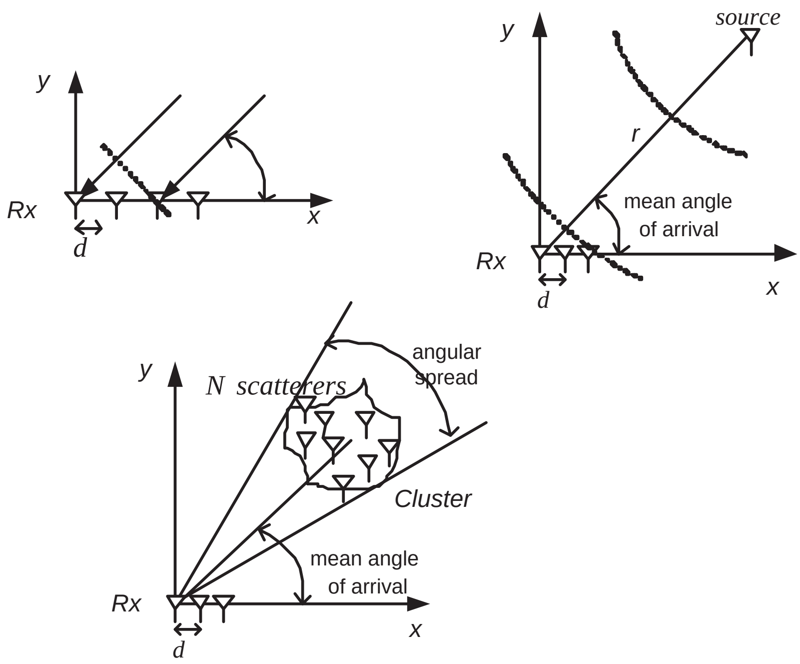


Figure 2.4: Model with local scatterers. Incident wave is approximately plane at the receiving array.

nals, large separations among the antennas may not be feasible. On the other hand, when the transmitter or receiver is not surrounded by scatterers, no local scattering or diversity occurs, and the spatial fading at the antennas is correlated. Hence, insufficient antenna spacing and lack of scattering cause the individual antennas to be correlated.

We next discuss the correlation model and the effect of antenna correlation on capacity. Following [17], assuming correlations at both the transmitter and receiver, the ($n_R \times n_T$) channel response matrix can be modeled as

$$\boldsymbol{H} = \boldsymbol{R}_r^{1/2} \boldsymbol{H}_w \boldsymbol{R}_t^{1/2} \tag{2.10}$$

with $\boldsymbol{H}_w$ being a ($n_R \times n_T$) matrix with i.i.d. $\mathcal{N}_c$(0,1) entries and $\boldsymbol{R}_t$ and $\boldsymbol{R}_r$, of size ($n_T \times n_T$) and ($n_R \times n_R$), representing the covariance matrices inducing transmit and receive correlations respectively. Note that for the case of uncorrelated transmitter (receiver), we have $\boldsymbol{R}_t = \mathbf{I}$ ($\boldsymbol{R}_r = \boldsymbol{I}$).

The form of cross-correlation between the waves impinging on antenna elements (i.e., $\boldsymbol{R}_r$ or $\boldsymbol{R}_t$) has been studied and modeled in several publications, e.g., [7, 17, 20, 36, 112]. These models use similar parameters to characterize the correlation. Specifically, assuming that no line of sight exists between the transmit and the receive antennas, the signal reaching the receive antennas can be modeled as arriving from a number of equivalent point sources or scatterers in the vicinity of the receiver as shown in Figure 2.4. Assuming that the antennas are omnidirectional (i.e. they radiate and receive from all directions in space), there are three main parameters that characterize the correlation between antennas (see Figure 2.4):

- Distance $d$ between antennas in terms of wavelengths,
- Angular spread of the arrival incident waves $a_o^{Rx}$,
- Mean angle of arrival of incident waves $f_o^{Rx}$.

Large values of the angular spread $a_o^{Rx}$ result in uncorrelated signals at each of the antennas. The angular spread is a function of the distance of the cluster to the antenna array and radius of the cluster. For example, in an outdoor environment, a cluster could be a building located far away from the antenna array yielding in a small angular spread $a_o^{Rx}$. In an indoor environment, the cluster of scatterers will be the walls surrounding the array. In this case, there will be signals impinging the antenna array from all directions resulting in a large value of angular spread; therefore, uncorrelated fading among the antennas can be expected. Figure 2.5

depicts various scattering scenarios similar to those defined for COST-259 models [112]. In this representation, the circle represents a cluster of scatterers. The five different scenarios correspond to:

- Uplink: This scenario corresponds to a base station operating as a receiver from some high point without any nearby scatterers. The receiver, usually a handset or small terminal, will be surrounded by scatterers. The angular spread at the receiver (i.e., base station) is very low, resulting in correlation among the receive antennas.

- Downlink: This scenario is similar to the uplink but with the base station acting as a transmitter.

- Urban area: Medium size angular spread for both the transmitter and the receiver. Scatterer clusters represent buildings.

- Rural area: Low angular spread for both the transmitter and the receiver. Scatterer clusters represent mountains and hills.

- Indoor: Large angular spread for both the transmitter and the receiver. Impinging waves arrive from all directions in space.

Figure 2.6 shows the 10% outage capacities for the different scenarios defined in Figure 2.5 with $n_T = n_R$ = 4 and an antenna spacing of $d = 0.5\lambda$. We assume that the channel is known at the receiver but not at the transmitter. We have used the correlation model described in [7]. We also show the SISO capacity for comparison. It is seen that urban and indoor scenarios with rich scattering offer much higher MIMO capacities than do rural environments.

Figure 2.7 shows the 10% outage capacities of a correlated MIMO channel with and without water-filling. The correlation scenario corresponds to the urban area depicted in Figure 2.5 with an antenna spacing of $d = 0.5\lambda$. Comparing with Figure 2.3, it is seen that significant capacity gain can be achieved with water-filling in the presence of antenna correlations however the channel must be known at both the transmitter and the receiver.

## 2.3 The BLAST System

The information theoretical results presented in the preceding section indicate the large capacity gains available by employing multiple antennas at both ends of the

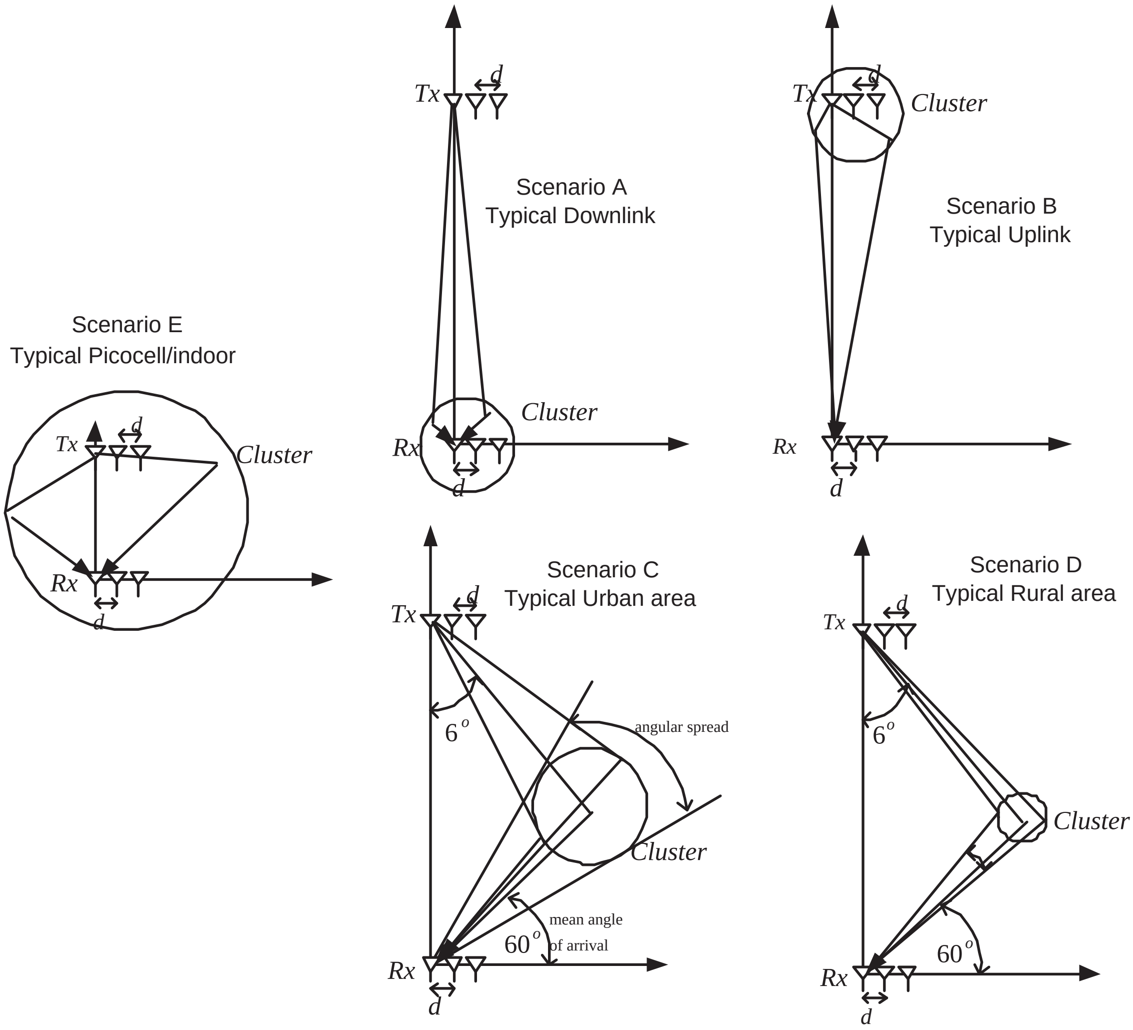


Figure 2.5: Various MIMO scattering scenarios.

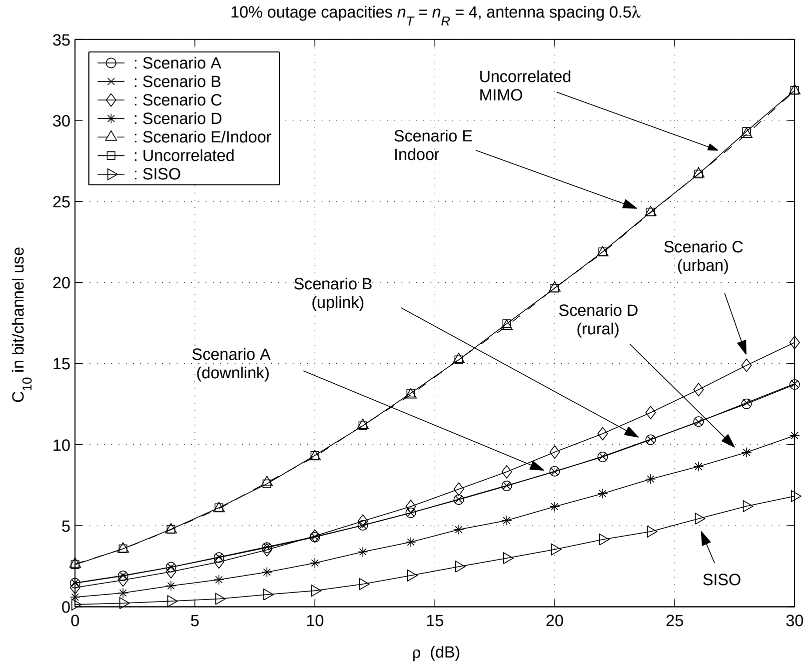


Figure 2.6: MIMO outage capacities for different channel scenarios described in Figure 2.5.

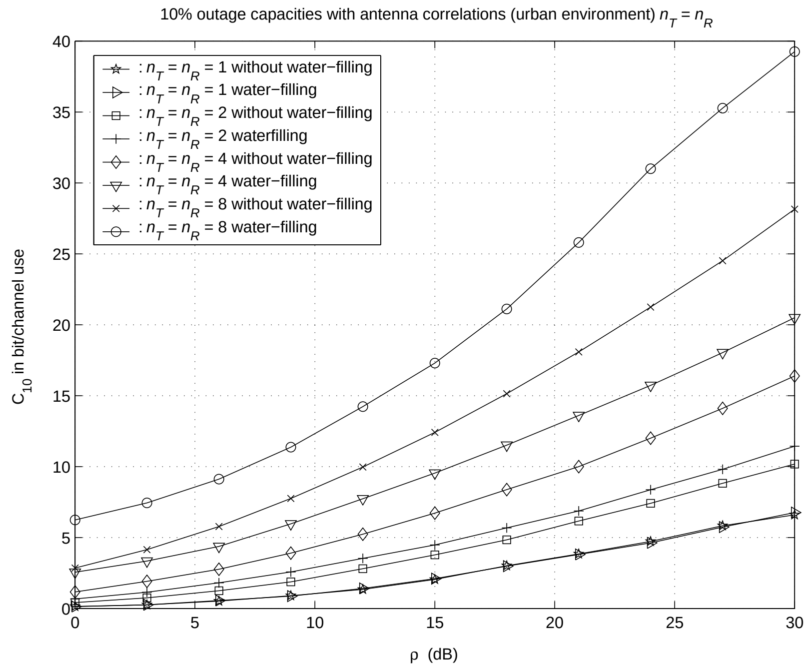


Figure 2.7: 10% outage capacities of a correlated MIMO channel corresponding to an urban scenario, with and without employing water-filling.

communication systems. Identifying such a large potential gain, researchers at Bell-Labs developed the first MIMO architecture for high-speed wireless communications, namely the BLAST systems.

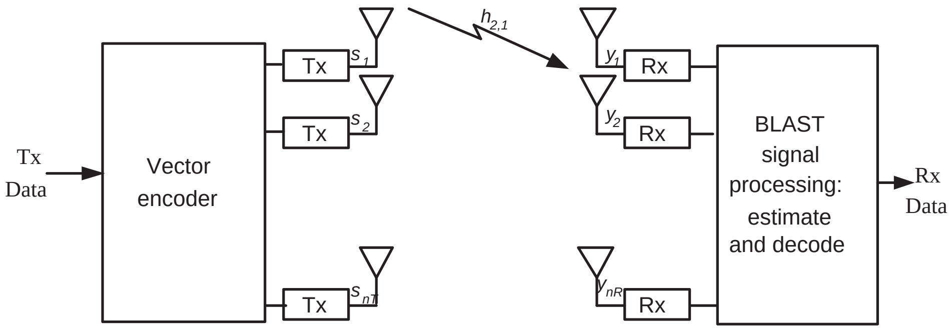


Figure 2.8: Schematic representation of a BLAST system.

BLAST (Bell-Labs Layered Space Time) [42, 131] is a high speed wireless communication scheme employing multiple antennas at both the transmitter and the receiver. In a BLAST system, the transmitted data is split equally into $n_T$ transmit antennas and then simultaneously sent to the channel overlapping in both time and frequency. The signals are received by $n_R$ receive antennas as shown in Figure 2.8 and signal processing at the receiver attempts to separate the received signals and recover the transmitted data. The input-output relationship of a BLAST system can be expressed as

$$\boldsymbol{y} = \sqrt{\frac{\rho}{n_T}}\boldsymbol{H}\boldsymbol{s} + \boldsymbol{v} \tag{2.11}$$

where $\boldsymbol{s} = [s_1, s_2, ..., s_{n_T}]^T$ is the $(n_T \times 1)$ transmit signal vector with $s_i$ belonging to a finite constellation $\mathcal{A}$, $\boldsymbol{v} = [v_1, v_2, ..., v_{n_R}]^T$ is the $(n_R \times 1)$ receive noise vector with $v_i \sim \mathcal{N}_c(0, 1)$, $\boldsymbol{H}$ is defined in (2.2) and $\rho$ is the total signal-to-noise ratio independent of the number of transmit antennas. Unitary power is assumed for the transmitted symbols, $E\left\{|s_i|^2\right\} = 1$.

### 2.3.1 BLAST Detection Algorithms

It is seen from (2.11) that the receive antennas see the superposition of all the transmitted signals. The task of a BLAST detector is to recover the transmitted data $\boldsymbol{s}$ from the received signal $\boldsymbol{y}$. Several BLAST detection algorithms will now be described [41, 48]. Here we assume the channel matrix $\boldsymbol{H}$ is known at the receiver. We will discuss channel estimation algorithms in Section 2.3.2.

### Maximum Likelihood (ML) Receiver

The ML detector is the optimal receiver in terms of bit error rate. Let $\mathcal{A}$ be the symbol constellation set (e.g., QPSK or $M$-QAM) whose size is $M$. Then, the ML detection rule is given by

$$\hat{\boldsymbol{s}} = \arg \min_{\boldsymbol{s} \in \mathcal{A}^{n_T}} \left\| \boldsymbol{y} - \sqrt{\frac{\rho}{n_T}} \boldsymbol{H} \boldsymbol{s} \right\|^2 . \tag{2.12}$$

Note that the minimization problem is performed over all possible transmitted signal vectors $\boldsymbol{s}$ in the set $\mathcal{A}^{n_T}$. The computational complexity of an exhaustive search is then $\mathcal{O}(M^{n_T})$. Hence, although the ML receiver is optimal, its complexity grows exponentially with the number of transmit antennas. A low complexity local search method called "sphere decoding" whose complexity is $\mathcal{O}(M^3)$ is developed in [26, 38].

### Zero Forcing and Cancellation Receiver

A more simpler receiver is known as the zero forcing (ZF) receiver. The ZF receiver considers the signal from each transmit antenna as the desired signal and the remainder as interferers. Nulling is performed by linearly weighting the received signals to satisfy the ZF criterion, i.e., by inverting the channel response. Furthermore, a superior performance can be obtained by using nonlinear techniques, for example cancellation. Using symbol cancellation, the previously detected and sliced symbol from each transmit antenna is subtracted out from the received signal vector, in a similar manner to that employed ino decision feedback equalization or multiuser detection with successive interference cancellation. Therefore, the next signal to be decoded will see one interferer less.

For simplicity, assume $n = n_T = n_R$. Denote the QR factorization of $\boldsymbol{H}$ as $\boldsymbol{H} = \boldsymbol{Q}\boldsymbol{R}$ where $\boldsymbol{Q}$ is unitary, i.e., $\boldsymbol{Q}\boldsymbol{Q}^H = \boldsymbol{I}$ and $\boldsymbol{R}$ is upper triangular. The nulling operation of the received vector $\boldsymbol{y}$ is performed by

$$\boldsymbol{z} = \boldsymbol{Q}^H \boldsymbol{y} = \sqrt{\frac{\rho}{n_T}} \boldsymbol{R}\boldsymbol{S} + \boldsymbol{Q}^H \boldsymbol{v}; \tag{2.13}$$

that is

$$\begin{bmatrix} z_1 \\ z_2 \\ \vdots \\ z_n \end{bmatrix} = \sqrt{\frac{\rho}{n}} \begin{bmatrix} r_{1,1} & r_{1,2} & \dots & r_{1,n} \\ 0 & r_{2,2} & \dots & r_{2,n} \\ \vdots & \ddots & \ddots & \vdots \\ 0 & \dots & 0 & r_{n,n} \end{bmatrix} \begin{bmatrix} s_1 \\ s_2 \\ \vdots \\ s_n \end{bmatrix} + \begin{bmatrix} w_1 \\ w_2 \\ \vdots \\ w_n \end{bmatrix}. \qquad (2.14)$$

Note that since $\boldsymbol{Q}$ is unitary, there is no noise amplification, i.e., $\boldsymbol{w} = \boldsymbol{Q}^H \boldsymbol{v}$ is also $\mathcal{N}_c(0, \boldsymbol{I})$. In (2.14), the decision statistic $z_n$ is just a noisy scaled version of $s_n$ which can be directly estimated and then subtracted from $z_{n-1}$. Repeating the estimating and subtracting operations until all transmitted signals are decoded, the complete algorithms is summarized in Algorithm 1 where the quantizer $\mathcal{Q}(\cdot)$ takes values from the constellation $\mathcal{A}$.

**Algorithm 1** ZF and cancellation BLAST receiver

$\hat{s}_n = \mathcal{Q}\left(\frac{1}{r_{n,n}}\sqrt{\frac{n}{\rho}}z_n\right)$

$\hat{s}_{n-1} = \mathcal{Q}\left(\frac{1}{r_{n-1,n-1}}\left(\sqrt{\frac{n}{\rho}}z_{n-1} - r_{n-1,n}\hat{s}_n\right)\right)$

$\vdots$

$\hat{s}_i = \mathcal{Q}\left(\frac{1}{r_{i,i}}\left(\sqrt{\frac{n}{\rho}}z_i - \sum_{k=i+1}^{n} r_{i,k}\hat{s}_k\right)\right)$

$\vdots$

$\hat{s}_1 = \mathcal{Q}\left(\frac{1}{r_{1,1}}\left(\sqrt{\frac{n}{\rho}}z_{n-1} - \sum_{k=2}^{n} r_{1,k}\hat{s}_k\right)\right)$

### Nulling and Cancellation Receivers with Ordering

In the decoding algorithm discussed above, an incorrect decision in the detection of a symbol adds interference to the next symbols to be detected. It is shown in [41, 48] that it is advantageous to first find and detect the symbol $s_k$ with the highest signal to-noise ratio, i.e., that with the highest reliability. The detected symbol is then subtracted from the rest of the received signals. Therefore, after cancelling $s_k$, we have a system with $n_T - 1$ transmit antennas and $n_R$ receive antennas, i.e., the corresponding channel matrix is obtained by removing column $k$ from $\boldsymbol{H}$. The same process is then applied on this $(n_T - 1, n_R)$ system and the algorithm continues until all transmitted symbols have been detected. That is, the nulling and cancellation operation is performed starting with the more reliable symbols and moving to the less reliable ones.

The nulling operation can be performed by means of ZF or the minimum mean-square error (MMSE) criterion. Similarly to ZF equalization in single antenna systems, the ZF criterion yields the following problems: (1) The algorithm can encounter singular matrices that are not invertible; and (2) ZF focuses on cancelling the interference (i.e., overlapping signals) completely at the expense of enhancing the noise, possibly significantly. On the other hand, the MMSE criterion minimizes the error due to the noise and the interference combined. In the ordering operation, the MMSE method nulls the component with the smallest MSE. Following [48], the BLAST decoding algorithm based on the MMSE nulling and cancellation with ordering is given in Algorithm 2.

**Algorithm 2** MMSE nulling and cancellation with ordering

$\boldsymbol{G} = \boldsymbol{H}$
$\boldsymbol{r} = \boldsymbol{y}$
FOR $i = 1 : n_T$ DO
  $\boldsymbol{P} = (\frac{\rho}{n}\boldsymbol{G}^H\boldsymbol{G} + \boldsymbol{I})^{-1}$
  $k_i = \operatorname{argmin}\{P_{j,j}\}, \quad j \notin \{k_1, k_2, ..., k_{i-1}\}$ (ordering: find min MSE)
  $\boldsymbol{w} = (\boldsymbol{G}\boldsymbol{P})(:, k_i)$ (nulling vector)
  $z = \boldsymbol{w}^H\boldsymbol{r}$
  $\hat{s}_{k_i} = \mathcal{Q}(z)$
  $\boldsymbol{r} = \boldsymbol{r} - \sqrt{\frac{\rho}{n}}\boldsymbol{H}(:, k_i)\hat{s}_{k_i}$ (cancellation)
  $\boldsymbol{G} = \boldsymbol{G} \setminus \boldsymbol{H}(:, k_i)$ (remove column of that transmit antenna)
END

Figure 2.9 compares the BER performance of the four detection methods discussed previously in a BLAST system with $n_T$ = $n_R$ = 4 antennas and QPSK modulation. It is seen that the ML decoder has the best BER performance although for every transmitted code vector, the receiver needs to evaluate (2.12) over $4^4 = 256$ possibilities. On the other hand, the MMSE nulling and cancellation algorithm with ordering exhibits the best performance among the suboptimal algorithms.

### 2.3.2 MIMO Channel Estimation Algorithms

So far, we have assumed that the MIMO channel matrix $\boldsymbol{H}$ is known at the receiver. In practice, the receiver needs to estimate this matrix prior to the start of the decoding process. We next discuss the channel estimation methods based on a training preamble [91].

Suppose $T \geq n_T$ MIMO training symbol vectors $\boldsymbol{s}(1)$, $\boldsymbol{s}(2)$, ..., $\boldsymbol{s}(T)$ are used

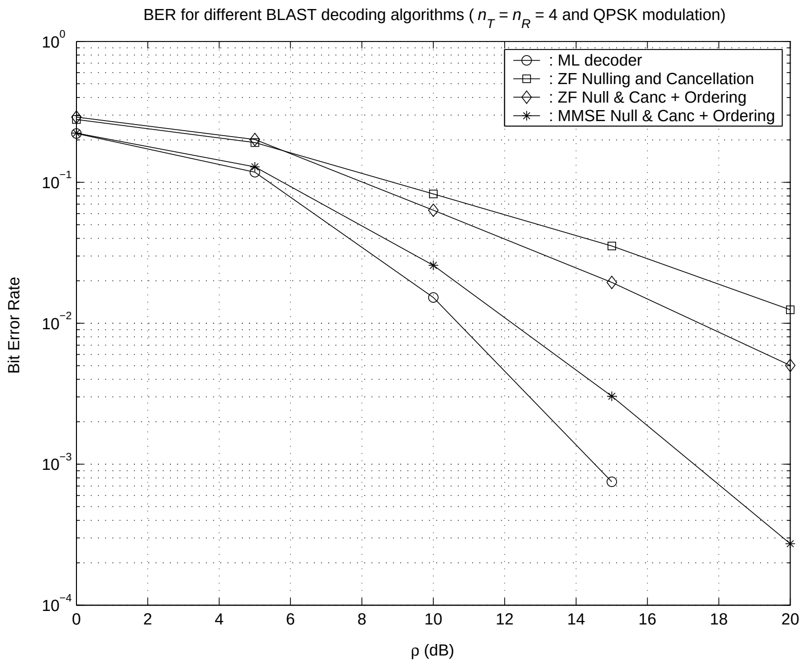


Figure 2.9: BER performance of different BLAST decoding algorithms with $n_T$ = $n_R$ = 4 and QPSK. Uncorrelated MIMO channels and perfect channel knowledge at the receiver are assumed.

to probe the channel. The received signals corresponding to these training symbols are

$$\boldsymbol{y}(i) = \sqrt{\frac{\rho}{n_T}}\boldsymbol{H}\boldsymbol{s}(i) + \boldsymbol{v}(i), \quad i = 1, 2, ..., T. \tag{2.15}$$

Denote $\boldsymbol{Y} = \left[ \; \boldsymbol{y}(1), \boldsymbol{y}(2), ..., \boldsymbol{y}(T) \; \right]$, $\boldsymbol{S} = \left[ \; \boldsymbol{s}(1), \boldsymbol{s}(2), ..., \boldsymbol{s}(T) \; \right]$ and $\mathbf{V} = \left[ \; \boldsymbol{v}(1), \boldsymbol{v}(2), ..., \boldsymbol{v}(T) \; \right]$. Then (2.15) can be written as

$$\boldsymbol{Y} = \sqrt{\frac{\rho}{n_T}}\boldsymbol{H}\boldsymbol{S} + \boldsymbol{V}. \tag{2.16}$$

The maximum likelihood estimate of the channel matrix $\boldsymbol{H}$ is given by

$$\begin{aligned} \hat{\boldsymbol{H}}_{ML} &= \arg\min_{\boldsymbol{H}} \left\| \boldsymbol{Y} - \sqrt{\frac{\rho}{n_T}}\boldsymbol{H}\boldsymbol{S} \right\|^2 \\ &= \sqrt{\frac{n_T}{\rho}}\boldsymbol{Y}\boldsymbol{S}^H(\boldsymbol{S}\boldsymbol{S}^H)^{-1}. \end{aligned} \tag{2.17}$$

According to [91], the optimal training symbol sequence $\boldsymbol{S}$ that minimizes the channel estimation error should satisfy

$$\boldsymbol{S}\boldsymbol{S}^H = T \cdot \boldsymbol{I}_{n_T}. \tag{2.18}$$

One way to generate such optimal training sequences is to use the Hadamard matrices [61] (when they exist for specific values of $n_T$). As an example, consider a system with $n_T$ = 4 and a training sequence of length $T$ = 16 symbol intervals. We first generate a $(4 \times 4)$ Hadamard matrix as

$$\boldsymbol{A} = \frac{1+i}{\sqrt{2}} \begin{bmatrix} 1 & 1 & 1 & 1 \\ 1 & -1 & 1 & -1 \\ 1 & 1 & -1 & -1 \\ 1 & -1 & -1 & 1 \end{bmatrix}. \tag{2.19}$$

Then the optimal training sequence can be constructed by concatenating four $\boldsymbol{A}$ matrices as

$$\boldsymbol{S} = \left[ \; \boldsymbol{A} \quad \boldsymbol{A} \quad \boldsymbol{A} \quad \boldsymbol{A} \; \right]. \tag{2.20}$$

As an alternative to the ML channel estimator, the linear MMSE channel estimator is obtained as a linear transformation of the received signals $\boldsymbol{Y}$ that minimizes the estimation error and it is given by

$$\hat{\boldsymbol{H}}_{MMSE} = \sqrt{\frac{\rho}{n_T}}\boldsymbol{Y}\boldsymbol{S}^H\left(\frac{\rho}{n_T}\boldsymbol{S}\boldsymbol{S}^H + \boldsymbol{I}\right)^{-1}. \tag{2.21}$$

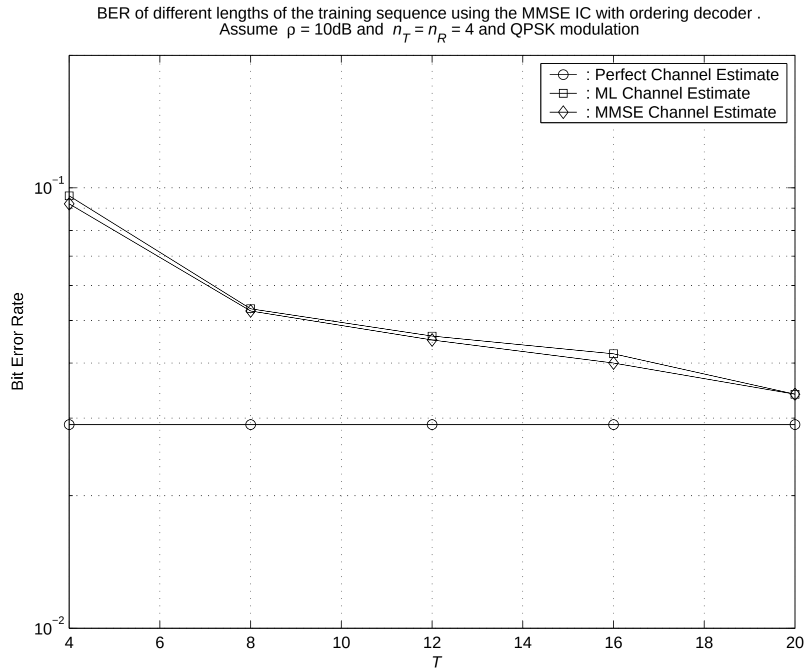


Figure 2.10: Effect of the training length $T$ on the BER performance.

We next give a simulation example. Consider a BLAST system with $n_T$ = $n_R$ = 4 antennas and QPSK modulation. We assume uncorrelated fading and a signal-to-noise ratio $\rho$ = 10dB. Figure 2.10 shows the BER for various channel estimation algorithms for different lengths of the optimal training sequence. The MMSE nulling and cancellation with ordering algorithm is employed as the decoder in all cases. It is seen that the MMSE and ML channel estimators have similar performance which gradually approaches optimum performance as $T$ is increased. Figure 2.11 compares the BER performance of the MMSE nulling and cancellation with ordering decoder using the ML channel estimator with different lengths of the optimal training sequence.

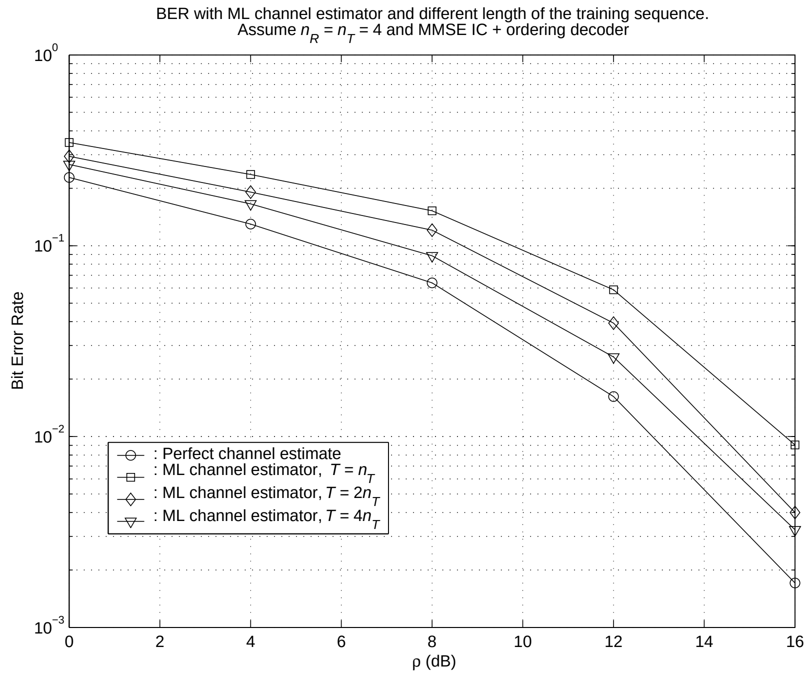


Figure 2.11: BER performance of the ML channel estimator with different lengths of the optimal training sequence.

## 2.4 Space-Time Coding

In the previous section, we discussed the BLAST system which increases the data rate by simultaneously transmitting symbols from multiple transmit antennas. However, the BLAST approach suffers from two major drawbacks: (1) it requires $n_R \geq n_T$ that is not always feasible when the receiver is a small or battery operated device; and (2) the performance of the suboptimal BLAST decoding algorithms is limited by error propagation. In this section, we discuss the space-time coding approach that exploits the concept of diversity.

### 2.4.1 The Concept of Diversity

With space-time codes (STC) [3, 114, 115, 118], instead of transmitting independent data streams as in BLAST, the same information is transmitted in an appropriate manner simultaneously from different transmit antennas in order to obtain transmit diversity. The underlying principle of transmit diversity is that if a message is lost in a channel with probability $p$ and if we can transmit replicas of the message over $n$ independent such channels, the loss probability becomes $p^n$. The use of diversity improves the reliability of detection which allows modulation employing higher order constellation to be used and so yielding a higher throughput , as is possible with the BLAST system. The main difference between BLAST and STC can be summarized as: (1) BLAST transmits more symbols, i.e., $n_T$ symbols/channel used; and (2) STC transmits only (at most) 1 *reliable* symbol/channel used by means of diversity.

As an example, consider a systems wishing to transmit 4 bit/s/Hz with 2 transmit antennas. BLAST would use QPSK symbols per antenna, i.e., 4 bit/s/Hz. STC can only send 1 symbol/channel used, therefore 16-QAM symbols would need to be employed. In this case, the same quantity of data is transmitted through the use of higher order constellations. There are two main types of STCs, namely space time trellis codes (STTC) [118] and space time block codes (STBC) [115].

The STTC is an extension of trellis coded modulation [15] to the case of multiple transmit and receive antennas. It provides both full diversity and coding gain. However, it has the disadvantage of high decoding complexity which grows exponentially with the number of antennas. Specific space-time trellis codes designed for two or four antennas perform very well in slow fading environments and come within 2-3 dB of the outage capacity. STTC's are designed to achieve full diversity and then, among the codes that achieve full diversity, maximize the coding gain. For further references on STTC refer to [11, 118].

In the hope of reducing the exponential decoding complexity of STTC, Alamouti proposed a simple space-time coding scheme using two transmit antennas [3]. Later, the STBC introduced in [114], generalized the Alamouti transmission scheme to an arbitrary number of transmit antennas. STBC achieves full diversity as does the STTC although they do not provide any coding gain. This is not a problem since they can be concatenated with an outer channel code [12]. Besides achieving full diversity, the main property of STBC is that there is a very simple ML decoding algorithm based only on linear processing. These codes are based on some specific linear matrices and the reduced complexity receiver is due to the orthogonal properties of these matrices.

### 2.4.2 Space-Time Block Codes

We assume a wireless communication system where the transmitter is equipped with $n_T$ and the receiver with $n_R$ antennas. A space time block code matrix is represented as

$$\begin{array}{c c} & \leftarrow\textbf{space}\rightarrow \\ \boldsymbol{C}_{p,n_T} = & \begin{bmatrix} c_{1,1} & c_{1,2} & \cdots & c_{1,n_T} \\ c_{2,1} & c_{2,2} & \cdots & c_{2,n_T} \\ \vdots & & \ddots & \vdots \\ c_{p,1} & c_{p,2} & \cdots & c_{p,n_T} \end{bmatrix} \end{array} \begin{array}{c} \uparrow \\ \textbf{time} \\ \downarrow \end{array} \tag{2.22}$$

At each time slot $t$, signals $c_{t,i}$, $i$=1,2,$\ldots$,$n_T$, are transmitted simultaneously from the $n_T$ transmit antennas as shown in Figure 2.12. Therefore, at time $t$, transmitter antenna $i$ will transmit $c_{t,i}$ in the matrix ($1 \leq t \leq p$ and $1 \leq i \leq n_T$, where $p$ is the length of the block code). Next, we describe the encoding and decoding operations of the STBC for two transmit antennas, namely the Alamouti code.

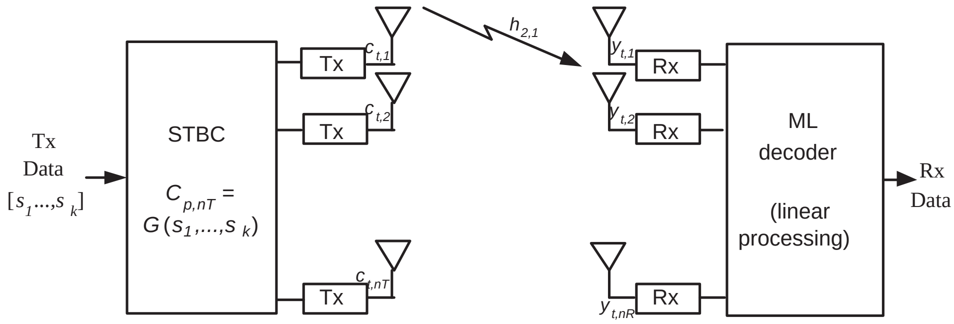


Figure 2.12: Schematic representation of an STBC system.

### STBC with $n_T$ = 2: Alamouti Code

The Alamouti code is an STBC using $n_T$ = 2 transmit antennas and any number of receive antennas. The Alamouti code matrix $\boldsymbol{O}_{c,2}$ is defined as [3]

$$\boldsymbol{O}_{c,2} = \begin{bmatrix} x_1 & x_2 \\ -x_2^* & x_1^* \end{bmatrix}. \tag{2.23}$$

Consider transmitting symbols of a signal constellation $\mathcal{A}$ of size $2^b$. Every two time slots, $2b$ bits arrive at the encoder and select constellation signals $s_1$ and $s_2$. Setting $x_1 = s_1$ and $x_2 = s_2$ in $\boldsymbol{O}_{c,2}$, we arrive at the following transmission matrix

$$\boldsymbol{C}_{2,2} = \begin{bmatrix} s_1 & s_2 \\ -s_2^* & s_1^* \end{bmatrix}. \tag{2.24}$$

Then, in the first time slot, antenna 1 transmits $s_1$ and antenna 2 transmits $s_2$. In the next time slot, antenna 1 transmits $-s_2^*$ and antenna 2 transmits $s_1^*$. Since two time slots are needed to transmit two symbols ($s_1$, $s_2$), the rate of the code is $R$ = 1 symbol/channel used.

At the receiver, the signal received by antenna $i$ during two consecutive time slots ($t$=1,2) is

$$\begin{aligned} \begin{bmatrix} y_{1,i} \\ y_{2,i} \end{bmatrix} &= \sqrt{\frac{\rho}{2}} \boldsymbol{C}_{2,2} \boldsymbol{h}_i + \boldsymbol{v}_i \\ &= \sqrt{\frac{\rho}{2}} \begin{bmatrix} s_1 & s_2 \\ -s_2^* & s_1^* \end{bmatrix} \begin{bmatrix} h_{i,1} \\ h_{i,2} \end{bmatrix} + \begin{bmatrix} v_{1,i} \\ v_{2,i} \end{bmatrix}, \quad i = 1, 2, \end{aligned} \tag{2.25}$$

which can be rewritten as

$$\underbrace{\begin{bmatrix} y_{1,i} \\ y_{2,i}^* \end{bmatrix}}_{\mathbf{y}_i} = \sqrt{\frac{\rho}{2}} \underbrace{\begin{bmatrix} h_{i,1} & h_{i,2} \\ h_{i,2}^* & -h_{i,1}^* \end{bmatrix}}_{\mathbf{H}_i} \underbrace{\begin{bmatrix} s_1 \\ s_2 \end{bmatrix}}_{\mathbf{s}} + \underbrace{\begin{bmatrix} v_{1,i} \\ \tilde{v}_{2,i} \end{bmatrix}}_{\tilde{\mathbf{v}}_i}, \quad i = 1, 2. \tag{2.26}$$

We note that the orthogonality of the code $\boldsymbol{O}_{c,2}$ implies the orthogonality of $\boldsymbol{H}_i$, i.e., $\boldsymbol{H}_i^H \boldsymbol{H}_i = \left(|h_{i,1}|^2 + |h_{i,2}|^2\right) \boldsymbol{I}_2$. Assuming that the receiver has knowledge of the channel coefficients $h_{i,j}$, we form a decision statistic at each receive antenna by left multiplying the received vector in (2.26) by $\boldsymbol{H}_i^H$ which results in

$$\boldsymbol{z}_i = \begin{bmatrix} z_{1,i} \\ z_{2,i} \end{bmatrix} = \boldsymbol{H}_i^H \boldsymbol{y}_i = \sqrt{\frac{\rho}{2}} \boldsymbol{H}_i^H \boldsymbol{H}_i \boldsymbol{s} + \boldsymbol{H}_i^H \tilde{\mathbf{v}}_i. \tag{2.27}$$

Hence, using the orthogonality property of $\boldsymbol{H}_i$ yields

$$\boldsymbol{z}_i = \begin{bmatrix} z_{1,i} \\ z_{2,i} \end{bmatrix} = \sqrt{\frac{\rho}{2}} \left(|h_{i,1}|^2 + |h_{i,2}|^2\right) \begin{bmatrix} s_1 \\ s_2 \end{bmatrix} + \begin{bmatrix} w_{1,i} \\ w_{2,i} \end{bmatrix}. \tag{2.28}$$

Adding all the decision statistics from all $n_R$ receive antennas we obtain

$$\begin{aligned} \boldsymbol{z} &= \begin{bmatrix} z_1 \\ z_2 \end{bmatrix} = \sum_{i=1}^{n_R} \begin{bmatrix} z_{1,i} \\ z_{2,i} \end{bmatrix} \\ &= \sqrt{\frac{\rho}{2}} \sum_{i=1}^{n_R} \left(|h_{i,1}|^2 + |h_{i,2}|^2\right) \begin{bmatrix} s_1 \\ s_2 \end{bmatrix} + \sum_{i=1}^{n_R} \begin{bmatrix} w_{1,i} \\ w_{2,i} \end{bmatrix}. \end{aligned} \tag{2.29}$$

In (2.29), in the absence of noise, $z_1$ will be just an scaled version of $s_1$ and $z_2$ will be an scale version of $s_2$ without any cross dependency. To estimate the symbols that were sent, we just scale and quantize the decisions statistics in (2.29) as

$$\begin{aligned}\hat{s}_1 &= Q(z_1),\\ \text{and} \quad \hat{s}_2 &= Q(z_2).\end{aligned} \tag{2.30}$$

We recall that the decoupling has been possible because of the orthogonality of the Alamouti code matrix.

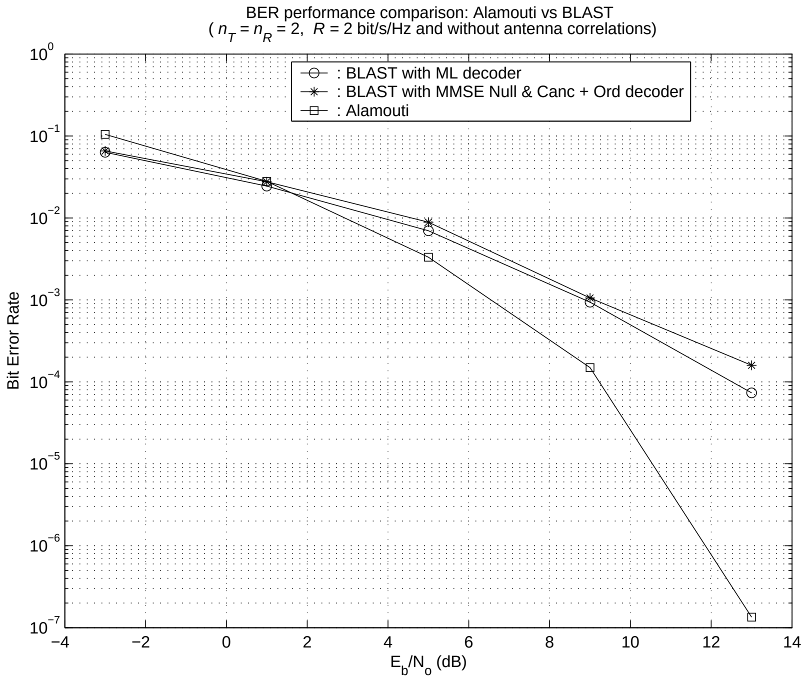


Figure 2.13: BER performance comparison between BLAST (BPSK modulation) and Alamouti (QPSK modulation) with $n_T = n_R = 2$ (transmission rate $R = 2$ bit/s/Hz). Uncorrelated MIMO channel and perfect channel knowledge at the receiver are assumed.

We now compare the performance of the Alamouti scheme with that of the BLAST system discussed in the previous section. For both systems, we consider $n_T = n_R = 2$. We assume that both schemes have a transmission rate $R = 2$ bit/s/Hz. This rate can be achieved using BLAST with BPSK or using the Alamouti code with QPSK modulation. For a fair comparison, we compare the two systems in terms of signal-to-noise ratio per bit, i.e., $E_b/N_o$. Assuming perfect channel estimation at the receiver and no antenna correlations, Figure 2.13 shows that Alamouti performs better than BLAST and this improvement is greater at higher signal-to-

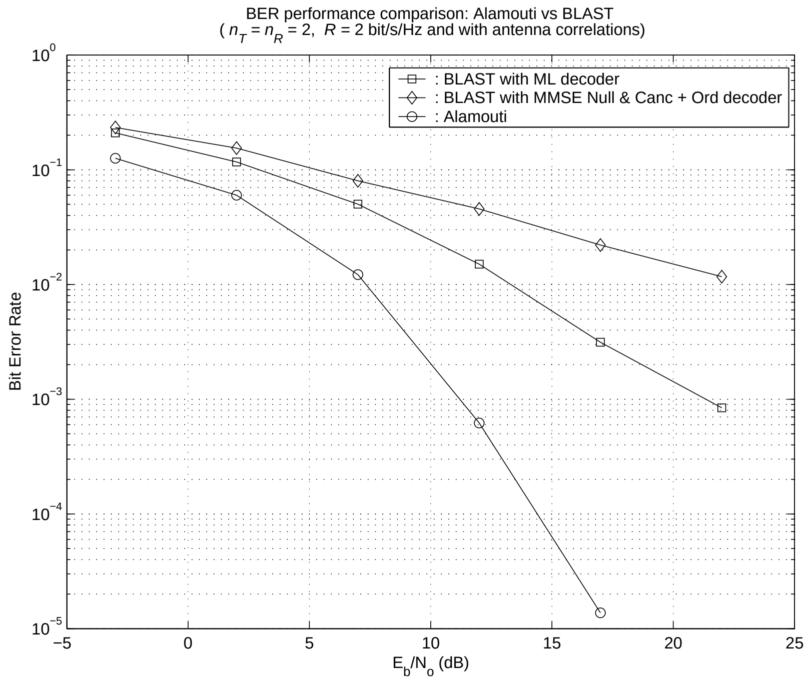


Figure 2.14: BER Performance comparison between BLAST (BPSK modulation) and Alamouti (QPSK modulation) with $n_T = n_R = 2$ (transmission rate $R = 2$ bit/s/Hz). Correlated MIMO channel (urban environment in Figure 2.5) and perfect channel knowledge at the receiver are assumed.

noise ratio. We next compare their performance in correlated MIMO channels. We consider a medium level of correlation typical of urban environments as described in Figure 2.5. It is seen from Figure 2.14 that Alamouti performs much better than BLAST in such a scenario.

#### General STBC Based on Orthogonal Designs ($n_T \geq 2$)

The Alamouti scheme presented previously only works with two transmit antennas. This scheme was later generalized in [114, 115] to an arbitrary number of transmit antennas. In a similar manner to the Alamouti code in (2.23), the general STBC is defined by a code matrix with orthogonal columns. Just like in the Alamouti scheme, a simple linear receiver is also obtained owing to the orthogonality of the columns of the code matrix. In general, an STBC is defined by a ($p \times n_T$) matrix $\boldsymbol{G}$. The entries of the matrix $\boldsymbol{G}$ are linear (possibly complex) combinations of the variables $x_1, x_2, ..., x_k$ (representing symbols). The columns of the matrix represent antennas and the rows time slots. Therefore, $p$ time slots are needed to transmit $k$ symbols, resulting in a code rate $R = k/p$ symbols/channel used. It is of special interest code matrices achieving the maximum transmission rate permitted by the STC theory, i.e, $R$ = 1 symbol/channel used. For a fixed $n_T$, among the code matrices that achieve the maximum rate, we will be interested in those with minimum values of $p$ or equivalently, the minimum number of time slots needed to transmit a block. These code matrices are referred as delay optimal and they are interesting because they minimize the memory requirements at the transmitter and at the receiver (i.e., encoding and decoding delay). We recall that $p \geq n_T$.

*STBC for real constellations*

For real signal constellations such as pulse amplitude modulation (PAM), the entries of the code matrices are only real linear combinations of $x_1, x_2, ..., x_k$. General STBC based on real orthogonal designs achieving full diversity and full rate, can be found for any number of transmit antennas $n_T$ [118]. Using $n_T$ = 2, 4 and 8 antennas, STBC code matrices can be found with $p = n_T$ (i.e., minimum possible delay in STBC). As an example, an STBC suitable for real constellations with $n_T$ = 4 is

$$\boldsymbol{G}_4 = \begin{bmatrix} x_1 & x_2 & x_3 & x_4 \\ -x_2 & x_1 & -x_4 & x_3 \\ -x_3 & x_4 & x_1 & -x_2 \\ -x_4 & -x_3 & x_2 & x_1 \end{bmatrix} \tag{2.31}$$

for which it can be verified that $\boldsymbol{G}_4^T \boldsymbol{G}_4 = \left( \sum_{i=1}^{4} x_i^2 \right) \cdot \boldsymbol{I}_4$. The encoding process at the transmitter is similar to that for the Alamouti code, as follows. Consider a real constellation of size $2^b$. At time instant 1, 4*b* bits arrive at the encoder and select symbols $s_1, s_2, s_3, s_4$. Let $x_i = s_i$ in matrix $\boldsymbol{G}_4$ in (2.31) to obtain the code matrix $\boldsymbol{C}_4$. At time $t$ = 1,2,3 and 4, the $t$-th row of $\boldsymbol{C}_4$ is transmitted from the four transmit antennas simultaneously. Therefore, with $n_T$ = 4 transmit antennas and employing the code matrix $\boldsymbol{C}_4$, four symbols are transmitted during four symbol intervals achieving $R$ = 1 symbol/channel used, i.e., the maximum rate allowed by the STC theory. At the receiver, the orthogonality of the matrix $\boldsymbol{C}_4$ simplifies the ML decoder by decoupling the detection of each of the transmitted symbols.

*STBC for complex constellations*

Complex STBC are analogous to the real ones except that the code matrices contain entries $\pm x_1, \pm x_2, ..., \pm x_k$, their conjugates, and them multiplied by $\sqrt{-1}$, making them useful for complex constellations such as M-PSK or M-QAM. As an example, an STBC with $n_T$ = 4 for complex constellations can be constructed using the real orthogonal design in (2.31) as

$$\boldsymbol{G}_{c,4} = \begin{bmatrix} \boldsymbol{G}_4 \\ \boldsymbol{G}_4^* \end{bmatrix} = \begin{bmatrix} x_1 & x_2 & x_3 & x_4 \\ -x_2 & x_1 & -x_4 & x_3 \\ -x_3 & x_4 & x_1 & -x_2 \\ -x_4 & -x_3 & x_2 & x_1 \\ x_1^* & x_2^* & x_3^* & x_4^* \\ -x_2^* & x_1^* & -x_4^* & x_3^* \\ -x_3^* & x_4^* & x_1^* & -x_2^* \\ -x_4^* & -x_3^* & x_2^* & x_1^* \end{bmatrix}. \tag{2.32}$$

As before, the code $\boldsymbol{C}_{c,4}$ can be obtained substituting $x_i$ by the data symbols $s_i$ in $\boldsymbol{G}_{c,4}$. In this code, transmitting each row at a time, 8 symbols intervals are needed to transmit 4 symbols, therefore giving a rate $R$ = 1/2 symbol/channel used, i.e., half of the maximum rate permitted by the STC theory. Complex STBC of $R$ = 1/2 achieving full diversity can be built for any number of transmit antennas $n_T$ from real STBC using $\boldsymbol{G}_{c,n_T} = \begin{bmatrix} \boldsymbol{G}_{n_T} \\ \boldsymbol{G}_{n_T}^* \end{bmatrix}$.

It has been shown that complex STBC having full symbol rate (i.e., $R$ = 1) only exist for $n_T$ = 2, i.e., the Alamouti code. In this sense, the Alamouti codes is unique. Codes that achieve a rate $R$ = 3/4 with complex constellations have been found with $n_T$ = 3 and $n_T$ = 4 [114].

## 2.5 MIMO systems in frequency selective channels

So far we have considered flat fading channels. In this section, in addition to showing how to extend MIMO detectors to frequency selective channels, we also introduce a new class of linear detectors, namely lattice-reduction-aided (LRA) detectors.

### 2.5.1 MIMO Frequency Selective System Model

An apparent disadvantage of single-carrier based MIMO systems in frequency selective channels is the fact that the computational complexity of the receiver (either a vector-MLSE or a multi-channel equalizer) will in general be very high. The use of orthogonal frequency division multiplexing (OFDM) alleviates this problem by turning the frequency-selective MIMO channel into a set of parallel narrowband MIMO channels [17, 98], which greatly simplifies the equalization process.

For the equivalent narrowband detection process, although the performance of the ML receiver is optimal, its complexity is very high. A number of other detectors, offer substantially lower complexity, but their performance is significantly worse. This section shows that a class of lattice-reduction-aided (LRA) receivers in MIMO-OFDM systems can achieve near maximum likelihood detector performance with low complexity. We extend the LRA receiver technique proposed in [133], applicable for a $2 \times 2$ system, to a general $n_R \times n_T$ system, where $n_R \geq n_T$. It will be shown that particularly with higher order constellations and when the channel is correlated, LRA significantly outperforms other suboptimal detectors in terms of BER.

Consider the equivalent discrete time baseband model for the MIMO-OFDM system shown in Figure 2.15 having $N_c$ carriers, $n_T$ transmit antennas, and $n_R$ receive antennas. Assuming that $x_v[t]$ is the output of the parallel-to-serial converter at the $v$-th transmit antenna at time $t$, the signal received at the $m$-th antenna can be written as

$$r_m[t] = \sum_{v=1}^{n_T} \sum_{l=0}^{L-1} \sqrt{\frac{\rho}{n_T}} h_{m,v}[l] x_v[t-l] + w_m[t], \qquad (2.33)$$

where $\rho$ is the received signal to noise ratio (SNR), $w_m[t]$ is the noise observed at the $m$-th receive antenna, distributed as $\mathcal{N}_c(0,1)$ and $h_{m,v}[l]$ represents the com-

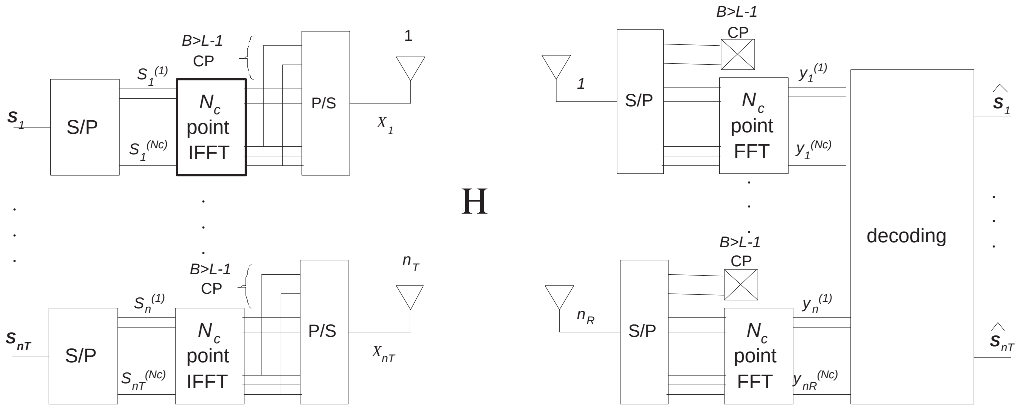


Figure 2.15: The block diagram of MIMO-OFDM transceiver.

plex channel gain between the $v$-th transmit antenna and the $m$-th receive antenna for the $l$-th path, where $l = 1, \ldots, L-1$. We consider $h_{m,v}[l] \sim \mathcal{N}_c(0, \sigma_{h,l}^2)$ with $\sum_{l=0}^{L-1} \sigma_{h,l}^2 = 1$.

Denoting $\boldsymbol{r}[t] = [r_1[t], \ldots, r_{n_R}[t]]^T$, $\boldsymbol{x}[t] = [x_1[t], \ldots, x_{n_T}[t]]^T$, and $\boldsymbol{w}[t] = [w_1[t], w_2[t], \ldots, w_{n_R}[t]]^T$, we can rewrite (2.33) as

$$\boldsymbol{r}[t] = \sum_{l=0}^{L-1} \sqrt{\frac{\rho}{n_T}} \boldsymbol{H}_l \boldsymbol{x}[t-l] + \boldsymbol{w}[t], \tag{2.34}$$

where the elements of the $(n_R \times n_T)$ matrix $[\boldsymbol{H}_l]_{m,v} = h_{m,v}[l]$.

The MIMO-OFDM structure is one way to avoid the complexity of time domain equalization to recover the transmitted signal in (2.34). MIMO-OFDM converts a frequency selective channel into a set of $N_c$ parallel frequency flat channels with $N_c$ subcarriers [17, 98]. In MIMO-OFDM systems, the transmitted signal at the $v$-th transmit antenna, $x_v[t]$, is generated by the IFFT of $N_c$ data symbols $s_v^{(1)}[i], \ldots, s_v^{(N_c)}[i]$, where $s_v^{(k)}[i]$ is the input data on the $v$-th antenna on the $k$-th subcarrier. A cyclic prefix (CP) is pre-appended at each block of the IFFT output as shown in Figure 2.15. The receiver at each antenna discards the CP from $r_m[t]$ and passes the remaining $N_c$ samples to the FFT block. If the length of the CP, $B \geq L-1$, then the system in (2.34) during the $i$-th MIMO-OFDM symbol can be written as

$$\boldsymbol{y}^{(k)}[i] = \sqrt{\frac{\rho}{n_T}} \boldsymbol{H}^{(k)} \boldsymbol{s}^{(k)}[i] + \boldsymbol{n}^{(k)}[i], \tag{2.35}$$

where the equivalent flat fading matrix $\boldsymbol{H}^{(k)}$ corresponding to the $k$-th subcarrier is denoted as

$$\boldsymbol{H}^{(k)} = \boldsymbol{H}(e^{j2\pi k/N_c}) = \frac{1}{\sqrt{N_c}} \sum_{l=0}^{L-1} \boldsymbol{H}_l e^{-j2\pi lk/N_c}, \tag{2.36}$$

and $\boldsymbol{s}^{(k)}[i]$ consists of the input data symbols of all the $n_T$ transmit antennas, $\boldsymbol{n}^{(k)}[i]$ is the noise at the $k$-th output of the FFT blocks at each of the $n_R$ receive antennas. Owing to the OFDM operations, ISI is avoided and for notational convenience, we will drop the time index $i$ in the remainder of this section, i.e., $\boldsymbol{s}^{(k)}[i] = [s_1^{(k)}, \ldots, s_{n_T}^{(k)}]^T$, $\boldsymbol{n}^{(k)} = [n_1^{(k)}, \ldots, n_{n_R}^{(k)}]^T$, and $\boldsymbol{y}^{(k)} = [y_1^{(k)}, \ldots, y_{n_R}^{(k)}]^T$. The MIMO-OFDM symbol has a duration $T$ equal to $N_c + B$ samples of the time domain signal $x_v[t]$.

### 2.5.2 Correlated Channel Model in Frequency Selective Channels

Consider that there is no line of sight between the transmit and receive antennas. Also assume that all the signals reflected from one cluster of scattering objects and arriving at the receiver can be considered as having undergone one path of the multipath channel as shown in Figure 2.16. If the angular spread $a_l^{Rx}$ of the arriving rays corresponding to one path/cluster is not large enough or if the distance between the antennas, $d$ is not sufficient, the signals arriving at different receive antennas will be correlated. Similar arguments apply to the transmit antennas.

Consider the matrix $\boldsymbol{H}_l$ whose entries $h_{m,v}[l]$ represent the complex channel gains between the $v$-th transmit and $m$-th receive antenna for the $l$-th path. When the channels are correlated at either the transmitter or the receiver sides, the elements of $\boldsymbol{H}_l$ cannot be considered as independent and in a similar manner that previously presented in section 2.2.2 the channel matrix response for the $l$-th transmission path can be modeled as [17]

$$\boldsymbol{H}_l = \boldsymbol{R}_{r,l}^{1/2} \boldsymbol{H}_{w,l} \boldsymbol{R}_{t,l}^{1/2}, \tag{2.37}$$

where $\boldsymbol{H}_{w,l}$ is an uncorrelated $n_R \times n_T$ matrix with i.i.d. entries, $\boldsymbol{R}_{t,l}$ is an $n_T \times n_T$ transmit covariance matrix for the $l$-th path corresponding to the correlation between transmit antennas, and $\boldsymbol{R}_{r,l}$ is an $n_R \times n_R$ receive covariance matrix for the $l$-th path. Note that when the $l$-th path is uncorrelated at the transmitter(receiver), $\boldsymbol{R}_{t,l} = \boldsymbol{I}(\boldsymbol{R}_{r,l} = \boldsymbol{I})$.

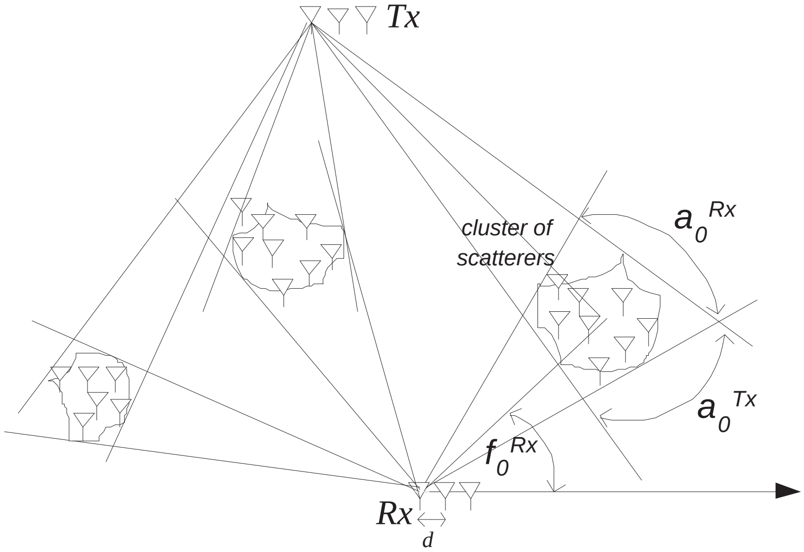


Figure 2.16: Geometry of the scattering scenario with $L = 3$ paths.

### 2.5.3 Basic Linear Receivers

Consider the received signal vector on the $k$-th OFDM carrier in (2.35). For this model, any of the BLAST detectors described in Section 2.3.1 can be applied. However, let us describe more simple receivers, namely linear detectors.

In a linear receiver, the received signal vector $\boldsymbol{y}^{(k)}$ in the $k$-th carrier is linearly transformed by a matrix equalizer $\boldsymbol{G}^{(k)}$ which basically undoes the effects of the channel to obtain

$$\boldsymbol{r}^{(k)} = \boldsymbol{G}^{(k)}\boldsymbol{y}^{(k)} = \sqrt{\frac{\rho}{n_T}}\boldsymbol{G}^{(k)}\boldsymbol{H}^{(k)}\boldsymbol{s}^{(k)} + \boldsymbol{G}^{(k)}\boldsymbol{w}^{(k)}, \qquad (2.38)$$

which is later quantized to obtain an estimate of the transmitted symbol vector, i.e., $\hat{\boldsymbol{s}}^{(k)} = Q(\boldsymbol{r}^{(k)})$. The whole process is shown in Figure 2.17. The matrix equalizer $\boldsymbol{G}^{(k)}$ can be computed according to different criteria. For the zero-forcing (ZF) criterion, the equalizer is given by $\boldsymbol{G}^{(k)} = \sqrt{\frac{n_T}{\rho}}\boldsymbol{H}^{(k)\dagger}$, where $\boldsymbol{H}^{(k)\dagger}$ denotes the pseudo-inverse. The ZF criterion suffers from noise enhancement since it focuses on cancelling the effects of the channel response at the expense of enhancing the noise, possibly significantly. On the other hand, the minimum mean-square error (MMSE) linear equalizer, $\boldsymbol{G}^{(k)} = \sigma_s^2\sqrt{\frac{\rho}{n_T}}\boldsymbol{H}^H\left(\frac{\sigma_s^2\rho}{n_T}\boldsymbol{H}^{(k)}\boldsymbol{H}^{(k)H} + \sigma_n^2\boldsymbol{I}_{M_R}\right)^{-1}$, minimizes the error due to the noise and the interference combined. The nonlinear BLAST receivers described in previous Section 2.3.1 offer better performance than linear receivers with a moderate increase in complexity. However, the performance of these receivers is far away from the much more complex ML receivers, especially in correlated channel scenarios.

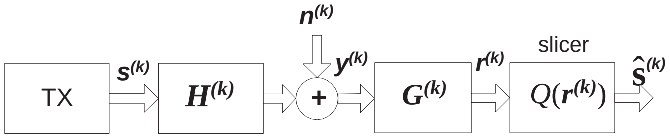


Figure 2.17: Traditional linear receiver.

### 2.5.4 Lattice-Reduction-Aided Receivers

#### Constellation, Lattices, and Basis Change

Let us first consider a real-valued MIMO-OFDM system with $n_T$=$n_R$=2 antennas, where the transmitted symbols $s_1^{(k)}$ and $s_2^{(k)}$ belong to a $2N+1$-PAM constellation, i.e. $s_i^{(k)} \in \{-N, -N+1, \dots, 0, \dots, N-1, N\}$. Assume that the channel matrix for the $k$-th OFDM carrier is $\boldsymbol{H}^{(k)} = [\boldsymbol{h}_1^{(k)}, \boldsymbol{h}_2^{(k)}] = \begin{bmatrix} 2 & 3 \\ 1 & 2 \end{bmatrix}$. Then, the received constellation will consist of a lattice of linear combinations of the columns of $\boldsymbol{H}^{(k)}$, i.e., $\boldsymbol{H}^{(k)}\boldsymbol{s}^{(k)} = s_1^{(k)}[2,1]^T + s_2^{(k)}[3,2]^T$. As shown in Figure 2.18, due to the equalizing operation and the direction of the basis vectors, the decision regions can be seen as parallelograms described by the columns of $\boldsymbol{H}^{(k)}$ [133]. In this case, it can be seen that when the angle between $\boldsymbol{h}_1^{(k)}$ and $\boldsymbol{h}_2^{(k)}$ is very narrow (i.e., the vectors are correlated), a small amount of noise can make a received symbol fall out of the decision region and cause the decoder to make a wrong decision [133].

The idea proposed in [133] is to change the original basis $\boldsymbol{H}^{(k)}$ to a new basis representing the same lattice in which its column vectors are less correlated, then decode the symbols in the new basis, and finally transform the decoded symbols into the original basis. All of these operations need to performed at the receiver. For example, as can be seen in Figure 2.19, the new basis, $\boldsymbol{h}_1^{\prime(k)}$ and $\boldsymbol{h}_2^{\prime(k)}$ is closer to orthogonal as compared to $\boldsymbol{h}_1^{(k)}$ and $\boldsymbol{h}_2^{(k)}$, and yet still generate the same lattice with better decision regions. Thus, with the new basis, the decision regions are more robust against noise and interference. In this section, we propose an extension of a reduction technique which first appeared in [133] for $2\times2$ systems, to a general $n_R \times n_T$ system.

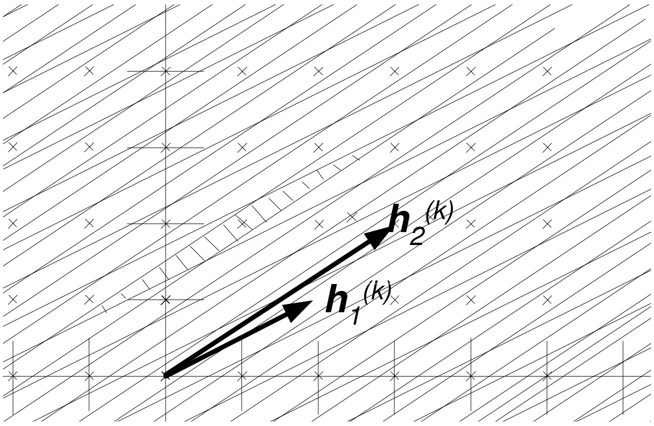


Figure 2.18: Original basis and decision regions.

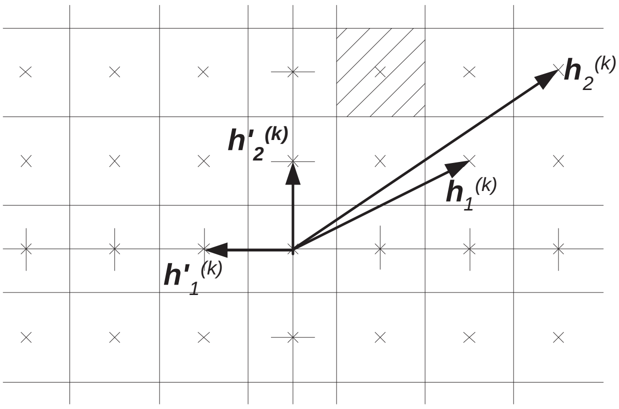


Figure 2.19: Original and new bases.

**Theorem 1** *[133]: If $\boldsymbol{H}$ is a basis of a lattice, $\boldsymbol{H}' = \boldsymbol{H}\boldsymbol{P}$ is also a basis of the same lattice if $\boldsymbol{P}$ and $\boldsymbol{P}^{-1}$ have integer (possibly complex) entries.*
For the problem in hand, the objective is to find a change of basis $\boldsymbol{P}^{(k)}$ which transforms $\boldsymbol{H}^{(k)}$ into $\boldsymbol{H}'^{(k)}$, for $k = 0, \ldots, N_c - 1$ such that the decision regions for a specific lattice and decoder are more robust against noise and interference.

### LRA Receiver

For general $n_T$ complex vectors and QAM input symbols, an input symbol vector of the $k$-th carrier represented by $\boldsymbol{s}^{(k)}$ in the original basis with elements in $\mathbb{Z}_{\mathbb{C}}$, where $\mathbb{Z}_{\mathbb{C}}$ is the set of complex integers, can be represented by $\boldsymbol{z}^{(k)} = (\boldsymbol{P}^{(k)})^{-1}\boldsymbol{s}^{(k)}$ in the new reduced basis. We can assume that the received vector $\boldsymbol{y}^{(k)}$ in (2.35) is already represented in the new reduced basis since

$$\boldsymbol{y}^{(k)} = \sqrt{\frac{\rho}{n_T}}\boldsymbol{H}'^{(k)}\boldsymbol{z}^{(k)} + \boldsymbol{n}^{(k)}. \tag{2.39}$$

Now $\boldsymbol{H}'^{(k)} = \boldsymbol{H}^{(k)}\boldsymbol{P}^{(k)}$, and so for the ZF receiver where $\boldsymbol{G}^{(k)} = \sqrt{\frac{n_T}{\rho}}(\boldsymbol{H}^{(k)}\boldsymbol{P}^{(k)})^{\dagger}$, (2.38) can be written as

$$\boldsymbol{r}^{(k)} = \sqrt{\frac{\rho}{n_T}}\boldsymbol{G}^{(k)}\boldsymbol{H}^{(k)}\boldsymbol{P}^{(k)}\boldsymbol{z}^{(k)} + \boldsymbol{G}^{(k)}\boldsymbol{n}^{(k)}. \tag{2.40}$$

The estimate of $\boldsymbol{z}^{(k)}$ is $\hat{\boldsymbol{z}}^{(k)} = \mathcal{Q}(\boldsymbol{r}^{(k)})$. Since the lattice points consist of elements in $\mathbb{Z}_{\mathbb{C}}$, the quantization consist of a rounding operation whereby the real and imaginary parts are rounded separately. Finally, $\hat{\boldsymbol{z}}^{(k)}$ is transformed to its original basis by performing the operation $\hat{\boldsymbol{s}}^{(k)} = \boldsymbol{P}^{(k)}\hat{\boldsymbol{z}}^{(k)}$.

To use the lattice theory and the decoding operation in (2.40), the original points in the constellation are required to consist of symbols in $\mathbb{Z}_{\mathbb{C}}$. Note that the origin $[0, \ldots, 0]^T$ also belongs to the lattice. Since ordinary QAM constellations consist neither of contiguous integers nor contain the origin, it is necessary to scale and shift the original constellation. In this section, we consider $M$-QAM constellations such that $\Re\{s_j^{(k)}\} \in \{-\sqrt{M}+1, \ldots, \sqrt{M}-1\}$ and $\Im\{s_j^{(k)}\} \in \{-\sqrt{M}+1, \ldots, \sqrt{M}-1\}$, thus, to convert the symbols into contiguous integers $s_j'^{(k)}$, we can shift the original constellation by $\boldsymbol{d} = [1+i, \ldots, 1+i]^T$ and scale by $1/2$. Since the transmitter might not know the type of receivers used, the scaling and shifting operations have to be done at the receiver.

Assuming the shifted and scaled constellation $\boldsymbol{s}'^{(k)}$ is transmitted, the received signal vector is

$$\boldsymbol{y}'^{(k)} = \sqrt{\frac{\rho}{n_T}}\boldsymbol{H}^{(k)}\boldsymbol{s}'^{(k)} = \sqrt{\frac{\rho}{n_T}}\boldsymbol{H}^{(k)}\frac{1}{2}\left[\boldsymbol{s}^{(k)} + \boldsymbol{d}\right]. \tag{2.41}$$

In terms of the signal received when the data bits are transmitted using the original constellation, $\boldsymbol{y}^{(k)}$, (2.41) can be rewritten as:

$$\boldsymbol{y}'^{(k)} = \frac{1}{2}\boldsymbol{y}^{(k)} + \frac{1}{2}\sqrt{\frac{\rho}{n_T}}\boldsymbol{H}^{(k)}\boldsymbol{d}. \tag{2.42}$$

To summarize, combining (2.40) and (2.42), the operations at the receiver consist

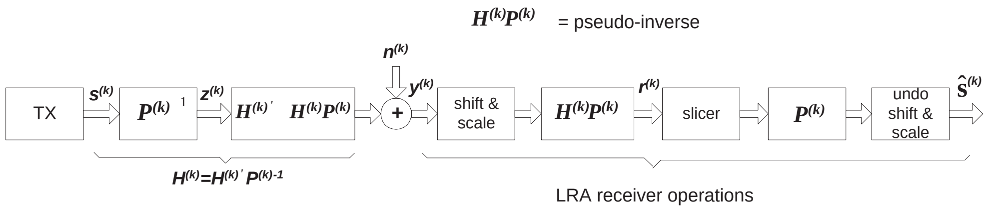


Figure 2.20: LRA linear receiver.

of two steps as shown in Figure 2.20: (a) scaling, shifting, and equalizing in the new basis

$$\boldsymbol{r}^{(k)} = \underbrace{\sqrt{\frac{n_T}{\rho}}\left(\boldsymbol{H}^{(k)}\boldsymbol{P}^{(k)}\right)^{\dagger}}_{\text{equalize in new basis}}\underbrace{\frac{1}{2}}_{\text{scale}}\left[\underbrace{\sqrt{\frac{\rho}{n_T}}\boldsymbol{H}^{(k)}\boldsymbol{s}^{(k)} + \boldsymbol{n}}_{\text{rx signal-}\boldsymbol{y}}\underbrace{\sqrt{\frac{\rho}{n_T}}(\boldsymbol{H}^{(k)}\boldsymbol{d})}_{\text{shift}}\right], \tag{2.43}$$

and (b) slicing, returning to the original basis, and undoing the scaling and shifting as

$$\hat{\boldsymbol{s}} = 2\boldsymbol{P}^{(k)}\mathcal{Q}(\boldsymbol{r}^{(k)}) - \boldsymbol{d}. \tag{2.44}$$

Note that the slicing $\mathcal{Q}(\cdot)$ is a rounding operation since the symbols in the lattice belong to $\mathbb{Z}_{\mathbb{C}}$. In general, LRA receivers are expected to have better performance than traditional linear receivers, especially in realistic communication systems scenarios, where the channel and therefore the column vectors are correlated to some degree. When the columns or rows of $\boldsymbol{H}^{(k)}$ are correlated, the inversion of channel matrix $\boldsymbol{H}^{(k)}$ in the ZF equalizer may enhance the noise significantly.

### 2.5.5 Basis Reduction Algorithm

Given the columns of $\boldsymbol{H}^{(k)}$, i.e., $\boldsymbol{h}_1^{(k)}, \ldots, \boldsymbol{h}_{n_T}^{(k)}$ are the basis of the lattice for the $k$-th OFDM carrier, let us consider the problem of finding a *good* change of basis $\boldsymbol{P}$ to transform $\boldsymbol{h}_1^{(k)}, \ldots, \boldsymbol{h}_2^{(k)}$ into $\boldsymbol{h}_1'^{(k)}, \ldots, \boldsymbol{h}_{n_T}'^{(k)}$ as illustrated in Figure 2.19 for the case of 2 transmit antennas. This problem is known as the basis reduction problem and borrows the ideas from Gram-Schmidt orthogonalization.

We first give an overview of the Gauss basis reduction algorithm limited to rank $n_T = 2$ which is used in [133]. The reduction algorithm uses a method similar to the Gram-Schmidt orthogonalization. Assume that $\boldsymbol{h}_1^{(k)}$ and $\boldsymbol{h}_2^{(k)}$ are a basis of the lattice. Define the Euclidean inner product as $\langle \boldsymbol{h}_1^{(k)}, \boldsymbol{h}_2^{(k)} \rangle = \boldsymbol{h}_1^{(k)H} \boldsymbol{h}_2^{(k)}$ and consider the Euclidean norm. Assuming that $\|\boldsymbol{h}_1^{(k)}\| < \|\boldsymbol{h}_2^{(k)}\|$, the basis reduction algorithm does operations in the basis vectors of the form

$$\boldsymbol{h}_2^{(k)} = \boldsymbol{h}_1^{(k)} - \mu \boldsymbol{h}_2^{(k)}, \tag{2.45}$$

which yields a different basis for the same lattice if $\mu \in \mathbb{Z}_{\mathbb{C}}$. Since the purpose of the lattice reduction is to make lattice basis vectors as close to orthogonal as possible, Gram-Schmidt orthogonalization can be used to find $\mu$ with the further constraint $\mu \in \mathbb{Z}_{\mathbb{C}}$. The ideal Gram-Schmidt orthogonalization, uses $\mu' = \frac{\langle \boldsymbol{h}_1^{(k)}, \boldsymbol{h}_2^{(k)} \rangle}{\langle \boldsymbol{h}_1^{(k)}, \boldsymbol{h}_2^{(k)} \rangle}$ but this operation would change the lattice since $\mu'$ is not in $\mathbb{Z}_{\mathbb{C}}$. The weakly reduced Gram-Schmidt orthogonalization, uses an integer rounding of the ideal Gram-Schmidt coefficient as $\mu = \lfloor \mu' \rceil$ where real and imaginary parts of complex numbers are rounded separately. Using a weak reduction, the lattice remains the same. Once $\boldsymbol{h}_2^{(k)}$ has been reduced with respect to $\boldsymbol{h}_1^{(k)}$, if $\boldsymbol{h}_2^{(k)} < \boldsymbol{h}_1^{(k)}$ we have the possibility of reducing $\boldsymbol{h}_1^{(k)}$ with respect to the new $\boldsymbol{h}_2^{(k)}$. We first swap $\boldsymbol{h}_1^{(k)}$ and $\boldsymbol{h}_2^{(k)}$. This second reduction will occur if such $\mu$ exists, i.e., if $|\Re\{\langle \boldsymbol{h}_1^{(k)}, \boldsymbol{h}_2^{(k)} \rangle\}| > \frac{1}{2}\|\boldsymbol{h}_1^{(k)}\|^2$ or $|\Im\{\langle \boldsymbol{h}_1^{(k)}, \boldsymbol{h}_2^{(k)} \rangle\}| > \frac{1}{2}\|\boldsymbol{h}_1^{(k)}\|^2$. The algorithm repeats this process until no more reduction is possible. As an example, for the basis given in Figure 2.21 we give the two steps performed in the algorithm.

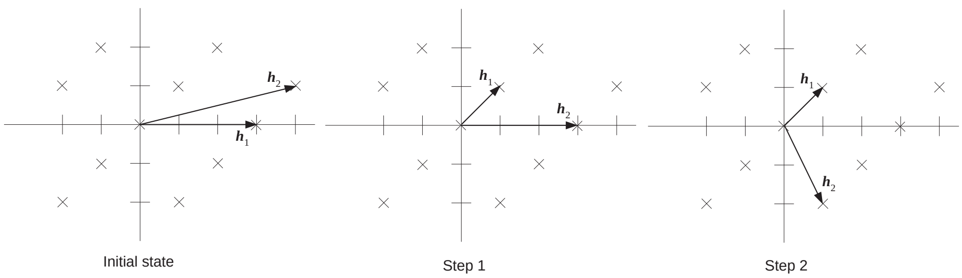


Figure 2.21: Lattice basis reduction using the Gauss reduction algorithm.

A notion of lattice reduction for a lattice basis $\boldsymbol{h}_1^{(k)}, ..., \boldsymbol{h}_{n_T}^{(k)}$ of arbitrary rank $n_T$ was proposed by Lenstra, Lenstra and Lovasz (LLL) [87]. It uses similar ideas to the Gauss reduction algorithm. For a given $\delta$, $\frac{1}{4} < \delta < 1$, the LLL reduction algorithm modifies an input basis $\boldsymbol{h}_1^{(k)}, ..., \boldsymbol{h}_{n_T}^{(k)}$ so the output basis satisfies the following $\delta$-reduction properties

$$\mu_{u,i} \leq \frac{1}{2} \quad \text{for} \quad 1 \leq i < u \leq n_T, \tag{2.46}$$

which guarantees that the next reduced vector cannot be further reduced with respect to the previously reduced vectors, and

$$\delta \cdot \|\hat{\boldsymbol{h}}_{i-1}^{(k)}\|^2 > \|\hat{\boldsymbol{h}}_i^{(k)} + \mu_{i,i-1}^{(k)} \hat{\boldsymbol{h}}_{i-1}^{(k)}\|^2, \tag{2.47}$$

where the vectors $\hat{\boldsymbol{h}}_1^{(k)}, ..., \hat{\boldsymbol{h}}_{n_T}^{(k)}$ denote the Gram-Schmidt orthogonalization of the output basis that can be obtained by the following recursion

$$\begin{aligned} \hat{\boldsymbol{h}}_1^{(k)} &= \boldsymbol{h}_1^{(k)}, \\ \hat{\boldsymbol{h}}_i^{(k)} &= \boldsymbol{h}_i^{(k)} - \sum_{j=1}^{i-1} \mu_{i,j} \hat{\boldsymbol{h}}_j^{(k)} \quad \text{for} \quad i = 2, ..., n_T, \end{aligned} \tag{2.48}$$

and the Gram-Schmidt coefficients, are equal to

$$\mu_{i,j} = \frac{\left\langle \hat{\boldsymbol{h}}_j^{(k)}, \boldsymbol{h}_i^{(k)} \right\rangle}{\left\langle \hat{\boldsymbol{h}}_j^{(k)}, \hat{\boldsymbol{h}}_j^{(k)} \right\rangle}. \tag{2.49}$$

A possible implementation of the LLL algorithm to obtain the reduced basis is given in Algorithm 3.

During the algorithm we keep two sets of vectors, namely the lattice reduced basis vectors $\{\boldsymbol{h}_1^{(k)}, ..., \boldsymbol{h}_u^{(k)}\}$ and the Gram-Schmidt vectors $\{\hat{\boldsymbol{h}}_1^{(k)}, ..., \hat{\boldsymbol{h}}_u^{(k)}\}$ (with the corresponding Gram-Schmidt coefficients $\mu_{u,i}^{(k)}$) which are continuously updated. Note that only adjacent vectors $\boldsymbol{h}_{u-1}$ and $\boldsymbol{h}_u$ may be exchanged. When the rank is $n_T = 2$ and $\delta = 1$, Algorithm 3 is identical to the Gauss reduction algorithm used in [133]. Reduced bases with better properties can be obtained when the constant $\delta$ is closer to one although the number of iterations of Algorithm 3 would increase. More efficient implementations of the algorithm can be found in [105] and [106].

Other types of reduced bases are the Korkin-Kolotarev (KZ) basis [10, 73, 79], the Minkowski basis [1, 62], the Seysen basis [80, 109] and hybrids [104] which have different reduction criteria. These bases have in general slightly better prop-

**Algorithm 3** LLL lattice-reduction algorithm

INPUT: Lattice basis $\boldsymbol{h}_1^{(k)} = \boldsymbol{H}^{(k)}[:,1], ..., \boldsymbol{h}_{n_T}^{(k)} = \boldsymbol{H}^{(k)}[:,n_T] \in \mathbb{C}^{n_R}$ and $\frac{1}{4} < \delta < 1$
FOR $k = 0, ..., N_c - 1$ DO for each carrier
  $u = 2$
  WHILE $u \leq n_T$ DO
    FOR $i = u-1, ..., 1$ DO
      $\boldsymbol{h}_u^{(k)} = \boldsymbol{h}_u^{(k)} - \left\lfloor \mu_{u,i}^{(k)} \right\rceil \boldsymbol{h}_i^{(k)}$; round real and imag separately
    END FOR
    Compute $\hat{\boldsymbol{h}}_u^{(k)}$ as in (2.48)
    IF $\delta \|\hat{\boldsymbol{h}}_{u-1}^{(k)}\|^2 > \|\hat{\boldsymbol{h}}_u^{(k)} + \mu_{u,u-1}^{(k)} \hat{\boldsymbol{h}}_{u-1}^{(k)}\|^2$ THEN
      $\boldsymbol{h}_{u-1}^{(k)} \leftrightarrow \boldsymbol{h}_u^{(k)}$ (exchange)
      $u = \max(u-1, 2)$
    ELSE $u = u + 1$
  END WHILE
END FOR
OUTPUT: Reduced lattice basis $\boldsymbol{H}'^{(k)} = [\boldsymbol{h}_1^{(k)}, ..., \boldsymbol{h}_{n_T}^{(k)}]$ and $\boldsymbol{P}^{(k)}$ defined as $\boldsymbol{H}'^{(k)} = \boldsymbol{H}^{(k)} \boldsymbol{P}^{(k)}$

erties although the reduction is more time consuming.

The performance of the LRA receivers will be closer to that of the ML receiver as the size of the QAM constellation increases. This occurs because LRA treats finite constellations as infinite and therefore, constellation points on the boundary of the constellation that originally had less constellation neighbors, end up having the same number of neighbors as the internal constellation points. Hence, this loss in performance will be smaller if the ratio of boundary constellation points and internal points becomes smaller which occurs in high order QAM constellations (e.g., 64-QAM or 256-QAM). Moreover, it is known that the computational complexity of the ML decoder in MIMO systems with large constellations or large number of transmit antennas becomes prohibitive. Therefore, LRA decoders are a good alternative when large order constellations or large number of transmit antennas are used. Note that the complexity of the LRA receivers has two parts: i) computing the reduced basis of the lattice, and ii) implement the linear equalizer. In quasi-static channels, the lattice is fixed during a long period of time, so the basis reduction is performed just once and then the resulting basis is stored for subsequent use. Thus, the complexity of solving i) is not of major concern.

### 2.5.6 Simulation Results

The simulations presented in this section were conducted with $N_c$=16 OFDM sub-carriers, 1000 symbols transmitted per carrier, $n_T$=3 transmit antennas, $n_R$=3 receive antennas, $\delta = 1$, and a multipath channel with $L$=3 resolvable paths. The distribution of the multipath complex channel gains is $h_{m,v}[l] \sim \mathcal{N}_c(0, \sigma^2_{h,l})$, for $m = 1, \ldots, n_R$ and $v = 1, \ldots, n_T$ with $\sigma^2_{h,0} = 0.44$, $\sigma^2_{h,1} = 0.34$, and $\sigma^2_{h,2} = 0.22$. Channel noise is complex Gaussian with symmetric density function $\mathcal{N}_c(0, 1)$. An uncoded system is considered and Gray coding is used for all cases (QPSK and 16-QAM). For the correlated channel case, scattering scenarios similar to the ones suggested in the COST-259 model [7, 112] is used. The mean angle of arrivals (AOA) at the transmitters are $f_0^{Tx} = 30^o$, $f_1^{Tx} = 45^o$ and $f_2^{Tx} = 60^o$, and at receiver side are $f_0^{Rx} = 50^o$, $f_1^{Rx} = 70^o$, $f_2^{Rx} = 100^o$. The rms angular spread at the transmitters are $a_0^{Tx} = 20^o$, $a_1^{Tx} = 22^o$ and $a_2^{Tx} = 17^o$, and at the receivers, $a_0^{Rx} = 20^o, a_1^{Rx} = 18^o$ and $a_2^{Rx} = 23^o$, respectively. Fifty independent realizations are simulated for each SNR and the BER results are averaged.

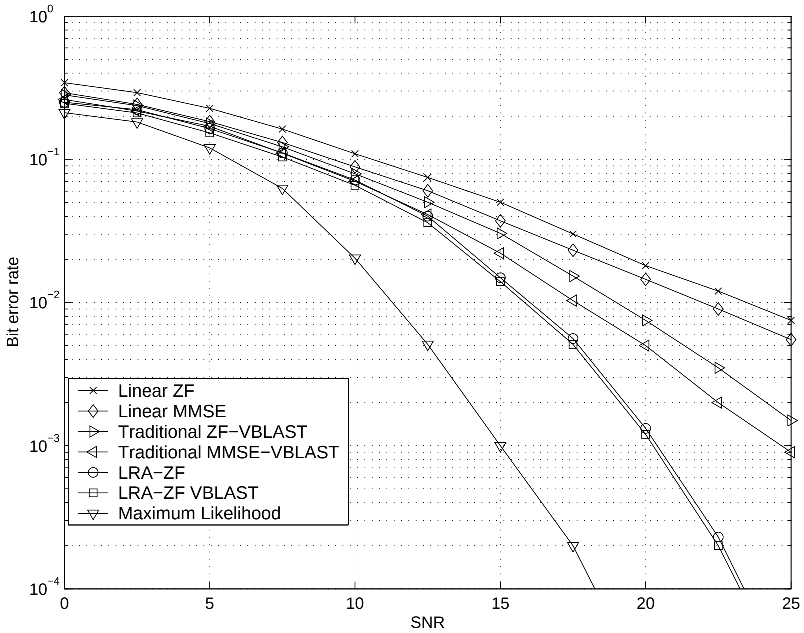


Figure 2.22: BER performance of a $3 \times 3$ system with QPSK modulation in an uncorrelated channel.

Comparing Figures 2.22 to 2.25, it can be seen that the performance of the LRA receivers approaches the ML receiver as the size of the QAM constellation is increased. This occurs because the LRA treats finite constellations as infinite and therefore, data points at the constellation boundary that originally have fewer

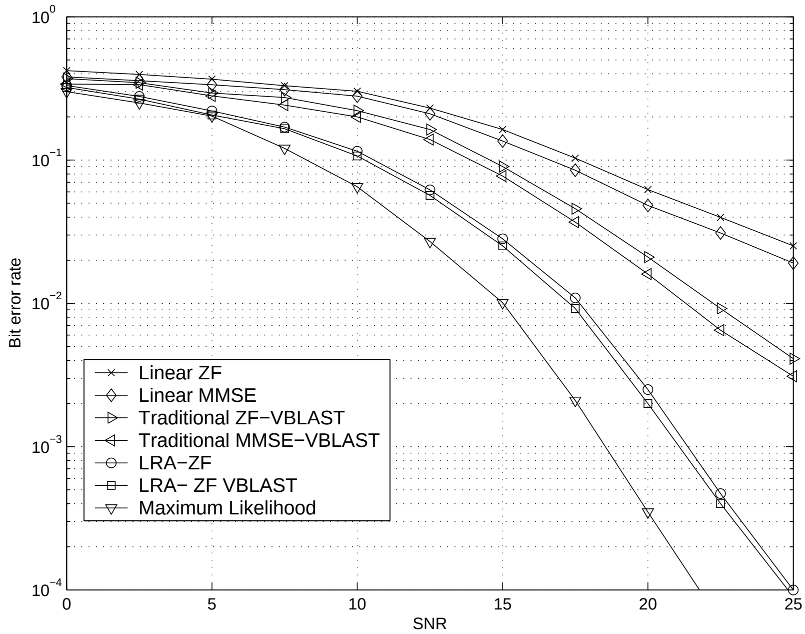


Figure 2.23: BER performance of a $3 \times 3$ system with QPSK modulation in a correlated channel.

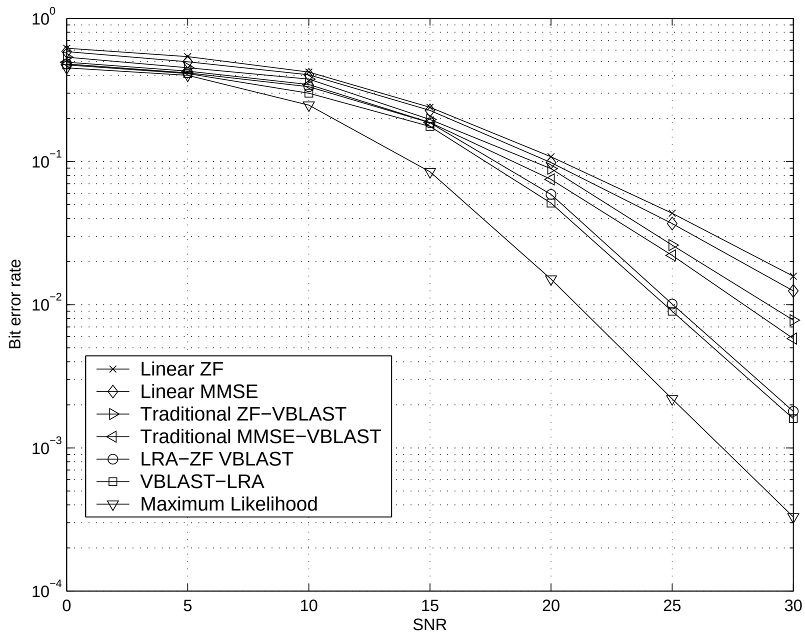


Figure 2.24: BER performance of a $3 \times 3$ system with 16-QAM modulation in an uncorrelated channel.

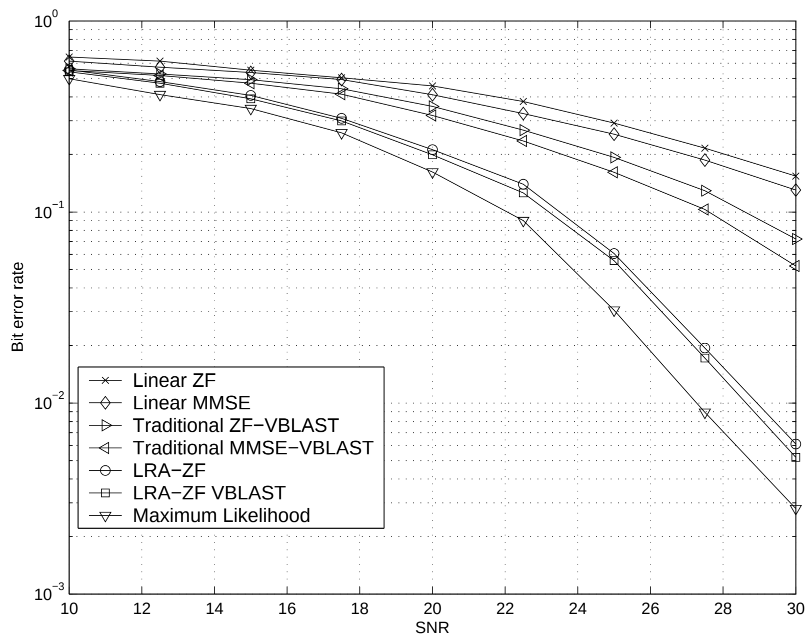


Figure 2.25: BER performance of a $3 \times 3$ system with 16-QAM modulation in a correlated channel.

neighbours end up having the same number of neighbours as the internal constellation points [133]. Due to the high computational complexity of the ML receiver, the LRA receiver is a promising alternative, especially if a large number of transmit antennas and large constellation are used. Recall that for 3 antennas transmitting 16-QAM symbols, the ML receiver performs 4096 comparisons to decode each symbol vector.

From Figures 2.23 and 2.25, it is observed that only the ML and LRA receivers are robust against correlated channels whereas the performance of traditional linear and V-BLAST receivers is very poor. Since LRA receivers use basis which are closer to orthogonal, there is less correlation between the columns of $\boldsymbol{H}'^{(k)}$, $k = 0, \ldots, N_c - 1$, as compared to the original $\boldsymbol{H}^{(k)}$, therefore it performs much better than the linear receiver in correlated channel. It can be seen that the LRA is an attractive method to improve the bit error rate performance when channel correlation is high. For all of the cases considered, it can be seen that the LRA and ML receivers achieve the same diversity order, where diversity is defined as $\gamma = -\lim_{\rho\to\infty} \frac{\log \mathrm{BER}(\rho)}{\log \rho}$.

## 2.6 Further Topics and Conclusions

In this chapter, we have discussed the huge increase in capacity that can be obtained in rich scattering environments by using multiple antennas at the transmitter and the receiver; and we have given an overview of the main classes of space-time techniques recently developed in the literature. In conclusion, the area of space-time coding and signal processing is new, active and full of challenges. The following is a list of some other important topics related to MIMO systems and space-time coding and signal processing:

- Space-time trellis codes (STTC): An STTC is basically a trellis-coded modulation (TCM) code, which can be defined in terms of a trellis tree. Rather than transmitting the output code symbols serially from a single transmitter antenna as in the traditional TCM scheme, in STTC all the output code symbols at each time are transmitted simultaneously from multiple transmitter antennas. The first STTC communication system was proposed in [118]. Some design criteria and performance analysis for STTC in the presence of channel estimation error are given in [117]. Some improved STTC codes found by exhaustive computer search are given in [11].

- Differential space-time codes: Previous sections have assumed that the receiver has knowledge of the channel matrix before starting the detection algorithms. In some situations, this is not possible since no training symbols are available. In some other situations, the channel changes so rapidly that channel estimation is difficult or requires training symbols to be sent very often. That is the reason why it is interesting to consider differential techniques that do not require estimation of the channel response neither at the receiver nor at the transmitter. Differential STBC based on orthogonal designs are proposed in [67, 113] and those based on unitary group codes were proposed in [66]. Similarly to the SISO case, differential decoding incurs a performance penalty of about 3dB compared with coherent detection.

- Space-time precoding: The space-time coding schemes presented in this chapter only require channel knowledge at the receiver. In some cases, channel status can be fedback to the transmitter or directly estimated by the transmitter such as in a TDD system. In such scenarios, the performance can be improved if the transmitter uses this channel information. Different precoding schemes have been proposed in [102].

- MIMO antenna selection: Usually, the RF chain (amplifier, digital-to-analog converters, etc.) in wireless devices is one of the most significant costs. A promising approach for reducing the cost and complexity while retaining a reasonably large fraction of the high potential data rate of a MIMO system is to employ a reduced number of RF chains at the receiver (or transmitter) and attempt to optimally allocate each chain to one of a larger number of receive (transmit) antennas. In this way, only the best set of antennas is used, while the remaining antennas are not employed, thus reducing the number of RF chains required. Different approaches to selecting those antennas have been recently proposed in the literature [51, 52, 59, 103].

- MIMO applications in OFDM and CDMA systems: Code design criteria for the MIMO OFDM systems are given in [89, 90], and specific code designs are given in [18]. Moreover, MIMO coding and signal processing techniques for code-division multiple-access (CDMA) systems are developed in [64, 100].

- Turbo processing for MIMO systems: Iterative or turbo demodulation and decoding for coded BLAST or coded STC systems have been investigated in [30, 55, 88, 90, 107, 120].

- Other space-time coding schemes: Other classes of codes are being developed for MIMO systems. As an example, linear dispersion (LD) codes [58] can be used with any configuration of transmit and receive antennas and they are designed to optimize the mutual information between the transmitted and received signals. The LD codes can be decoded using any BLAST detection algorithm. Moreover, layered space-time coding schemes are proposed in [44, 116] and LAttice Space-Time codes have been proposed in [43].

# Chapter 3

# MIMO Antenna Selection

## 3.1 Introduction

Multiple-input multiple-output (MIMO) systems can offer significant capacity gains over traditional single-input single-output (SISO) systems [40, 119]. However, multiple antennas require multiple RF chains which consist of amplifiers, analog to digital converters, mixers, etc., that are typically very expensive. An approach for reducing the cost while maintaining the high potential data rate of a MIMO system is to employ a reduced number of RF chains at the receiver (or transmitter) and attempt to optimally allocate each chain to one of a larger number of receive (transmit) antennas which are usually cheaper elements. In this way, only the best set of antennas is used, while the remaining antennas are not employed, thus reducing the number of RF chains required.

Originally, antenna selection was proposed for systems having a single transmit antenna and multiple antennas at the receiver employed for standard diversity purposes at the receiver [72, 129]. Recently, for multiple transmit and multiple receive antennas several algorithms have been developed for selecting the optimal antenna subset given a particular channel realization. In [95] it is proposed to select the subset of transmit or receive antennas based on the maximum mutual information criterion and [93] gives an upper bound on the capacity of a system with antenna selection. A suboptimal algorithm that does not need to perform an exhaustive search over all possible subsets is proposed in [46] and [53]. Antenna selection algorithms that minimize the bit error rate (BER) of linear receivers in spatial multiplexing systems are presented in [59]. In [51], antenna selection algorithms are proposed to minimize the symbol error rate when orthogonal space-time block coding is used in MIMO systems. Selection algorithms that only assume knowledge of the second order statistics of the MIMO channels are also presented in [49, 59]. Theoretical studies in [9] and [53] show that the diversity order achieved through antenna selection is the same as that of the system using the whole set of antennas in spatial multiplexing and space-time coding systems, which motivates the use of antenna selection.

All the algorithms appeared in the literature assume perfect channel knowledge to find the optimal antenna configuration. Moreover, these algorithms cannot naturally cope with time-varying channels. This chapter presents discrete stochastic approximation algorithms for selecting the optimal antenna subset based on advanced discrete stochastic optimization techniques that can be found in the recent operations research literature [5, 6, 28]. These techniques optimize an objective function (e.g., maximum mutual information or minimum error rate) over a set of feasible parameters (e.g., antenna subsets to be used) when the objective function cannot be evaluated analytically but can only be estimated. The methods are in the same spirit as traditional adaptive filtering algorithms, for example the least mean-squares (LMS) algorithm in which at each iteration, the algorithms make computationally simple updates to move towards a better solution. Consequently the performance is successively improved until converging to the optimal solution. But in this case, the parameters to be optimized take discrete values (i.e., antenna indices to be used). In a similar manner to the continuous parameter case, the discrete adaptive algorithms asymptotically converge to the optimum solution. The algorithms also have an attractive property, in that it can be proved that they spend more time at the optimum value than at any other parameter value. In the transient phase, the algorithms converge geometrically fast toward the vicinity of the optimum point [6]. These techniques have recently been applied to solve several other problems in wireless communications [8, 74].

When the MIMO channel is time-varying, the optimal antenna subset is no longer fixed. To cope with this situation we extend our proposed algorithms to be able to track the time-varying optimal antenna configurations. The first of the proposed adaptive algorithms uses a fixed step size which acts as a forgetting factor to be able to track the optimal antenna subset. The motivation is the same as in the adaptive filtering applications with a continuous parameter space, such as LMS, in non-stationary environments, where the computation is distributed over time enabling slowly varying dynamics to be tracked. The choice of the step-size value has important effects in the tracking performance in terms of convergence rate and stability. However, its value is difficult to select when the dynamics of the channel are unknown. Hence, we may optimize the tracking performance by superimposing an adaptive algorithm for the purpose of tuning the step-size parameter. Thus, we propose a second adaptive algorithm comprising two cross-coupled adaptive algorithms: (1) a discrete algorithm to adaptively select the best antenna subset and (2) a continuous algorithm to adaptively optimize the step size. This second combination is attractive when the details of the underlying physical model of the MIMO channel and its variability are unknown. To the best of our knowledge, such adaptive discrete stochastic approximation algorithms are new and have not been used previously for antenna selection.

In the final part of this chapter we consider new antenna selection criteria for different MIMO configurations. The motivation for considering these scenarios is that they permit the introduction of suboptimal fast (i.e., low complexity) antenna selection algorithms based on greedy selection as was recently proposed for other selection criteria in [46, 53]. That is, in the incremental greedy selection algorithms we begin with the full set of antennas available and then remove one antenna per step. In each step, the antenna with lowest contribution to the optimization of the objective function of the system is removed. Similarly, we consider incremental greedy selection algorithms in which we start without selecting any antenna and at each step of the algorithm, a new antenna is added until enough antennas have been selected.

The remainder of this chapter is organized as follows. In Section 3.2, the MIMO system model with antenna selection is presented. We also formulate the antenna selection problem as a discrete stochastic optimization problem. In Section 3.3, two general discrete stochastic optimization algorithms are presented and their convergence properties are summarized. In Section 3.4, several antenna selection criteria are presented, including maximum mutual information, minimum bound on error rate, maximum signal-to-noise ratio, and *minimum error rate*. The performance of the corresponding stochastic approximation algorithms is demonstrated through several numerical examples. In Section 3.5, antenna selection in time-varying channels is addressed. In Section 3.6, new antenna selection criteria are developed for different MIMO system configurations and their fast antenna selection algorithm counterparts are also presented. Section 3.7 presents the conclusions.

## 3.2 System Description

### 3.2.1 MIMO System with Antenna Selection

Consider a MIMO system as shown in Figure 3.1 with $n_T$ transmit and $n_R$ receive RF chains and suppose that there are $N_T \geq n_T$ transmit and $N_R \geq n_R$ receive antennas. The channel is represented by an $(N_R \times N_T)$ matrix $\boldsymbol{H}$ whose element $h_{ij}$ represents the complex gain of the channel between the $j$th transmit antenna and the $i$th receive antenna. We assume a flat fading channel remaining constant over several bursts. In this chapter we first concentrate on antenna selection implemented only at the receiver and therefore $N_T = n_T$. The subset of $n_R \leq N_R$ receive antennas to be employed is determined by the selection algorithm operating at the receiver which selects the optimal subset $\omega$ of all possible $\binom{N_R}{n_R}$ subsets of $n_R$ receive antennas. More generally, antenna selection can also be implemented at the transmitter with similar selection algorithms although the channel information needs to be known at the transmitter side. This is the case when there exists a full feedback channel so the receiver can return channel state information to the transmitter. In the case of limited feedback between the transmitter and the receiver, the selection algorithm can be implemented at the receiver and only information about the antenna indices to be used is fedback to the transmitter. Another situation where the selection algorithm is implemented at the transmitter occurs, for example, when the system employs time-division duplex (TDD) transmission so that both the uplink and downlink channels are reciprocal. In the case of antenna selection at both sides of the transmission, the same selection algorithms can be used although the amount of possible solutions, $\binom{N_R}{n_R}\binom{N_T}{n_T}$, increases dramatically. We note that loading is generally implemented when the transmitter has knowledge of the channel [102]. Therefore, if antenna selection is implemented at the transmitter, different optimality criteria will be considered to select the best antenna subset.

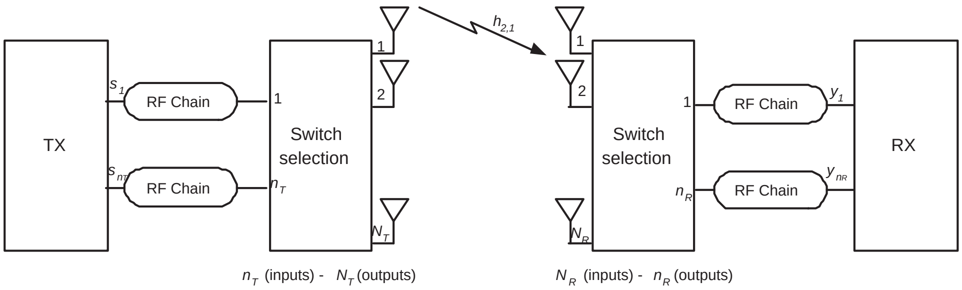


Figure 3.1: Schematic representation of a MIMO system with antenna selection.

Denote $\boldsymbol{H}[\omega]$ as the $(n_R \times n_T)$ channel submatrix corresponding to the receive antenna subset $\omega$, i.e., rows of $\boldsymbol{H}$ corresponding to the selected antennas. The corresponding received signal is then

$$\boldsymbol{y} = \sqrt{\frac{\rho}{n_T}}\boldsymbol{H}[\omega]\boldsymbol{s} + \boldsymbol{n} \tag{3.1}$$

where $\boldsymbol{s} = [s_1, s_2, ..., s_{n_T}]^T$ is the $(n_T \times 1)$ transmitted signal vector, $\boldsymbol{y} = [y_1, y_2, ..., y_{n_R}]^T$ is the $(n_R \times 1)$ received signal vector, $\boldsymbol{n}$ is the $(n_R \times 1)$ received noise vector, and

$\rho$ is the total signal-to-noise ratio independent of the number of transmit antennas. The entries of $\boldsymbol{n}$ are i.i.d. circularly symmetric complex Gaussian variables with unit variance, i.e., $n_i \sim \mathcal{N}_c(0,1)$. It is assumed that the transmitted symbols have unit power, i.e., $E\left\{|s_i|^2\right\} = 1$.

For the problems that we are looking at in this paper, the receiver is required to estimate the channel. One way to perform channel estimation at the receiver is to use a training preamble [91]. Suppose each block of symbols comprises of $T \geq n_T$ MIMO training symbols $\boldsymbol{s}(1)$, $\boldsymbol{s}(2)$, ..., $\boldsymbol{s}(T)$ which are used to probe the channel. In our numerical examples we use $T = 2$, $T = 4$ or $T = 6$. The received signals corresponding to these training symbols are

$$\boldsymbol{y}(i) = \sqrt{\frac{\rho}{n_T}}\boldsymbol{H}[\omega]\boldsymbol{s}(i) + \boldsymbol{n}(i), \quad i = 1, 2, ..., T. \tag{3.2}$$

Denote $\boldsymbol{Y} = [\boldsymbol{y}(1), \boldsymbol{y}(2), ..., \boldsymbol{y}(T)]$, $\boldsymbol{S} = [\boldsymbol{s}(1), \boldsymbol{s}(2), ..., \boldsymbol{s}(T)]$ and $\boldsymbol{N} = [\boldsymbol{n}(1), \boldsymbol{n}(2), ..., \boldsymbol{n}(T)]$. Then (3.2) can be written as

$$\boldsymbol{Y} = \sqrt{\frac{\rho}{n_T}}\boldsymbol{H}[\omega]\boldsymbol{S} + \boldsymbol{N} \tag{3.3}$$

and the maximum likelihood estimate of the channel matrix $\boldsymbol{H}[\omega]$ is given by

$$\hat{\boldsymbol{H}}[\omega] = \arg \min_{\boldsymbol{H} \in \mathbb{C}^{n_R \times n_T}} \left\| \boldsymbol{Y} - \sqrt{\frac{\rho}{n_T}}\boldsymbol{H}\boldsymbol{S} \right\|^2 = \sqrt{\frac{n_T}{\rho}}\boldsymbol{Y}\boldsymbol{S}^H(\boldsymbol{S}\boldsymbol{S}^H)^{-1}.$$

According to [91], the optimal training symbol sequence $\boldsymbol{S}$ that minimizes the channel estimation error should satisfy

$$\boldsymbol{S}\boldsymbol{S}^H = T \cdot \boldsymbol{I}_{n_T}. \tag{3.4}$$

In an uncorrelated MIMO channel, the channel estimates $\hat{h}_{i,j}[\omega]$ computed using (3.4) with orthogonal training symbols are statistically independent Gaussian variables with [91]

$$\hat{h}_{i,j}[\omega] \sim \mathcal{N}_c\Big(h_{i,j}[\omega], \frac{n_T}{T\rho}\Big). \tag{3.5}$$

### 3.2.2 Problem Statement

We now formulate the antenna selection problem as a discrete stochastic optimization problem. Denote each of the antenna subsets as $\omega = \{Ant(1), Ant(2), ..., Ant(n_R)\}$ (e.g., selecting the first, second and sixth antennas is equivalent to $\omega = \{1, 2, 6\}$).

Denote the set of all $P = \binom{N_R}{n_R}$ possible antenna subsets as $\Omega = \{\omega_1, \omega_2, ..., \omega_P\}$. Then, the receiver selects one of the antenna subsets in $\Omega$ to optimize a certain objective function $\Phi(\boldsymbol{H}[\omega])$ according to some specific criterion, e.g., maximum mutual information between the transmitter and the receiver, maximum signal-to-noise ratio or minimum error rate. Thus, the discrete optimization problem becomes

$$\omega^* = \arg\max_{\omega \in \Omega} \Phi(\boldsymbol{H}[\omega]), \tag{3.6}$$

where we use $\omega^*$ to denote the global maximizer of the objective function. In practice, however, the exact value of the channel $\boldsymbol{H}[\omega]$ is not available. Instead, we typically have a noisy estimate $\hat{\boldsymbol{H}}[\omega]$ of the channel.

Suppose that at time $n$ the receiver obtains an estimate of the channel, $\hat{\boldsymbol{H}}[n, \omega]$, and computes a noisy estimate of the objective function $\Phi(\boldsymbol{H}[\omega])$ denoted as $\phi[n, \omega]$. Given a sequence of i.i.d. random variables $\{\phi[n, \omega], n = 1, 2, ...\}$, if each $\phi[n, \omega]$ is an unbiased estimate of the objective function $\Phi(\boldsymbol{H}[\omega])$, then (3.6) can be reformulated as the following discrete stochastic optimization problem

$$\omega^* = \arg\max_{\omega \in \Omega} \Phi(\boldsymbol{H}[\omega]) = \arg\max_{\omega \in \Omega} E\left\{\phi[n, \omega]\right\}. \tag{3.7}$$

Note that existing works on antenna selection assume perfect channel knowledge and therefore treat deterministic combinatorial optimization problems. On the other hand, we assume that only noisy estimates of the channel are available and hence the corresponding antenna selection problem becomes a discrete stochastic optimization problem. In what follows we first discuss a general discrete stochastic approximation method to solve the discrete stochastic optimization problem in (3.7) and then we treat different forms of the objective function under different criteria, e.g., maximum mutual information, minimum error rate, etc.

## 3.3 Discrete Stochastic Approximation Algorithms

There are several methods that can be used to solve the discrete stochastic optimization problem in (3.7). An inefficient method to solve (3.7) is to compute $N$ estimates of the objective function for each of the antenna subsets $\omega \in \Omega$ and compute an empirical average which approximates the exact value of the objective function. That is, for each $\omega \in \Omega$ compute

$$\hat{\phi}_N(\omega) = \frac{1}{N} \sum_{n=1}^{N} \phi[n, \omega] \tag{3.8}$$

and then perform and exhaustive search to find $\omega^* = \max_{\omega\in\Omega}\{\hat{\phi}_N(\omega)\}$. Since for any fixed $\omega \in \Omega$, $\{\phi[n,\omega]\}$ is an i.i.d. sequence of random variables, by the strong law of large numbers, $\hat{\phi}_N(\omega) \to E\{\phi[n,\omega]\}$ almost surely as $N \to \infty$. Using the finite number of antenna combinations in $\Omega$ implies that as $N \to \infty$

$$\arg\max_{\omega\in\Omega} \hat{\phi}_N(\omega) \to \arg\max_{\omega\in\Omega} E\{\phi[n,\omega]\} = \arg\max_{\omega\in\Omega} \Phi(\boldsymbol{H}[\omega]). \tag{3.9}$$

Although the method can in principle find the optimal solution, it is highly inefficient from the antenna selection problem point of view. For each antenna subset in $\Omega$, $N$ estimates of the objective function would need to be computed and hence it would need to be estimated $N\binom{N_R}{n_R}$ times in total. These computations are mostly wasted in the sense that only the estimate corresponding to the optimal set $\omega^*$ is eventually useful. Moreover, when the channel is time-varying, this method cannot naturally track the time-varying optimum solution.

More efficient methods to solve (3.7) have been proposed in the operations research literature (see [6] for a survey). The ranking and selection methods, and multiple comparison methods [63] can be used to solve the problem. However, when the number of feasible solutions $P$ increases (usually $P > 20$ antenna subsets), the complexity becomes prohibitive. More recently, a number of discrete stochastic approximation algorithms haven been proposed to solve the problem in (3.7), including simulated annealing type procedures [4], stochastic ruler [132], and nested partition methods [110]. In this section, we construct iterative algorithms that resemble a stochastic approximation algorithm in the sense that they generate a sequence of estimates of the solution where each new estimate is obtained from the previous one by taking a small step in a good direction toward the global optimizer. In particular we present two different discrete stochastic approximation algorithms based on ideas in the recent operations research literature. The most important property of the proposed algorithms is their self-learning capability – most of the computational effort is spent at the global or local optimizer of the objective function. As we will show, an attractive property of these methods is that they can be modified to track the optimum antenna subset in time-varying scenarios.

### 3.3.1 Aggressive Discrete Stochastic Approximation Algorithm

We now present an aggressive stochastic approximation algorithm based on [5]. We use the $P = \binom{N_R}{n_R}$ unit vectors as labels for the $P$ possible antenna subsets, i.e., $\xi = \{\boldsymbol{e}_1, \boldsymbol{e}_2, ..., \boldsymbol{e}_P\}$, where $\boldsymbol{e}_i$ denotes the $(P \times 1)$ vector with a one in the $i$th position and zeros elsewhere. At each iteration, the algorithm updates the

$(P \times 1)$ probability vector $\boldsymbol{\pi}[n] = \Big[\pi[n,1], ..., \pi[n,P]\Big]^T$ representing the state occupation probabilities with elements $\pi[n,i] \in [0,1]$ and $\sum_i \pi[n,i] = 1$. Let $\omega^{(n)}$ be the antenna subset chosen at the $n$-th iteration. For notational simplicity, it is convenient to map the sequence of antenna subsets $\{\omega^{(n)}\}$ to the sequence $\{\boldsymbol{D}[n]\} \in \xi$ of unit vectors where $\boldsymbol{D}[n] = \boldsymbol{e}_i$ if $\omega^{(n)} = \omega_i$, $i = 1, ..., P$.

**Algorithm 3.1** Aggressive discrete stochastic approximation algorithm

```
□ Initialization
    n ⇐ 0
    select initial antenna subset ω^(0) ∈ Ω
    set π[0, ω^(0)] = 1
    set π[0, ω] = 0 for all ω ≠ ω^(0)
for n = 0, 1, ... do
  □ Sampling and evaluation
      given ω^(n) at time n, obtain φ[n, ω^(n)]
      choose another ω̃^(n) ∈ Ω\ω^(n) uniformly
      obtain an independent observation φ[n, ω̃^(n)]
  □ Acceptance
      if φ[n, ω̃^(n)] > φ[n, ω^(n)] then
        set ω^(n+1) = ω̃^(n)
      else
        ω^(n+1) = ω^(n)
      end if
  □ Adaptive filter for updating state occupation
      probabilities
      π[n+1] = π[n] + μ[n+1](D[n+1] − π[n])
      with the decreasing step size μ[n] = 1/n
  □ Computing the maximum
      if π[n+1, ω^(n+1)] > π[n+1, ω̂^(n)] then
        ω̂^(n+1) = ω^(n+1)
      else
        set ω̂^(n+1) = ω̂^(n)
      end if
end for
```

We assume that in a realistic communications scenario, each iteration of the above algorithm operates on a block of symbols comprising of $T > 0$ training symbols (see description above (3.2). These $T$ training symbols are used to obtain the channel estimates $\hat{\boldsymbol{H}}[n, \omega^{(n)}]$ and hence the noisy estimate of the cost $\phi[n, \omega^{(n)}]$. In our numerical examples, we use $T = 2, T = 4$ or $T = 6$. At the end of each iteration, antenna subset $\hat{\omega}^{(n)}$ will be selected for the next iteration.

In the `Sampling and Evaluation` step in Algorithm 3.1, the candidate antenna subset $\tilde{\omega}^{(n)}$ is chosen uniformly from $\Omega \backslash \omega^{(n)}$. There are several variations for selecting a candidate antenna subset $\tilde{\omega}^{(n)}$. One possibility is to select a new antenna subset $\tilde{\omega}^{(n)}$ by replacing only one antenna in $\omega^{(n)}$. Define the distance $d(\tilde{\omega}^{(n)}, \omega^{(n)})$ as the number of different antennas between the two antenna subsets $\tilde{\omega}^{(n)}$ and $\omega^{(n)}$. Hence, we can select $\tilde{\omega}^{(n)} \in \Omega \backslash \omega^{(n)}$ such that $d(\tilde{\omega}^{(n)}, \omega^{(n)}) = 1$. More generally we can select a new subset $\tilde{\omega}^{(n)}$ with arbitrary distance $d(\tilde{\omega}^{(n)}, \omega^{(n)}) = D$, where $1 \leq D \leq \min(n_R, N_R - n_R)$. Note that any variation for selecting a candidate need to be taken into account to prove global convergence.

To obtain the independent observations in the `Sampling and Evaluation` step in Algorithm 3.1 we proceed as follows. At time $n$, we collect training symbols to estimate the channel and compute $\phi[n, \omega]$. Now, collect other training symbols from another antenna subset and compute $\phi[n, \tilde{\omega}]$. Therefore, $\phi[n, \omega]$ and $\phi[n, \tilde{\omega}]$ are independent observations.

*Remark: Heuristic variations of* `Sampling and Evaluation` *step with correlated observations*. The above procedure of using independent samples to evaluate the objective function allows us to rigorously prove convergence and efficiency of the algorithm. Here we briefly discuss three heuristic variations of the `Sampling and Evaluation` step that use correlated observations of the objective function. In numerical simulations we observed that these variations also yield excellent results – however, due to the statistically correlated observations of the objective function, the proof of convergence is intractable. The first possibility is to reuse same channel observation multiple times (i.e., use the same channel estimate to compute several observations of the objective function under different antenna configurations). Another heuristic variation is to incorporate the greedy antenna selection solutions (note that this is another form of correlation) or reduce the dimension of the possible transition states (i.e., possible solutions) in the Markov chain. A third possibility is to devise hybrid solutions based on a combination of Algorithm 3.1 and batch processing (e.g., exhaustive search based on noisy channel estimates or greedy selections).

The sequence $\{\omega^{(n)}\}$ generated by Algorithm 3.1 is a Markov chain on the state space $\Omega$ which is not expected to converge and may visit each element in $\Omega$ infinitely often. On the other hand, under certain conditions the sequence $\{\hat{\omega}^{(n)}\}$

converges almost surely to the global maximizer $\omega^*$. Therefore, $\hat{\omega}^{(n)}$ can be viewed as an estimate at time $n$ of the optimal antenna subset $\omega^*$.

In the `Adaptive filter for updating state occupation probabilities` step in Algorithm 3.1, $\boldsymbol{\pi}[n] = \left[\pi[n,1], \pi[n,2], ..., \pi[n,P]\right]$ denotes the empirical state occupation probability at time $n$ of the Markov chain $\{\omega^{(n)}\}$. If we denote $W^{(n)}[\omega]$ for each $\omega \in \Omega$ as a counter of the number of times the Markov chain has visited antenna subset $\omega^{(n)}$ by time $n$, we can observe that $\boldsymbol{\pi}[n] = \frac{1}{n}\left[W^{(n)}[\omega_1],...,W^{(n)}[\omega_P]\right]^T$. Hence, the algorithm chooses the antenna subset which has been visited most often by the Markov chain $\{\omega^{(n)}\}$ so far.

### Global Convergence of Algorithm 3.1

A sufficient condition for Algorithm 3.1 to converge to the global maximizer of the objective function $\Phi(\boldsymbol{H}[\omega])$ is as follows [5]. For $\widetilde{\omega} \neq \omega^*, \omega \neq \omega^*$, and independent observations $\phi[n,\omega^*]$, $\phi[n,\widetilde{\omega}]$, $\phi[n,\omega]$

$$Pr\left\{\phi[n,\omega^*] > \phi[n,\omega]\right\} > Pr\left\{\phi[n,\omega] > \phi[n,\omega^*]\right\}, \tag{3.10}$$

$$Pr\left\{\phi[n,\omega^*] > \phi[n,\widetilde{\omega}]\right\} > Pr\left\{\phi[n,\omega] > \phi[n,\widetilde{\omega}]\right\}. \tag{3.11}$$

It is shown in [5] that if the conditions (3.10) and (3.11) are satisfied, the sequence $\{\omega^{(n)}\}$ is an homogeneous irreducible and aperiodic Markov chain with state space $\Omega$. Moreover, the sequence $\{\hat{\omega}^{(n)}\}$ converges almost surely to $\omega^*$ in the sense that the Markov chain $\{\omega^{(n)}\}$ spends more time in $\omega^*$ than any other state. The transition kernel for the Markov chain $\{\omega^{(n)}\}$ is given by a transition probability matrix $\boldsymbol{K}$ whose elements are given by

$$k_{i,j} = Pr\left\{\omega^{(n+1)} = \omega_j \mid \omega^{(n)} = \omega_i\right\} = \frac{1}{|\Omega|-1} Pr\left\{\phi[n,\omega_j] > \phi[n,\omega_i]\right\} \tag{3.12}$$

for all $i, j \in \{1,...,P\}, \quad i \neq j$, and

$$k_{i,i} = 1 - \sum_{j\in\{1,...,P\}, j\neq i} k_{i,j} = \frac{1}{|\Omega|-1} \sum_{j\in\{1,...,P\}, j\neq i} Pr\left\{\phi[n,\omega_j] \leq \phi[n,\omega_i]\right\} \tag{3.13}$$

for all $i \in \{1,...,P\}$ (assuming that the observations $\phi[n,\omega]$ are independent for all $n$ and $\omega$).

The two conditions in (3.10) and (3.11) basically state the conditions that the Markov transition matrix defined in (3.12) and (3.13) need to satisfy. Condition (3.10) states that $k_{j,i} > k_{i,j}$ for $\omega_i = \omega^*$ and $\omega_j \neq \omega^*$, i.e., it is more probable for the Markov chain to move into a state corresponding to $\omega^*$ from a state that does not correspond to $\omega^*$ than in the other direction. And condition (3.11) states that $k_{j,i} > k_{j,\ell}$ for $\omega_i = \omega^*$ and $\omega_\ell \neq \omega^*$, $\omega_j \neq \omega^*$, i.e., once the Markov chain is in a state that does not correspond to $\omega^*$, it is more probable to move into a state that corresponds to $\omega^*$ than into any other state.

The major difficulty of Algorithm 3.1 is to choose estimators that can be proved to satisfy properties (3.10) and (3.11). Next, we propose a conservative algorithm that converges to the global optimizer of the objective function under less restrictive conditions.

### 3.3.2 Conservative Discrete Stochastic Approximation Algorithm

Now, we present a conservative discrete stochastic approximation algorithm based on ideas in [28] with less restrictive conditions for global convergence.

**Algorithm 3.2** Conservative discrete stochastic approximation algorithm

□ `Initialization`

  $n \Leftarrow 0$

  `select initial antenna subset` $\omega^{(0)} \in \Omega$

  `Initialize` $P$`-dimensional vectors` $\boldsymbol{h}[0], \boldsymbol{l}[0]$ `and` $\bar{\boldsymbol{k}}[0]$ `to zero`

**for** $n = 0, 1, ...$ **do**

  □ `Sampling, evaluation and update`

    `choose another` $\tilde{\omega}^{(n)} \in \Omega \backslash \omega^{(n)}$ `uniformly`

    `obtain an independent observation` $\phi[n, \tilde{\omega}^{(n)}]$ `and update:`

      $\boldsymbol{l}[n+1, \tilde{\omega}^{(n)}] = \boldsymbol{l}[n, \tilde{\omega}^{(n)}] + \phi[n, \tilde{\omega}^{(n)}]$   (Accumulated cost)

      $\bar{\boldsymbol{k}}[n+1, \phi[n, \tilde{\omega}^{(n)}]] = \bar{\boldsymbol{k}}[n, \phi[n, \tilde{\omega}^{(n)}]] + 1$   (Occupation time)

      $\boldsymbol{h}[n, \phi[n, \tilde{\omega}^{(n)}]] = \boldsymbol{l}[n+1, \phi[n, \tilde{\omega}^{(n)}]] / \bar{\boldsymbol{k}}[n+1, \phi[n, \tilde{\omega}^{(n)}]]$   (Average cost vector)

  □ `Acceptance`

    `if` $\boldsymbol{h}[n, \tilde{\omega}^{(n)}] > \boldsymbol{h}[n, \omega^{(n)}]$ `then`

      `set` $\omega^{(n+1)} = \tilde{\omega}^{(n)}$

    `else`

      $\omega^{(n+1)} = \omega^{(n)}$

    `end if`

  □ `Update estimate of optimum subset`

$\hat{\omega}^{(n+1)} = \omega^{(n+1)}$

**end for**

As in the `Adaptive filter` step of Algorithm 3.1, the `Sampling, evaluation and update` step in Algorithm 3.2 can be rewritten as an adaptive algorithm with a decreasing step size as: update the occupation time diagonal matrix $\boldsymbol{K}[\cdot]$ as $\boldsymbol{K}[n+1] = \boldsymbol{K}[n] + \mu[n+1](\mathbf{diag}(\boldsymbol{D}_1[n], ..., \boldsymbol{D}_P) - \boldsymbol{K}[n])$ and

$$\boldsymbol{h}[n+1] = \boldsymbol{h}[n] + \mu[n+1]\boldsymbol{K}^{-1}[n+1]\left(\phi[n, \tilde{\omega}^{(n)}]\boldsymbol{D}[n] - \mathbf{diag}(\boldsymbol{D}_1[n], ..., \boldsymbol{D}_P)\boldsymbol{h}[n]\right) \tag{3.14}$$

where as in Algorithm 3.1, $\mu[n] = 1/n$, $\boldsymbol{D}[n] = \boldsymbol{e}_i$ if $\tilde{\omega}^{(n)} = \omega_i$ and $\boldsymbol{D}_i[n]$ represents the $i$th component of $\boldsymbol{D}[n]$. The $(P \times P)$-dimensional matrix $\boldsymbol{K}[n]$ in (3.14) is initialized to $\boldsymbol{K}[0] = \boldsymbol{I}_P$. The *conservative* name refers to the convergence of the Markov chain $\{\omega^{(n)}\}$ in Algorithm 3.2 since the sequence $\{\omega^{(n)}\}$ in Algorithm 3.1 is not expected to converge – in Algorithm 3.1 only $\{\hat{\omega}^{(n)}\}$ converges. Note that in Algorithm 3.2, we only require one estimate of the objective function per iteration and in general, the complexity is similar to the one of Algorithm 3.1.

**Global convergence of Algorithm 3.2**

As proved in [28], a sufficient condition for Algorithm 3.2 to converge to the global optimum is to use unbiased observations of the objective function.

## 3.4 Adaptive Antenna Selections Under Different Criteria

In this section we use the optimization algorithms to optimize four different objective functions $\Phi(\boldsymbol{H}[\omega])$. These are (i) MIMO mutual information, (ii) bounds on error rate, (iii) SNR, and (iv) error rate. Simulation results are provided in each case to demonstrate the performance of the corresponding stochastic approximation algorithm.

### 3.4.1 Maximum MIMO Mutual Information

Assuming that the channel matrix $\boldsymbol{H}[\omega]$ is known at the receiver, but not at the transmitter, the mutual information between the transmitter and receiver is given by [40, 119]

$$\mathcal{I}[\omega] = \log\det\left(\boldsymbol{I}_{n_T} + \frac{\rho}{n_T}\boldsymbol{H}^H[\omega]\boldsymbol{H}[\omega]\right) \text{bit/s/Hz}. \tag{3.15}$$

One criterion for selecting the antennas is to maximize the above mutual information, i.e., choosing the objective function $\Phi(\boldsymbol{H}[\omega]) = \mathcal{I}[\omega]$.

**Aggressive Algorithm to optimize the mutual information**

We now present an implementation of Algorithm 3.1 to find the maximum of the mutual information in (3.15) using

$$\phi[n,\omega] = \log\det\left(\boldsymbol{I}_{n_T} + \frac{\rho}{n_T}\hat{\boldsymbol{H}}[n,\omega]^H\hat{\boldsymbol{H}}[n,\omega]\right). \tag{3.16}$$

**Notes on convergence**
To prove the convergence to the global optimum when we use (3.16) in Algorithm 3.1, we need to verify that conditions (3.10) and (3.11) are satisfied. We propose the following result that will help us to verify these conditions.

**Proposition 1** *:* The random variable in (3.16) can be accurately approximated by the Gaussian distribution

$$\phi[n,\omega] \sim \mathcal{N}\left(\mu_{\mathcal{I}_\omega}, \sigma^2_{\mathcal{I}_\omega}\right), \tag{3.17}$$

where

$$\begin{aligned} \mu_{\mathcal{I}_\omega} &= E_{\hat{\boldsymbol{H}}}\left\{\log\det\left(\boldsymbol{I}_{n_T} + \frac{\rho}{n_T}\hat{\boldsymbol{H}}[n,\omega]^H\hat{\boldsymbol{H}}[n,\omega]\right)\right\} \\ &= \frac{e^{\mathrm{tr}(\Lambda[\omega])}}{ln(2)(\Gamma(t-s+1)^s\det(\boldsymbol{V})}\sum_{k=1}^{s}\det(\Psi(k)), \end{aligned} \tag{3.18}$$

with $\det(\Psi(k)), k = 1, ..., s$ are $(s \times s)$ matrices with entries

$$\{\Psi(k)\}_{i,j} = \begin{cases} \int_0^\infty y^{t-i}\ln(1+\alpha y)e^{-y}{}_0F_1(t-s+1, y\lambda_j[\omega])dy, & j = k \\ \Gamma(t-i+1){}_1F_1(t-i+1, t-s+1, \lambda_j[\omega]), & j \neq k \end{cases} \tag{3.19}$$

where $t = \max(n_T, n_R)$ and $s = \min(n_T, n_R)$, $\alpha = \frac{\rho}{n_T}\cdot\frac{n_T}{\rho T} = \frac{1}{T}$, $0 < \lambda_1[\omega] < \lambda_2[\omega] < ... < \lambda_s[\omega] < \infty$ are the non-zero ordered eigenvalues of $\frac{n_T}{T\rho}\boldsymbol{H}^H\boldsymbol{H}$, $\Lambda[\omega] = \mathrm{diag}(\lambda_1[\omega], ..., \lambda_s[\omega])$, $\boldsymbol{V}$ is an $(s \times s)$ matrix with determinant $\det(\boldsymbol{V}) = \Pi_{1\leq i<j\leq s}(\lambda_i[\omega] - \lambda_j[\omega])$, ${}_0F_1(\cdot,\cdot)$ is the generalized hypergeometric function defined in [[54], Eqn. (9.14.1)] as ${}_0F_1(a, z) = \sum_{k=0}^{\infty}\frac{z^k}{(a)_k k!}$, $\Gamma(\cdot)$ is the gamma function [[54], Eqn. (8.31.1)], ${}_1F_1(\cdot,\cdot,\cdot)$ is the confluent hypergeometric

function [[54], Eqn. (9.210.1)] defined as

$$ {}_1F_1(a;b;z) = \sum_{k=0}^{\infty} \frac{(a)_k}{(b)_k} \frac{z^k}{k!}, \tag{3.20} $$

and $(a)_k = a(a+1)...(a+k-1)$ is the Pochhammer symbol. The second moment of the estimator is

$$ E\{\hat{\mathcal{I}}_\omega^2\} = \frac{e^{\mathrm{tr}(\Lambda[\omega])}}{\ln^2(2)(\Gamma(t-s+1)^s \det(\boldsymbol{V})} \sum_{k=1}^{s} \sum_{l=1}^{s} \det(\Psi(k,l)), \tag{3.21} $$

where $\det(\Psi(k,l)), k, l = 1, ..., s$ are $(s \times s)$ matrices with entries

$$ \{\Psi(k)\}_{i,j} = \begin{cases} \int_0^\infty y^{t-i} \ln^2(1+\alpha y) e^{-y} {}_0F_1(t-s+1, y\lambda_j[\omega]) dy, & j = k = l \\ \int_0^\infty y^{t-i} \ln(1+\alpha y) e^{-y} {}_0F_1(t-s+1, y\lambda_j[\omega]) dy, & j = k, \mathrm{or} j = l; k \neq l \\ \Gamma(t-i+1) {}_1F_1(t-i+1, t-s+1, \lambda_j[\omega]), & j \neq k; j \neq l \end{cases} \tag{3.22} $$

and the variance in (3.17) can be computed as

$$ \sigma_{\mathcal{I}_\omega}^2 = E\{\hat{\mathcal{I}}_\omega^2\} - \mu_{\mathcal{I}_\omega}^2. \tag{3.23} $$

**Proof**: The channel estimate in (3.16) with orthogonal training symbols in (3.4) contains independent elements $\hat{h}_{ij[\omega]} = \mathcal{N}_c\left(h_{ij}[\omega], \frac{n_T}{T\rho}\right)$. Therefore, the channel estimate can be written as $\hat{\boldsymbol{H}}[n,\omega] = \boldsymbol{H}[\omega] + \Delta\boldsymbol{H}[n,\omega]$ which contains a constant term $\boldsymbol{H}[\omega]$ and a random complex Gaussian matrix $\Delta\boldsymbol{H}[n,\omega]$ of zero mean. Then, the estimate of the mutual information function can be written as

$$ \phi[n,\omega] = \log\det\left(\boldsymbol{I}_{n_T} + \frac{\rho}{n_T} (\boldsymbol{H}[\omega] + \Delta\boldsymbol{H}[n,\omega])^H (\boldsymbol{H}[\omega] + \Delta\boldsymbol{H}[n,\omega])\right), \tag{3.24} $$

which is equivalent to the mutual information of a Rician flat fading MIMO channel with a non-zero mean matrix $\boldsymbol{H}[\omega]$. The expressions of the mean and variance of the capacity of a non-iid Rician are derived in [71] which correspond to (3.18) and (3.23) respectively. ∎

In particular, under the maximum mutual information criterion, we note that the estimator in (3.16) has a positive bias, i.e., $\mu_{\mathcal{I}_\omega} > \mathcal{I}[\omega]$ in (3.15). This fact can be also understood with the results in [71] and the parallelism of the estimate of the mutual information computed with noisy channel estimates and capacity results of the Rician channel. Moreover, it has been observed that although the estimator is biased,

$$\text{if} \quad \mathcal{I}[\omega_i] > \mathcal{I}[\omega_k], \quad \text{then} \quad \mu_{\mathcal{I}_{\omega_i}} > \mu_{\mathcal{I}_{\omega_k}}, \forall i, k \in \{1, ..., P\}, \tag{3.25}$$

which again can be intuitively deduced with the parallelism with a Rician channel.

To prove the convergence to the global optimum using (3.16) in Algorithm 3.1, we still need to verify that conditions (3.10) and (3.11) are satisfied. Consider three different antenna subsets $\omega_i = \omega^*$ and $\omega_l, \omega_j \in \{\Omega \backslash \omega^*\}$. From (3.16) and (3.17), we have independent random variables $\phi[n, \omega_i] \sim \mathcal{N}(\mu_{\mathcal{I}_{\omega_i}}, \sigma^2_{\mathcal{I}_{\omega_i}}), \phi[n, \omega_j] \sim \mathcal{N}(\mu_{\mathcal{I}_{\omega_j}}, \sigma^2_{\mathcal{I}_{\omega_j}})$ and $\phi[n, \omega_l] \sim \mathcal{N}(\mu_{\mathcal{I}_{\omega_l}}, \sigma^2_{\mathcal{I}_{\omega_l}})$. Condition (3.10) can be written as

$$Pr\left(\phi[n, \omega_i] - \phi[n, \omega_j] > 0\right) > Pr\left(\phi[n, \omega_j] - \phi[n, \omega_i] > 0\right), \tag{3.26}$$

and since samples of $\phi$ are independent and Gaussian distributed, (3.26) is equivalent to

$$Pr\left(\mathcal{N}\left(\mu_{\mathcal{I}_{\omega_i}} - \mu_{\mathcal{I}_{\omega_j}}, \sigma^2_{\mathcal{I}_{\omega_i}} + \sigma^2_{\mathcal{I}_{\omega_j}}\right) > 0\right) > Pr\left(\mathcal{N}\left(\mu_{\mathcal{I}_{\omega_j}} - \mu_{\mathcal{I}_{\omega_i}}, \sigma^2_{\mathcal{I}_{\omega_j}} + \sigma^2_{\mathcal{I}_{\omega_i}}\right) > 0\right). \tag{3.27}$$

From (3.25) we have $\max\{\mu_{\mathcal{I}_{\omega_i}}, \mu_{\mathcal{I}_{\omega_j}}, \mu_{\mathcal{I}_{\omega_l}}\} = \mu_{\mathcal{I}_{\omega_i}}$ which implies $(\mu_{\mathcal{I}_{\omega_i}} - \mu_{\mathcal{I}_{\omega_j}}) > (\mu_{\mathcal{I}_{\omega_j}} - \mu_{\mathcal{I}_{\omega_i}})$. Therefore (3.26) holds since both terms have the same variance. Consider now condition (3.11). We can express it as

$$Pr\left(\mathcal{N}\left(\mu_{\mathcal{I}_{\omega_i}} - \mu_{\mathcal{I}_{\omega_j}}, \sigma^2_{\mathcal{I}_{\omega_i}} + \sigma^2_{\mathcal{I}_{\omega_j}}\right) > 0\right) > Pr\left(\mathcal{N}\left(\mu_{\mathcal{I}_{\omega_l}} - \mu_{\mathcal{I}_{\omega_j}}, \sigma^2_{\mathcal{I}_{\omega_l}} + \sigma^2_{\mathcal{I}_{\omega_j}}\right) > 0\right),$$

which can be rewritten as

$$Pr\left(\phi[n, \omega_i] - \phi[n, \omega_j] > 0\right) > Pr\left(\phi[n, \omega_l] - \phi[n, \omega_j] > 0\right), \tag{3.28}$$

that is equivalent to

$$\frac{\mu_{\mathcal{I}_{\omega_i}} - \mu_{\mathcal{I}_{\omega_j}}}{\sqrt{\sigma^2_{\mathcal{I}_{\omega_i}} + \sigma^2_{\mathcal{I}_{\omega_j}}}} > \frac{\mu_{\mathcal{I}_{\omega_l}} - \mu_{\mathcal{I}_{\omega_j}}}{\sqrt{\sigma^2_{\mathcal{I}_{\omega_l}} + \sigma^2_{\mathcal{I}_{\omega_j}}}}. \tag{3.29}$$

The inequality in (3.29) has been observed to hold after extensive simulations using the expressions of the mean and the variance given in (3.18) and (3.23) respectively.

### Conservative algorithm to optimize the mutual information

We now present an implementation of the conservative algorithm and prove that it converges to the global maximum of the mutual information in (3.15). Since the logarithm is a monotonically increasing function, the antenna subset $\omega^*$ maximizing $\log\det(\cdot)$ is identical to that maximizing $\det(\cdot)$.

In the `Sampling, evaluation and update` step of Algorithm 3.2 choose

$$\phi[n,\omega] = \det\left(\boldsymbol{I}_{n_T} + \frac{\rho}{n_T}\hat{\boldsymbol{H}}_1^H[n,\omega]\hat{\boldsymbol{H}}_2[n,\omega]\right), \tag{3.30}$$

where the channel estimates $\hat{\boldsymbol{H}}_1[n,\omega]$ and $\hat{\boldsymbol{H}}_2[n,\omega]$ are obtained from independent training blocks. We consider the case in which $\hat{\boldsymbol{H}}_1[n,\omega]$ and $\hat{\boldsymbol{H}}_2[n,\omega]$ satisfy (3.5).

**Theorem 2** *With $\phi[n,\omega]$ computed according to (3.30), the sequence $\{\hat{\omega}^{(n)}\}$ generated by Algorithm 3.2 converges to the antenna subset $\omega^*$ corresponding to the global maximizer of the MIMO mutual information in (3.15).*
**Proof**: To prove global convergence, we only need to show that $\phi[n,\omega]$ of (3.30) is unbiased, which is proved in Appendix A.

To reduce the training symbols needed to estimate the channel in Algorithm 3.2, in practical systems we can use a single sample of the channel $\hat{\boldsymbol{H}}_1[n,\omega]$ and choose

$$\phi[n,\omega] = \det\left(\boldsymbol{I}_{n_T} + \frac{\rho}{n_T}\hat{\boldsymbol{H}}_1[n,\omega]^H\hat{\boldsymbol{H}}_1[n,\omega]\right). \tag{3.31}$$

Although this sample is biased, numerical results can show that Algorithm 3.2 still converges to the global optimum.

### Simulation Results

We consider the performance of Algorithm 3.1 which selects the antenna subset maximizing the MIMO mutual information using (3.31) as an estimate of the objective function. We consider $n_T = 2$, $N_R = 8$ and $n_R = 4$ antennas. We use the ML channel estimate in (3.4) with $T = 4$ orthogonal training symbols. We set $\rho = 10$dB. The $(N_R \times n_T)$ channel $\boldsymbol{H}$ is randomly generated and fixed during the whole simulation. The initial antenna subset was randomly selected. From a practical point of view, there are several variations for selecting $\omega^{(0)}$. For instance, based on a noisy channel estimate, select the antenna subset whose matrix $\hat{\boldsymbol{H}}[0,\omega^{(0)}]$ has maximum Frobenius norm. Figure 3.2 shows one run of the algorithm. In the same figure we show the mutual information of the best antenna subset and the worst antenna subset, as well as the median mutual information among the $\binom{8}{4} = 70$ antenna configurations, found by exhaustive search. Next, in Figure 3.3 we consider 700 iterations per execution and we average the mutual information of the antenna subset selected at all iterations over 1000 channel realizations. In the same figure we also show the performance of Algorithm 3.2. It is seen that in the transient phase, Algorithm 3.2 has slightly better convergence behavior than Algorithm 3.1 although in the long term, Algorithm 3.1 performs better. From both figures, it is seen that the algorithms adaptively move to the best antenna subset. We observe that although the algorithms take some time to converge to the optimal antenna subset, they move very fast to an antenna subset inducing high MIMO mutual information.

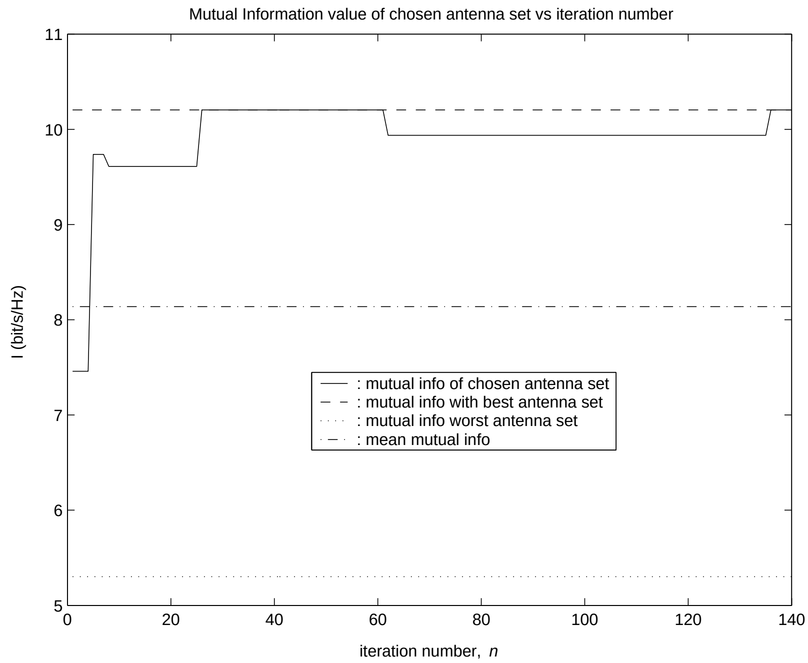


Figure 3.2: Single run of Algorithm 3.1: mutual information value of the chosen antenna subset versus iteration number $n$.

From a practical point of view, instead of initializing the algorithm by choosing a random antenna subset, there are several variations for selecting $\omega^{(0)}$ to avoid the initial transient phase (i.e., *hot start* initialization). For instance, based on a noisy channel estimate, select the antenna subset whose matrix $\hat{\boldsymbol{H}}[0, \omega^{(0)}]$ has maximum Frobenius norm (i.e., select the antennas that receive maximum power). Consider a system with $N_R = 5, n_T = n_R = 2, T = 4$, and SNR= 6dB. Figure 3.4 shows the average mutual information over 100 initial channel realizations versus the iteration number with the *hot start* adaptive algorithm based on the maximum

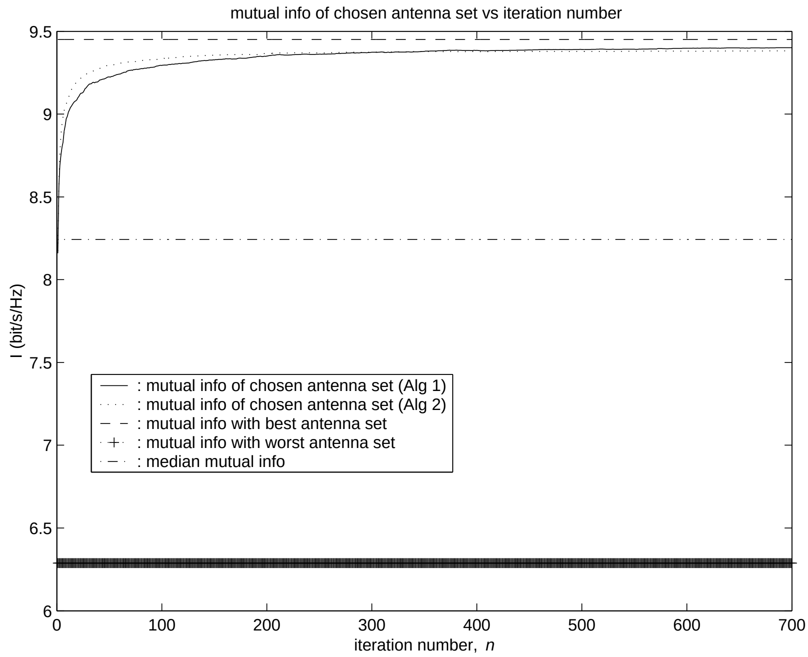


Figure 3.3: The average of the mutual information values of chosen antenna subsets by Algorithm 3.1 and Algorithm 3.2 (over 3000 runs) versus iteration number $n$.

Frobenius norm initial selection. It is seen that from the very first iteration the adaptive algorithm is close to the optimal solution. In the same figure we show the mutual information of the antenna subset selected based on the maximum mutual information criterion found by exhaustive search using noisy channel estimates.

### 3.4.2 Minimum Bounds on Error Rate

Consider the system in Figure 3.1 where the transmitted data $\boldsymbol{s}$ is multiplexed into the $n_T$ transmit antennas. The input-output relationship is expressed in (3.1) where in this case, the transmitted symbols $s_i$ belong to a finite constellation $\mathcal{A}$ of size $|\mathcal{A}|$. The receive antennas see the superposition of all transmitted signals. The task of the receiver is to recover the transmitted data $\boldsymbol{s}$. The ML detection rule is given by

$$\hat{\boldsymbol{s}} = \arg \min_{\boldsymbol{s} \in \mathcal{A}^{n_T}} \left\| \boldsymbol{y} - \sqrt{\frac{\rho}{n_T}} \boldsymbol{H}[\omega] \boldsymbol{s} \right\|^2 . \tag{3.32}$$

At high signal-to-noise ratio, we can upper bound the probability of error of the ML detector using the union bound [59] which is a function of the squared minimum

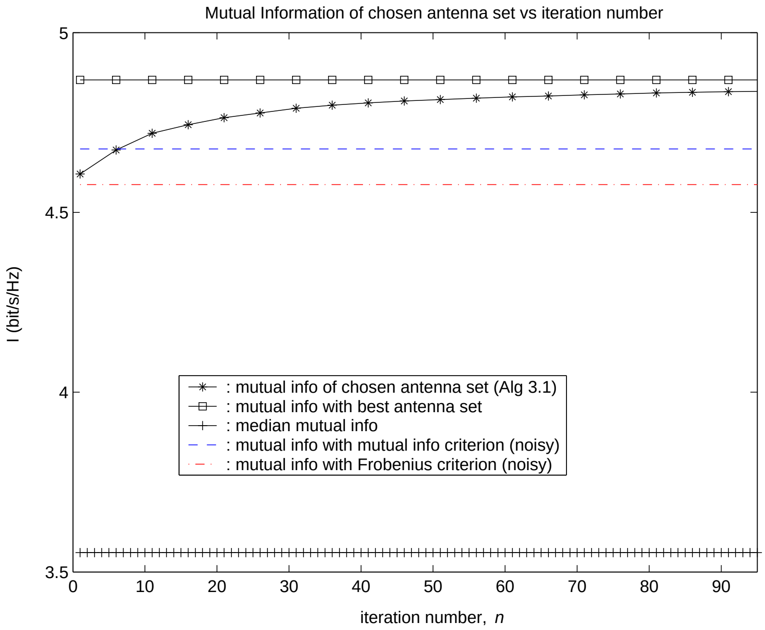


Figure 3.4: The average of the mutual information values of chosen antenna subsets versus iteration number with a *hot start* adaptive algorithm.

distance $d^2_{\min,r}$ of the received constellation given by [60]

$$d^2_{\min,r}[\omega] = \min_{\substack{\boldsymbol{s}_i,\boldsymbol{s}_j \in \mathcal{A}^{n_T} \\ \boldsymbol{s}_i \neq \boldsymbol{s}_j}} \|\boldsymbol{H}[\omega]\left(\boldsymbol{s}_i - \boldsymbol{s}_j\right)\|^2. \tag{3.33}$$

Therefore, minimizing the union bound on error probability is equivalent to maximizing $d^2_{\min,r}$. In Algorithm 3.1, we use $\phi[n,\omega] = \min_{\substack{\boldsymbol{s}_i,\boldsymbol{s}_j \in \mathcal{A}^{n_T} \\ \boldsymbol{s}_i \neq \boldsymbol{s}_j}} \left\|\hat{\boldsymbol{H}}[n,\omega]\left(\boldsymbol{s}_i - \boldsymbol{s}_j\right)\right\|^2$. In Algorithm 3.2, we propose the following theorem.

**Theorem 3** *With*

$$\phi[n,\omega] = \min_{\substack{\boldsymbol{s}_i,\boldsymbol{s}_j \in \mathcal{A}^{n_T} \\ \boldsymbol{s}_i \neq \boldsymbol{s}_j}} \left[\hat{\boldsymbol{H}}_1[n,\omega]\left(\boldsymbol{s}_i - \boldsymbol{s}_j\right)\right]^H \left[\hat{\boldsymbol{H}}_2[n,\omega]\left(\boldsymbol{s}_i - \boldsymbol{s}_j\right)\right] \tag{3.34}$$

*the sequence $\{\hat{\omega}^{(n)}\}$ generated by Algorithm 3.2 converges to the global maximizer $\omega^*$ of (3.33).*

**Proof**: Applying similar arguments to the proof of Proposition 1 it follows that the estimate of the objective function in (3.34) satisfies the requirements of global convergence specified by Algorithm 3.2.

To reduce the number of required training symbols in the implementation of Algorithm 3.2, we can use a biased estimator of $d^2_{\min,r}[\omega]$ using only one estimate of the channel as in Algorithm 3.1.

Note that the computation of $d^2_{\min,r}[\omega]$ is performed over $|\mathcal{A}|^{n_T}(|\mathcal{A}|^{n_T}-1)$ possibilities for each antenna subset which can be prohibitive for large $|\mathcal{A}|$ or $n_T$. Let $\lambda_{\min}[\omega]$ be the smallest singular value of $\boldsymbol{H}[\omega]$ and let the minimum squared distance of the transmit constellation be $d^2_{\min,t} = \min_{\boldsymbol{s}_i,\boldsymbol{s}_j \in \mathcal{A}^{n_T}} \|(\boldsymbol{s}_i - \boldsymbol{s}_j)\|^2$. Then, it is shown in [60] that $d^2_{\min,r}[\omega] \geq \lambda^2_{\min}[\omega] d^2_{\min,t}$ . Therefore, a selection criterion can be simplified to select the antenna subset $\omega \in \Omega$ whose associated channel matrix $\boldsymbol{H}[\omega]$ has the largest minimum singular value. In our problem, based on an estimate of the channel at time $n$ we let $\phi[n,\omega] = \hat{\lambda}_{\min}[n,\omega]$.

### Simulation Results

We consider the performance of Algorithm 3.1 with $N_R = 10$, $n_R = 2$ (45 different antenna subsets) and $n_T = 2$ with ML channel estimate and $T = 2$ orthogonal training symbols. The channel $\boldsymbol{H}$ is assumed to be fixed during the whole run of the algorithm and we set $\rho = 10$dB. We compare three antenna configuration: (a) best antenna set: antenna set with $\max_{\omega_i}(\lambda_{\min}[\omega_i])$; (b) worst antenna set: antenna set with $\min_{\omega_i}(\lambda_{\min}[\omega_i])$; and (c) the antenna set chosen by the algorithm at iteration $n$, i.e., $\hat{\omega}^{(n)}$. Antenna sets (a) and (b) are found by an exhaustive search assuming that the channel is perfectly known. We performed 90 iterations of the algorithm. Figure 3.5 shows a single run of the algorithm. Figure 3.6 shows the average of 100 runs of the algorithm over the same fixed channel $\boldsymbol{H}$. It is observed from the two figures that the algorithm converges and as in the maximum of the mutual information case, it is seen that although it takes some time to converge, it moves quite fast to an antenna subset whose channel has a high $\lambda_{\min}$.

It is important to point out that Algorithm 3.1 using the above cost functions converges to the antenna subset which maximizes $d_{\min,r}$ or $\lambda_{\min}$. However, these criteria do not necessarily minimize the bit error probability since they are based on bounds. Actually, we can show situations in which both cases converge to different antenna subsets and none of them correspond to the antenna subset minimizing the bit error probability. The main reason for this is that the bound is tight only for high signal-to-noise ratio. To observe this phenomenon we consider a system with $N_R = 10$, $n_R = 2$, $n_T = 2$, and $\rho = 10$dB. We average the BER of 30 different channels realizations $\boldsymbol{H}$ and with each channel realization and each antenna subset within the same channel we send 14000 QPSK symbols to compute the BER. Performing an exhaustive search (assuming perfect knowledge of the channel), we find

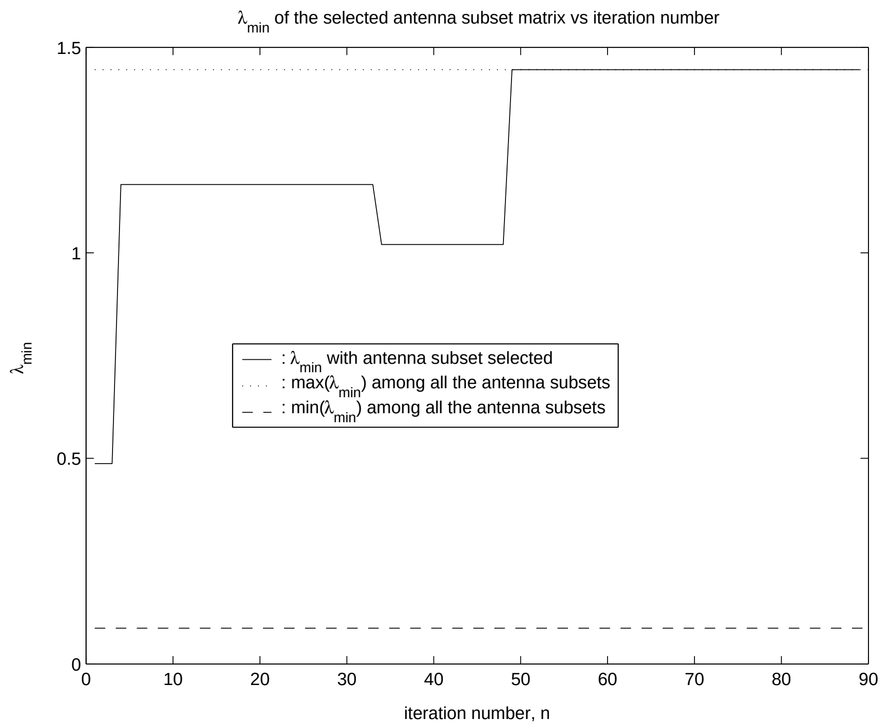


Figure 3.5: Single run of Algorithm 3.1: minimum singular value of the antenna subset selected versus iteration number $n$.

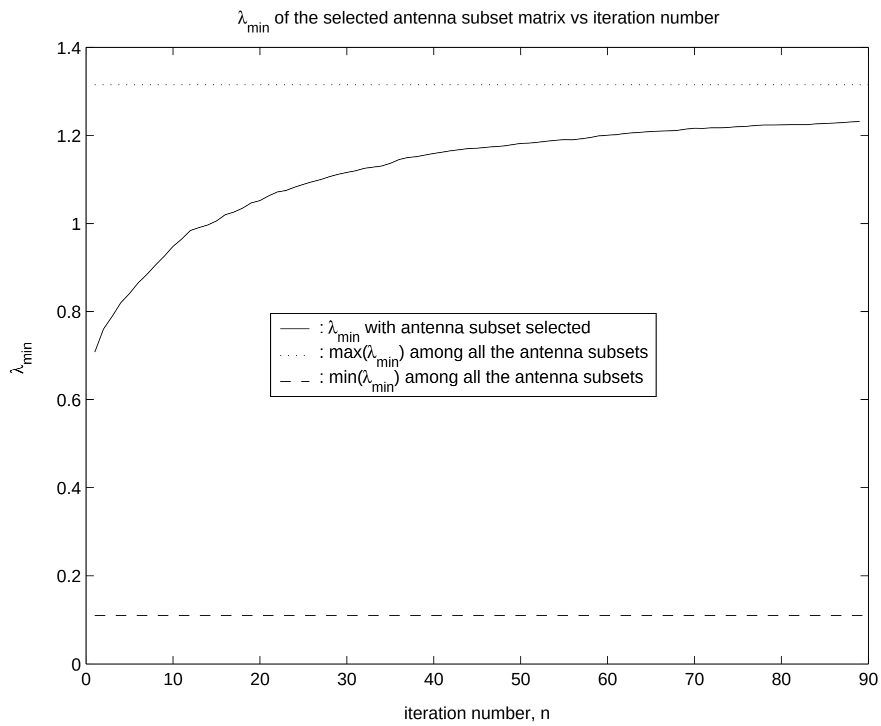


Figure 3.6: The average (over 100 runs) of the minimum singular value of the channel of the chosen antenna subsets versus iteration number $n$.

the antenna subsets under each criterion. We observe that with the $\mathcal{I}_{\max}$ criterion, the antenna subset selected obtains a BER of 0.00054, with the $\lambda_{\min}$ criterion the BER is 0.00049, with the $d_{\min,r}$ criterion the BER is 0.00039, and the minimum BER of all antenna subsets is 0.00035.

### 3.4.3 Maximum SNR

Linear receivers for the system in (3.1) are simpler receivers in which the received vector $\boldsymbol{y}$ is linearly transformed to obtain

$$\boldsymbol{z} = \boldsymbol{G}\boldsymbol{y} = \sqrt{\frac{\rho}{n_T}}\boldsymbol{G}\boldsymbol{H}[\omega]\boldsymbol{s} + \boldsymbol{G}\boldsymbol{n}. \tag{3.35}$$

For linear receivers, the symbol error probability is influenced by the post processing signal-to-noise ratio. For the minimum mean-square error (MMSE) receiver, after applying the equalizer matrix $\boldsymbol{G} = \sqrt{\frac{\rho}{n_T}}\left(\frac{\rho}{n_T}\boldsymbol{H}^H[\omega]\boldsymbol{H}[\omega] + \boldsymbol{I}_{n_T}\right)^{-1}\boldsymbol{H}^H[\omega]$ the signal-to-noise ratio for each of the $n_T$ transmitted data streams can be expressed as [59]

$$\mathrm{SNR}_i^{(MMSE)}[\omega] = \frac{1}{\left(\frac{\rho}{n_T}\boldsymbol{H}^H[\omega]\boldsymbol{H}[\omega] + \boldsymbol{I}_{n_T}\right)^{-1}_{ii}} - 1 \quad \text{for} \quad i = 1, ..., n_T. \tag{3.36}$$

Correspondingly, in Algorithm 3.1 we set

$$\phi[n,\omega] = \max_{i\in[1,n_T]}\left(\frac{\rho}{n_T}\hat{\boldsymbol{H}}^H[n,\omega]\hat{\boldsymbol{H}}[n,\omega] + \boldsymbol{I}_{n_T}\right)^{-1}_{ii}. \tag{3.37}$$

For the zero-forcing (ZF) receiver, $\boldsymbol{G} = \sqrt{\frac{n_T}{\rho}}\boldsymbol{H}^{\dagger}[\omega]$, where $\dagger$ denotes the pseudo-inverse. For each of the $n_T$ transmitted data streams, the signal-to-noise ratio after applying the equalizer matrix $\boldsymbol{G}$ can be expressed as [59]

$$\mathrm{SNR}_i^{(ZF)}[\omega] = \frac{\rho}{n_T\left(\boldsymbol{H}^H[\omega]\boldsymbol{H}[\omega]\right)^{-1}_{ii}} \quad \text{for} \quad i = 1, ..., n_T \tag{3.38}$$

and correspondingly, in Algorithm 3.1 we use

$$\phi[n,\omega] = \max_{i\in[1,n_T]}\left(\hat{\boldsymbol{H}}^H[n,\omega]\hat{\boldsymbol{H}}[n,\omega]\right)^{-1}_{ii}. \tag{3.39}$$

Another case of interest is when the orthogonal space-time block codes are employed. Using the coding and decoding algorithms in [3, 114], the receiver signal-to-noise ratio of the data stream is given by [51]

$$\mathrm{SNR}[\omega] = \frac{\rho}{n_T} \mathrm{trace}\left(\boldsymbol{H}^H[\omega]\boldsymbol{H}[\omega]\right) = \frac{\rho}{n_T} \|\boldsymbol{H}[\omega]\|_F^2 \tag{3.40}$$

where $\|\cdot\|_F^2$ indicates the Frobenius norm. Therefore, in Algorithm 3.1 we may use $\phi[n,\omega] = \left\|\hat{\boldsymbol{H}}[n,\omega]\right\|_F^2$. With Algorithm 3.2, we propose the following theorem to obtain an unbiased estimate of the objective function.

**Theorem 4** *With*

$$\phi[n,\omega] = trace\left[\hat{\boldsymbol{H}}_1^H[n,\omega]\hat{\boldsymbol{H}}_2^H[n,\omega]\right] \tag{3.41}$$

*the sequence* $\{\hat{\omega}^{(n)}\}$ *generated by Algorithm 3.2 converges to the global maximizer of (3.40).*

**Proof**: Applying similar arguments to the proof of Theorem 1 it follows that the estimate of the objective function in (3.41) satisfies the requirements of global convergence specified by Algorithm 3.2.

### 3.4.4 Minimum Error Rate

As shown in Section 4.2 for the ML receiver, the antenna subset chosen by the different criteria based on bounds do not necessarily choose the antenna subset minimizing the bit error rate (BER). In this section, we propose an antenna selection algorithm that directly minimizes the symbol or bit error rate of the system under any type of receivers.

In the proposed method, a noisy estimate of the *simulated* error rate is used as the cost function in the stochastic approximation algorithm instead of a noisy estimate of a bound. The method proceeds as follows. Assume for example that the ML decoding algorithm in (3.32) is used. At time $n$, estimate the channel $\hat{\boldsymbol{H}}[n,\omega]$ with antenna subset $\omega$. At the receiver, generate $m$ *fake* random symbol vectors $\boldsymbol{S}_f = [\boldsymbol{s}_f(1), ..., \boldsymbol{s}_f(m)]$ with $s_{f,k}(i) \in \mathcal{A}$ and perform a simulation of the form

$$\boldsymbol{Y}_f = \sqrt{\frac{\rho}{n_T}}\hat{\boldsymbol{H}}[n,\omega]\boldsymbol{S}_f + \boldsymbol{N} \tag{3.42}$$

where the $(n_R \times m)$ matrix $\boldsymbol{N}$ contains i.i.d. $\mathcal{N}_c(0,1)$ samples. Perform the ML detection on (3.42) to obtain

$$\hat{\boldsymbol{S}}_f = \arg \min_{\boldsymbol{S} \in \mathcal{A}^{n_T \times m}} \left\| \boldsymbol{Y}_f - \sqrt{\frac{\rho}{n_T}} \hat{\boldsymbol{H}}[n,\omega] \boldsymbol{S} \right\|^2 \tag{3.43}$$

and estimate the bit error rate $\widehat{\mathrm{BER}}[n,\omega]$ by comparing $\hat{\boldsymbol{S}}_f$ and $\boldsymbol{S}_f$. In this way, at time $n$, an estimate of the real $\mathrm{BER}[\omega]$ has been obtained. Note that the noise in the estimate of the BER is due to the error in the estimate of the channel and to the limitation in the number of fake symbols used in the simulations. The number of fake symbol vectors required to obtain a good estimate of the BER depends on the signal-to-noise ratio $\rho$ of the channel. For low signal-to-noise ratio, only short fake sequences are needed. The estimated BER will become more accurate as we increase the number $m$ of the fake symbols although the complexity of the algorithm will grow accordingly. Therefore, in Algorithm 3.1 we use $\phi[n,\omega] = -\widehat{\mathrm{BER}}[n,\omega]$ as an observation of the cost function.

Note that the fake symbols $\boldsymbol{s}_f$ are *not* actually sent through the channel. They are merely generated at the receiver to estimate the BER. It is important to point that this method uses an *estimate* of the BER and a closed-form BER expression is not needed, which makes it appealing for other receivers for which even a tight bound is difficult to find. Among these receivers, we may cite the ordered nulling and cancellation BLAST receivers [48]. Obviously, the same method can be used in antenna selection for MIMO systems employing various space-time coding schemes. Moreover, it is straightforward to modify the algorithm to minimize the symbol error rate or frame error rate as well.

The main disadvantage of this approach is that in the high SNR regime, the BER can be very low and therefore, a large amount of fake symbols need to be used if we want to obtain a good estimate of the BER. On the other hand, it has been observed by simulations that the antenna subset having the minimum BER at a SNR value $\rho_1$, corresponds to the antenna subset having the minimum BER for a range of SNR values around $\rho_1$ as long as there is not a large difference in the SNR. Therefore, we can reduce the SNR of the simulation to find the best antenna subset when the SNR is high. In this way, a smaller number of fake symbols will be needed to obtain a good estimate of the error rate and the complexity can be considerably reduced.

### Simulation Results

To show the performance of this method in Algorithm 3.1 we consider first an ML receiver. We use QPSK symbols and we consider $N_R = 6$, $n_R = 2$ (i.e., 15 different antenna configurations) and $n_T = 2$. The $(N_R \times n_T)$ channel $\boldsymbol{H}$

is randomly generated and fixed during the whole simulation. We set $\rho = 9$dB and we use $T = 6$ orthogonal training symbols to estimate the channel. Before starting the algorithm, long simulations are performed assuming perfect channel knowledge over all antenna configurations to find the BER associated with each antenna subset (including the worst and best antenna subset). We run $n = 60$ iterations of the algorithm with $m = 500$ fake symbols per iteration. Figure 3.7 shows the BER of the antenna selected by the algorithm comparing it with the median, the best and the worst BER. It is seen that the algorithm converges to the optimal antenna subset. Moreover, it is observed that antenna selection at the receiver can improve the BER by more than two orders of magnitude with respect to the median BER even for such small values of the signal-to-noise ratio in the channel.

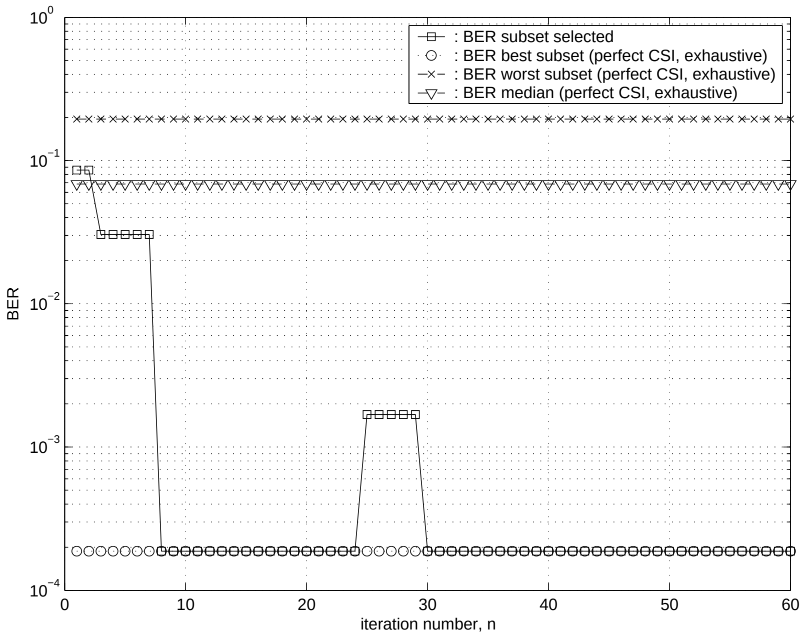


Figure 3.7: Single run of Algorithm 3.1: BER of the of the chosen antenna subset versus iteration number $n$ employing an ML receiver.

Now, we consider the performance of this method in a system employing the ordered nulling and cancellation BLAST receiver. We consider the MMSE criterion for the nulling operation [48]. We use the same channel realization and system parameters as in the ML case. Before starting the algorithm, long simulations are performed assuming perfect channel knowledge over all antenna configurations to find the BER associated with each antenna subset. We use 400 fake symbols per iteration. Figure 3.8 shows the BER of the antenna selected by the algorithm and we compare it with the median, the best and the worst BER. As in the ML case,

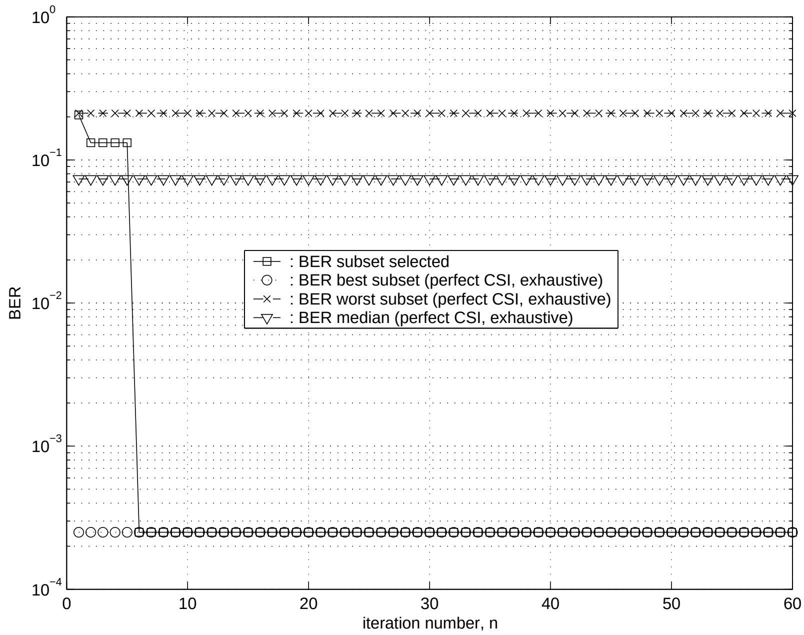


Figure 3.8: Single run of Algorithm 3.1: BER of the of the chosen antenna subset versus iteration number $n$ in a system employing the ordered nulling (MMSE) and cancellation BLAST receiver.

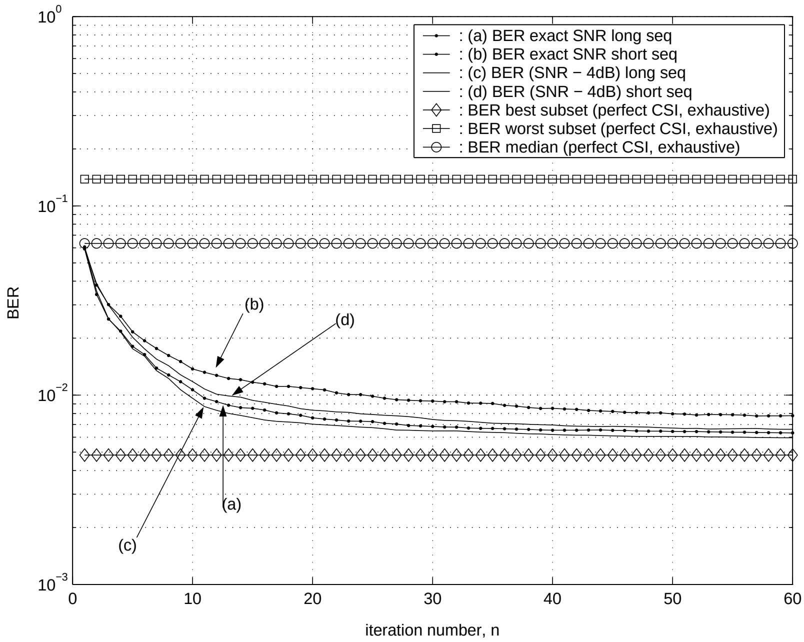


Figure 3.9: The average of 2000 runs of the algorithm: Exact BER of the chosen antenna subset versus iteration number $n$ in a system employing the ordered nulling (MMSE) and cancellation BLAST receiver.

it is seen that the algorithm converges to the optimal antenna subset. Moreover, it is observed that antenna selection at the receiver improves the BER by more than two orders of magnitude with respect to the median BER.

We now consider the average of 2000 runs of the algorithm over a new channel realization employing the ordered nulling and cancellation BLAST receiver. We set $\rho = 9$dB and we use $T = 6$ orthogonal training symbols to estimate the channel. Before starting the algorithm, long simulations are performed assuming perfect channel knowledge over all antenna configurations to find the exact BER associated with each antenna subset. We consider four different implementations of the algorithm depending on the length of the fake sequence $m$ and the $\rho$ used in the simulations: (a) the simulation to estimate the BER at every iteration of the algorithm is performed with the exact $\rho$ of the channel and $m = 500$ fake symbols; (b) to reduce the complexity, the simulation is performed with the exact SNR of the channel $\rho = 9dB$ but with only $m = 20$ fake symbols; (c) the SNR is reduced to $\rho = 5$dB and $m = 500$ fake symbols are employed; and (d) the SNR is reduced to $\rho = 5$dB and only $m = 20$ fake symbols are employed. In Figure 3.9, the average of the exact BER selected by the algorithm at each iteration is plotted. In the same figure we show the BER of the best antenna subset and worst antenna subset, as well as the median BER among the 15 antenna configurations, found by exhaustive search. It is seen that the algorithm moves towards the optimal antenna configuration in the four cases considered. Comparing the performance of cases (a) and (b), we observe that (a) has a better convergence behavior because by using longer fake sequences, the estimate of the BER is less noisy. Comparing the performance of cases (a) and (d) we find that the behavior is very close although in (d) we have reduced the complexity by more than one order of magnitude. Comparing the performance of (b) and (d), we observe that although (b) uses the real $\rho$ of the channel to estimate the BER, the behavior is worse. This result is due to the fact that at very low values of the exact BER (i.e., high SNR) we cannot obtain a good estimate of the BER with only $m = 20$ symbols. Moreover, we observe that case (c) has the best performance since with $m = 500$ symbols we can have a better estimate of the BER when the SNR is 5dB. However, although not plotted in the figure, if the number $m$ of fake symbols became larger, the performance of (a) would become better than the one of (c). In summary, we can reduce the complexity without incurring in a convergence penalty by reducing the SNR of the simulations (assuming that the SNR difference is not large) and using a shorter sequence of fake symbols $m$.

## 3.5 Adaptive Algorithms for Antenna Selection in Time-varying Channels

In the previous section, we described discrete stochastic approximation algorithms for antenna selection in static MIMO channels. Now we consider nonstationary environments for which the optimum antenna subset takes on a time-varying form, $\omega^*[n] \in \Omega$, since the MIMO channel is time-varying. Consequently, the MIMO antenna selection algorithms should be able to track the best antenna subset if the variation of the channel is *slow* for tracking to be feasible. The adaptive discrete stochastic approximation algorithms proposed in this section are directly applicable to any of the objective functions discussed in Section 4.

### 3.5.1 Fixed Step-size Discrete Stochastic Approximation Algorithm

In the static channel environment discussed in the previous section, in order for the method to converge, it was necessary for the method to become progressively more and more conservative as the number of iterations grew. Consequently, a decreasing step size, $\mu[n] = 1/n$, was used, in order to avoid moving away from a promising point unless there was a strong evidence that the move will result in an improvement. In the time-varying case, we require a step size that permits moving away from a state as the optimal antenna subset changes [74]. Therefore, to track the optimal antenna subset, we replace the `Adaptive filter for updating state occupation probabilities` step in Algorithm 3.1 by

$$\boldsymbol{\pi}[n+1] = \boldsymbol{\pi}[n] + \mu(\boldsymbol{D}[n+1] - \boldsymbol{\pi}[n]) \tag{3.44}$$

where $0 < \mu \leq 1$. A fixed step size $\mu$ in (3.44) introduces an exponential forgetting factor of the past occupation probabilities and allows to track slowly time-varying optimal antenna subset $\omega^*[n]$. The same arguments can be used to extend the application of Algorithm 3.2 to time-varying channels by using a fixed step size $\mu$ in (3.14).

For $\boldsymbol{\pi}[n]$ being a probability vector (i.e., the elements add 1 and are non-negative) the step size must satisfy $0 < \mu \leq 1$. Note that $\mathbf{1}^T(\boldsymbol{D}[n+1] + \boldsymbol{\pi}[n]) = 0$ implying that $\mathbf{1}^T\boldsymbol{\pi}[n+1] = \mathbf{1}^T\boldsymbol{\pi}[n] = 1$. Expressing (3.44) as $(1-\mu)\boldsymbol{\pi}[n] + \mu\boldsymbol{D}[n+1]$ we observe that the elements of $\boldsymbol{\pi}[n+1]$ are non-negative, which proves that $\boldsymbol{\pi}$ is a probability vector.

It has been observed that time-varying channels modify the optimal antenna subset over the time although most of the antennas in the optimal antenna subset remain the same. Hence, in time-varying channels, we can modify the `Sampling` `and Evaluation` step in Algorithm 3.1 to select a candidate solution $\tilde{\omega}^{(n)}$ uniformly from $\Theta \backslash \omega^{(n)}$ where $\Theta$ is defined as the set of antenna subsets $\tilde{\omega}^{(n)} \in \Omega$ such that the distance $d(\tilde{\omega}^{(n)}, \omega^{(n)}) = D$, where we choose $D < \min(n_R, N_R - n_R)$.

**Simulation Results**

We demonstrate the tracking performance of this version of the algorithm under the maximum mutual information criterion in time-varying channels. We use (3.31) as an estimate of the objective function. We assume that each channel gain $h_{i,j}$ between a transmit and receive antenna remains constant over $\tau$ frame intervals (we assume that each frame interval corresponds to one iteration of the algorithm) and follows a first order AR dynamics over $\tau$ written as

$$h_{i,j}(t) = \alpha h_{i,j}(t-1) + \beta \upsilon_{i,j}(t) \quad i = 1, ..., N_R \quad \text{and} \quad j = 1, ..., N_T \tag{3.45}$$

where $\alpha$ and $\beta$ are the fixed parameters of the model related through $\beta = (1 - \alpha^2)^{1/2}$ and $\upsilon_{i,j} \sim \mathcal{N}_c(0, 1)$. The parameter $\alpha$ can be related to the maximum Doppler frequency $f_d$ as $\alpha = J_0(2\pi f_d \tau T_f)$ where $J_0(\cdot)$ is the zeroth order Bessel function of the first kind and $T_f$ is the duration of one frame. In the simulations we set $\alpha = 0.9$, $\tau = 500$ and the constant step size $\mu = 0.002$. We consider $N_R = 12$, $n_R = 6$ and $n_T = 2$. We set $\rho = 10$dB and we use the ML channel estimate with $T = 6$ orthogonal training symbols. It has also been observed that in most cases $d(\omega^*[n], \omega^*[n-\tau]) \leq 2$ and therefore we set $D = 2$. The tracking performance of the algorithm is shown in Figure 3.10. The maximum, minimum and median values of the mutual information as a function of time are also shown. It is seen that the algorithm closely tracks the best antenna subset.

### 3.5.2 Adaptive Step-size Discrete Stochastic Approximation Algorithm

In the previous version of the algorithm, the choice of the fixed step size $\mu$ has high influence in the performance of the algorithm. The faster the channel changes or the further away of the current subset estimate of the optimal antenna subset, the larger $\mu$ should be. On the other hand, the larger the effects of the observation noise or the closer we are from the optimal antenna subset, the smaller $\mu$ should be [76]. However, in practice, one does not know the dynamics of the channel in advance.

In this section we present a method to adaptively adjust the step size $\mu[n]$ as the algorithm evolves. In this way, at each iteration $n$, our stochastic approximation algorithm has two estimation problems to contend with. The first is the estimation of $\omega^*[n]$ and the second is the estimation of $\mu[n]$. Since the $\mu[n]$ is a continuous variable, we can use an adaptive algorithm similar to the gradient descent algorithm [14]. This underlying adaptive algorithm to adjust $\mu[n]$ would use estimates of the derivative of the mean square error with respect to the step size $\mu$. These ideas are based on [14, 77] and have been further exploited in [74, 75].

Within this new framework, the estate occupation probability vector depends on $\mu$. Denote the mean-square derivative $(\partial/\partial\mu)\boldsymbol{\pi}^{\mu}[n]$ by $\boldsymbol{J}^{\mu}[n]$, i.e.,

$$\lim_{\Delta\to 0} E\left\{\left|\frac{\boldsymbol{\pi}^{\mu+\Delta}[n]-\boldsymbol{\pi}^{\mu}[n]}{\Delta}-\boldsymbol{J}^{\mu}[n]\right|^2\right\}=0. \tag{3.46}$$

Define the error,

$$\boldsymbol{e}^{\mu}[n]=\boldsymbol{D}[n+1]-\boldsymbol{\pi}^{\mu}[n] \tag{3.47}$$

and differentiate the square of the error with respect $\mu$ as

$$\frac{\partial}{\partial\mu}\left(\boldsymbol{e}^{\mu}[n]\boldsymbol{e}^{\mu}[n]^T\right)=-2\left(\boldsymbol{D}[n+1]-\boldsymbol{\pi}^{\mu}[n]\right)^T\boldsymbol{J}^{\mu}[n]. \tag{3.48}$$

Next, differentiating $\boldsymbol{\pi}[n+1]$ in (3.44) with respect to $\mu$, yields

$$\boldsymbol{J}^{\mu}[n+1]=\boldsymbol{J}^{\mu}[n]-\mu\boldsymbol{J}^{\mu}[n]+\left(\boldsymbol{D}[n+1]-\boldsymbol{\pi}^{\mu}[n]\right). \tag{3.49}$$

The proposed scheme aims to minimize the expectation of (3.47) by scaling $\mu[n]$ depending on the error in (3.47). The following adaptive step-size discrete stochastic approximation algorithm is adopted as a modification of Algorithm 3.1.

**Algorithm 3.3** Adaptive step-size discrete stochastic approximation algorithm

□ Initialization, Sampling, and Acceptance: the same as Algorithm 3.1

□ Substitute the update of the state occupation probabilities by

$$\begin{aligned}
\boldsymbol{e}[n] &= \boldsymbol{D}[n+1]-\boldsymbol{\pi}[n],\\
\boldsymbol{\pi}[n+1] &= \boldsymbol{\pi}[n+1]+\mu[n]\boldsymbol{e}[n],\\
\mu[n+1] &= \left\{\mu[n]+\eta\boldsymbol{e}^T[n]\boldsymbol{J}[n]\right\}_{\mu_-}^{\mu_+},\\
\boldsymbol{J}[n+1] &= \left(1-\mu[n]\right)\boldsymbol{J}[n]+\boldsymbol{e}[n], \quad \boldsymbol{J}[0]=\mathbf{0}.
\end{aligned} \tag{3.50}$$

□ Compute the maximum: the same as Algorithm 3.1

In the algorithm $\eta$ denotes the learning rate. As $\eta$ decreases, the rate of adaptation decreases. If the learning rate $\eta = 0$, then the algorithm reduces to the fixed step-size algorithm. $\{X\}_{\mu_-}^{\mu_+}$ denotes the projection of $X$ onto the interval $[\mu_-, \mu_+]$ with $0 < \mu_- \leq \mu_+$. For fast speed of tracking and good transient behavior, one seeks $\mu_+$ as large as possible but not greater than the instability value. We note that the sequence $\mu[n]$ will not go to zero unless the optimal antenna subset remains constant.

We point out that Algorithm 3.3 is composed of three parts: (1) A random search of a next candidate $\omega^{(n)}$ over $\Omega$; (2) a continuous adaptive LMS algorithm which updates the step size $\mu[n]$; and (3) a discrete adaptive algorithm that updates the state probability vector $\boldsymbol{\pi}[n]$, where the last two adaptive algorithms are cross-coupled. Assuming that there is a unique local minimum $\mu^*$ of $E\{\|\boldsymbol{e}^{\mu}[n]\|^2\}$, it can be proved that $\mu[n]$ converges weakly to $\mu^*$, where we consider weak convergence as a generalization of convergence in distribution [74].

An interesting feature of the algorithm is that it does not assume anything about the dynamics of the problem. It self adapts to track the dynamics of the channel and consequently, the best antenna subset $\omega^*[n]$.

**Simulations Results**

To demonstrate the performance of this version of the algorithm, we consider the same system parameters as in Section 5.1. The bounds for the step size are chosen as $\mu_- = 0$ and $\mu_+ = 0.003$ and the learning rate is set to $\nu = 0.0005$. We restrict the candidate solution to antenna subsets with $D = 2$. Figure 3.11 shows the performance of the algorithm. The maximum, minimum and median values of the mutual information as a function of time are also shown for comparison. It is seen that the adaptive step-size algorithm has a better tracking performance than the constant step-size algorithm.

## 3.6 Fast Antenna Selection Algorithms

### 3.6.1 Transmit antenna selection in linear receivers: geometrical approach

Next we consider transmit antenna subset selection in spatial multiplexing systems and perfect CSI at the receiver. In particular, we propose selection algorithms aiming to minimize the error rate when linear detectors are used at the receiver. In [50], selection criteria have been proposed which attempt to minimize the error rate when linear receivers are used. In that work, the signal-to-noise ratio prior to

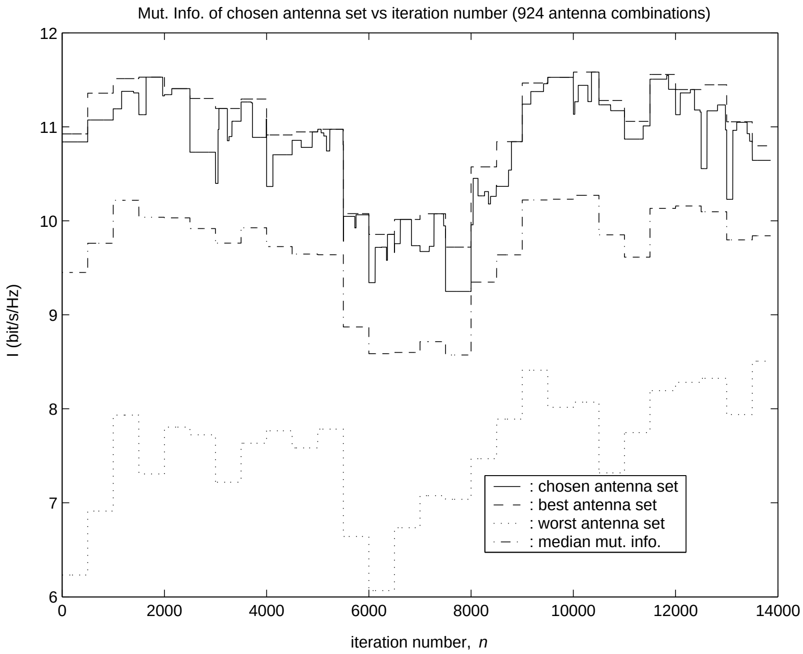


Figure 3.10: The mutual information values of the chosen antenna subsets versus iteration number $n$ (fixed step-size).

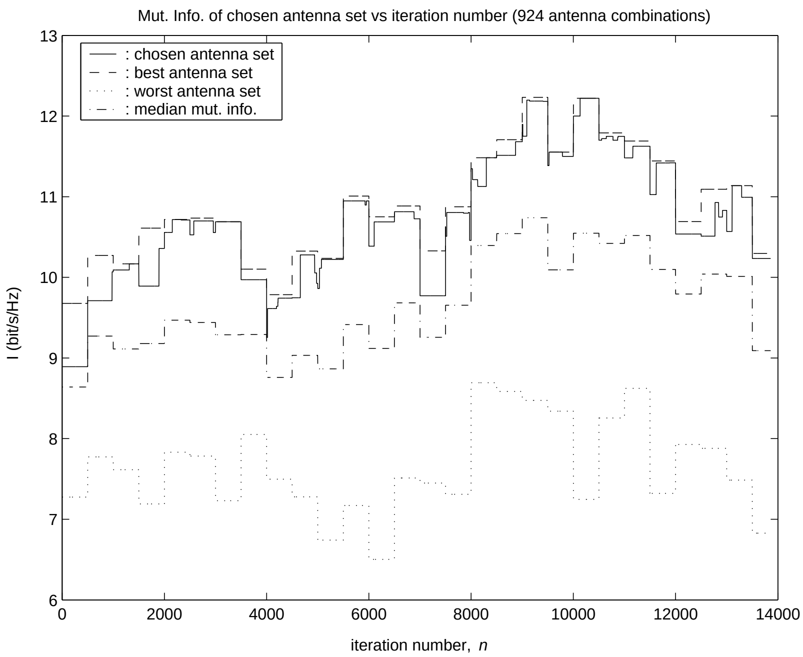


Figure 3.11: The mutual information values of the chosen antenna subsets versus iteration number $n$ (adaptive step-size).

the slicing operation is considered as the objective function to be optimized. In this section, we propose a selection metric based upon the geometrical interpretation of the decoding process in a linear receiver. This interpretation also permits us to develop a suboptimal algorithm that yields a considerable complexity reduction with only a small loss in performance.

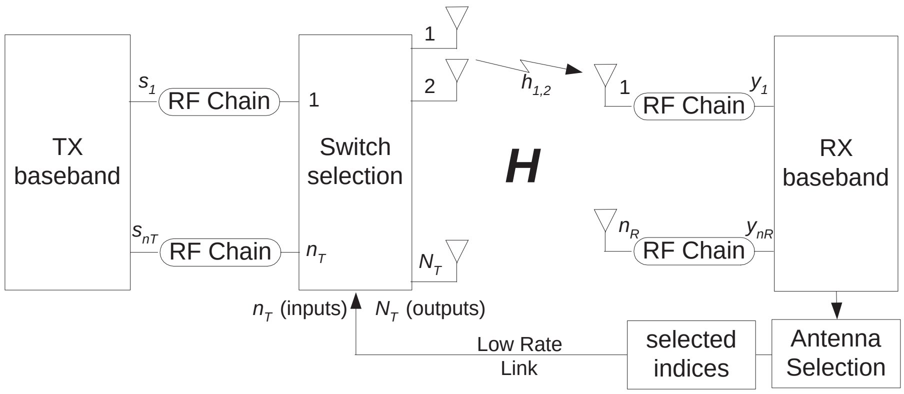


Figure 3.12: MIMO system with antenna selection at the transmitter.

Consider the system shown in Figure 3.12 with $n_T$ transmit and $n_R$ receive RF chains. We assume that the receiver is equipped with equal number of antennas and RF chains whereas the transmitter is equipped with $N_T$ antenna elements. Thus, the selection algorithm consists of selecting the best $n_T$ transmit antennas out of the $\binom{N_T}{n_T}$ different combinations according to certain optimization criterion. The wireless channel is assumed to be quasi-static and flat fading and can be represented by a $(n_R \times N_T)$ matrix $\boldsymbol{H}$ whose element $h_{ij}$ represents the complex gain of the channel between the $j$-th transmit antenna and the $i$-th receive antenna. Denote each of the transmit antenna subsets as $\omega_i = \{Ant_1, ..., Ant_{n_T}\}$. Define the set of all $P = \binom{N_T}{n_T}$ antenna subsets as $\Omega = \{\omega_1, ..., \omega_P\}$ and denote $\boldsymbol{H}[\omega]$ as the $(n_R \times n_T)$ submatrix corresponding to the columns of $\boldsymbol{H}$ selected by $\omega$. We assume that the channel state information is available at the receiver but not at the transmitter. Thus, the selection algorithms are implemented at the receiver and the antennas indices to be used are fedback to the transmitter assuming that there exists a low rate link between the receiver and the transmitter.

In spatial multiplexing systems, different data streams are transmitted from different antennas. Assume that $\boldsymbol{s} = [s_1, ..., s_{n_T}]^T$ is the transmitted symbol vector with $E\{s_i^* s_i\} = 1$. Then, the received signal when the transmit antenna subset selected is $\omega$ can be expressed as $\boldsymbol{y} = \sqrt{\frac{\rho}{n_T}}\boldsymbol{H}[\omega]\boldsymbol{s} + \boldsymbol{n}$, where $\boldsymbol{y} = [y_1, ..., y_{n_R}]$ is the received signal vector, $\boldsymbol{n}$ is the received noise vector distributed as $\mathcal{N}_c(\mathbb{0}, \boldsymbol{I}_{n_R})$ and $\rho$ is the total signal-to-noise ratio independent of the number of transmit antennas. In linear receivers, a spatial linear equalizer $\boldsymbol{G}[\omega]$ is applied to recover the transmitted symbol vector. The equalizer can be optimized according to the ZF criterion, $\boldsymbol{G}[\omega] = \sqrt{\frac{n_T}{\rho}}\boldsymbol{H}[\omega]^\dagger$, where $\dagger$ denotes the pseudo-inverse, or the MMSE criterion, $\boldsymbol{G}[\omega] = \sqrt{\frac{\rho}{n_T}}\boldsymbol{H}[\omega]^H(\frac{\rho}{n_T}\boldsymbol{H}[\omega]\boldsymbol{H}[\omega]^H + \boldsymbol{I}_{n_R})^{-1}$. Since at high signal-to-noise ratio with antenna selection the MMSE solution tends to the ZF solution, we will focus on the ZF solution. As has been shown in [133] and Chapter 2, the decision regions in linear receivers consist of $n_T$-dimensional complex parallelepipeds formed by the column vectors of $\boldsymbol{H}[\omega]$. Therefore, from a geometrical perspective, we propose a simple transmit antenna selection criterion consisting of selecting the columns of $\boldsymbol{H}$ such that the decision region minimizes the error rate. At a high signal-to-noise ratio, the error rate performance will be limited by the minimum error vector that makes a symbol fall out of the decision region. Denote $\boldsymbol{h}_1[\omega], ..., \boldsymbol{h}_{n_T}[\omega]$ as the $n_T$ columns of $\boldsymbol{H}$ selected by $\omega$. Then, considering that the symbol is located in the center of the $n_T$-dimensional parallelepiped, the minimum length of a vector to make an error is

$$d[\omega] = \min_{1\leq i\leq n_T} \frac{1}{2}\|\pi^\perp(\boldsymbol{h}_i[\omega])\|^2, \tag{3.51}$$

where $\pi^\perp(\boldsymbol{h}_i[\omega])$ denotes the projection of $\boldsymbol{h}_i[\omega]$ on $span(\{\boldsymbol{h}_1[\omega], ..., \boldsymbol{h}_{n_T}[\omega]\}\backslash\boldsymbol{h}_i[\omega])^\perp$ and $(\cdot)^\perp$ denotes the orthogonal complement. Then, the selection criterion becomes

$$\omega^* = \arg\max_{\omega\in\Omega}\left\{\min_{1\leq i\leq n_T}\frac{1}{2}\|\pi^\perp(\boldsymbol{h}_i[\omega])\|^2\right\}. \tag{3.52}$$

*a) Low Complexity Algorithms*: The selection process in (3.52) could be highly complex when the number of antenna combinations is large. One solution to reduce the complexity consists of employing sub-optimal incremental or decremental greedy algorithms similar to that proposed in [53] for the capacity case. In the decremental approach, we start considering the whole $N_T$ columns and at every step, we remove the column that has the minimum projection onto the orthogonal complement of the span of the remaining $N_T - 1$ columns. The process is repeated with the remaining columns until only $n_T$ columns are left. The inconvenience of this approach is that the system requires not only $n_R \geq n_T$ but $n_R \geq N_T$ which is not always true. In the incremental approach, we start by selecting one column that has the maximum 2-norm. Then, at every step of the algorithm, we add the column with the largest projection onto the orthogonal complement of the subspace spanned by the columns already selected. This approach greatly reduces the complexity in the situation where $n_T$ is small in comparison to $N_T$. A very low complexity implementation of incremental selection is given in Algorithm 4.

In the algorithm, $\mu_{p,j}$ denotes the Gram-Schmidt coefficient $\mu_{p,j} = \hat{\boldsymbol{h}}_p^H \boldsymbol{h}_j$ and $\Theta_i$ represents the subset of antennas selected up to the $i$-th step.

**Algorithm 4** Reduced complexity incremental selection

INPUT: all column vectors $\boldsymbol{h}_1, ..., \boldsymbol{h}_{N_T}$ in $\boldsymbol{H}$
$k_1 = \arg\max_{i \le N_T} \{\boldsymbol{h}_i^H \boldsymbol{h}_i\}$;
$\hat{\boldsymbol{h}}_1 = \boldsymbol{h}_{k_1} / \|\boldsymbol{h}_{k_i}\|$; $\Theta_1 = \{k_1\}$;
FOR $i = 2 : n_T$
  FOR EVERY $j \in \{\{1, ..., N_T\} \backslash \Theta_{i-1}\}$
    $\boldsymbol{b}_j = \boldsymbol{h}_j - \sum_{p=1}^{i-1} \mu_{p,j} \hat{\boldsymbol{h}}_p$;
  END FOR
  $k_i = \arg\max_j \{\boldsymbol{b}_j^H \boldsymbol{b}_j\}$;
  $\hat{\boldsymbol{h}}_i = \boldsymbol{b}_{k_i} / \|\boldsymbol{b}_{k_i}\|$; $\Theta_i = \{\Theta_{i-1}\} \cup \{k_i\}$;
END FOR
OUTPUT: selected antenna indices: $\Theta_{n_T}$

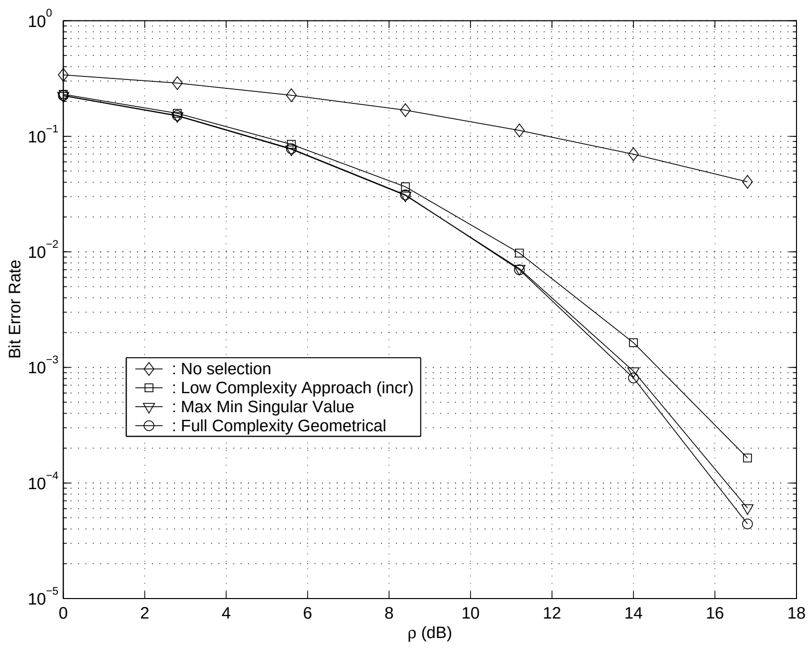


Figure 3.13: Selection criteria comparison.

### Simulations Results

In Figure 3.13 we show the performance of the antenna selection algorithms in a system with $n_R = 4$ receive antennas and $N_T = 8$ antennas where only $n_T = 4$

are actually used. We average the results over several channel realizations. In the same figure we also show the error rate of a system employing a selection criterion that maximizes the minimum eigenmode [50] and also the error rate of a system without antenna selection. It is seen that the geometrical approach obtains the best performance although its complexity is very high (although similar to the complexity of the eigenmode criterion). On the other hand, the much less complex incremental algorithm only shows a small loss of performance.

### 3.6.2 Antenna selection in the downlink of linearly precoded MISO systems

We consider the downlink of multiuser multiple-input single-output (MISO) wireless systems, where the base station is equipped with multiple antennas and each mobile user is constrained to a single antenna. In particular, we consider linear precoded systems such that the single antenna receivers do not have to estimate the channel, but only scale and quantize the received data. In this scenario, we propose low complexity antenna selection algorithms. The highly complex optimal antenna selection algorithm is first derived, and then, a low complexity greedy optimization algorithm is proposed. It will be shown that the proposed algorithm obtains nearly optimal performance.

#### System Model

We consider a multiuser MISO wireless system consisting of a single base station and $K$ mobile units scattered over the service area. We assume that the base station is equipped with multiple antennas and each receiver is constrained to a single antenna. Precoding schemes for broadcast channels effectively transfer the signal processing for interference suppression from the mobile receiver to the base station transmitter. This approach is feasible if the base station can estimate the downlink channels of all users (e.g., in systems employing time division duplexing (TDD) where the uplink and downlink channels are reciprocal). Different practical techniques (linear [70] and non-linear [130]) have been proposed to approach the downlink capacity. We consider the case in which the transmit signal is precompensated such that the single antenna receivers do not have to estimate the channel, but only quantize the received data. Linear precoding is the simplest method to perform precoding. In this case, the receiver simply quantizes the received signal to the original symbol constellation, which translates to a reduction in power consumption and decrease in the cost of the terminals.

In the downlink of multiuser MISO systems, different data streams are trans-

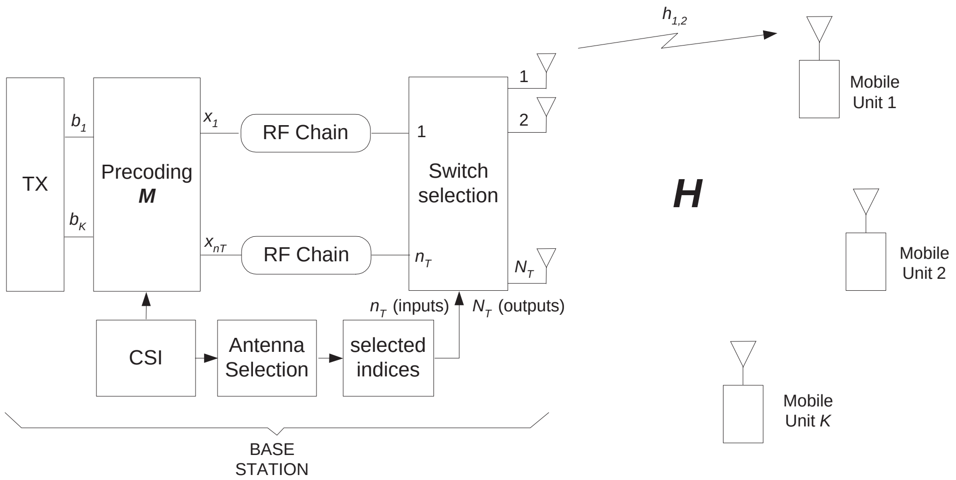


Figure 3.14: Downlink multiuser MISO system with antenna selection.

mitted for each of the users. Consider first a system with $K$ users and $n_T$ antennas ($n_T \geq K$). Assume that $\boldsymbol{b} = [b_1, ..., b_K]^T$ is the transmitted symbol vector with $E\{|b_i|^2\} = 1, i = 1, ..., K$. The base station computes the precoding matrix $\boldsymbol{M} \in \mathbb{C}^{n_T \times K}$ with the knowledge of the CSI of every user with the constraint of the total power budget available at the transmitter $P_T$, where $P_T$ is independent of the number of transmit antennas. Then, the $n_T \times 1$ precoded signal ready to be transmitted is given by $\boldsymbol{x} = \boldsymbol{M}\boldsymbol{b}$. By stacking the received signal from all the mobile units in a single vector $\boldsymbol{y} = [y_1, ..., y_K]^T$ we can write

$$\boldsymbol{y} = \boldsymbol{H}\boldsymbol{M}\boldsymbol{b} + \boldsymbol{n}, \tag{3.53}$$

where $\boldsymbol{H} \in \mathbb{C}^{K \times n_T}$ corresponds to the flat fading channel whose element $h_{ij}$ represents the complex gain of the channel between the $j$-th transmit antenna and the $i$-th mobile unit, and $n_i$ is the noise at the $i$-th receiver distributed as $\mathcal{N}(0, \sigma_{n,i}^2)$.

The spatial linear precoder $\boldsymbol{M}$ optimized according to the MMSE criterion is given by $\boldsymbol{M}^{(u)} = \boldsymbol{H}^\dagger$, where $(\cdot)^\dagger$ denotes the pseudo-inverse [70]. Notice that the precoding matrix $\boldsymbol{M}^{(u)} = \boldsymbol{H}^\dagger$ places no explicit constraint on average transmit power and a power normalization factor is required. Assuming that the total available power at the transmitter is $P_T$, the scaling factor is given by $\beta^2 = P_T/\text{tr}(\boldsymbol{H}^\dagger \boldsymbol{H}^{\dagger H})$ and the precoding matrix becomes $\boldsymbol{M} = \beta \boldsymbol{M}^{(u)} = \beta \boldsymbol{H}^\dagger$. Then the $k$-th receiver makes a decision based on $y_k = \beta b_k + n_k$. With the precoding matrix $\boldsymbol{M}$, the received SNR is equal across the users and is given by

$$\text{SNR}_k = \frac{\beta^2}{\sigma_n^2} = \frac{P_T}{\text{tr}(\boldsymbol{H}^\dagger \boldsymbol{H}^{\dagger H})\sigma_n^2}. \tag{3.54}$$

**Antenna Selection**

Although $n_T = K$ is sufficient to implement linear precoding, it has been shown in [97] that there is an optimum ratio of antennas-to-users ($n_T/K > 1$) such that linear precoding can achieve around 80% of the sum capacity of the downlink channel computed at the same ratio. At other ratios the difference between the capacity with linear precoding and the downlink capacity can become much more pronounced. In particular, when $K = n_T$, the sum rate capacity of the linearly precoded system does not increase linearly with $n_T$ (or $K$), while the capacity of the downlink channel does. Similarly, when $n_T = K$, linear precoding exhibits a poor BER performance. The optimal ratio implies that the number of transmit antennas $n_T$ needs to be not equal but larger than the number of mobile units $K$. However, when multiple users $K$ want to communicate concurrently with the base station, one major concern to implement $n_T > K$ antenna systems is the high cost due to the expense of the RF chains required for each antenna. A technique to reduce the cost of the multiple antenna system while maintaining part of the capacity is the use of antenna selection [92] (see Fig. 3.14). In this section, we choose to select the $n_T$ antennas (i.e., $n_T$ columns in $\boldsymbol{H}$) that maximize the signal to noise ratio across the users in (3.54). Although a combinatorial exhaustive search of the $\binom{N_T}{n_T}$ antenna subsets can find the optimal solution, the selection would become highly complex since for every new antenna subset, a $n_T \times n_T$ matrix pseudo-inverse needs to be computed. In this section, motivated by the greedy algorithms in [53] we propose sub-optimal low complexity antenna selection algorithms that only show a minimum loss of performance. In particular, we consider a solution using decremental selection.

This solution begins by considering that all available antennas can be used in the transmission, and at every step, an antenna is de-activated such that $\text{SNR}_k$ decreases as low as possible. The process is repeated with the remaining antennas until only $n_T$ antennas are left. Recall that removing one antenna is equivalent to removing one column in $\boldsymbol{H}$ while the rest of the columns remain unchanged.

Consider first the full matrix $\boldsymbol{H} \in \mathbb{C}^{K \times N_T}$, and let $\boldsymbol{h}_i$ and $\boldsymbol{H}_i$ denote the $i$th column in $\boldsymbol{H}$, and the submatrix of $\boldsymbol{H}$ after removing the $i$th column, respectively. Therefore, in the decremental algorithm we remove the $i$-th column in $\boldsymbol{H}$ such that the submatrix left $\boldsymbol{H}_i$ minimizes the denominator in (3.54), i.e.,

$$i^* = \arg \min_{i=1,\dots,N_T} \operatorname{tr}\left(\left(\boldsymbol{H}_i \boldsymbol{H}_i^H\right)^{-1}\right). \tag{3.55}$$

Notice that $(3.55)$ requires the inversion of $N_T$ matrices of size $K \times K$. Here we make use of the following equality

$$\boldsymbol{H}_i \boldsymbol{H}_i^H = \boldsymbol{H}\boldsymbol{H}^H - \boldsymbol{h}_i \boldsymbol{h}_i^H, \tag{3.56}$$

and (3.55) becomes

$$i^* = \arg \min_{i=1,\dots,N_T} \operatorname{tr}\left(\left(\boldsymbol{H}\boldsymbol{H}^H - \boldsymbol{h}_i^H \boldsymbol{h}_i\right)^{-1}\right). \tag{3.57}$$

Denote $\boldsymbol{A} = \boldsymbol{H}\boldsymbol{H}^H$. Using the matrix inversion lemma we can write

$$\left(\boldsymbol{A} - \boldsymbol{h}_i^H \boldsymbol{h}_i\right)^{-1} = \boldsymbol{A}^{-1} + \boldsymbol{A}^{-1}\boldsymbol{h}_i \left(1 - \boldsymbol{h}_i^H \boldsymbol{A}^{-1} \boldsymbol{h}_i\right) \boldsymbol{h}_i^H \boldsymbol{A}^{-1}. \tag{3.58}$$

Then, applying tr$(\boldsymbol{U} + \boldsymbol{V}) =$ tr$(\boldsymbol{U}) +$ tr$(\boldsymbol{V})$ we can express (3.57) as

$$i^* = \min_i \left\{ \operatorname{tr}\left(\boldsymbol{A}^{-1}\boldsymbol{h}_i \left(1 - \boldsymbol{h}_i^H \boldsymbol{A}^{-1} \boldsymbol{h}_i\right) \boldsymbol{h}_i^H \boldsymbol{A}^{-1}\right)\right\}. \tag{3.59}$$

Notice that now, for the $N_T$ possible antennas that can be removed, only one matrix inverse has to be computed, $(\boldsymbol{H}\boldsymbol{H}^H)^{-1}$. Next assume that after removing one antenna, the number of antennas is still excessive. Then, a second antenna needs to be removed from the remaining $N_T - 1$ columns in $\boldsymbol{H}_{i^*}$, and the inverse of $(\boldsymbol{H}_{i^*}\boldsymbol{H}_{i^*}^H)^{-1}$ is required. However, this inverse has already been computed using the matrix inversion lemma when we removed the $i^*$-th column in (3.58) (i.e., we do not need to explicitly compute a new matrix inverse at each step of the algorithm). Hence, we iteratively remove one column until only $n_T$ antennas are left. The algorithm is shown in Algorithm 5 below. It is straightforward to prove that with $N_T = n_T + 1$, the algorithm is optimal. Note that the algorithm also provides us with the unconstrained precoding matrix $\boldsymbol{M}^{(u)} = \boldsymbol{H}[\omega]^\dagger$. Also note that the operations in the “update inverse” step are computed in the previous step.

### Simulation Results

In the simulations we compare the BER obtained by the different antenna selection criteria with a system without antenna selection, i.e., $N_T = n_T$ and a system that

**Algorithm 5** Decremental antenna subset selection algorithm

INPUT: $\boldsymbol{H}$; $N_T \geq n_T \geq K$;
$\omega = \{1, ..., K\}$ % start with all antennas selected ;
$\boldsymbol{A}^{-1} = (\boldsymbol{H}^H \boldsymbol{H})^{-1}$ %this is the only inverse computed;
FOR $i = 1 : N_T - n_T$ DO
  find $i^* = \arg\min_{i \in \omega} \mathrm{tr}(\boldsymbol{A}^{-1}\boldsymbol{h}_i(1 - \boldsymbol{h}_i^H \boldsymbol{A}^{-1}\boldsymbol{h}_i)\boldsymbol{h}_i^H \boldsymbol{A}^{-1})$;
  $\boldsymbol{A}^{-1} = \boldsymbol{A}^{-1} + \boldsymbol{A}^{-1}\boldsymbol{h}_{i^*}(1 - \boldsymbol{h}_{i^*}^H \boldsymbol{A}^{-1}\boldsymbol{h}_{i^*})\boldsymbol{h}_{i^*}^H \boldsymbol{A}^{-1}$; %update inverse
  $\boldsymbol{H} = \boldsymbol{H} \backslash \boldsymbol{h}_{i^*}$; %remove the column
  $\omega = \omega \setminus i^*$; %remove that antenna index from the selected subset
END FOR
OUTPUT: $\omega$, $\boldsymbol{H}[\omega] = \boldsymbol{H}$ and $\boldsymbol{M}^{(u)} = \boldsymbol{H}_\omega^H \boldsymbol{A}^{-1}$.

employs the $N_T$ available transmit antennas. The BER is approximated by BER = $Q(\sqrt{(}\mathrm{SNR}_k))$, which is constant across the users because of the precoding operation. Fig. 3.15 illustrates the BER when $N_T = 6$, $n_T = 4$, $K = 4$ and $\sigma_n^2 = 1$, where the BER is averaged over 1000 different channel realizations. It is seen that antenna selection in MISO systems can bring an important performance improvement over systems without antenna selection. Note that the maximus Frobenius norm antenna selection criterion (i.e., select the antennas that see the best propagation channel in terms of power) is not a good approach in multiuser MISO systems. On the other hand, the suboptimal decremental selection algorithm achieves approximately the same performance as the optimal antenna selection (the curves overlap). It is also seen that antenna selection achieves the same diversity as the full system, where diversity is defined as $\gamma = -\lim_{P_T \to \infty} \frac{\log \mathrm{BER(P_T)}}{\log P_T}$ and the power loss is around 1.5dB. Therefore, antenna selection can be seen as a good alternative to boost the performance of this systems. Fig. 3.16 shows similar results for $N_T = 12$, $n_T = 6$ and $K = 6$; and Fig. 3.17 for $N_T = 6, n_T = 5$ and $K = 5$. Even with only one extra antenna element, the performance improvement is considerably.

## 3.7 Conclusions

We have developed MIMO antenna selection algorithms based on various performance criteria in situations where only noisy estimates of the channels are available. The proposed techniques are based on the discrete stochastic approximation algorithms found in the recent operations research literature, which generate a sequence of antenna subsets where each new subset is obtained from the previous one by taking a small step in a good direction towards the global optimizer. One

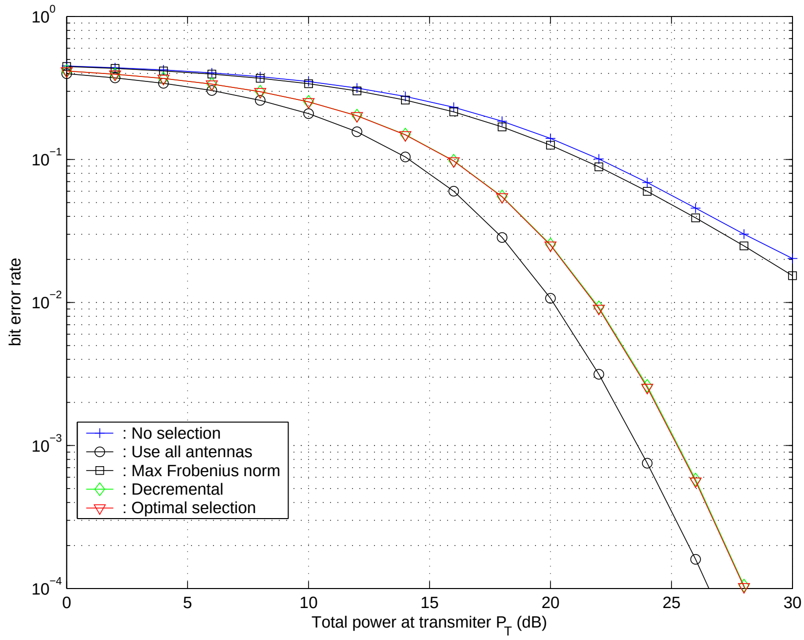


Figure 3.15: bit error rate for different transmit antenna selection algorithms ($N_T = 6, n_T = 4, K = 4$).

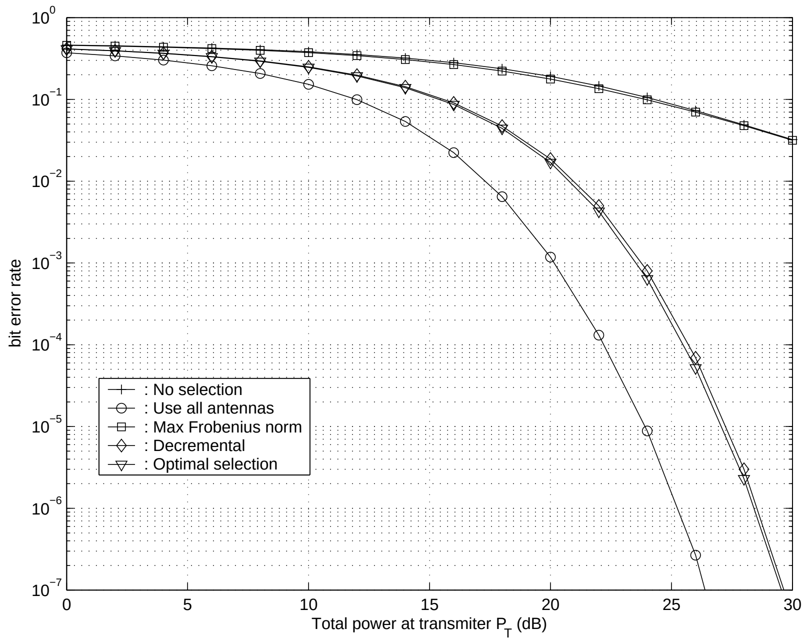


Figure 3.16: bit error rate for different transmit antenna selection algorithms ($N_T = 12, n_T = 6, K = 6$).

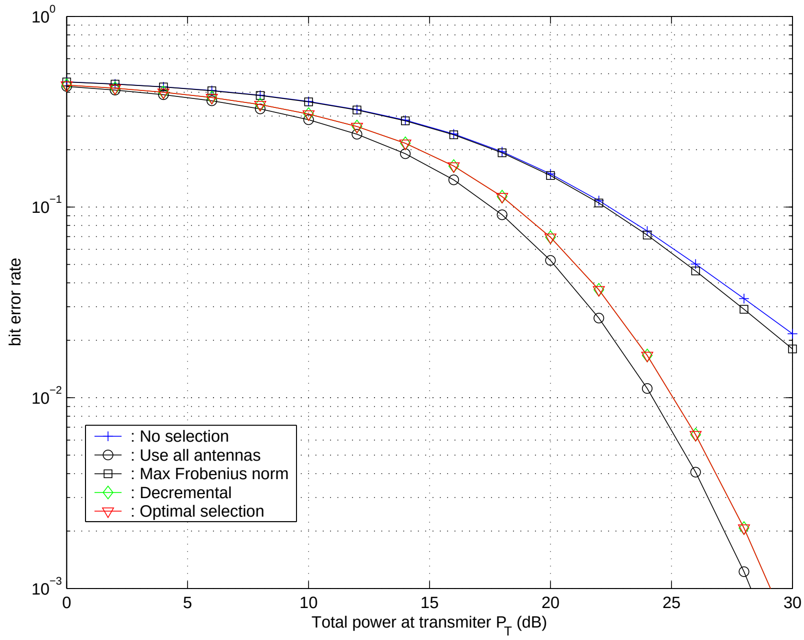


Figure 3.17: bit error rate for different transmit antenna selection algorithms ($N_T = 6, n_T = 5, K = 5$).

salient feature of the proposed approach is that no closed-form expression for the objective function is needed and only an estimate of it is sufficient. Therefore, the algorithm is able to choose the antenna subset that minimize the bit, symbol or frame error rate, under any MIMO techniques (e.g., BLAST, space-time coding) and any receiver detection methods.

We have also developed antenna selection algorithms for time-varying scenarios where the optimal antenna subset is slowly varying. By employing the constant or adaptive step-size discrete stochastic approximation algorithms, the time-varying optimal antenna configuration can be closely tracked. We have provided extensive simulation results to demonstrate the performance of these new MIMO antenna selection algorithms under various selection criteria.

Finally, we have presented very low complexity greedy antenna selection algorithms that can achieve nearly optimum performance in various MIMO configurations.

# Chapter 4

# Design of minimum error rate LAttice Space-Time (LAST) codes

## 4.1 Introduction

Wireless communications using multiple transmit and receive antennas can increase the multiplexing gain (i.e., throughput) and diversity gain (i.e., robustness) in fading channels [136]. It has been shown in [136] that for any given number of antennas there is a fundamental tradeoff between these two gains. That work establishes a framework to compare existing space-time systems against the optimal multiplexing-diversity tradeoff curve. Pioneering works on space-time architectures have focused on maximizing either the diversity gain [114, 115, 118] or the multiplexing gain [42]. More recent contributions have proposed space-time architectures that achieve simultaneously good diversity and multiplexing performance [58, 116] and other space-time architectures have been shown to achieve the optimal diversity-multiplexing tradeoff curve for some specific number of antennas and code length [13, 27, 32, 43, 108, 134]. In particular, in [43] the authors propose lattice space-time (LAST) codes that achieve the optimum diversity-multiplexing tradeoff in delay-limited MIMO channels with the use of low complexity lattice decoders in combination with a minimum mean square error generalized decision feedback equalizer (MMSE-GDFE) front-end. Unfortunately, the diversity-multiplexing tradeoff framework does not quantify the coding gain or error rate at the signal-to-noise (SNR) ratio of interest (notice that the tradeoff gives asymptotic results). That is, for two LAST code designs with the same tradeoff, different error rate performance can be obtained at the SNR of interest.

Minimum-error rate high dimensional lattice codes have been extensively studied for AWGN single-input single-output (SISO) channels when maximum likelihood (ML) decoding or lattice decoding are used [22]. In general, these lattice codes have been obtained using algebraic number theoretic tools and assuming the optimal ML (or lattice) decoder. However, these lattice codes are not necessarily optimal in the sense of minimum error rate for MIMO fading channels or for other receiver structures. In this chapter, we propose to design spherical LAST codes under a minimum error-rate criterion by employing a stochastic approximation technique based on the well known Robbins-Monro algorithm [101] together with unbiased gradient estimation. Stochastic optimization techniques focus on problems where the objective function, in this case the error rate, is sufficiently complex so that it is not possible to obtain a closed-form analytical solution. In our problem, we minimize the error rate function over a set of possible vector parameters (i.e., possible generators of the LAST codebook) satisfying some constraints, in this case the average power at the transmitter. An iterative algorithm is used (a step-by-step procedure) for moving from an initial guess to a final value that is expected to be closer to the true optimum. This is in contrast to classical deterministic search and optimization, where it is assumed that one has perfect information about the objective function and derivatives and that this information is used to determine the search direction in a deterministic manner at every step of the algorithm. Our designs can be tailored to optimize the spherical LAST codes given a particular SNR, channel statistics, and receiver scheme. We show that the design procedure is universal in the sense that it permits the design of LAST codes for a wide range of channel statistics, receiver structures or even for cooperative relying environments. Loosely speaking, the problem of finding a good LAST code for MIMO transmission can be seen as finding a $n$-dimensional constellation belonging to a $n$-dimensional lattice such that the error rate is minimized given a specific receiver structure and channel statistics, subject to a maximum transmission power constraint. Numerical results show that our codes generally outperform lattice codes that are designed for AWGN channels with optimal ML decoding when they are employed in MIMO fading channels.

The rest of the chapter is organized as follows. Section 4.2 introduces the system model for LAST codes, codebook construction, and various LAST detectors. In Section 4.3 we discuss the LAST code design procedure and the proposed stochastic optimization algorithm. In Section 4.4 some simulation results are provided. Section 4.5 extends the LAST design to a space-time cooperative scenario, while Section 4.6 concludes the chapter.

## 4.2 System Model and LAST Codes

In this section we review the MIMO communication system used in LAST code transmission [43]. Consider the $n_T$-transmit $n_R$-receive multiple-input multiple-output (MIMO) channel with no channel state information (CSI) at the transmitter and perfect CSI at the receiver. The wireless channel is assumed to be quasistatic and flat fading and can be represented by a $n_R \times n_T$ matrix $\boldsymbol{H}^c$ whose element $h_{ij}^c$ represents the complex gain of the channel between the $j$th transmit antenna and the $i$th receive antenna and is assumed to remain fixed for $t = 1, ..., T$. The received signal can be expressed as

$$\boldsymbol{y}_t^c = \sqrt{\frac{\rho}{n_T}} \boldsymbol{H}^c \boldsymbol{x}_t^c + \boldsymbol{w}_t^c, \tag{4.1}$$

where $\{\boldsymbol{x}_t^c \in \mathbb{C}^{n_T} : t = 1, ..., T\}$ is the transmitted signal, $\{\boldsymbol{y}_t^c \in \mathbb{C}^{n_R} : t = 1, ..., T\}$ is the received signal, $\{\boldsymbol{w}_t^c \in \mathbb{C}^{n_R} : t = 1, ..., T\}$ denotes the channel Gaussian noise, and with the power constraint $E\{\frac{1}{T}\sum_{t=1}^{T} |\boldsymbol{x}_t^c|^2\} \leq n_T$, the parameter $\rho$ is the average SNR per receive antenna independent of the number of transmit antennas. The entries of $\boldsymbol{w}_t$ are independent and identically distributed (i.i.d) circularly symmetric complex Gaussian variables with unit variance, i.e., $\boldsymbol{w}_{t,i} \sim \mathcal{N}_c(0, 1)$. The equivalent real channel model corresponding to $T$ symbol intervals can be written as

$$\boldsymbol{y} = \boldsymbol{H}\boldsymbol{x} + \boldsymbol{w}, \tag{4.2}$$

where $\boldsymbol{x} = [\boldsymbol{x}_1^T, ..., \boldsymbol{x}_T^T]^T \in \mathbb{C}^{2n_T T}$ is a codeword belonging to a codebook $\mathcal{C}$ with

$$\boldsymbol{x}_t^T = [\Re\{\boldsymbol{x}_t^c\}^T, \Im\{\boldsymbol{x}_t^c\}^T]^T, \tag{4.3}$$

$\boldsymbol{w} = [\boldsymbol{w}_1^T, ..., \boldsymbol{w}_T^T]^T \in \mathbb{C}^{2n_R T}$ with

$$\boldsymbol{w}_t^T = [\Re\{\boldsymbol{w}_t^c\}^T, \Im\{\boldsymbol{w}_t^c\}^T]^T \tag{4.4}$$

and

$$\boldsymbol{H} = \sqrt{\frac{\rho}{n_T}} \boldsymbol{I} \otimes \begin{bmatrix} \Re\{\boldsymbol{H}^c\} & -\Im\{\boldsymbol{H}^c\} \\ \Im\{\boldsymbol{H}^c\} & \Re\{\boldsymbol{H}^c\} \end{bmatrix}. \tag{4.5}$$

The goal of this chapter is the design of the codebook $\mathcal{C} \subseteq \mathbb{R}^{2n_T T}$ with the constraint that the codewords $\boldsymbol{x} \in \mathcal{C}$ belong to a lattice and satisfy the average power constraint

$$\frac{1}{|\mathcal{C}|} \sum_{\boldsymbol{x} \in \mathcal{C}} |\boldsymbol{x}|^2 \leq T n_T. \tag{4.6}$$

Note that the rate of the code is $R = \frac{1}{T}\log_2 |\mathcal{C}|$ bit/s/Hz. Next we review some lattice properties.

***Basic Lattice Definitions :*** An $n$-dimensional lattice $\Lambda$ is defined by a set of $n$ basis (column) vectors $\boldsymbol{g}_1, ..., \boldsymbol{g}_n$ in $\mathbb{R}^n$ [22]. The lattice is composed of all integral combinations of the basis vectors, i.e.,

$$\Lambda = \{\boldsymbol{x} = \boldsymbol{G}\boldsymbol{z} : \boldsymbol{z} \in \mathbb{Z}^n\} \tag{4.7}$$

where $\mathbb{Z} = \{0, \pm 1, \pm 2, ...\}$, and the $n \times n$ generator matrix $\boldsymbol{G}$ is given by $\boldsymbol{G} = [\boldsymbol{g}_1, \boldsymbol{g}_2, \cdots, \boldsymbol{g}_n]$. Note that the zero vector is always a lattice point and $\boldsymbol{G}$ is not unique for a given $\Lambda$. In the Euclidean space, the closest lattice point quantizer $\mathcal{Q}(\cdot)$ associated with $\Lambda$ is defined by

$$\mathcal{Q}(\boldsymbol{r}) = \boldsymbol{x} \in \Lambda, \quad \text{if} \quad \|\boldsymbol{r} - \boldsymbol{x}\| \le \|\boldsymbol{r} - \boldsymbol{x}'\|, \quad \forall \boldsymbol{x}' \in \Lambda. \tag{4.8}$$

The Voronoi cell of $\Lambda$ is the set of points in $\mathbb{R}^n$ closest to the zero codeword, i.e.,

$$\mathcal{V}_0 = \{\boldsymbol{r} \in \mathbb{R}^n : \mathcal{Q}(\boldsymbol{r}) = \boldsymbol{0}\} \tag{4.9}$$

The Voronoi cell associated with each $\boldsymbol{x} \in \Lambda$ is a shift of $\mathcal{V}_0$ by $\boldsymbol{x}$. The volume of the Voronoi cell is given by $V(\Lambda) = \sqrt{\det(\boldsymbol{G}^T\boldsymbol{G})}$.

***LAST codebook construction :*** Consider the dimension of the lattice generated by $\boldsymbol{G}$ to be $n = 2n_T T$. A finite set of points in the $n$-dimensional lattice can be used as codewords of a codebook $\mathcal{C}$. Given a bit rate $R$ bit/s/Hz, the codebook will contain $|\mathcal{C}| = 2^{T \cdot R}$ lattice points. In particular, the codewords consist of all lattice points inside a shaping region $\mathcal{S}$. In spherical LAST codes, the shaping region is a sphere, having in general the lowest possible energy. To find the code with smallest total average power, we consider the codebook obtained using a sphere centered at $-\boldsymbol{u} \in \mathbb{R}^n$ and the codeword coordinates are given by the Euclidean difference between the center of the sphere and the lattice points. That is, the code is specified by the generator matrix $\boldsymbol{G}$, the translation vector $\boldsymbol{u}$, and the radius of the sphere, i.e.,

$$\mathcal{C} = (\Lambda + \boldsymbol{u}) \cap \mathcal{S} \tag{4.10}$$

where the cardinality of the codebook (i.e., the rate) is a function of the radius of the sphere. If we form the intersection of the sphere of volume $V(\mathcal{S})$ with the lattice of Voronoi volume $V(\Lambda)$ we could expect to obtain a code with about $V(\mathcal{S})/V(\Lambda)$ codewords. In fact, the value $V(\mathcal{S})/V(\Lambda)$ is correct on average although it is clear that there are some codes that have more and some that have less. It is easily proven

[86] that at least one value of $\boldsymbol{u} \in \mathbb{R}^n$ exists, such that $|(\Lambda+\boldsymbol{u})\cap\mathcal{S}| \geq V(\mathcal{S})/V(\Lambda)$. Among all the possible choices for $\boldsymbol{u}$, we are interested in the one that leads to a code of the smallest average energy $\frac{1}{|\mathcal{C}|}\sum_{\boldsymbol{x}\in\mathcal{C}}|\boldsymbol{x}|^2$. Using the centroid, an iterative algorithm is shown in [23] to find the translation vector $\boldsymbol{u}$ which generates a codebook with minimum energy. Hence, given a translation vector, the codewords

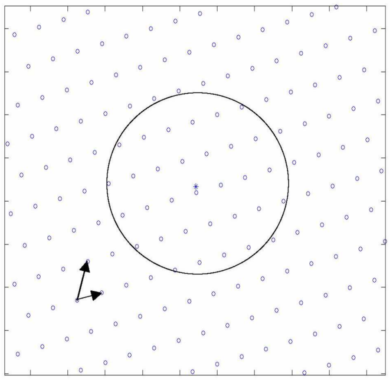

Figure 4.1: A 2-dimensional lattice (two basis vectors $\boldsymbol{g}_1$ and $\boldsymbol{g}_2$), translation vector, and spherical shaping region.

are obtained by taking $|\mathcal{C}|$ lattice points in the shifted lattice $\Lambda + \boldsymbol{u}$ that are closer to $\boldsymbol{u}$ as shown in Figure 4.1 for the hypothetical 2-dimensional case [1]. A method to enumerate all the lattice points in a sphere is given in Appendix B. To speed up the enumeration of all the lattice points inside the sphere centered at $\boldsymbol{u}$, the radius of the sphere or the lattice generator should be scaled such that $V(\mathcal{S})/V(\Lambda) \simeq |\mathcal{C}|$ [2]. Once the codewords have been found, a second scaling factor $\beta$ should be applied to guarantee the energy constraint at the transmitter $Tn_T$, i.e.,

$$\beta = \left(\frac{MT|\mathcal{C}|}{\sum_{\boldsymbol{x}\in\mathcal{C}}|\boldsymbol{x}|^2}\right)^{1/2} \tag{4.11}$$

and the translation vector and the generator are scaled as $\beta\boldsymbol{G}$ and $\beta\boldsymbol{u}$, respectively.

### 4.2.1 LAST detectors

Given the input-output relation in (4.2) the task of a LAST detector is to recover the transmitted codeword $\boldsymbol{x}$ (or its corresponding integer coordinates $\boldsymbol{z}$) from the

[1]In this chapter we use either $\boldsymbol{x}$ or its integer coordinates $\boldsymbol{z}$ to refer to each codeword, since for any codeword $\boldsymbol{x}$ there is a univocal relation $\boldsymbol{x} = \boldsymbol{G}\boldsymbol{z} + \boldsymbol{u}$.

[2]The volume of a $n$-dimensional sphere (hypersphere) of radius $\rho$ and $n$ even is computed as $V_n = V_n^{(1)}\rho^n$ where $V_n^{(1)}$ is the volume of a sphere of radius 1 and is given by $V_n^{(1)} = \frac{\pi^{n/2}}{(n/2)!}$.

received signal $\boldsymbol{y}$. Next we overview some LAST detectors, which are also outlined in Fig. 4.2.

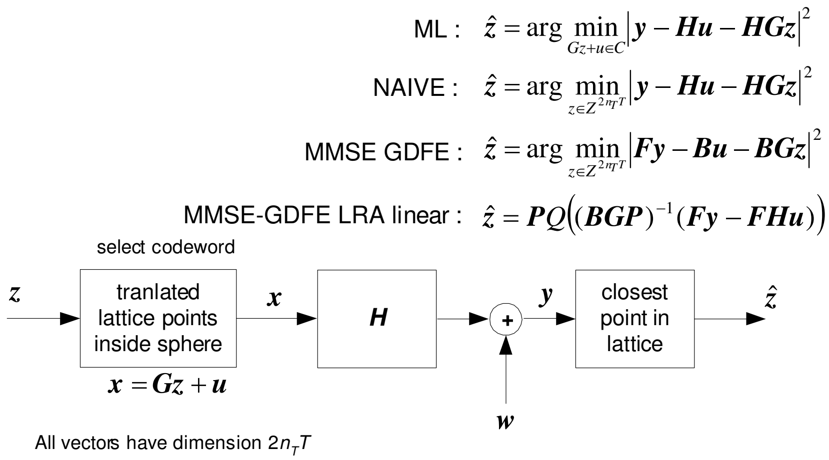


Figure 4.2: Spherical LAST codes and different detectors.

***Maximum likelihood decoding:*** The maximum likelihood detector (ML) is the optimal receiver in terms of error rate. The ML detection rule is given by

$$\hat{\boldsymbol{z}} = \arg \min_{\boldsymbol{Gz}+\boldsymbol{u}\in\mathcal{C}} \|\boldsymbol{y} - \boldsymbol{Hu} - \boldsymbol{HGz}\| . \tag{4.12}$$

The minimization is performed over all possible codewords in the codebook $\mathcal{C}$. Note that the decoding regions are not identical due to the boundary of the codebook and in fact some are not bounded. This breaks the symmetry of the lattice structure in the decoding process, making the decoding process too complex.

***MMSE-GDFE lattice decoder:*** In lattice decoding, the receiver is not aware of the boundary of the codebook (e.g., the spherical shaping region $\mathcal{S}$ employed in spherical LAST codes) and assumes that any point in the infinite lattice may be transmitted, corresponding to infinite power and transmission rate. For a given lattice, the lattice decoder will search for the lattice point that is nearest to the received vector, whether or not this point lies in $\mathcal{S}$. This decoder is known as the naive closest point in the lattice

$$\hat{\boldsymbol{z}} = \arg \min_{\boldsymbol{z}\in\mathbb{Z}^{2Tn_T}} \|\boldsymbol{y} - \boldsymbol{Hu} - \boldsymbol{HGz}\| . \tag{4.13}$$

Note that this receiver should be distinguished from the nearest-codeword decoder, which decodes to the nearest lattice point inside $\mathcal{S}$. The attractive symmetry and periodic properties commonly associated with lattices allows low complexity algorithms to solve the closest point in the lattice problem expressed in (4.13) (see [2] for an overview).

More recently, based on initial results presented in [35] it has been shown in [43] that a MMSE-GDFE front-end can further improve the performance of the lattice decoding algorithms in MIMO systems. Given uncorrelated inputs and noise, with mean zero and covariance $\boldsymbol{I}$, the feedforward (FF) and feedback (FB) MMSE-GDFE matrices are denoted by $\boldsymbol{F}$ and $\boldsymbol{B}$ respectively. In particular, $\boldsymbol{B}$ is obtained from the Cholesky factorization $\boldsymbol{B}^T\boldsymbol{B} = \boldsymbol{I}_{2Tn_T} + \boldsymbol{H}^T\boldsymbol{H}$ and is upper triangular with positive diagonal elements and $\boldsymbol{F}^T = \boldsymbol{H}\boldsymbol{B}^{-1}$. In this case, the MMSE-GDFE closest point lattice decoder returns

$$\hat{\boldsymbol{z}} = \arg\min_{\boldsymbol{z}\in\mathbb{Z}^{2Tn_T}} \|\boldsymbol{F}\boldsymbol{y} - \boldsymbol{B}\boldsymbol{u} - \boldsymbol{B}\boldsymbol{G}\boldsymbol{z}\|\,, \tag{4.14}$$

which essentially finds the point in the lattice generated by $\boldsymbol{B}\boldsymbol{G}$ that is closer to the point $\boldsymbol{F}\boldsymbol{y} - \boldsymbol{B}\boldsymbol{u}$.

***MMSE-GDFE lattice-reduction-aided linear receiver:*** A combination of the MMSE-GDFE front-end and the lattice-reduction-aided (LRA) linear receiver described in Section 2.5.4 can be used to simplify the detector. The LRA receiver makes a change of basis such that the decision regions of the detectors are improved and more robust to noise. The change of basis is obtained via lattice reduction. Consider the MMSE-GDFE matrices $\boldsymbol{F}$ and $\boldsymbol{B}$. Applying the MMSE-GDFE front-end and removing the translation vector gives

$$\boldsymbol{y}' = \boldsymbol{F}\boldsymbol{y} - \boldsymbol{F}\boldsymbol{H}\boldsymbol{u} = \boldsymbol{B}\boldsymbol{G}\boldsymbol{z} + \underbrace{\boldsymbol{F}\boldsymbol{w} - [\boldsymbol{B} - \boldsymbol{F}\boldsymbol{H}]\boldsymbol{G}\boldsymbol{z}}_{\boldsymbol{n}} = \boldsymbol{B}\boldsymbol{G}\boldsymbol{z} + \boldsymbol{n}. \tag{4.15}$$

Consider the lattice with generator matrix $\boldsymbol{B}\boldsymbol{G}$. If $\boldsymbol{B}\boldsymbol{G}$ is a basis of the lattice, $\boldsymbol{B}\boldsymbol{G}\boldsymbol{P}$ also is a basis of the same lattice if $\boldsymbol{P}$ and $\boldsymbol{P}^{-1}$ have integer entries. The aim of the LRA receiver is to find a change of basis $\boldsymbol{P}$ that transforms the generator into $\boldsymbol{B}\boldsymbol{G}\boldsymbol{P}$ to optimize the decision regions of the detector [133]. This problem is known as the lattice reduction problem. The goal of lattice basis reduction is, given an arbitrary lattice basis, to obtain a basis of the shortest possible vectors; that is, vectors as close as possible to being mutually orthogonal. The simplest way to reduce the basis is the LLL reduction algorithm [87]. Other types of reduced bases are the Korkin-Zolotarev (KZ) basis [10, 73], the Minkowski basis [1], the Seysen basis [109], and hybrids [104], which have different reduction criteria. These bases have, in general, slightly better properties, although the reduction is more time consuming. The idea behind LRA linear receivers is to assume that the signal was transmitted in the reduced basis, i.e., $\boldsymbol{y}' = \boldsymbol{B}\boldsymbol{G}\boldsymbol{P}(\boldsymbol{P}^{-1}\boldsymbol{z}) + \boldsymbol{n}$, to equalize in the new basis, which is more robust against noise enhancement, and then return the decoded symbol to the original basis. That is,

$$\hat{\boldsymbol{z}} = \boldsymbol{P}\mathcal{Q}\left((\boldsymbol{BGP})^{-1}\boldsymbol{y}'\right) \tag{4.16}$$

where the quantizer $\mathcal{Q}(\cdot)$ rounds to the nearest integer.
***Other receivers:*** Other receivers can be used to decode LAST codes for example standard linear receivers (based either on MMSE of ZF) or nulling and cancellation in combination with lattice reduction and the MMSE-GDFE front-end.

## 4.3 Spherical LAST codes optimization

In this section we describe a systematic procedure for designing the minimum error rate spherical LAST codes.

### 4.3.1 Lattice design in AWGN SISO channels and ML decoding

In an $n$-dimensional Euclidean space and for AWGN channels the lattice code design asks for the best arrangement of points in the space such that for a given number of codewords, transmit power constraint, and noise statistics, the probability of error of the maximum likelihood decoder is minimized. In this situation, there are a number of desirable properties that a code should satisfy: a) the number of code vectors should be large; b) the average energy (or alternatively the peak energy) should be small, that is, the regions of space defining the code should be as nearly spherical as possible; c) the minimum distance between codewords should be large; mapping and demapping should be easily implemented; d) given an arbitrary point in the space, it should be easy to find the closest codeword. The lattice design problem has been extensively studied in the literature and good lattice codes have been found for different dimensions [22, 33, 86]. However, wireless MIMO communications do not signal over AWGN channels but over fading channels, with some known statistics. Moreover, the receiver is not necessarily the complex ML decoder. It turns out that good lattice codes for AWGN SISO channels and ML decoder are not necessarily good for MIMO fading channels. In the following sections we propose a procedure to design error efficient lattices that are tailored for the specific receiver structure and MIMO channel statistics (i.e., when these are known a priori).

### 4.3.2 Preliminaries concerning stochastic optimization and problem formulation

Note that the analytical expression for the error rate performance in any of the detectors presented previously is intractable. Simulation-based optimization turns out to be powerful for this scenario [111]. In particular, we consider simulation-based algorithms where only noisy information about the objective function and gradient can be obtained via the simulation.

Our goal is to compute the optimal lattice generator matrix $\boldsymbol{G}$ so as to minimize the average block error rate probability denoted as $\Upsilon(\boldsymbol{G})$ (i.e., objective function) with the following power constraint

$$\min_{\boldsymbol{G}\in\Theta} \Upsilon(\boldsymbol{G}), \quad \text{with} \quad \Theta = \{\boldsymbol{G} : \sum_{\boldsymbol{Gz}+\boldsymbol{u}\in\mathcal{C}} |\boldsymbol{Gz}+\boldsymbol{u}|^2 \leq MT\} \tag{4.17}$$

where $\Theta$ represents the set of lattice generators that satisfy the energy constraint at the transmitter. The constraint is achieved through the scaling factor $\beta$ in (4.11). Notice that we use either $\boldsymbol{x}$ or $\boldsymbol{Gz}+\boldsymbol{u}$ to refer to the codewords. Denote $\gamma(\boldsymbol{y}, \boldsymbol{z}, \boldsymbol{H}, \boldsymbol{G})$ as the empirical (i.e., noisy) block error rate for a given generator matrix $\boldsymbol{G}$, transmitted coordinates $\boldsymbol{z}$, received signal $\boldsymbol{y}$, and channel matrix $\boldsymbol{H}$, i.e., $\gamma(\boldsymbol{y}, \boldsymbol{z}, \boldsymbol{H}, \boldsymbol{G}) = 1$, if $\hat{\boldsymbol{z}} = \boldsymbol{z}$ (i.e., the decoded vector is equivalent to the transmitted vector) and 0 otherwise. Then the average block error rate is obtained by $\Upsilon(\boldsymbol{G}) = E\{\gamma(\boldsymbol{y}, \boldsymbol{z}, \boldsymbol{H}, \boldsymbol{G})\}$.

Since in general there is no closed form expression for the average block error rate $\Upsilon(\boldsymbol{G})$ we propose to use a stochastic gradient algorithm to optimize it. The aim of gradient estimation is to compute an unbiased estimate of the true gradient. Let $\hat{g}(\boldsymbol{G})$ denote an estimate of $\nabla_G \Upsilon(\boldsymbol{G})$. We consider the case in which $E\{\hat{g}(\boldsymbol{G})\} = \nabla_G \Upsilon(\boldsymbol{G})$. The constrained Robbins-Monro (R-M) simulation-based algorithm [101] is of the form

$$\boldsymbol{G}_{k+1} = \Pi_\Theta(\boldsymbol{G}_k - a_k \hat{\boldsymbol{g}}(\boldsymbol{G}_k)) \tag{4.18}$$

where $\boldsymbol{G}_k$ is the solution after the $k$th iteration, $\hat{g}(\boldsymbol{G}_k)$ is an estimate of $\nabla_G \Upsilon(\boldsymbol{G})|_{G=G_k}$, $\{a_k\}$ is a decreasing step size sequence of positive real numbers such that $\sum_{k=1}^{\infty} a_k = \infty$ and $\sum_{k=1}^{\infty} a_k^2 < \infty$, and the function $\Pi_\Theta$ projects each matrix $\boldsymbol{G}_k$ into the nearest point in $\Theta$. For the R-M algorithm to converge, the gradient estimate should be unbiased. The step-size sequence $\{a_k\}$ is usually chosen as the harmonic series $a_k = c/k$, where $c$ is a positive scalar. The R-M algorithm will converge with probability one to a local stationary point of $\Upsilon(\boldsymbol{G})$ [78].

### 4.3.3 Lattice Design via Stochastic Approximation based on Gradient Estimation

Consider again the LAST system model

$$\boldsymbol{y} = \boldsymbol{H}(\boldsymbol{G}\boldsymbol{z} + \boldsymbol{u}) + \boldsymbol{w}. \tag{4.19}$$

The average block error rate is obtained by $\Upsilon(\boldsymbol{G}) = E\{\gamma(\boldsymbol{y}, \boldsymbol{z}, \boldsymbol{H}, \boldsymbol{G})\}$, where $\gamma(\boldsymbol{y}, \boldsymbol{z}, \boldsymbol{H}, \boldsymbol{G})$ is the empirical block error-rate given $\boldsymbol{H}, \boldsymbol{G}$, and $\boldsymbol{z}$. We can write,

$$\begin{aligned} \Upsilon(\boldsymbol{G}) &= E(\gamma(\boldsymbol{y}, \boldsymbol{z}, \boldsymbol{H}, \boldsymbol{G})) \\ &= \int\int\int \gamma(\boldsymbol{y}, \boldsymbol{z}, \boldsymbol{H}, \boldsymbol{G}) p(\boldsymbol{y}, \boldsymbol{z}, \boldsymbol{H}|\boldsymbol{G}) d\boldsymbol{y} d\boldsymbol{z} d\boldsymbol{H}, \end{aligned} \tag{4.20}$$

where $p(\boldsymbol{y}, \boldsymbol{z}, \boldsymbol{H}|\boldsymbol{G})$ is the joint probability density function (pdf) of $(\boldsymbol{y}, \boldsymbol{z}, \boldsymbol{H})$ for a given $\boldsymbol{G}$. Note that the empirical block error rate $\gamma(\cdot)$ cannot usually be given in closed form and it also depends on the structure of the receiver. Therefore, (4.20) cannot be evaluated analytically. The design goal is to solve the minimization problem $\min \Upsilon_{\boldsymbol{G}\in\Theta}(\boldsymbol{G})$, where the constraint $\Theta$ guarantees the average power of the codewords. Note that

$$\Upsilon(\boldsymbol{G}) = E_z E_H E_{y|z,H,G}\{\gamma(\boldsymbol{y}, \boldsymbol{z}, \boldsymbol{H}, \boldsymbol{G})\}, \tag{4.21}$$

where

$$E_{y|z,H,G}\{\gamma(\boldsymbol{y}, \boldsymbol{x}, \boldsymbol{H}, \boldsymbol{G})\} = \int \gamma(\boldsymbol{y}, \boldsymbol{x}, \boldsymbol{H}, \boldsymbol{G}) p(\boldsymbol{y}|\boldsymbol{z}, \boldsymbol{H}, \boldsymbol{G}) d\boldsymbol{y}. \tag{4.22}$$

For a given channel realization $\boldsymbol{H}$, codeword $\boldsymbol{z}$, and lattice generator $\boldsymbol{H}$, $\boldsymbol{y}$ in (4.19) is Gaussian with mean $\boldsymbol{H}\boldsymbol{G}\boldsymbol{z} + \boldsymbol{H}\boldsymbol{u}$ and covariance matrix $\frac{1}{2}\boldsymbol{I}_{2MT}$, specifically

$$p(\boldsymbol{y}|\boldsymbol{z}, \boldsymbol{H}, \boldsymbol{G}) = \pi^{-TM} \exp\left[-(\boldsymbol{y}-\boldsymbol{H}\boldsymbol{G}\boldsymbol{z}-\boldsymbol{H}\boldsymbol{u}^*)^T(\boldsymbol{y}-\boldsymbol{H}\boldsymbol{G}\boldsymbol{z}-\boldsymbol{H}\boldsymbol{u}^*)\right]. \tag{4.23}$$

On the other hand, $\nabla_G \Upsilon(\boldsymbol{G})$ cannot be computed analytically, and therefore the constrained R-M iterative optimization algorithm in (4.18) is not straightforward to apply. Fortunately, the parameters $\Upsilon(\boldsymbol{G})$ and $\nabla_G \Upsilon(\boldsymbol{G})$ can be estimated. The gradient of $\Upsilon(\boldsymbol{G})$ with respect to $\boldsymbol{G}$ for a given $\boldsymbol{G}$ is given as

$$\begin{aligned}\nabla_G \Upsilon(\boldsymbol{G}) &= E_z E_H \Big[\nabla_G E_{y|z,H,G}\{\gamma(\boldsymbol{y},\boldsymbol{z},\boldsymbol{H},\boldsymbol{G})\}\Big] \\ &= E_z E_H \int \nabla_G \Big\{\gamma(\boldsymbol{y},\boldsymbol{z},\boldsymbol{H},\boldsymbol{G}) p(\boldsymbol{y}|\boldsymbol{z},\boldsymbol{H},\boldsymbol{G})\Big\} d\boldsymbol{y} \\ &= E_z E_H \int \Big\{ \underbrace{\Big(\nabla_G \gamma(\boldsymbol{y},\boldsymbol{z},\boldsymbol{H},\boldsymbol{G})\Big)}_{0} p(\boldsymbol{y}|\boldsymbol{z},\boldsymbol{H},\boldsymbol{G}) \\ &\quad + \gamma(\boldsymbol{y},\boldsymbol{z},\boldsymbol{H},\boldsymbol{G}) \Big(\nabla_G p(\boldsymbol{y}|\boldsymbol{z},\boldsymbol{H},\boldsymbol{G})\Big)\Big\} d\boldsymbol{y} \\ &= E_z E_H \int \gamma(\boldsymbol{y},\boldsymbol{z},\boldsymbol{H},\boldsymbol{G}) \nabla_G p(\boldsymbol{y}|\boldsymbol{z},\boldsymbol{H},\boldsymbol{G}) d\boldsymbol{y} \qquad (4.24)\end{aligned}$$

where in (4.24), due to the discrete nature of $\boldsymbol{z} \in \mathbb{Z}^n$ and the definition of $\gamma(\cdot)$, we have applied that with probability one we have [127]

$$[\nabla_G \gamma(\boldsymbol{y},\boldsymbol{z},\boldsymbol{H},\boldsymbol{G})] = \mathbf{0}. \qquad (4.25)$$

Property (4.25) follows using that for $\boldsymbol{z} \in \mathbb{Z}^n$ and sufficiently small $\delta$ we have $\gamma(\boldsymbol{y},\boldsymbol{z},\boldsymbol{H},\boldsymbol{G}+\delta\boldsymbol{G}) = \gamma(\boldsymbol{y},\boldsymbol{z},\boldsymbol{H},\boldsymbol{G})$, see [127]. Then, we can rewrite (4.24) as

$$\begin{aligned}\nabla_G \Upsilon(\boldsymbol{G}) &= E_z E_H \int \gamma(\boldsymbol{y},\boldsymbol{z},\boldsymbol{H},\boldsymbol{G}) \underbrace{\frac{\nabla_G p(\boldsymbol{y}|\boldsymbol{z},\boldsymbol{H},\boldsymbol{G})}{p(\boldsymbol{y}|\boldsymbol{z},\boldsymbol{H},\boldsymbol{G})}}_{\nabla \log p(\boldsymbol{y}|\boldsymbol{z},\boldsymbol{H},\boldsymbol{G})} p(\boldsymbol{y}|\boldsymbol{z},\boldsymbol{H},\boldsymbol{G}) d\boldsymbol{y} \\ &= E_z E_H E_{y|z,H,G}\Big[\gamma(y,z,H,G) \nabla_G \log p(\boldsymbol{y}|\boldsymbol{z},\boldsymbol{H},\boldsymbol{G})\Big]. \qquad (4.26)\end{aligned}$$

We need to compute $\nabla_G \log p(\boldsymbol{y}|\boldsymbol{z},\boldsymbol{H},\boldsymbol{G})$, when $\boldsymbol{y} = \boldsymbol{H}(\boldsymbol{G}\boldsymbol{z} + \boldsymbol{u}) + \boldsymbol{w}$ and $p(\boldsymbol{y}|\boldsymbol{z},\boldsymbol{H},\boldsymbol{G})$ is given in (4.23). Notice that computing $\nabla_G \log p(\boldsymbol{y}|\boldsymbol{z},\boldsymbol{H},\boldsymbol{G})$ is equivalent to computing the gradient of $f(\cdot)$ with respect to $\boldsymbol{G}$, where we define $f(\cdot)$ as the exponent of (4.23) given by

$$\begin{aligned}f(\boldsymbol{G}) &= -(\boldsymbol{y} - \boldsymbol{H}\boldsymbol{G}\boldsymbol{z} - \boldsymbol{H}\boldsymbol{u}^*)^T(\boldsymbol{y} - \boldsymbol{H}\boldsymbol{G}\boldsymbol{z} - \boldsymbol{H}\boldsymbol{u}^*) \\ &= -\boldsymbol{y}^T\boldsymbol{y} + 2\boldsymbol{y}^T\boldsymbol{H}\boldsymbol{G}\boldsymbol{z} + 2\boldsymbol{y}^T\boldsymbol{H}\boldsymbol{u}^* - 2\boldsymbol{u}^{*T}\boldsymbol{H}^T\boldsymbol{H}\boldsymbol{G}\boldsymbol{z} \\ &\quad -\boldsymbol{u}^{*T}\boldsymbol{H}^T\boldsymbol{H}\boldsymbol{u}^* - \underbrace{\boldsymbol{z}^T\boldsymbol{G}^T\boldsymbol{H}^T\boldsymbol{H}\boldsymbol{G}\boldsymbol{z}}_{v(\boldsymbol{G})}. \qquad (4.27)\end{aligned}$$

The $(n,l)$th entry of the gradient of $v(\boldsymbol{G})$ defined in (4.27) can be computed as

$$\begin{aligned}\left[\frac{\partial v(\boldsymbol{G})}{\partial \boldsymbol{G}}\right]_{n,l} &= \lim_{\delta\to 0}\frac{v(\boldsymbol{G}+\delta\boldsymbol{e}_n\boldsymbol{e}_l^T)-v(\boldsymbol{G})}{\delta}\\ &= \lim_{\delta\to 0}\frac{2\boldsymbol{z}^T\boldsymbol{e}_l\boldsymbol{e}_n^T\boldsymbol{H}^T\boldsymbol{H}\boldsymbol{G}\boldsymbol{z}\delta+\boldsymbol{z}^T\boldsymbol{e}_l\boldsymbol{e}_n^T\delta\boldsymbol{H}^T\boldsymbol{H}\boldsymbol{e}_n\boldsymbol{e}_l^T\delta\boldsymbol{z}}{\delta}\\ &= 2\boldsymbol{z}_T\boldsymbol{e}_l\boldsymbol{e}_n^T\boldsymbol{H}^T\boldsymbol{H}\boldsymbol{G}\boldsymbol{z} \end{aligned}\tag{4.28}$$

where $\boldsymbol{e}_n$ is the $2MT$ vector with a one in the $n$-th position and zeros elsewhere. Therefore,

$$\left[\frac{\partial f(\boldsymbol{G})}{\partial \boldsymbol{G}}\right]_{n,l} = 2\boldsymbol{y}^T\boldsymbol{H}\boldsymbol{e}_n\boldsymbol{e}_l^T\boldsymbol{z}-2\boldsymbol{u}^T\boldsymbol{H}^T\boldsymbol{H}\boldsymbol{e}_n\boldsymbol{e}_l^T\boldsymbol{z}-2\boldsymbol{z}^T\boldsymbol{e}_l\boldsymbol{e}_n^T\boldsymbol{H}^T\boldsymbol{H}\boldsymbol{G}\boldsymbol{z}. \tag{4.29}$$

### 4.3.4 The algorithm

Assume that at the $k$th iteration the current lattice generator is $\boldsymbol{G}_k$. Perform the following steps during the next iteration to generate $\boldsymbol{G}_{k+1}$.
**Step 1 -** Composition method to generate mixture sample:

1. Draw $L$ coordinate vectors $\boldsymbol{z}_1,...,\boldsymbol{z}_L$ uniformly from the set of possible coordinates that generate the codebook.
2. Simulate $L$ observations $\boldsymbol{y}_1,...,\boldsymbol{y}_L$ where each $\boldsymbol{y}_i$ is generated according to the system model $\boldsymbol{y}_i = \boldsymbol{H}_i(\boldsymbol{G}_k\boldsymbol{z}_i+\boldsymbol{u}_k)+\boldsymbol{w}_i, \quad i=1,...,L$.
3. Using the given decoding algorithm, decode $\boldsymbol{z}_i$ based on the observations $\boldsymbol{y}_i$ and the channel value $\boldsymbol{H}_i, i=1,...,L$. Compute the empirical block error rate $\gamma(\boldsymbol{y}_i,\boldsymbol{z}_i,\boldsymbol{H}_i,\boldsymbol{G}_k)$.

**Step 2 -** Score function method for gradient estimation: Use (4.26), generate

$$\hat{g}(\boldsymbol{G}_k)=\frac{1}{L}\sum_{i=1}^{L}\gamma(\boldsymbol{y}_i,\boldsymbol{z}_i,\boldsymbol{H}_i,\boldsymbol{G}_k)\left[\nabla_G \log p(\boldsymbol{y}_i|\boldsymbol{z}_i,\boldsymbol{H}_i,\boldsymbol{G})|_{\boldsymbol{G}=\boldsymbol{G}_k}\right], \tag{4.30}$$

where the gradient is given in (4.29)
**Step 3 -** Update new lattice generator matrix $\boldsymbol{G}_{k+1}$: Generate

$$\boldsymbol{G}_{k+1}=\Pi_\Theta(\boldsymbol{G}_k-a_k\hat{g}(\boldsymbol{G}_k)), \tag{4.31}$$

where $a_k=c/k$ for some positive constant $c$. For a given lattice generator matrix $\boldsymbol{G}_k$, the projection function $\Pi_\Theta$ is defined as a scaling factor $\beta$ and translation vector ($\boldsymbol{u}_{k+1}$) so the power constraint in (4.17) is satisfied with equality. Note that the gradient estimator is unbiased for any integer $L$, but the variance decreases for larger values of $L$.

### Implementation aspects of the algorithm

There are some practical issues about the algorithm which are worth mentioning.

1. At each iteration of the algorithm the projection $\Pi_{\Theta}(\cdot)$ proceeds as follows: (1) Enumerate the $|\mathcal{C}|$ lattice points closer to $-\boldsymbol{u}$ (e.g., using the procedure given in Appendix B); (2) scale the generator matrix $\boldsymbol{G}$ using $\beta$ in (4.11) to satisfy (4.17). In our implementation we have assumed $\boldsymbol{u} = \mathbf{0}$ and the translation vector has been updated after the last iteration.

2. The speed of convergence of the algorithm is highly dependent upon the choice of the step-size $a_k = c/k$. The value of $c$ needs to be large enough so the step-size does not decrease too fast before moving to the vicinity of the optimal generator matrix. On the other hand, it should be small to make the solutions stable as soon as possible. A *good* vale of $c$ can be obtained heuristically comparing the initial Frobenius norm of $\boldsymbol{G}$ and the Frobenius norm of the estimated gradient.

3. It can be proved that the gradient estimator is unbiased and its variance decays with the number of samples $L$ in Step 1 of the algorithm. Hence, a larger number of samples $L$ can provide a better estimator of the gradient although it will slow the simulation. Instead of increasing the number of samples $L$, a different possibility is to use the same step-size value over multiple iterations, i.e., $a_k = c/\lceil (k/p) \rceil$, where $p$ is the number of iterations for which the step-size remains constant.

## 4.4 Simulation results

In this section, we provide multiple examples to show the performance of the new LAST codes obtained by the design procedure described in the previous section. We will see that the codes optimized for a particular SNR work acceptably over a wide range of SNR values of interest.

***LAST code design with MMSE-GDFE lattice decoder:*** Consider first $n_T = n_R = T = 2$ and $R = 4$ bit/s/Hz (i.e., a codebook with 256 codewords, and dimension $n = 8$). In the first iteration of the algorithm we use a random initial guess $\boldsymbol{G}_0$

properly scaled to satisfy $\Theta$. The code is designed for $\rho = 16$dB. We assume MMSE-GDFE lattice decoding. The code optimized for this scenario is given by [3]

$$\boldsymbol{G} = \begin{bmatrix} 0.6115 & 0.7220 & 0.1828 & 0.0047 & 0.4083 & 0.2432 & 0.3809 & 0.5912 \\ 0.2330 & 0.0415 & -0.6020 & 0.2606 & 0.3728 & -0.8860 & -0.4119 & 0.2633 \\ 0.5702 & -0.2313 & -0.4036 & 0.4560 & 0.2410 & 0.1998 & 0.4884 & -0.7502 \\ 0.5638 & -0.4284 & 0.2143 & 0.5062 & -0.2804 & 0.4311 & -0.6880 & 0.3297 \\ -0.4046 & 0.1748 & -0.0495 & 0.0595 & 0.8929 & 0.5190 & -0.5679 & -0.2452 \\ 0.1475 & 0.8923 & 0.0621 & 0.1454 & -0.5027 & -0.0977 & -0.4464 & -0.5875 \\ -0.2845 & -0.0036 & 0.8151 & 0.7903 & 0.2233 & -0.4233 & 0.2114 & -0.0767 \\ 0.5586 & -0.2500 & 0.6112 & -0.6839 & 0.3271 & -0.3490 & -0.2370 & -0.3855 \end{bmatrix}. \tag{4.32}$$

The block error rate convergence of the algorithm is shown in Fig. 4.3 averaged over 88 random initial lattice generators. The number of samples in the algorithm was set to $L = 17000$. It is seen that during the first iterations the algorithm rapidly moves towards a lattice generator with low block error rate. Next, for comparison purposes we report the block error rate performance using the LAST codebook obtained with the $8$-dimensional generator matrix given in El Gamal et. al [43] that we denote as GCD, and also for the LAST codebook obtained from the Gosset lattice $E_8$ given in [23], which is known to be good for most purposes in AWGN SISO channels. In Fig. 4.4 it is seen that in excess of a SNR of 12dB our optimized code obtains better performance than the other LAST codes.

Now consider $n_T = n_R = 2$ and $T = 3$. We select the rate as $R = 4$ bit/s/Hz (i.e., a codebook with 4096 codewords, and dimension $n = 12$). Fig. 4.5 illustrates the block error rate performance. For comparison purposes we report the results of a LAST code obtained using construction A [4] [22, 43] and we also show the outage error probability. It is seen that the new LAST code have slightly better performance than the code obtained via construction A.

***LAST code design with MMSE-GDFE lattice-reduction-aided linear receiver:*** We consider the MMSE-GDFE lattice-reduction-aided linear receiver with $n_T = T = 2$ and $n_R = 3$ . Fig. 4.6 shows the performance results of different LAST codes with MMSE-GDFE LRA linear receivers. It is seen that the new code slightly outperforms the other implemented codes.

***LAST code design with MMSE-GDFE lattice decoder in spatially correlated***

[3] Notice that multiple generator matrices $\boldsymbol{G}$ can obtain the same codebook or same error rate results, e.g., unitary transformations on $\boldsymbol{G}$, or equivalent lattices through lattice reduction, mirroring, etc.

[4] The author would like to thank M.O. Damen for providing the lattice generator of Construction A.

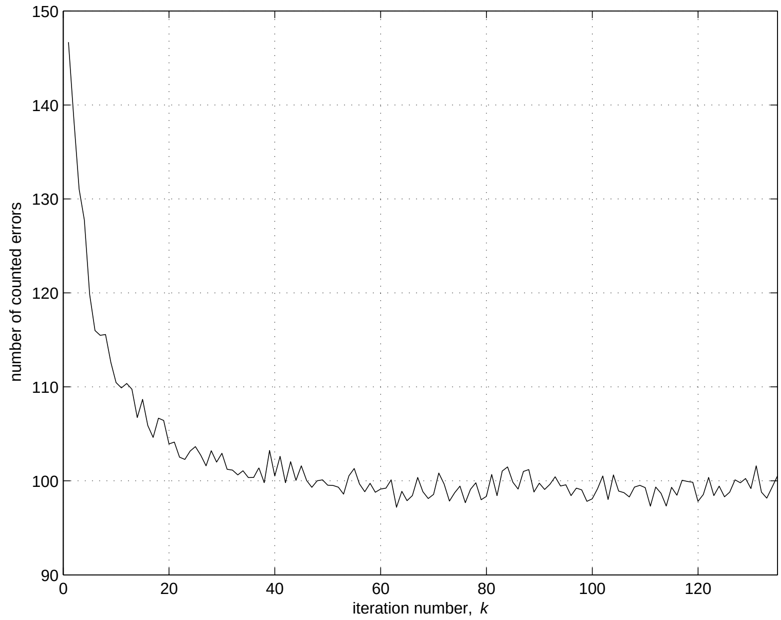


Figure 4.3: Convergence of the algorithm: average of the block error rate at different iteration indices.

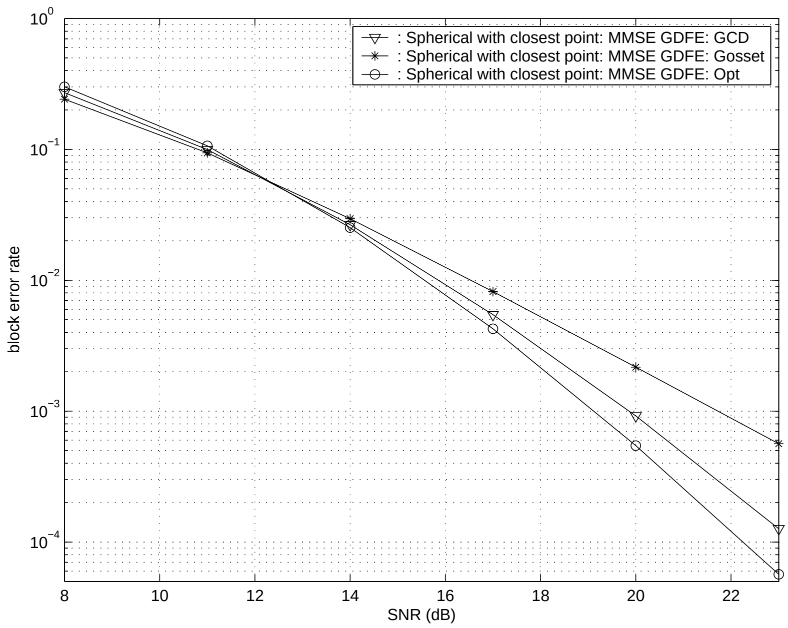


Figure 4.4: Block error rates of LAST codes with $n_T = n_R = T = 2$, rate $R =$ 4bit/s/Hz with MMSE-GDFE lattice decoder.

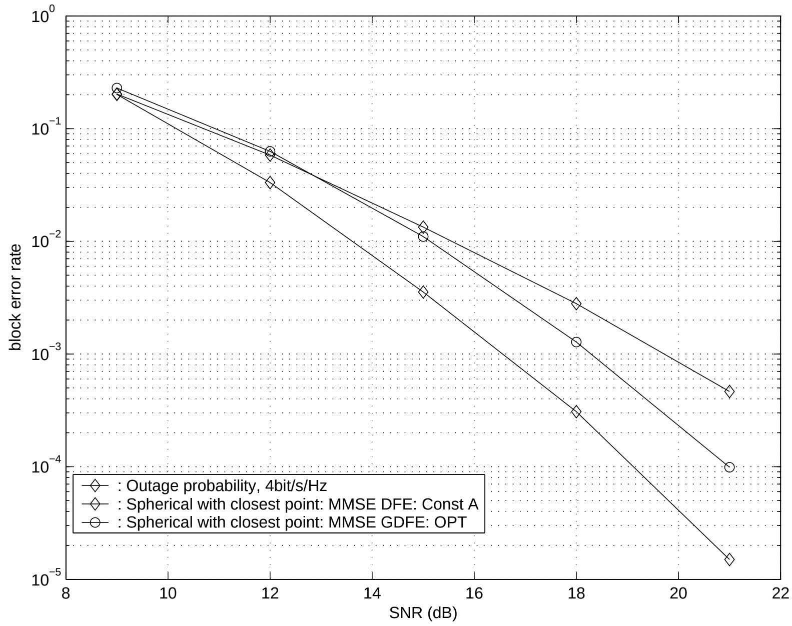


Figure 4.5: Block error rates of LAST codes with $n_T = n_R = 2$, $T = 3$, rate $R =$ 4bit/s/Hz and MMSE-GDFE lattice decoder.

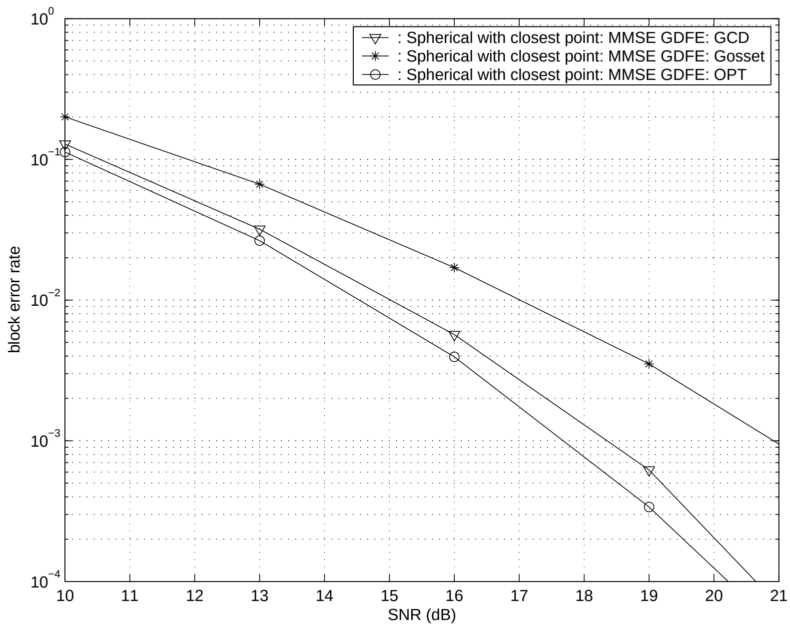


Figure 4.6: Block error rates of LAST codes with $T = n_T = 2$, $n_R = 3$, rate $R =$ 4bit/s/Hz and MMSE-GDFE LRA linear decoder (designed for SNR= $18$dB).

***channel:*** We consider a $2 \times 2$ MIMO channel with equal spatial correlation at both the transmitter and the receiver. We consider a urban scenario with medium correlated spatial channel represented by the covariance matrix

$$\boldsymbol{R}_r = \boldsymbol{R}_t = \begin{bmatrix} 1 & 0.88 - 0.3i \\ 0.88 + 0.3i & 1 \end{bmatrix} \tag{4.33}$$

and $\boldsymbol{H}_t^c = \boldsymbol{R}_r^{1/2} \boldsymbol{H}_{w,t}^c \boldsymbol{R}_t^{T/2}$, with $\boldsymbol{H}_{w,t}^c$ being a $2 \times 2$ uncorrelated matrix with i.i.d. $\mathcal{N}_c(0, 1)$ entries. Note that the new codes are optimized specifically for this correlation scenario (this is achieved using the correlated MIMO channel in Step 1.2 of the algorithm). The convergence of the algorithm is shown in Fig 4.7. The block error rate performance is shown in Fig. 4.8. It is seen that the new code outperform the lattice codes obtained with either of the other generator matrices considered.

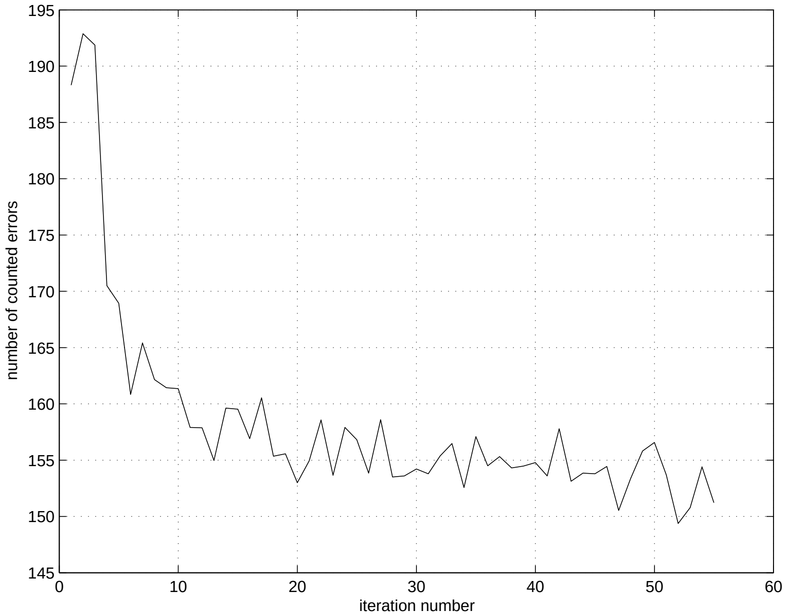


Figure 4.7: Convergence of the algorithm: average of the block error rate at different iteration indices with correlated channels.

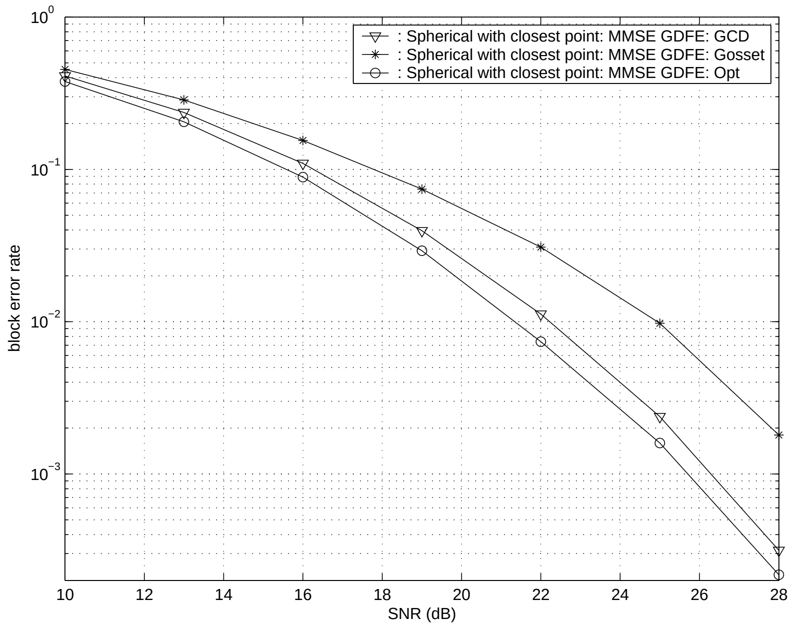


Figure 4.8: Block error rates of LAST codes with $n_T = n_R = T = 2$, rate $R =$ 4bit/s/Hz with MMSE-GDFE lattice decoder and spatial correlation (code designed for SNR=20dB) .

## 4.5 LAST codes with cooperative relays

Next we consider LAST codes with cooperative relaying [81] where idle nodes assist the active node in the communication of the LAST codewords $\boldsymbol{x} = \boldsymbol{G}\boldsymbol{z} + \boldsymbol{u}$. For the purpose of demonstrating the flexibility of our method and its application in this scenario we only consider a simple cooperative strategy. In particular, we only consider the design of the LAST code for a predetermined cooperative strategy and power allocation, and we claim that for this particular fixed cooperative strategy, the LAST codes obtained are block error optimal.

We consider a 2-hop relay network using amplify and forward relay nodes. This relaying technique allows a lower power consumption at the relaying nodes because there is no need to consume power for decoding [56]. All terminals are equipped with single antenna transmitters and receivers. Without loss of generality we only consider the amplify and forward relaying protocol in which the source terminal $S$ communicates simultaneously with one relay $R$ and destination terminal $D$ over the first time slot. In the second time slot, $R$ and $S$ simultaneously communicate with $D$ [96]. We consider perfect synchronization and perfect channel state information at the receivers. The channel between $S$ and $R$ is also known by the destination $D$. Two consecutive time slots are shown in Fig. 4.9. For simplicity we assign equivalent power to $S$ and $R$. We remark that a joint optimization of the assigned powers and code design can be formulated, complicating the derivation of the gradient required in the algorithm described in Section 4.3.4.

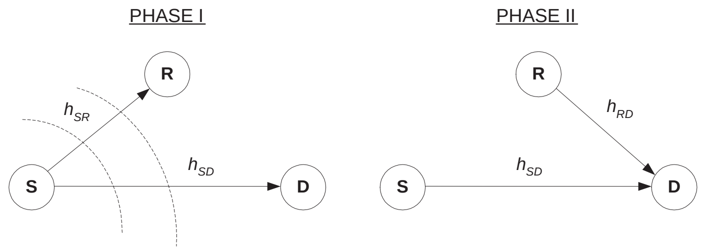


Figure 4.9: Cooperative scenario.

Consider $T$ intervals in the original MIMO case with $n_T$ co-located antennas, which translates in $T_c = Tn_T$ time intervals in the cooperative case. For example, to mimic the performance of a $n_T = T = 2$ LAST code, cooperative relaying requires $T_c = 4$ symbol intervals. Notice that due to the symmetry and periodicity of the lattice in the $n$-dimensional space and the spherical carving region $\mathcal{S}$, it can be observed that the LAST codeword coordinates are uniformly distributed around the sphere $\mathcal{S}$ (spherical uniform random vector). The power of each coordinate can be determined from this marginal density. The components of a spherically uniform vector are clearly identically distributed and the variance on one component is $r^2/(n+2)$, where $r$ is the radius of the $n$-dimensional sphere [82, p.665]. Using a discrete uniform distribution instead of a continuous uniform distribution and considering the total available power, the marginal density of each codeword component satisfies $\mathbb{E}\{|x_i|^2\} \cong 1/2, i = 1, ..., n$.

We consider *cheap* relays, which in a particular time slot can only operate as receivers or transmitters. Among the $T_c$ channel uses, we assign $T_c/2$ channel uses to the relay to operate as a transmitter and $T_c/2$ channel uses to operate as a receiver. During the first time slot the complex signals received at the destination and the relay are given by

$$\begin{aligned} y^c_{D,1} &= \sqrt{\rho} h^c_{SD}(x_1 + jx_2) + n^c_{D,1} \\ y^c_{R,1} &= \sqrt{\rho} h^c_{SR}(x_1 + jx_2) + n^c_{R,1}, \end{aligned} \tag{4.34}$$

where the random variables $h^c_{SD}$ and $h^c_{SR}$ are the unit-power complex gains between source and destination, and source and relay, respectively. We consider that the noise at the destination and the relay is distributed as $\{n^c_{D,t}, n^c_{R,t}\} \sim \mathcal{N}_c(0, 1)$. The received signal at the relay is normalized to have unit average power, i.e., $\sqrt{E\{|y^c_{R,1}|^2\}} = \sqrt{\rho + 1}$. The relay forwards it to the destination during the second time slot – notice that in the second time slot, the source also transmits. The received signal at $D$ during the second interval is given by

$$\begin{aligned} y^c_{D,2} &= \sqrt{\rho} h^c_{SD}(x_3 + jx_4) + \sqrt{\rho} h^c_{RD} \frac{y^c_{R,1}}{\sqrt{\rho+1}} + n^c_{D,2} \\ &= \sqrt{\rho} h^c_{SD}(x_3 + jx_4) + \frac{\sqrt{\rho\rho}}{\sqrt{\rho+1}} h^c_{RD} h^c_{SR}(x_1 + jx_2) + \underbrace{\sqrt{\frac{\rho}{\rho+1}} h_{RD} n^c_{R,1} + n^c_{D,2}}_{\tilde{n}^c_{D,2}} \end{aligned}$$

where it follows that $\tilde{n}^c_{D,2} \sim \mathcal{N}_c(0, 1 + \frac{\rho|h_{RD}|^2}{\rho+1})$. To keep the variance of the noise equal in the first and second time slot we normalize the received signal during the second slot by $\omega = \sqrt{1 + \frac{\rho|h_{RD}|^2}{\rho+1}})$. The equivalent Real input-output relation during the first two time slots (phase I and II) can be written as

$$\boldsymbol{y}^{(1)} = \mathcal{H}\boldsymbol{x}^{(1)} + \boldsymbol{n}^{(1)} \tag{4.35}$$

where $\boldsymbol{y}^{(1)} = [\Re\{y^c_{D,1}\}, \Im\{y^c_{D,1}\}, \Re\{\frac{1}{\omega} y^c_{D,2}\}, \Im\{\frac{1}{\omega} y^c_{D,2}\}]^T$, $\boldsymbol{x}^{(1)} = [x_1, x_2, x_3, x_4]^T$, and

$$\mathcal{H} = \begin{bmatrix} \sqrt{\rho}\Re\{h^c_{SD}\} & -\sqrt{\rho}\Im\{h^c_{SD}\} & 0 & 0 \\ \sqrt{\rho}\Im\{h^c_{SD}\} & \sqrt{\rho}\Re\{h^c_{SD}\} & 0 & 0 \\ \frac{1}{\omega}\sqrt{\frac{\rho^2}{\rho_{SR}+1}}\Re\{h^c_{SR}h^c_{RD}\} & -\frac{1}{\omega}\sqrt{\frac{\rho^2}{\rho+1}}\Im\{h^c_{SR}h^c_{RD}\} & \frac{\sqrt{\rho}}{\omega}\Re\{h^c_{SD}\} & -\frac{\sqrt{\rho}}{\omega}\Im\{h^c_{SD}\} \\ \frac{1}{\omega}\sqrt{\frac{\rho^2}{\rho_{SR}+1}}\Im\{h^c_{SR}h^c_{RD}\} & \frac{1}{\omega}\sqrt{\frac{\rho^2}{\rho+1}}\Re\{h^c_{SR}h^c_{RD}\} & \frac{\sqrt{\rho}}{\omega}\Im\{h^c_{SD}\} & \frac{\sqrt{\rho}}{\omega}\Re\{h^c_{SD}\} \end{bmatrix}. \tag{4.36}$$

To mimic a LAST code of length $T$ (i.e., $T_c = 2T$), we write the same model for $\boldsymbol{x}^{(i)}, i = 2, ..., T$ (i.e., time intervals $3, ..., 2T_c$) and we can finally write the equivalent MIMO system

$$\boldsymbol{y} = \boldsymbol{H}\boldsymbol{x} + \boldsymbol{n} \tag{4.37}$$

where $\boldsymbol{x} = [\boldsymbol{x}^{(1)T}, ..., \boldsymbol{x}^{(T)T}]^T = [x_1, ..., x_n]^T = \boldsymbol{G}\boldsymbol{z} + \boldsymbol{u}$, $\boldsymbol{y} = [\boldsymbol{y}^{(1)T}, ..., \boldsymbol{y}^{(T)T}]^T$, $\boldsymbol{H} = \boldsymbol{I}_T \otimes \mathcal{H}$ is the equivalent $n \times n$ MIMO channel, and $\boldsymbol{n}$ conditioned on the channel $\boldsymbol{H}$ is circularly symmetric complex Gaussian noise with $E\{\boldsymbol{n}|\boldsymbol{H}\} = \boldsymbol{0}$ and $E\{\boldsymbol{n}\boldsymbol{n}^H|\boldsymbol{H}\} = \frac{1}{2}\boldsymbol{I}$. Note that multiplexing gain is absent, since time is expanded to create a virtual MIMO channel thereby negating any multiplexing gain. Here the purpose is to obtain diversity gain.

With this system model, we still have

$$p(\boldsymbol{y}|\boldsymbol{z}, \boldsymbol{H}, \boldsymbol{G}) = \pi^{-TM} \exp\left[-(\boldsymbol{y} - \boldsymbol{H}\boldsymbol{G}\boldsymbol{z} - \boldsymbol{H}\boldsymbol{u}^*)^T(\boldsymbol{y} - \boldsymbol{H}\boldsymbol{G}\boldsymbol{z} - \boldsymbol{H}\boldsymbol{u}^*)\right] \tag{4.38}$$

and thus the algorithm described in Section 4.4.3 to design the generator $\boldsymbol{G}$ of LAST codes is applicable.

### 4.5.1 Simulation results

We consider rate $R$ =4bit/s/Hz and the length of the code $T = 2$, i.e., $T_c = 4$ time intervals are required to transmit each LAST codeword. The LAST code is designed for $\rho = 22$dB. Fig. 4.10 illustrates the block error rate for the new LAST codes and we also present the performance of the LAST codes obtained with the GCD lattice and the Gosset lattice. It is seen that our LAST code gives the best performance.

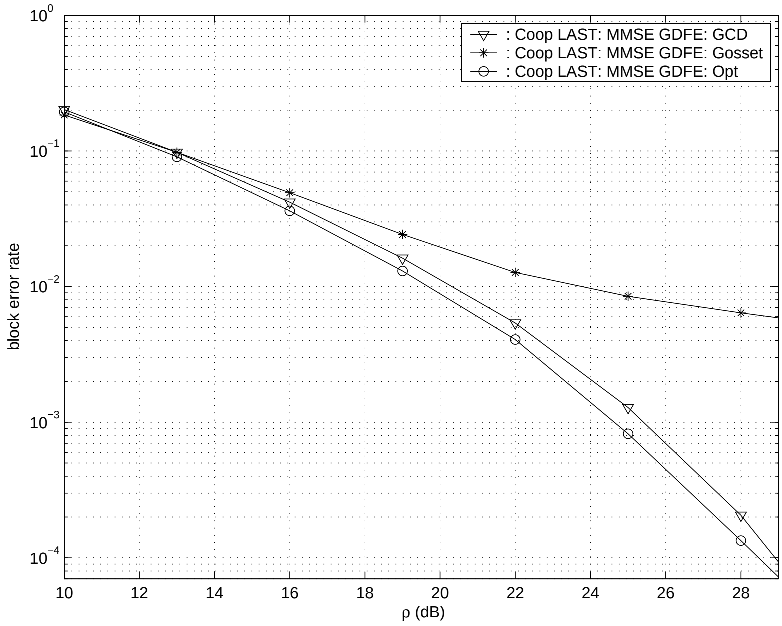


Figure 4.10: Cooperative results ($T = 2$, $R = 4$bit/s/Hz).

## 4.6 Conclusions

In this chapter we have proposed a systematic method for designing minimum block error rate spherical lattice space-time codes taking into account the detector architecture and the channel statistics. The design method has been shown to be universal in the sense that can be applied to optimize the LAST codes for a wide range of receivers schemes, channel statistics, or even cooperative relying.

# Chapter 5

# MIMO Precoding

## 5.1 Introduction

Multiuser detection techniques are considered powerful for interference suppression in CDMA systems, especially in uplinks, where the base-station receiver has the knowledge of all users' spreading sequences and channel states, and so has the opportunity to perform sophisticated signal processing [123]. In the downlinks, however, the mobile receiver typically only has the knowledge of its own spreading sequence and channel state. Although adaptive linear multiuser detection (either training-based or blind) can be employed for such scenario, the performance can be limited due to the limited power available at the detector for signal processing. On the other hand, precoding schemes for downlink CDMA effectively transfer the signal processing for interference suppression from the mobile receiver to the base-station transmitter. This approach is feasible if the base-station can estimate the downlink channels of all users (e.g., in time-division duplex (TDD) systems, the base station can exploit channel reciprocity if the time difference between uplink and downlink transmission is shorter than the channel coherence time, or alternatively the use of channel prediction techniques [31]). In [37] a precoding method has been proposed which is essentially an implementation of the RAKE receiver at the transmitter. Hence this approach does not attempt to mitigate the multiple-access interference (MAI). Recently, different linear precoding techniques have been proposed to combat MAI and inter-chip interference but without considering inter-symbol interference (ISI) [126]. If ISI is present then the complexity of these techniques becomes prohibitive since the dimension of the matrix filter is proportional to the data frame length multiplied by the number of users (i.e., block processing) [126]. More recently, bit-wise linear precoding methods have been proposed to reduce the precoding complexity in the presence of ISI [45].

Downlink CDMA is a special case of a broadcast channels. There has been significant recent interest in characterizing the capacity of broadcast channels. In particular, it has been shown that when the interference is non-causally known to the transmitter and unknown to the receiver, the capacity is the same as if the interference were not present – a result known as “dirty paper coding”. These results were originally proved for Gaussian channels [24], and have been generalized to other types of causal interference [19, 21, 34]. Several practical suboptimal implementations of dirty paper coding have been proposed, e.g., for digital subscriber line (DSL) systems [47] and for multi-antenna systems [130]. These implementations use successive interference cancellation combined with Tomlinson-Harashima (TH) precoding [57, 121].

In this chapter, we first obtain the capacity regions of a downlink CDMA system employing either multiuser detection (i.e., receiver processing) or precoding (transmitter processing). It is seen that these two approaches provide similar capacity regions, suggesting that precoding can potentially achieve similar performance to that offered by multiuser detection. This motivates the development of practical precoding solutions for downlink TDD-CDMA systems.

Then we consider linear precoders with very simple receivers, i.e., only a fixed matched-filter to the *own* spreading sequence is required and therefore CSI is not required. We propose several bit-wise and chip-wise linear precoders and corresponding power control algorithms to meet certain performance criteria at the receiver. We also consider the performance comparisons between linear precoding and linear MUD. The comparison metric is the total required power at the transmitter to achieve a minimum QoS requirement at each of the receivers. Our results show that linear precoding offers similar performance to linear MUD in most cases; but in some specific cases, linear precoding is more effective. Moreover, the proposed linear precoding techniques with only a matched-filter (to the spreading sequence) at the receiver can outperform the linear precoder with a RAKE receiver (i.e., with CSI at the receiver) proposed in [126]. These results motivate the use of linear precoding techniques in the downlink of TDD-CDMA systems. Among the advantages of using precoding we have:

- Receiver terminals are simply a fixed matched-filter corresponding to the *own* spreading sequence. This translates into a power consumption reduction and a decrease in price of the terminals since they do not have to perform sophisticated signal processing for channel estimation and interference mitigation. Note that variations in channel conditions and the number of active users in the network do not affect the receiver operations.

- A reduced amount of control data is required in the precoding solution. The reason is that in MUD, every user requires to know the own channel response plus the spreading sequences and the CSI of all other active users in the network. Moreover, mobile units do not need to be informed when users are added to (or removed from) the network.

- Power control is easy to implement with precoding since the transmitter has information about the quality of each link and it does not require extra feedback information. Note that MUD requires a feedback link to find the power loading value assigned to each user.

- User scheduling based on the knowledge of CSI can be implemented jointly with linear precoding to increase the system throughput.

In the final part of the chapter we consider nonlinear precoding techniques based on TH-precoding, which offer superior performance compared to linear precoding. We extend the precoding method in [39] to systems with ISI. We also propose a new chip-wise precoding scheme that combines spreading and TH-precoding operations. The main difference between our solution and the TH solution in [39, 130] is that our non-linear precoder does not require CSI at the mobile receiver and yet the performance is similar (note that in the TH precoding solution in [39, 130] each user implements a RAKE receiver and therefore CSI is required). Furthermore, efficient algorithms for multiuser power loading and cancelation ordering are developed. Implementation of the proposed TH-precoding schemes in time-varying channels based on channel prediction is also addressed.

The remainder of this chapter is organized as follows. In Section 5.2, we obtain and compare the capacity regions of multiuser detection and precoding in the downlink of CDMA systems. In Section 5.3 we briefly summarize two well-known linear MUD methods and we propose several forms of linear precoding techniques. We also present simulation comparisons between linear MUD and linear precoding. In Section 5.4, we develop new TH-precoding schemes for downlink TDD-CDMA systems over multipath channels. Power loading and cancellation ordering are also addressed. Simulation results under both perfectly known channels and predicted channels are also presented. In Section 5.5 we discuss low-complexity user scheduling algorithms based on our precoding schemes. Finally, Section 5.6 concludes the chapter.

## 5.2 Downlink Capacity Regions of Multiuser Detection and Precoding

In time-division duplexing (TDD) systems, the uplink channel and the downlink channel for each individual user is the same. Hence the base station can use the uplink channel information to perform preprocessing for the downlink and thereby transfer sophisticated signal processing from the receiver end to the transmitter end, i.e., to replace multiuser detection (receiver processing) by precoding (transmitter processing). In this section, we present and compare the capacity results of precoding and multiuser detection in the downlink of a CDMA system. These two approaches for downlink CDMA are illustrated schematically in Fig. 5.1. Note that this is a special case of the MIMO broadcast channel for which recent progressive developments [19, 16, 124, 125, 135] have lead to the final solution to the capacity region for the general broadcast channel [128]. Consider a synchronous CDMA system with $K$ users signalling over a real-valued AWGN channel. Let $f_k$ and $\boldsymbol{s}_k$ be the channel gain and the spreading signature of the $k$-th user, respectively. Denote $\boldsymbol{S} = [\boldsymbol{s}_1, \cdots, \boldsymbol{s}_K]$. Then $\boldsymbol{R} = \boldsymbol{S}^T\boldsymbol{S}$ is the $K \times K$ cross-correlation matrix of the spreading waveforms of all users.

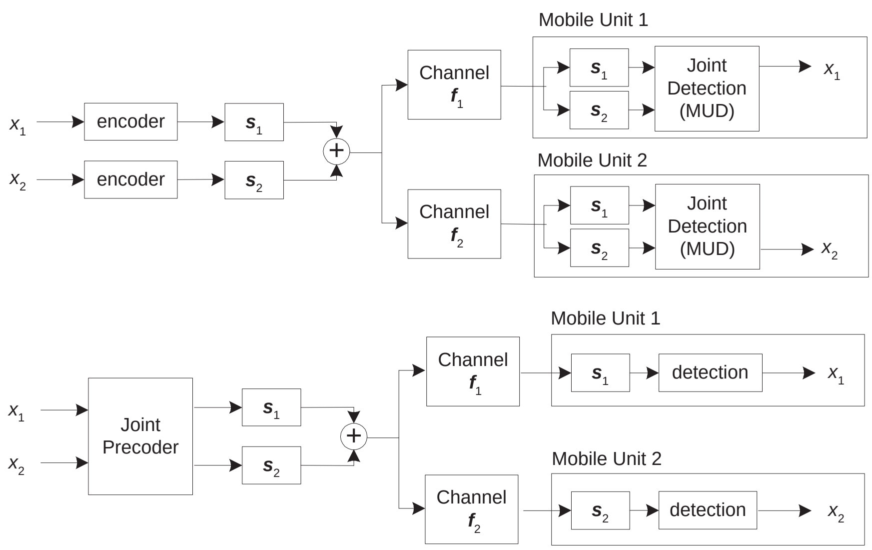


Figure 5.1: Schematic illustration of MUD and Precoding in downlink CDMA systems.

### 5.2.1 Multiuser Detection

Assume that the users are ordered according to their path gains so that $f_1 \geq f_2 \geq \cdots \geq f_K$. The received signal at the $k$-th mobile receiver is given by $\boldsymbol{r}_k = f_k \sum_{\ell=1}^{K} x_\ell \boldsymbol{s}_\ell + \boldsymbol{n}_k$, where $\boldsymbol{n}_k \sim \mathcal{N}(\boldsymbol{0}, \boldsymbol{I})$. Note that in this case symbols from different users $x_1, \cdots, x_K$ are independently encoded. Denote $\boldsymbol{x} = [x_1, \cdots, x_K]^T$. A sufficient statistic for $\boldsymbol{x}$ is the output of a bank of matched-filters [123],

$$\boldsymbol{y}_k \triangleq \left[\boldsymbol{s}_1^T \boldsymbol{r}_k,\, \boldsymbol{s}_2^T \boldsymbol{r}_k,\, \cdots, \boldsymbol{s}_K^T \boldsymbol{r}_k\right] = f_k \boldsymbol{R}\boldsymbol{x} + \boldsymbol{v}_k, \tag{5.1}$$

with $E\{\boldsymbol{v}_k \boldsymbol{v}_k^T\} = \boldsymbol{R}$. The $k$-th user then makes a decision on its own data $x_k$ based on $\boldsymbol{y}_k$. Denote $\boldsymbol{\rho}_k$ as the $k$-th column of $\boldsymbol{R}$ and

$$\boldsymbol{Q}_k \triangleq \boldsymbol{R} + f_k^2 \sum_{\ell=1}^{k-1} P_\ell \boldsymbol{\rho}_\ell \boldsymbol{\rho}_\ell^T, \tag{5.2}$$

where $P_k \triangleq E\{x_k^2\}$. Denote $P_T \triangleq \sum_{k=1}^{K} P_k$ as the total transmit power. We have the following result regarding an outer bound on the rate region.

**Proposition 2** *Consider the channel model (5.1) and suppose that each user's data is encoded independently. Then the multiuser rate tuple* $(R_1, \ldots, R_K)$ *must satisfy*

$$R_k \leq \frac{1}{2} \log\left(1 + P_k f_k^2\, \boldsymbol{\rho}_k^T \boldsymbol{Q}_k^{-1} \boldsymbol{\rho}_k\right), \quad k = 1, \cdots, K, \tag{5.3}$$

*for some* $P_k, k = 1, \ldots, K$, *satisfying* $P_k \geq 0$ *and* $\sum_{k=1}^{K} P_k = P_T$.

*Proof:* Define $\boldsymbol{y}'_k = \boldsymbol{y}_k / f_k$. Then we can rewrite the following equivalent model to (5.1):

$$\boldsymbol{y}'_1 = \boldsymbol{R}\boldsymbol{x} + \boldsymbol{v}'_1, \ \text{ and } \ \boldsymbol{y}'_k = \boldsymbol{y}'_{k-1} + \boldsymbol{v}'_k, \qquad k = 2, \ldots, K, \tag{5.4}$$

where the $\boldsymbol{v}'_1, \cdots, \boldsymbol{v}'_K$ are independent, zero-mean Gaussian vectors, and $E\{\boldsymbol{v}'_k \boldsymbol{v}'^T_k\} = \left(f_k^{-2} - f_{k-1}^{-2}\right) \boldsymbol{R}$. The model (5.4) is the same as the aligned degraded broadcast channel (ADBC) model in [128]. The difference is that here each $x_k$ is encoded *independently*. This corresponds to the model in [128] with $\boldsymbol{B}_i$ zero except for the $i$-th diagonal element and $\boldsymbol{S}$ a diagonal matrix. It can be checked that the proof still applies with these restrictions, and we therefore get a rate given by Eq.(2)-(3)

in [128], which here becomes

$$
\begin{aligned}
R_k &\leq \frac{1}{2}\log\left(\frac{\det\left(\sum_{\ell=1}^{k} P_\ell \boldsymbol{\rho}_\ell \boldsymbol{\rho}_\ell^T + \sum_{\ell=1}^{k} E\{\boldsymbol{v}'_\ell \boldsymbol{v}'^T_\ell\}\right)}{\det\left(\sum_{\ell=1}^{k-1} P_\ell \boldsymbol{\rho}_\ell \boldsymbol{\rho}_\ell^T + \sum_{\ell=1}^{k} E\{\boldsymbol{v}'_\ell \boldsymbol{v}'^T_\ell\}\right)}\right) \\
&= \frac{1}{2}\log\left(\frac{\det\left(\boldsymbol{Q}_k + f_k^2 P_k \boldsymbol{\rho}_k \boldsymbol{\rho}_k^T\right)}{\det \boldsymbol{Q}_k}\right). \qquad (5.5)
\end{aligned}
$$

Let $\boldsymbol{F}_k$ be a Cholesky factor of $\boldsymbol{Q}_k$, i.e., $\boldsymbol{F}_k \boldsymbol{F}_k^T = \boldsymbol{Q}_k$. Then

$$
\begin{aligned}
\det\left(\boldsymbol{Q}_k + P_k f_k^2 \boldsymbol{\rho}_k \boldsymbol{\rho}_k^T\right) &= \det\left[\boldsymbol{F}_k\left(\boldsymbol{I} + \left(\sqrt{P_k} f_k \boldsymbol{F}_k^{-1}\boldsymbol{\rho}_k\right)\left(\sqrt{P_k} f_k \boldsymbol{F}_k^{-1}\boldsymbol{\rho}_k\right)^T\right)\boldsymbol{F}_k^T\right] \\
&= \left(1 + P_k f_k^2 \boldsymbol{\rho}_k^T \boldsymbol{Q}_k^{-1} \boldsymbol{\rho}_k\right)\det \boldsymbol{Q}_k, \qquad (5.6)
\end{aligned}
$$

where in (5.6) we used the following identity $\det(\boldsymbol{AB}) = \det(\boldsymbol{BA}) = \det(\boldsymbol{A})\det(\boldsymbol{B})$, and $\det\left(\boldsymbol{I} + \boldsymbol{a}\boldsymbol{a}^T\right) = \boldsymbol{a}^T\boldsymbol{a} + 1$ where $\boldsymbol{a}$ is a vector. Substituting (5.6) into (5.5) we obtain (5.3).

The rate in Proposition 2 is achievable with a multiuser detector that performs serial interference cancellation on weak users and linear MMSE interference suppression on strong users. In particular, user $k$ can decode the data intended for users $k+1, \ldots, K$ as user $k$ receives the same signal but with higher SNR. Suppose that user $k$ has decoded users $k+1, \ldots, K$. It then subtracts the signals of these users from $\boldsymbol{y}_k$ in (5.1) to obtain

$$
\begin{aligned}
\tilde{\boldsymbol{y}}_k &= \boldsymbol{y}_k - f_k \sum_{\ell=k+1}^{K} \boldsymbol{\rho}_\ell x_\ell \\
&= f_k \sum_{\ell=1}^{k} \boldsymbol{\rho}_\ell x_\ell + \boldsymbol{v}_k \\
&= f_k \boldsymbol{\rho}_k x_k + f_k \sum_{\ell=1}^{k-1} \boldsymbol{\rho}_\ell x_\ell + \boldsymbol{v}_k. \qquad (5.7)
\end{aligned}
$$

It now applies a linear MMSE filter on $\tilde{\boldsymbol{y}}_k$. Note that the covariance matrix of the noise and interference is given by $\boldsymbol{Q}_k$ in (5.2). The linear MMSE filter output is given by

$$
\hat{x}_k =_k^T \tilde{\boldsymbol{y}}_k, \quad \text{with} \quad _k = f_k \boldsymbol{Q}_k^{-1} \boldsymbol{\rho}_k. \qquad (5.8)
$$

This gives a rate

$$
\begin{aligned}
R_k &= \frac{1}{2}\log\left(1+\frac{\left(\boldsymbol{\rho}_k^T\boldsymbol{Q}_k^{-1}\boldsymbol{\rho}_k\right)^2 P_k f_k^2}{\boldsymbol{\rho}_k^T\boldsymbol{Q}_k^{-1}\boldsymbol{\rho}_k}\right)\\
&= \frac{1}{2}\log\left(1+P_k f_k^2\boldsymbol{\rho}_k^T\boldsymbol{Q}_k^{-1}\boldsymbol{\rho}_k\right). \qquad (5.9)
\end{aligned}
$$

When $K=2$, denote $\rho \triangleq \rho_{1,2}=\rho_{2,1}$. The above rate region can be easily evaluated as

$$
\begin{aligned}
R_1 &= \frac{1}{2}\log(1+P_1 f_1^2), \qquad (5.10)\\
R_2 &= \frac{1}{2}\log\left(1+\frac{1+P_1 f_2^2(1-\rho^2)}{1+P_1 f_2^2}P_2 f_2^2\right)\\
&= \frac{1}{2}\log\left(1+\left(1-\rho^2\frac{P_1 f_2^2}{1+P_1 f_2^2}\right)P_2 f_2^2\right). \qquad (5.11)
\end{aligned}
$$

### 5.2.2 Precoding

In systems employing precoding, each downlink user simply applies a filter matched to its *own* spreading sequence. The output of this matched-filter is given by $y_k = f_k\boldsymbol{\rho}_k^T\boldsymbol{x}+v_k$, where $\boldsymbol{x}$ is the precoded vector. Stacking the output of the matched-filters of all users in a single vector, we then obtain the downlink precoding signal model: $\boldsymbol{y}=\boldsymbol{A}\boldsymbol{R}\boldsymbol{x}+\boldsymbol{v}$, where $\boldsymbol{A}=\mathrm{diag}(f_1,...,f_K)$ and $E\{\boldsymbol{v}\boldsymbol{v}^T\}=\boldsymbol{I}$. This is similar to a multiple-antenna broadcast channel [19]. However, note that here the power of the transmitted signal is $E\left\{\boldsymbol{x}^T\boldsymbol{R}\boldsymbol{x}\right\}$. Therefore the power constraint is $E\left\{\boldsymbol{x}^T\boldsymbol{R}\boldsymbol{x}\right\}\le P_T$, which is different than [19]. This is easily fixed: let $\boldsymbol{F}$ be the Cholesky factor of $\boldsymbol{R}$, i.e., $\boldsymbol{F}\boldsymbol{F}^T=\boldsymbol{R}$. Define $\boldsymbol{u}=\boldsymbol{F}^T\boldsymbol{x}$. Then $\boldsymbol{u}$ should satisfy the power constraint $E\left\{\boldsymbol{u}^T\boldsymbol{u}\right\}\le P_T$, and we can write the received signal as

$$
\boldsymbol{y} = \boldsymbol{A}\boldsymbol{R}\boldsymbol{F}^{-T}\boldsymbol{u}+\boldsymbol{v} = \boldsymbol{A}\boldsymbol{F}\boldsymbol{u}+\boldsymbol{v}. \qquad (5.12)
$$

This is the same as the model in [19] for a broadcast channel with $K$ antennas at the base station and one antenna at each terminal, with $\boldsymbol{H}\triangleq\boldsymbol{A}\boldsymbol{F}$. In [19] Costa's "dirty-paper coding" was suggested, and very recently in [128] it was shown that this scheme actually gives the capacity region. Hence the results in [19] apply to the current problem and the following rate is achievable [124]

$$R_k = \frac{1}{2}\log\frac{\det\left(\boldsymbol{I}+\boldsymbol{h}_k^T\left(\sum_{\ell=k}^{K}\boldsymbol{\Sigma}_\ell\right)\boldsymbol{h}_k\right)}{\det\left(\boldsymbol{I}+\boldsymbol{h}_k^T\left(\sum_{\ell=k+1}^{K}\boldsymbol{\Sigma}_\ell\right)\boldsymbol{h}_k\right)}, \tag{5.13}$$

where $\boldsymbol{\Sigma}_1,\ldots,\boldsymbol{\Sigma}_K$ are positive semidefinite matrices satisfying $\operatorname{tr}\left(\sum_{k=1}^{K}\boldsymbol{\Sigma}_k\right) \leq P_T$ and $\boldsymbol{h}_k^T$ is the $k$-th row of $\boldsymbol{H}$. The capacity region, as proven in [128], is the convex union over all matrices $\boldsymbol{\Sigma}_1,\ldots,\boldsymbol{\Sigma}_K$ and all orderings of the users. Unfortunately, except for the two-user case solved in [19] no closed-form solution for the capacity region has been found. For the case of $K = 2$, we can obtain explicit expressions for the capacity region. In [19] it was proven that the capacity region is given by

$$R_1 \leq \log\left(1+\frac{\alpha c_1 P_T}{1+q(1-\alpha)c_1P_T}\right), \tag{5.14}$$

$$R_2 \leq \log\Big(1+p(1-\alpha)c_1P_T\Big), \qquad 0\leq q\leq 1, 0\leq\alpha\leq 1. \tag{5.15}$$

where $c_1 \triangleq \boldsymbol{h}_1^T\boldsymbol{h}_1$, $c_2 \triangleq |\det(\boldsymbol{H})|^2/c_1$, $c_3 \triangleq |\boldsymbol{h}_1^T\boldsymbol{h}_2|^2/c_1^2$, and

$$p = \left(\sqrt{c_3 q}+\sqrt{\frac{c_2}{c_1}(1-q)}\right)^2. \tag{5.16}$$

We can obtain a more explicit expression as follows. First set equality in (5.14) and solve for $q$, to obtain

$$q = \frac{2^{R_1}-1-\alpha c_1 P_T}{(1-\alpha)c_1P_T(1-2^{R_1})}. \tag{5.17}$$

Then substitute (5.17) into (5.16) and in (5.15) with equality, and solve for $\alpha$ from $\frac{dR_2}{d\alpha} = 0$, to obtain the unique solution

$$\alpha = \frac{-c_1^2P_T+2^{R_1}c_1^2c_3P_T-2^{2R_1}c_2-c_1c_3+2^{3R_1}c_2+2^{R_1}c_1c_3}{(c_1c_3+2^{R_1}c_2)2^{R_1}c_1P_T}. \tag{5.18}$$

Substituting (5.18) into (5.14) and (5.15) we obtain

$$R_1 \leq \log\left(1 + c_1 P_T\right), \tag{5.19}$$

$$R_2 \leq \log\left(1 + \frac{c_1^2 c_3 P_T + c_1 c_3 + 2^{R_1}(c_1 c_2 P_T + c_2 - c_1 c_3 - c_2 2^{R_1})}{c_1 2^{R_1}}\right) \tag{5.20}$$

Now substituting (5.19) with equality into (5.20), and using the definitions of $c_i$ and $\boldsymbol{H} \triangleq \boldsymbol{AF}$, after some straightforward but tedious simplifications, we obtain

$$R_1 \leq \frac{1}{2}\log\left(1 + P_1 f_1^2\right), \tag{5.21}$$

$$R_2 \leq \frac{1}{2}\log\left(1 + \left(1 - \rho^2 \frac{P_1 f_1^2}{1 + P_1 f_1^2}\right) P_2 f_2^2\right). \tag{5.22}$$

If we swap the order of the users we get another region, and the total region is the convex closure of these two regions.

### 5.2.3 Comparisons

We next provide some numerical results comparing the downlink CDMA capacity regions for multiuser detection (MUD) and precoding with $K = 2$. First we notice that the two capacity expressions (5.10)-(5.11) and (5.21)-(5.22) are very similar. Figure 5.2 shows typical rate regions, one for high SNR and one for low SNR. There are two curves for the precoding case because of the dependency on user ordering (the capacity region is the convex union) and one curve for the MUD case. It is seen that the regions are quite similar. The maximum sum rate is slightly larger for MUD; whereas the maximum equal rate (i.e., $R_1 = R_2$) is slightly larger for precoding. This turns out to be general, as the following numerical results show. Figure 5.3 shows the sum rate as a function of $f_2/f_1$ and $\rho \in [0, 1]$ with $f_1$ fixed. It is seen that the sum rate for MUD is consistently better, but only slightly. Similar observation can be made for maximum equal rate in Fig. 5.4. In summary it is seen that precoding can potentially provide similar capacity as MUD, which motivates the development of practical transmitter precoding techniques as an alternative to MUD to reduce the complexity of the mobile receiver. In the following sections, we propose suboptimal approaches to “dirty-paper coding” based on linear precoding and the Tomlinson-Harashima (TH) precoding technique in multipath channels.

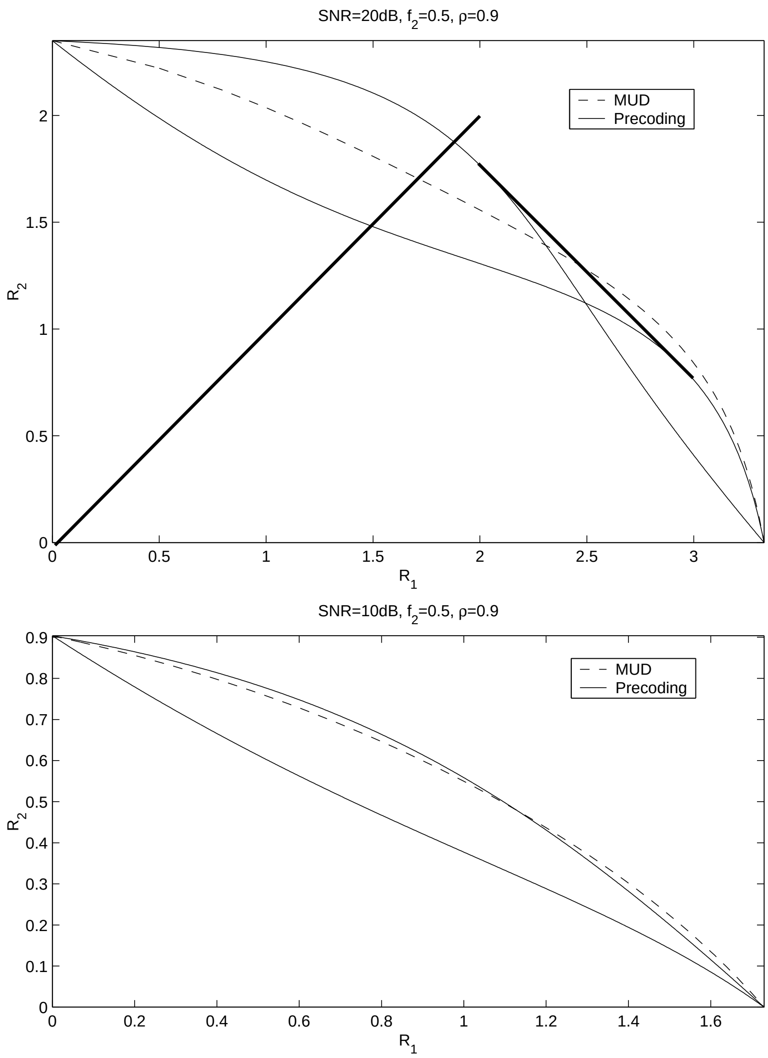


Figure 5.2: Comparisons of rate regions for MUD and precoders with $K = 2$.

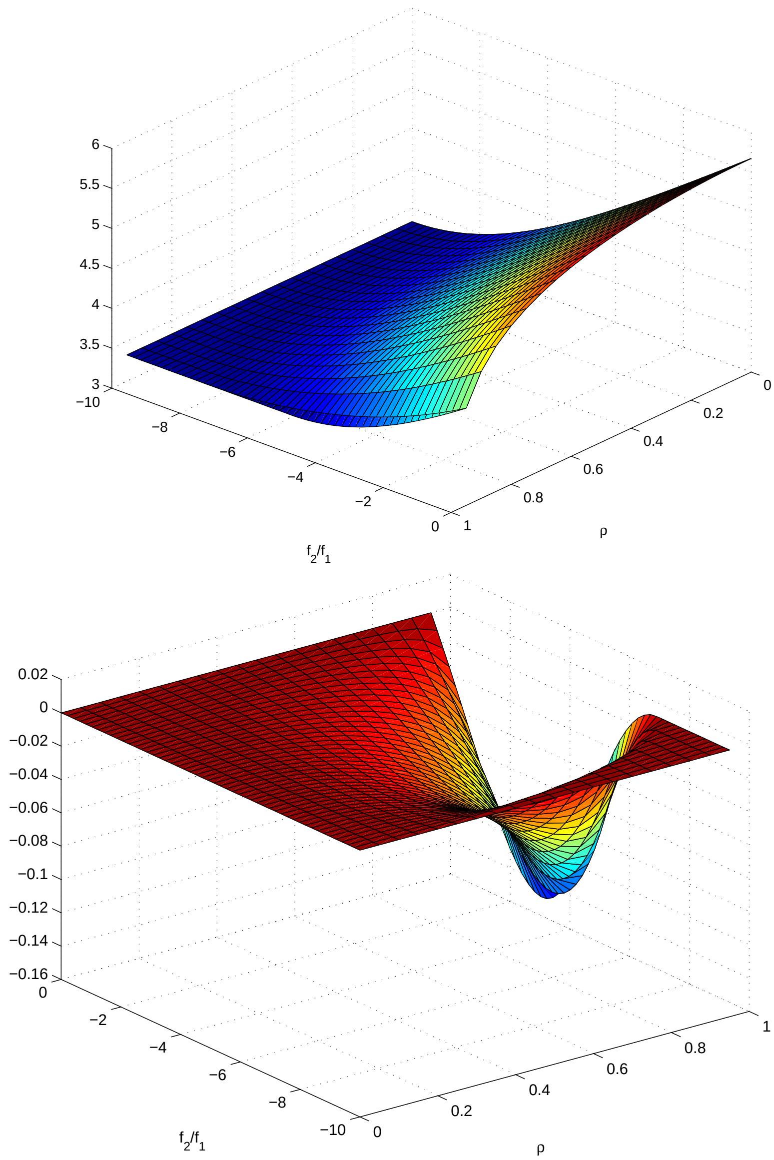


Figure 5.3: Sum rate for precoding and MUD as a function of $\rho$ and $f_2/f_1$ (almost equal, so the two surfaces are nearly indistinguishable); and difference between sum rates for precoding and MUD ($R_{\text{precoding}} - R_{\text{MUD}}$). The SNR is 20dB for user 1.

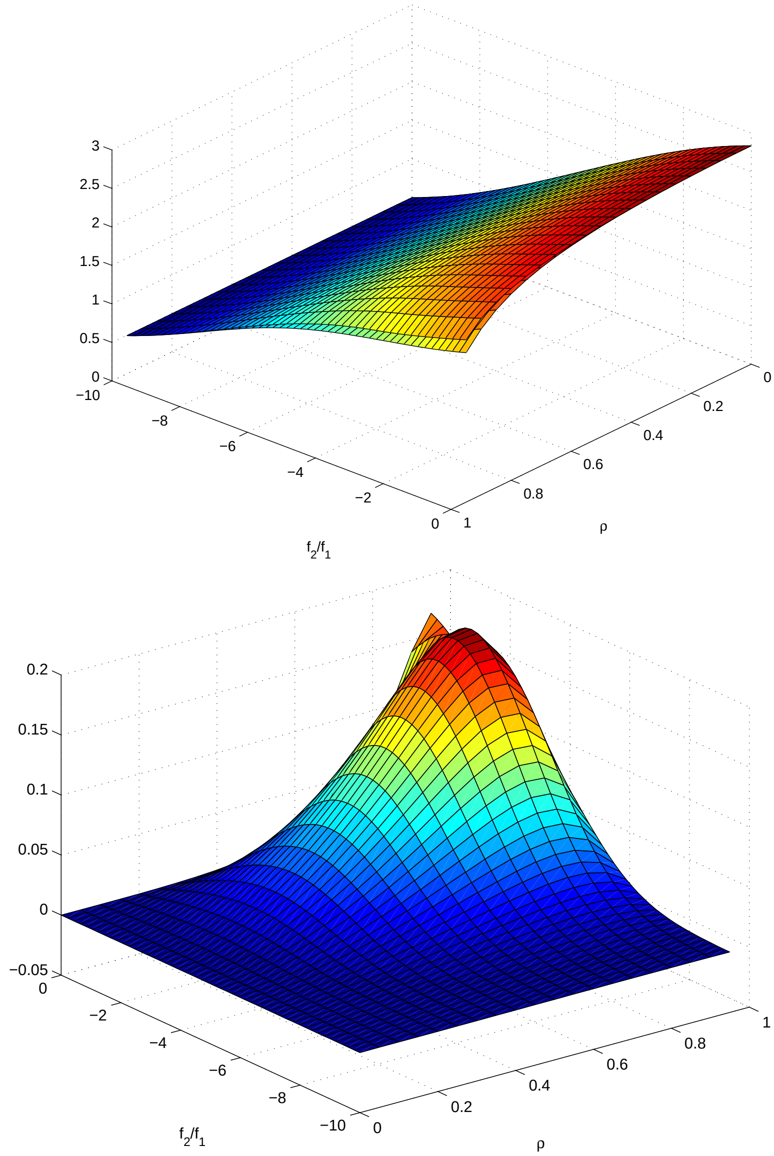


Figure 5.4: Equal rate for precoding and MUD as a function of $\rho$ and $f_2/f_1$ (almost equal, so the two surfaces are nearly indistinguishable); and difference between equal rates for precoding and MUD ($R_{\text{precoding}} - R_{\text{MUD}}$). The SNR is 20dB for user 1.

# 5.3 Linear Precoding versus Linear Multiuser Detection

## 5.3.1 Linear MUD Methods

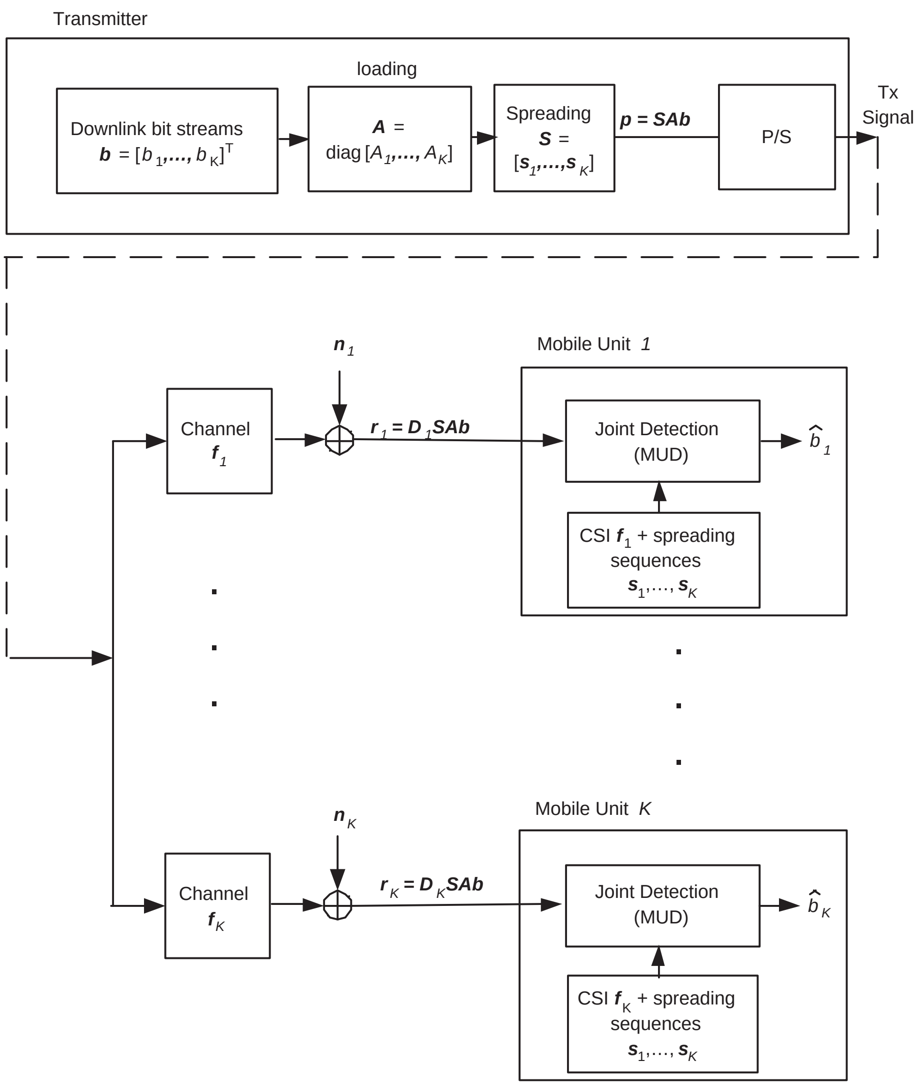


Figure 5.5: Downlink MUD.

We consider a $K$-user discrete-time synchronous multipath CDMA system. Define $b_k[i]$ from a constellation $\mathcal{A}$ as the symbol of the $k$-th user transmitted during the $i$-th symbol interval with $E\{|b[i]|^2\} = 1$ and $\boldsymbol{b}[i] = [b_1[i], ..., b_K[i]]^T$. Denote $N$ as the spreading factor and $\boldsymbol{s}_k = [s_{k,1}, ..., s_{k,N}]^T$ as the normalized spreading waveform of the $k$-th user. Then, the signal transmitted from the base station during the $i$-th symbol interval can be written as $\boldsymbol{p}[i] = \boldsymbol{SAb}[i]$, where $\boldsymbol{S} =$

$[\boldsymbol{s}_1, \boldsymbol{s}_2, ..., \boldsymbol{s}_K]$ is the matrix of spreading waveforms; and $\boldsymbol{A} = \mathrm{diag}(A_1, ..., A_K)$ contains the user signal amplitudes. The vector $\boldsymbol{p}[i]$ is passed through a parallel-to-serial converter and transmitted over the multipath channel. The path delays are assumed to be an integral number of chip periods. Denote the multipath channel seen by the $k$-th user as $\boldsymbol{f}_k = [f_{k,1}, f_{k,2}, ..., f_{k,L}]^T$, where $L$ is the number of resolvable paths and $f_{k,l}$ is the complex fading gain corresponding to the $l$-th path of the $k$-th user. We assume that $L < N$. At the $k$-th user's receiver, the $N \times 1$ received signal during $N$ consecutive chip intervals corresponding to $\boldsymbol{b}[i]$ is given by

$$\boldsymbol{r}_k[i] = \underbrace{\boldsymbol{D}_k \boldsymbol{S}}_{\boldsymbol{H}_k} \boldsymbol{A}\boldsymbol{b}[i] + \boldsymbol{n}_k[i] \quad \text{with } \boldsymbol{D}_k = \begin{bmatrix} f_{k,1} & 0 & \cdots & \cdots & 0 \\ \vdots & \ddots & \ddots & & \vdots \\ f_{k,L} & \ddots & f_{k,1} & \ddots & \\ 0 & \ddots & & \ddots & 0 \\ 0 & \cdots & f_{k,L} & \cdots & f_{k,1} \end{bmatrix}_{N\times N}, \tag{5.23}$$

where $\boldsymbol{r}_k[i] = [r_{k,1}[i], ..., r_{k,N}[i]]^T$ is the received signal, $\boldsymbol{n}_k[i] \sim \mathcal{N}_c\left(\boldsymbol{0}, \sigma^2 \boldsymbol{I}_N\right)$ is the complex white Gaussian noise vector at the $k$-th receiver, and $\boldsymbol{H}_k = \boldsymbol{D}_k \boldsymbol{S}$. Notice that we have assumed that ISI can be ignored either by being truncated or by inserting a guard interval. At the $k$-th receiver, a linear detector to recuperate the signal $b_k[i]$ can be represented by an $N$-dimensional vector $\boldsymbol{w}_k \in \mathbb{C}^N$, which is correlated with the received signal $\boldsymbol{r}_k[i]$ in (5.23) to obtain $z_k[i] = \boldsymbol{w}_k^H \boldsymbol{r}_k[i]$, and the $k$-th mobile unit makes a decision $\hat{b}_k[i] = \mathcal{Q}(z_k[i])$, where $\mathcal{Q}$ rounds to the closest point in the constellation.

***Linear Decorrelating Detector:*** The decorrelating detector completely eliminates the multiuser interference (MUI) and interchip interference (ICI), at the expense of enhancing the noise. The linear decorrelating detector for user $k$ is given by [123]

$$\boldsymbol{w}_k = \boldsymbol{H}_k^{\dagger H} \boldsymbol{e}_k = \boldsymbol{H}_k (\boldsymbol{H}_k^H \boldsymbol{H}_k)^{-1} \boldsymbol{e}_k, \tag{5.24}$$

where $\boldsymbol{e}_k$ denotes a $K$-dimensional vector with all entries zeros, except for the $k$-th entry, which is 1. The output of this detector is given by

$$z_k[i] = \boldsymbol{w}_k^H \boldsymbol{r}_k[i] = A_k b_k[i] + \boldsymbol{w}_k^H \boldsymbol{n}_k[i] \implies \mathrm{SINR}_k = \frac{A_k^2}{\sigma^2 \|\boldsymbol{w}_k\|^2}, \tag{5.25}$$

where $\mathrm{SINR}_k$ is the signal-to-interference-plus-noise ratio for the $k$-th user. Suppose that the QoS requirement for user $k$ is such that $\mathrm{SINR}_k \geq \gamma_k$, where $\gamma_k$ is the minimum acceptable SINR value for user $k$. Hence we have $A_k^2 = \sigma^2\gamma_k\|\boldsymbol{w}_k\|^2$. And the total required transmit power is given by

$$P_T = \sum_{k=1}^{K} A_k^2 = \sum_{k=1}^{K} \sigma^2\gamma_k\, \boldsymbol{e}_k^H(\boldsymbol{S}^H\boldsymbol{D}_k^H\boldsymbol{D}_k\boldsymbol{S})^{-H}\boldsymbol{e}_k. \tag{5.26}$$

***Linear MMSE Detector:*** The linear MMSE detector for user $k$ is given by [123]

$$\boldsymbol{w}_k = \arg\min_{\boldsymbol{w}_k\in\mathbb{C}^N} E\left\{|b_k[i] - \boldsymbol{w}_k^H\boldsymbol{r}_k[i]|^2\right\} = A_k(\boldsymbol{H}_k\boldsymbol{A}^2\boldsymbol{H}_k^H + \sigma^2\boldsymbol{I}_N)^{-1}\boldsymbol{H}_k\boldsymbol{e}_k. \tag{5.27}$$

The SINR for this detector is given by

$$\text{SINR}_k = \frac{A_k^2\|\boldsymbol{w}_k^H\boldsymbol{H}_k\boldsymbol{e}_k\|^2}{\sum_{j\neq k} A_j^2\|\boldsymbol{w}_k^H\boldsymbol{H}_k\boldsymbol{e}_j\|^2 + \sigma^2\|\boldsymbol{w}_k\|^2}. \tag{5.28}$$

We seek to minimize the total power $P_T$ such that $\text{SINR}_k \geq \gamma_k$. The iterative power control algorithm for linear MMSE MUD proposed in [122] can be extended to the downlink scenario. At the $(n+1)$-th iteration, the MMSE filter $\boldsymbol{w}_k(n+1)$ is constructed using the current power matrix $\boldsymbol{A}(n)$. Then, the power matrix $\boldsymbol{A}(n+1)$ is updated using the new filter coefficients $\boldsymbol{w}_k(n+1)$.

**Algorithm 6** Power control algorithm for linear MMSE MUD in the downlink

INPUT: $\boldsymbol{H}_k, \gamma_k, \sigma^2$.
FOR $n = 0, 1, 2, ...$ DO
  FOR $k = 1, 2, ..., K$ DO

$$\begin{aligned} \boldsymbol{w}_k(n+1) &= (\boldsymbol{H}_k\boldsymbol{A}^2(n)\boldsymbol{H}_k^H + \sigma^2\boldsymbol{I})^{-1}A_k(n)\boldsymbol{H}_k\boldsymbol{e}_k \\ A_k^2(n+1) &= \gamma_k\frac{\sum_{j=1,j\neq k}^{K} A_j^2(n)\|\boldsymbol{w}_k^H(n+1)\boldsymbol{H}_k\boldsymbol{e}_j\|^2 + \sigma^2(\boldsymbol{w}_k^H(n+1)\boldsymbol{w}_k(n+1))}{\|\boldsymbol{w}_k^H(n+1)\boldsymbol{H}_k\boldsymbol{e}_k\|^2} \end{aligned}$$

  END FOR;
END FOR;
OUTPUT: assigned powers $A_k$ and linear MMSE filters $\boldsymbol{w}_k$, $k = 1, ..., K$.

### 5.3.2 Linear Precoding Schemes

In this section we consider different approaches to implement linear precoding assuming that the transmitter has perfect CSI.

### Bit-wise Linear Precoding

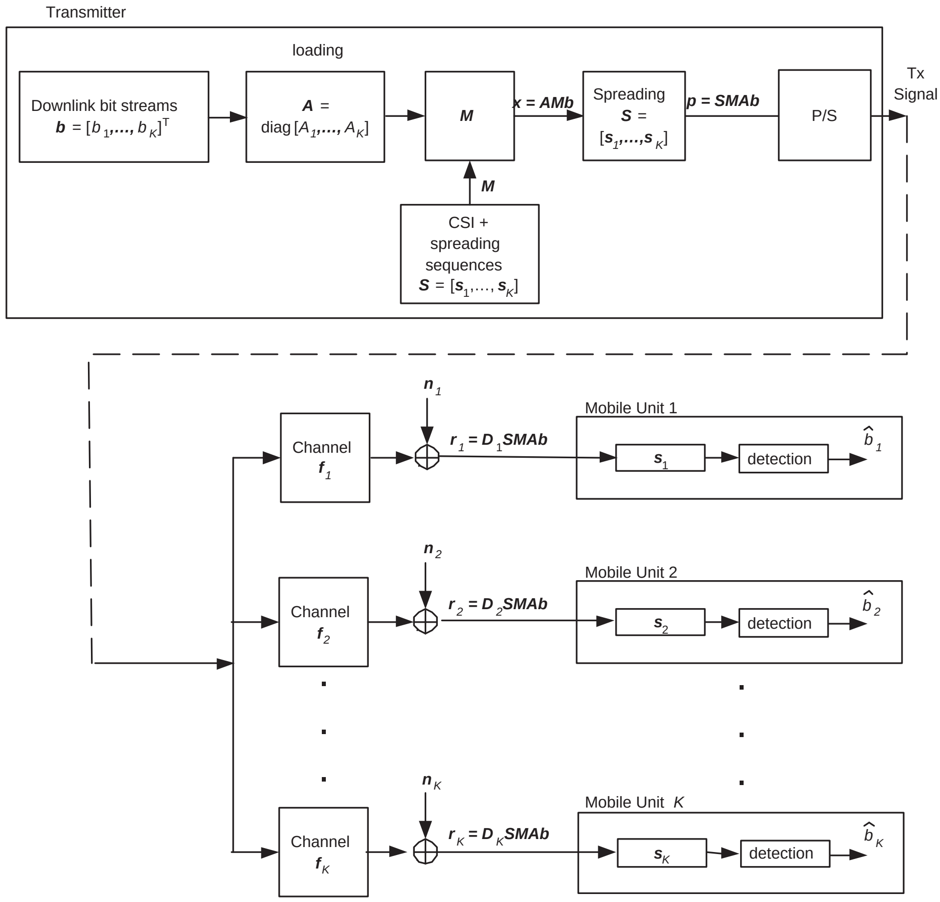


Figure 5.6: Downlink linear precoding.

We assume that each mobile unit employs only a filter matched to its *own* spreading sequence, and it does not need to know other users' spreading sequences or to estimate the channel. Denote the symbol by symbol bit-wise precoding operation as $\boldsymbol{x}[i] = \boldsymbol{M}_b\boldsymbol{A}\boldsymbol{b}[i]$, where $\boldsymbol{x}[i]$ is the precoded symbol vector and $\boldsymbol{M}_b \in \mathbb{C}^{K\times K}$ is the bit-wise linear precoding matrix. Then, after spreading the precoded data, the signal transmitted from the base station during the $i$-th symbol interval can be written as $\boldsymbol{p}[i] = \boldsymbol{S}\boldsymbol{x}[i] = \boldsymbol{S}\boldsymbol{M}_b\boldsymbol{A}\boldsymbol{b}[i]$. The vector $\boldsymbol{p}[i]$ is passed through a parallel-to-serial converter and transmitted through the channel. The signal received by the $k$-th user is then given by

$$\boldsymbol{r}_k[i] = \boldsymbol{D}_k\boldsymbol{S}\boldsymbol{M}_b\boldsymbol{A}\boldsymbol{b}[i] + \boldsymbol{n}_k[i], \tag{5.29}$$

where $\boldsymbol{D}_k$ is given in (5.23). Then the corresponding matched filter $\boldsymbol{s}_k$ is applied to $\boldsymbol{r}_k[i]$. Stacking the outputs of the $K$ matched-filters we obtain

$$\underbrace{\begin{bmatrix} \boldsymbol{s}_1^H \boldsymbol{r}_1[i] \\ \boldsymbol{s}_2^H \boldsymbol{r}_2[i] \\ \vdots \\ \boldsymbol{s}_K^H \boldsymbol{r}_K[i] \end{bmatrix}}_{\boldsymbol{y}[i]} = \underbrace{\begin{bmatrix} \boldsymbol{s}_1^H \boldsymbol{D}_1 \boldsymbol{S} \\ \boldsymbol{s}_1^H \boldsymbol{D}_2 \boldsymbol{S} \\ \vdots \\ \boldsymbol{s}_K^H \boldsymbol{D}_K \boldsymbol{S} \end{bmatrix}}_{\boldsymbol{H}_b} \boldsymbol{M}_b \boldsymbol{A} \boldsymbol{b}[i] + \underbrace{\begin{bmatrix} \boldsymbol{s}_1^H \boldsymbol{n}_1[i] \\ \boldsymbol{s}_2^H \boldsymbol{n}_2[i] \\ \vdots \\ \boldsymbol{s}_K^H \boldsymbol{n}_K[i] \end{bmatrix}}_{\boldsymbol{v}[i]}. \tag{5.30}$$

The $k$-th receiver makes a decision $\hat{b}_k[i] = \mathcal{Q}(y_k[i])$. Therefore the precoder design problem involves designing the precoding matrix $\boldsymbol{M}_b$ such that $\boldsymbol{y}[i]$ is as close to $\boldsymbol{b}[i]$ as possible.

***Bit-wise Linear MMSE Precoder:*** Assuming that the spreading sequences are normalized, the linear MMSE precoder chooses the precoding matrix $\boldsymbol{M}_b$ to minimize $E\{\|\boldsymbol{b}-\boldsymbol{y}\|^2\}$, and is given by [126] $\boldsymbol{M}_b = \beta \boldsymbol{H}_b^{-1}$, with $\beta = \sqrt{\frac{P_T}{\text{tr}\left(\boldsymbol{S}\boldsymbol{H}_b^{-1}\boldsymbol{A}^2\boldsymbol{H}_b^{-H}\boldsymbol{S}^H\right)}}$. Note that such a linear MMSE precoder also zero-forces the interference. If the constraint is the minimum SINR at each receiver $\gamma_k$, we obtain the unconstrained precoding solution $\boldsymbol{M}_b = \boldsymbol{H}_b^{-1}$. Thus we have $\text{SINR}_k = \frac{A_k^2}{\sigma^2}$; and the power assigned to the $k$-th user becomes $A_k^2 = \sigma^2\gamma_k$. Then the total power required at the transmitter becomes $P_T = E\{\|\boldsymbol{S}\boldsymbol{M}_b\boldsymbol{A}\boldsymbol{b}[i]\|^2\} = \text{tr}(\boldsymbol{S}\boldsymbol{M}_b\boldsymbol{A}^2\boldsymbol{M}_b^H\boldsymbol{S}^H)$.

***Bit-wise Wiener Precoder:*** The bit-wise Wiener precoder is proposed in [69, 70] as the matrix $\boldsymbol{M}_b$ and constant $\beta$ that minimize $E\left\{\|\boldsymbol{b}[i] - \beta^{-1}\boldsymbol{y}[i]\|^2\right\}$, subject to $E\{\|\boldsymbol{M}_b\boldsymbol{A}\boldsymbol{b}[i]\|^2\} = P_T$. Given the total transmit power $P_T$, the Wiener precoder is given by

$$\boldsymbol{M}_b = \beta \boldsymbol{J}^{-1}\boldsymbol{H}_b^H, \tag{5.31}$$

with

$$\beta = \sqrt{\frac{P_T}{\text{tr}\left(\boldsymbol{J}^{-2}\boldsymbol{H}_b^H\boldsymbol{A}^2\boldsymbol{H}_b\right)}} \ \text{ and } \ \boldsymbol{J} = \boldsymbol{H}_b^H\boldsymbol{H}_b + \frac{K\sigma^2}{P_T}\boldsymbol{I}_N. \tag{5.32}$$

***Optimal Transmit Spreading Sequences:*** Besides optimizing the precoding matrix $\boldsymbol{M}_b$ for a given channel realization, we can also optimize the transmit spreading sequences. Denote $\boldsymbol{s}_1, ..., \boldsymbol{s}_K$ as the fixed spreading sequences used at the mobile units (i.e., the matched -filters) and $\tilde{\boldsymbol{s}}_1, ..., \tilde{\boldsymbol{s}}_K$ as the optimized spreading sequences used at the transmitter. Denote $\tilde{\boldsymbol{S}} = [\tilde{\boldsymbol{s}}_1, ..., \tilde{\boldsymbol{s}}_K]$. Similarly to (5.30), the received signal can be written as

$$\underbrace{\begin{bmatrix} \boldsymbol{s}_1^H \boldsymbol{r}_1[i] \\ \boldsymbol{s}_2^H \boldsymbol{r}_2[i] \\ \vdots \\ \boldsymbol{s}_K^H \boldsymbol{r}_K[i] \end{bmatrix}}_{\boldsymbol{y}[i]} = \underbrace{\begin{bmatrix} \boldsymbol{s}_1^H \boldsymbol{D}_1 \\ \boldsymbol{s}_1^H \boldsymbol{D}_2 \\ \vdots \\ \boldsymbol{s}_K^H \boldsymbol{D}_K \end{bmatrix}}_{\boldsymbol{H}_c} \tilde{\boldsymbol{S}} \boldsymbol{M}_b \boldsymbol{A} \boldsymbol{b}[i] + \underbrace{\begin{bmatrix} \boldsymbol{s}_1^H \boldsymbol{n}_1[i] \\ \boldsymbol{s}_2^H \boldsymbol{n}_2[i] \\ \vdots \\ \boldsymbol{s}_K^H \boldsymbol{n}_K[i] \end{bmatrix}}_{\boldsymbol{v}[i]}. \tag{5.33}$$

Following [99], it can be easily shown that the linear MMSE precoding matrix is given by $\boldsymbol{M}_b = (\boldsymbol{H}_c \tilde{\boldsymbol{S}})^{-1}$ (for details see Appendix C), and $A_k^2 = \sigma^2 \gamma_k, k = 1, \ldots, K$. Next we show that for any given propagation channel $\boldsymbol{D}_1, ..., \boldsymbol{D}_K$, original spreading sequences $\boldsymbol{S}$, and minimum SINR requirements, we can explicitly find the optimal spreading matrix $\tilde{\boldsymbol{S}}^* \in \mathbb{C}^{N \times K}$ such that the total transmit power $P_T$ is minimized. Assume that the $K \times N$ matrix $\boldsymbol{H}_c$ has rank $K$, where $N \geq K$. Define the SVD $\boldsymbol{H}_c = \boldsymbol{U}_c \boldsymbol{\Sigma}_c \boldsymbol{V}_c^H$, where $\boldsymbol{U}_c$ is a $K \times K$ unitary matrix, $\boldsymbol{V}_c^H$ is an $N \times N$ unitary matrix and $\boldsymbol{\Sigma}_c$ is a $K \times N$ diagonal matrix with $[\boldsymbol{\Sigma}_c]_{i,i} = \lambda_{c,i}$ being the positive square root of the $i$-th eigenvalue of $\boldsymbol{H}_c \boldsymbol{H}_c^H$.

**Proposition 3** *Given the channels $\boldsymbol{D}_1, \ldots, \boldsymbol{D}_K$, the receiver matched-filters $\boldsymbol{s}_1, \ldots, \boldsymbol{s}_K$, and the target SINR $\gamma_1, \ldots, \gamma_K$ of all users, by optimizing the transmit spreading matrix $\tilde{\boldsymbol{S}}$ used in the bit-wise linear MMSE precoder, the minimum achievable transmit power is given by*

$$P_T^* = \min_{\tilde{\boldsymbol{S}} \in \mathbb{C}^{N \times K}} \operatorname{tr}(\tilde{\boldsymbol{S}} \boldsymbol{M}_b \boldsymbol{A}^2 \boldsymbol{M}_b^H \tilde{\boldsymbol{S}}^H) = \sum_{k=1}^{K} A_k^2 \lambda_{c,k}^{-2}, \tag{5.34}$$

*where $A_k^2 = \sigma^2 \gamma_k, k = 1, ..., K$ are the assigned powers. One solution to the optimization problem in (5.34) (i.e., the optimal transmit spreading matrix) is given by the $N \times K$ matrix $\tilde{\boldsymbol{S}}^* = \boldsymbol{H}_c^H$.*

**Proof:** Note that $\boldsymbol{M}_b = (\boldsymbol{H}_c \tilde{\boldsymbol{S}})^{-1}$ and therefore the transmitted vector is given by $\boldsymbol{p}[i] = \tilde{\boldsymbol{S}} \boldsymbol{M}_b \boldsymbol{A} \boldsymbol{b}[i] = \tilde{\boldsymbol{S}} (\boldsymbol{H}_c \tilde{\boldsymbol{S}})^{-1} \boldsymbol{A} \boldsymbol{b}[i]$. Denote the SVDs of $\boldsymbol{H}_c$ and $\tilde{\boldsymbol{S}}$ by $\tilde{\boldsymbol{H}}_c = \boldsymbol{U}_c \boldsymbol{\Sigma}_c \boldsymbol{V}_c^H$ and $\tilde{\boldsymbol{S}} = \boldsymbol{U}_{\tilde{s}} \boldsymbol{\Sigma}_{\tilde{s}} \boldsymbol{V}_{\tilde{s}}^H$, respectively. Then the total transmit power is

$$\begin{aligned}
P_T &= E\{\boldsymbol{p}^H[i]\boldsymbol{p}[i]\} = \mathrm{tr}(\tilde{\boldsymbol{S}}(\boldsymbol{H}_c\tilde{\boldsymbol{S}})^{-1}\boldsymbol{A}^2(\boldsymbol{H}_c\tilde{\boldsymbol{S}})^{-H}\tilde{\boldsymbol{S}}^H) \\
&= \mathrm{tr}(\boldsymbol{U}_{\tilde{s}}\boldsymbol{\Sigma}_{\tilde{s}}\boldsymbol{V}_{\tilde{s}}^H(\boldsymbol{U}_c\underbrace{\boldsymbol{\Sigma}_c\boldsymbol{V}_c^H\boldsymbol{U}_{\tilde{s}}\boldsymbol{\Sigma}_{\tilde{s}}}_{\boldsymbol{T}}\boldsymbol{V}_s^H)^{-1}\boldsymbol{A}^2(\boldsymbol{U}_c\boldsymbol{\Sigma}_c\boldsymbol{V}_c^H\boldsymbol{U}_{\tilde{s}}\boldsymbol{\Sigma}_{\tilde{s}}\boldsymbol{V}_{\tilde{s}}^H)^{-H}\boldsymbol{V}_{\tilde{s}}\boldsymbol{\Sigma}_{\tilde{s}}^H\boldsymbol{U}_{\tilde{s}}^H) \\
&= \mathrm{tr}(\boldsymbol{\Sigma}_{\tilde{s}}\boldsymbol{V}_{\tilde{s}}^H\boldsymbol{V}_{\tilde{s}}\boldsymbol{T}^{-1}\boldsymbol{U}_c^H\boldsymbol{A}^2\boldsymbol{U}_c\boldsymbol{T}^{-H}\boldsymbol{V}_{\tilde{s}}^H\boldsymbol{V}_{\tilde{s}}\boldsymbol{\Sigma}_{\tilde{s}}^H) \\
&= \mathrm{tr}(\boldsymbol{\Sigma}_{\tilde{s}}\boldsymbol{T}^{-1}\boldsymbol{A}^2\boldsymbol{T}^{-H}\boldsymbol{\Sigma}_{\tilde{s}}^H) \;=\; \mathrm{tr}(\boldsymbol{A}^2\boldsymbol{\Sigma}_{\tilde{s}}^2\boldsymbol{T}^{-1}\boldsymbol{T}^{-H}), \qquad (5.35)
\end{aligned}$$

where $\boldsymbol{T} = \boldsymbol{\Sigma}_c\boldsymbol{V}_c^H\boldsymbol{U}_{\tilde{s}}\boldsymbol{\Sigma}_{\tilde{s}}$ is a $K \times K$ matrix; $\boldsymbol{\Sigma}_{\tilde{s}}^2 = \boldsymbol{\Sigma}_{\tilde{s}}^H\boldsymbol{\Sigma}_{\tilde{s}}$ is a $K \times K$ diagonal matrix; and we used the fact that $\boldsymbol{U}_{\tilde{s}}, \boldsymbol{U}_c, \boldsymbol{V}_c$ and $\boldsymbol{V}_{\tilde{s}}$ are unitary.

Consider $\boldsymbol{T}$ expressed in terms of the matrices obtained with the thin SVD [65], $\boldsymbol{T} = \boldsymbol{\Sigma}_c^{(t)}\boldsymbol{C}\boldsymbol{\Sigma}_{\tilde{s}}^{(t)}$, where $\boldsymbol{\Sigma}_c^{(t)}$ and $\boldsymbol{\Sigma}_{\tilde{s}}^{(t)}$ are the $K$-th leading submatrix of $\boldsymbol{\Sigma}_c$ and $\boldsymbol{\Sigma}_{\tilde{s}}$, respectively; and $\boldsymbol{C} = \boldsymbol{V}_c^{(t)H}\boldsymbol{U}_s^{(t)}$ is a $K \times K$ matrix (where $\boldsymbol{V}_c^{(t)}$ and $\boldsymbol{U}_s^{(t)}$ denote the matrices consisting of the first $K$ columns of $\boldsymbol{U}_{\tilde{s}}$ and $\boldsymbol{V}_c$, respectively). Denoting $\{\boldsymbol{v}_{c,1}, ..., \boldsymbol{v}_{c,K}\}$ and $\{\boldsymbol{u}_{\tilde{s},1}, ..., \boldsymbol{u}_{\tilde{s},K}\}$ as the first $K$ columns of $\boldsymbol{V}_c$ and $\boldsymbol{U}_{\tilde{s}}$, respectively, we have $[\boldsymbol{C}]_{ij} = \langle \boldsymbol{v}_{c,i}, \boldsymbol{u}_{\tilde{s},j}\rangle, i, j = 1, ..., K$. Next we show that the eigenvalues of $\boldsymbol{C}$ denoted as $\phi_i,\ i = 1, .., K$, always satisfy $|\phi_i| \leq 1$.

Denote $\{\boldsymbol{e}_1, ..., \boldsymbol{e}_K\}$ as the orthogonal basis of the $K$-dimensional space. Then the $l$-th component of the $\boldsymbol{C}$ transform of the $j$-th basis is given by $[\boldsymbol{e}'_j]_l = [\boldsymbol{C}\boldsymbol{e}_j]_l = [\boldsymbol{C}]_{l,j} = \langle \boldsymbol{v}_{c,l}, \boldsymbol{u}_{\tilde{s},j}\rangle$, where $\langle\cdot,\cdot\rangle$ denotes the inner product. Hence $\|\boldsymbol{e}'_j\|^2 = \sum_{l=1}^K |\langle \boldsymbol{v}_{c,l}, \boldsymbol{u}_{\tilde{s},j}\rangle|^2$. Notice that since $\boldsymbol{V}_c$ and $\boldsymbol{U}_{\tilde{s}} \in \mathrm{SU}(N)$ (i.e., special unitary group), then $\boldsymbol{V}_c^H\boldsymbol{U}_{\tilde{s}}$ also belongs to the SU$(N)$; and therefore the $L_2$ norm of each column vector of the $N \times N$ matrix $\boldsymbol{V}_c^H\boldsymbol{U}_{\tilde{s}}$ equals to one, i.e., $\sum_{l=1}^N |\langle \boldsymbol{v}_{c,l}, \boldsymbol{u}_{\tilde{s},j}\rangle|^2 = 1, j = 1, ..., N$. Since $N \geq K$, we have $\|\boldsymbol{e}'_j\|^2 = \sum_{l=1}^K |\langle \boldsymbol{v}_{c,l}, \boldsymbol{u}_{\tilde{s},j}\rangle|^2 \leq 1, j = 1, ..., K$. This is, the $L_2$ norm of the transformation by $\boldsymbol{C}$ of every basis vector is always less or equal to 1. Every vector in the $K$-dimensional space can be written as a linear combination of the basis and therefore, the $\boldsymbol{C}$ transform applied to any vector reduces the norm. In particular, it reduces the norm of the eigenvectors of $\boldsymbol{C}$. Therefore, we conclude that the eigenvalues of $\boldsymbol{C}$ satisfy $|\phi_i| \leq 1, \forall i$.

Substituting $\boldsymbol{T}^{-1} = [\boldsymbol{\Sigma}_{\tilde{s}}^{(t)}]^{-1}\boldsymbol{C}^{-1}[\boldsymbol{\Sigma}_c^{(t)}]^{-1}$ and the eigenvalue decomposition of $\boldsymbol{C} = \boldsymbol{W}\boldsymbol{\Phi}\boldsymbol{W}^{-1}$ (where $\boldsymbol{\Phi} = \mathrm{diag}(\phi_1, \ldots, \phi_K)$) in (5.35) we obtain

$$\begin{aligned}
P_T &= \mathrm{tr}(\boldsymbol{A}^2\boldsymbol{\Sigma}_{\tilde{s}}^2\boldsymbol{T}^{-1}\boldsymbol{T}^{-H}) = \mathrm{tr}(\boldsymbol{A}^2\boldsymbol{C}^{-1}\boldsymbol{C}^{-H}\boldsymbol{\Sigma}_c^{-2}) = \mathrm{tr}(\boldsymbol{A}^2\boldsymbol{\Phi}^{-1}\boldsymbol{\Phi}^{-H}\boldsymbol{\Sigma}_c^{-2}) \\
&= \sum_{i=1}^K A_i^2\lambda_{c,i}^{-2}|\phi_i|^{-2} \geq \sum_{i=1}^K A_i^2\lambda_{c,i}^{-2}. \qquad (5.36)
\end{aligned}$$

Denote the thin SVD of $\tilde{\boldsymbol{S}} = \boldsymbol{U}_{\tilde{s}}^{(t)}\boldsymbol{\Sigma}_{\tilde{s}}^{(t)}\boldsymbol{V}_{\tilde{s}}^{(t)}$. Finally, with $\tilde{\boldsymbol{S}}^* = \boldsymbol{H}_c^H$, the thin SVD decomposition becomes $\tilde{\boldsymbol{S}}^* = (\boldsymbol{U}_c^{(t)}\boldsymbol{\Sigma}_c^{(t)}\boldsymbol{V}_c^{(t)H})^H = \boldsymbol{V}_c^{(t)}\boldsymbol{\Sigma}_c^{(t)H}\boldsymbol{U}_c^{(t)H}$, i.e.,

$\boldsymbol{U}_{\tilde{s}}^{(t)} = \boldsymbol{V}_c^{(t)}$. Therefore $\boldsymbol{C} = \boldsymbol{V}_c^{(t)H}\boldsymbol{U}_{\tilde{s}}^{(t)} = \boldsymbol{I}_K$, and $\boldsymbol{C}$ has unit eigenvalues. Hence we have equality in (5.36) and $\tilde{\boldsymbol{S}}^* = \boldsymbol{H}_c^H$ is an optimal spreading matrix for linear MMSE precoding. ■

*Remark:* There are many other forms of the optimal spreading matrix $\tilde{\boldsymbol{S}}^*$ such that $\boldsymbol{C} = \boldsymbol{V}_c^{(t)H}\boldsymbol{U}_{\tilde{s}}^{(t)}$ has unit eigenvalues. Specifically, we need to construct an $N \times N$ matrix $\boldsymbol{U}_{\tilde{s}}$ that rotates the first $K$ columns vectors of $\boldsymbol{V}_c$ in the same $K$-dimensional subspace and keep invariant the $N-K$-dimensional subspace spanned by the $N-K$ remaining vectors. Consider first the real case. The constraints on the $K$ first columns of $\boldsymbol{U}_{\tilde{s}}$ are: (a) $\sum_{l=1}^{K} |\langle \boldsymbol{v}_{c,l}, \boldsymbol{u}_{\tilde{s},j}\rangle|^2 = 1, j = 1, ..., K$. [$K$ equations.] (b) $\langle \boldsymbol{u}_{\tilde{s},i}, \boldsymbol{v}_{c,m}\rangle = 0, i = 1, ..., K; m = K+1, ..., N$. [$K \cdot (N-K)$ equations.] (c) $\langle \boldsymbol{u}_{\tilde{s},i}, \boldsymbol{u}_{\tilde{s},j}\rangle = \delta_{ij}, i, j = 1, ..., K$. [$(K-1) + (K-2) + ... + (K-K+1) + (K-K) = K^2 - \frac{1}{2}K(K+1)$ equations.] To construct $\boldsymbol{U}_{\tilde{s}}$, there are $NK$ variables in the $K$ first columns of $\boldsymbol{U}_{\tilde{s}}$. After subtracting the number of constraints, we have $(K^2-K)/2$ degrees of freedom, which is nothing more than the dimension of the O($K$) (i.e., orthogonal group) as expected. In the complex case, there are $2NK$ variables in the first $K$ columns of $\boldsymbol{U}_{\tilde{s}}$ and it can be shown that the solution generalizes to $(K^2-1)$ degrees of freedom that is the number of free parameters of the SU($K$). To summarize, to construct the optimal spreading matrix with SVD decomposition $\tilde{\boldsymbol{S}} = \boldsymbol{U}_{\tilde{s}}\boldsymbol{\Sigma}_{\tilde{s}}\boldsymbol{V}_{\tilde{s}}^H$, we only have to find the unitary matrix $\boldsymbol{U}_{\tilde{s}}$ satisfying the above constraints on its $K$ first column vectors (i.e., range of $\tilde{\boldsymbol{S}}$). Moreover, there are $(K^2-1)$ degrees of freedom to select it.

### Chip-wise Linear Precoding

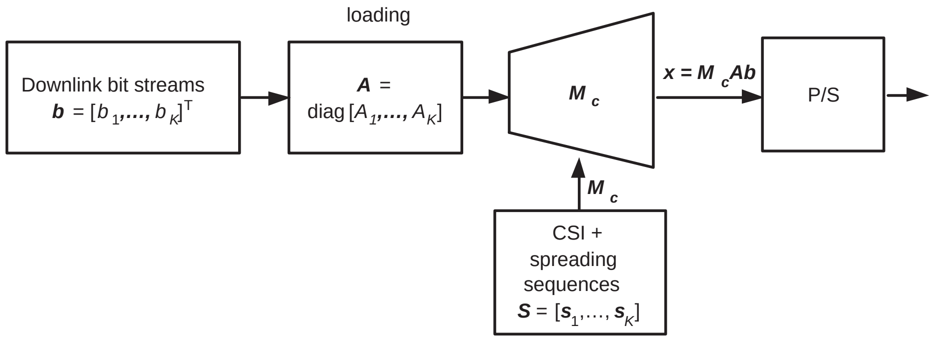


Figure 5.7: Downlink chipwise linear precoding.

In chip-wise precoding, we do not explicitly use any spreading matrix at the transmitter. This is, the precoder takes $K$ symbols and outputs the spread vector of length $N$. Hence the spreading and precoding operations are effectively combined.

The received signal at the $k$th receiver is given by

$$\boldsymbol{r}_k[i] = \boldsymbol{D}_k \boldsymbol{A} \boldsymbol{M}_c \boldsymbol{b}[i] + \boldsymbol{n}_k[i], \tag{5.37}$$

where $\boldsymbol{M}_c \in \mathbb{C}^{N \times K}$ is the chip-wise precoding matrix. At each receiver $k$, the matched-filter $\boldsymbol{s}_k$ is applied to $\boldsymbol{r}_k[i]$. By stacking the outputs of all $K$ matched-filters we obtain

$$\underbrace{\begin{bmatrix} \boldsymbol{s}_1^H \boldsymbol{r}_1[i] \\ \boldsymbol{s}_2^H \boldsymbol{r}_2[i] \\ \vdots \\ \boldsymbol{s}_K^H \boldsymbol{r}_K[i] \end{bmatrix}}_{\boldsymbol{y}[i]} = \underbrace{\begin{bmatrix} \boldsymbol{s}_1^H \boldsymbol{D}_1 \\ \boldsymbol{s}_2^H \boldsymbol{D}_2 \\ \vdots \\ \boldsymbol{s}_K^H \boldsymbol{D}_K \end{bmatrix}}_{\boldsymbol{H}_c} \boldsymbol{M}_c \boldsymbol{A} \boldsymbol{b}[i] + \underbrace{\begin{bmatrix} \boldsymbol{s}_1^H \boldsymbol{n}_1[i] \\ \boldsymbol{s}_2^H \boldsymbol{n}_2[i] \\ \vdots \\ \boldsymbol{s}_K^H \boldsymbol{n}_K[i] \end{bmatrix}}_{\boldsymbol{v}[i]}. \tag{5.38}$$

Differently from the bit-wise system model, here the channel matrix $\boldsymbol{H}_c$ is not a square matrix but has dimension $K \times N$ with $N \geq K$.

***Chip-wise MMSE Precoding:*** Using an argument similar to [99] and given in Appendix C, the linear MMSE chip-wise precoder is given by

$$\boldsymbol{M}_c = \boldsymbol{H}_c^{\dagger} = \boldsymbol{H}_c^H (\boldsymbol{H}_c \boldsymbol{H}_c^H)^{-1}. \tag{5.39}$$

It is easily seen that the SINR for each user is given by

$$\text{SINR}_k = \frac{A_k^2}{\sigma^2}, \quad k = 1, ..., K. \tag{5.40}$$

As before, if we assume that the required SINR for user $k$ is $\gamma_k$, the required power assigned to the $k$-th user becomes $A_k^2 = \sigma^2 \gamma_k$. Due to the precoding matrix, the required total transmit power becomes

$$P_T = \text{tr}(\boldsymbol{H}_c^{\dagger} \boldsymbol{A}^2 \boldsymbol{H}_c^{\dagger H}) = \text{tr}(\boldsymbol{A}^2 (\boldsymbol{H}_c \boldsymbol{H}_c^H)^{-1}). \tag{5.41}$$

*Remark:* Note that under a fixed transmit power budget $P_T$, the linear MMSE precoder is given by $\boldsymbol{M}_c = \beta \boldsymbol{H}_c^{\dagger}$ with $\beta = \sqrt{P_T / \text{tr}(\boldsymbol{A}^2 (\boldsymbol{H}_c \boldsymbol{H}_c^H)^{-1})}$ and $\text{SINR}_k = \frac{(\beta A_k)^2}{\sigma^2}$.

**Proposition 4** *The above chip-wise linear MMSE precoding method is equivalent to the bit-wise linear MMSE precoding method with the optimal spreading matrix at the transmitter $\tilde{\boldsymbol{S}}^*$.*

**Proof:** Using the SVD of $\boldsymbol{H}_c = \boldsymbol{U}_c \boldsymbol{\Sigma}_c \boldsymbol{V}_c^H$, the total transmit power required in the linear MMSE chip-wise precoder is given by

$$\begin{aligned} P_T &= \text{tr}(\boldsymbol{H}_c^{\dagger} \boldsymbol{A}^2 \boldsymbol{H}_c^{\dagger H}) = \text{tr}(\boldsymbol{V}_c \boldsymbol{\Sigma}_c^{-1} \boldsymbol{U}_c^H \boldsymbol{A}^2 \boldsymbol{U}_s \boldsymbol{\Sigma}_c^{-1} \boldsymbol{V}_c^H) \\ &= \text{tr}\left(\boldsymbol{A}^2 \boldsymbol{\Sigma}_c^{-2}\right) = \sum_{i=1}^{K} A_i^2 \lambda_{c,i}^{-2}. \end{aligned} \tag{5.42}$$

Hence the transmit power with the chip-wise linear MMSE precoder is equal to the minimum transmit power in the bit-wise solution given in (5.34). ■

*Remark:* The above result shows that it is not necessary to optimize the spreading operation at the transmitter. That is, by applying the simple chip-wise precoding operation we can obtain the optimal performance.

***Chip-wise Wiener Precoding:*** The Wiener precoder given in (5.31) can be used in our chip-wise scheme by subsituting $\boldsymbol{H}_b$ by $\boldsymbol{H}_c$, resulting in the precoding matrix $\boldsymbol{M}_c \in \mathbb{C}^{N \times K}$. Next we propose a power loading algorithm that can be applied to both the bit-wise and chip-wise Wiener precoders. Consider the signal model (5.38). Define $\boldsymbol{G} = \boldsymbol{H}_c \boldsymbol{M}_c$. Then we can write $y_k[i] = A_k \boldsymbol{G}_{kk} b_k[i] + \sum_{i=1, i \neq k}^{K} A_i \boldsymbol{G}_{ki} b_i[i] + v_k[i], k = 1, ..., K$. In the Wiener precoder $\boldsymbol{M}_c$ is not the pseudo-inverse of $\boldsymbol{H}_c$ and therefore $\boldsymbol{G}$ is not a diagonal matrix. Hence, for a fixed loading matrix $\boldsymbol{A}$, the received SINR is given by

$$\text{SINR}_k = \frac{A_k^2 \|\boldsymbol{G}_{kk}\|^2}{\sigma^2 + \sum_{i=1, i \neq k}^{K} A_i^2 \|\boldsymbol{G}_{ki}\|^2}. \tag{5.43}$$

To achieve the target SINR $\gamma_k$ for each user $k$, we need to find the optimal powers $A_k^2, k = 1, ..., K$. Now, different from the linear MMSE precoding, the power allocation problem is coupled with the problem of finding the optimal precoding matrix. Following the ideas of [122] we propose the following iterative algorithm to solve the joint problem. In the algorithm we first fix the power loading values $\boldsymbol{A}(n)$ to find the precoding matrix and then, based on the precoding matrix, the power loading values are updated. Simulations show that the algorithm converges in about two or three iterations.

### 5.3.3 Simulation Results

***Chip-wise precoding vs. bit-wise precoding:*** We first compare the bit-wise linear MMSE precoding (without optimizing the spreading sequences at the transmitter) with the chip-wise linear MMSE precoding. We assume that the target SINR per

**Algorithm 7** Power control algorithm for Wiener precoder

```
INPUT: $\boldsymbol{H}_c, \sigma^2$ and $\gamma_k, k = 1, ..., K$;
FOR $n = 1, 2, ...$ DO
  $\boldsymbol{D}(n+1) = \boldsymbol{H}_c^H \boldsymbol{H}_c + \frac{K\sigma^2}{P_T(n)} \boldsymbol{I}_N$
  $\beta(n+1) = \sqrt{\frac{P_T(n)}{\mathrm{tr}(\boldsymbol{J}^{-2}(n+1)\boldsymbol{H}_c^H \boldsymbol{A}^2(n)\boldsymbol{H}_c)}}$
  $\boldsymbol{M}_c(n+1) = \beta(n+1)\boldsymbol{J}^{-1}(n+1)\boldsymbol{H}_c^H$;
  $\boldsymbol{G}(n+1) = \boldsymbol{H}_c \boldsymbol{M}_c(n+1)$;
  FOR $k = 1 : K$ DO
    $A_k^2(n+1) = \gamma_k \frac{\sum_{i=1, i\neq k}^{K} A_i^2(n) \|\boldsymbol{G}_{ki}(n+1)\|^2 + \sigma^2}{\|\boldsymbol{G}_{kk}(n+1)\|^2}$;
  END;
  $P_T(n+1) = E\{\|\boldsymbol{M}_c(n+1)\boldsymbol{A}(n+1)\boldsymbol{b}\|^2\} = \mathrm{tr}(\boldsymbol{M}_c(n+1)\boldsymbol{A}^2(n+1)\boldsymbol{M}_c^H(n+1))$;
END FOR;
OUTPUT: precoding matrix $\boldsymbol{M}_c(n+1)$, and assigned powers $\boldsymbol{A}(n+1)$
```

user is constant for all users, $\gamma_k = 10$dB, $k = 1, \ldots, K$. We consider random codes and Gold codes with spreading gain $N = 31$ and the total number of users $K = 15$. We assume that each mobile user experiences an independent multipath channel $\boldsymbol{f}_k = [f_{k,1}, ..., f_{k,L}]^T$ with $L = 3$ resolvable paths, and the transmitter has perfect CSI of all users. The path gains are generated according to $f_{k,i} \sim \mathcal{N}_c(0, \frac{1}{L})$. The results are averaged over 1000 different channel realizations. The cumulative distribution function (CDF) of the required power at the transmitter to achieve the minimum SINR at the receivers is shown in Fig. 5.8. It is seen that under this severe multipath, the suboptimal bit-wise solution incurs a large performance degradation.

***Chip-wise precoding with matched-filter vs. bit-wise precoding with RAKE receiver:*** The bit-wise linear MMSE precoding with a RAKE receiver was proposed in [126]. The difference with the linear MMSE precoder considered in the Section 3.1 is that the receiver must also estimate the channel and apply a RAKE receiver, consequently, increasing the number of pilot symbols and the complexity of the receiver. We discuss this method only for comparison since we seek precoding solutions with simple receivers with no receiver CSI. The RAKE receiver can be implemented with a matched filter using the effective spreading sequence (i.e., the $k$-th effective spreading sequence is $\bar{\boldsymbol{s}}_k = \boldsymbol{f}_k \star \boldsymbol{s}_k$) instead of the original spreading sequence. With our notation, the $k$-th effective spreading sequence is given by the convolution $\bar{\boldsymbol{s}}_k = \boldsymbol{D}_k \boldsymbol{S} \boldsymbol{e}_k = \boldsymbol{D}_k \boldsymbol{s}_k$, where we have limited the convolution to $N$ chip samples. Then, with the RAKE receiver the system model can be written as

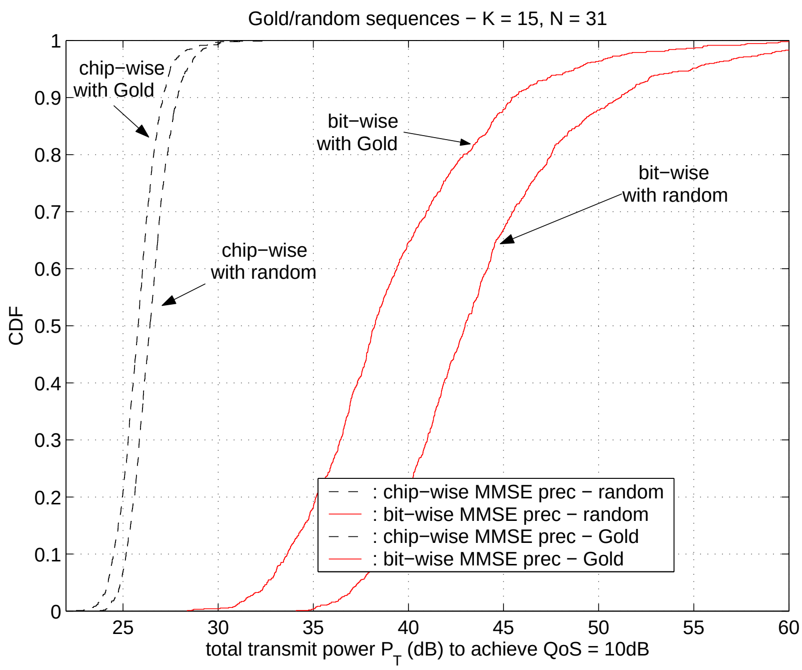


Figure 5.8: Chip-wise precoding vs. bit-wise precoding: CDF of the required power $P_T$ at the transmitter to achieve $\gamma_k = 10$dB, $\forall k$. Spreading gain $N = 31$, $K = 15$ users.

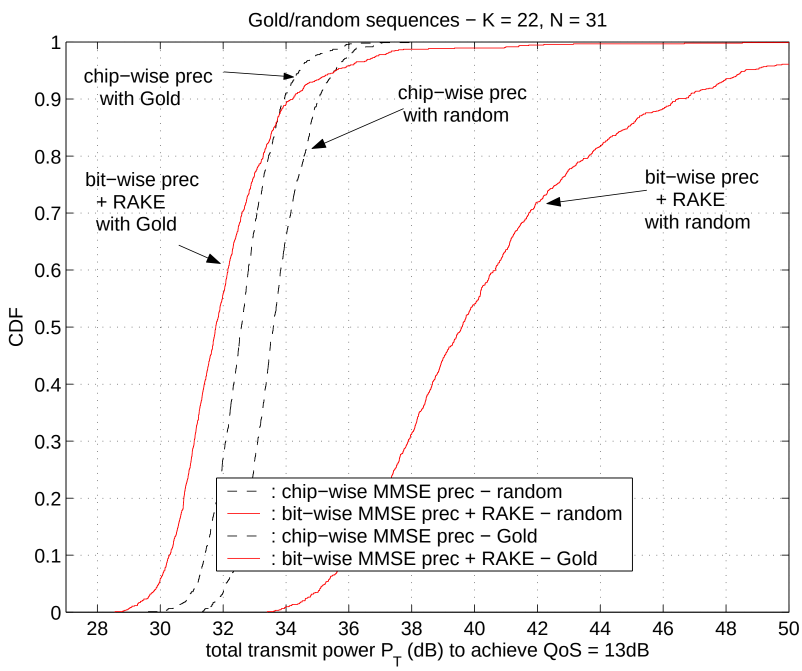


Figure 5.9: Chip-wise precoding with matched-filter vs. bit-wise precoding with RAKE receiver: CDF of the required power $P_T$ at the transmitter to achieve $\gamma_k =$ 13dB, $\forall k$. Spreading gain $N = 31$, $K = 22$ users.

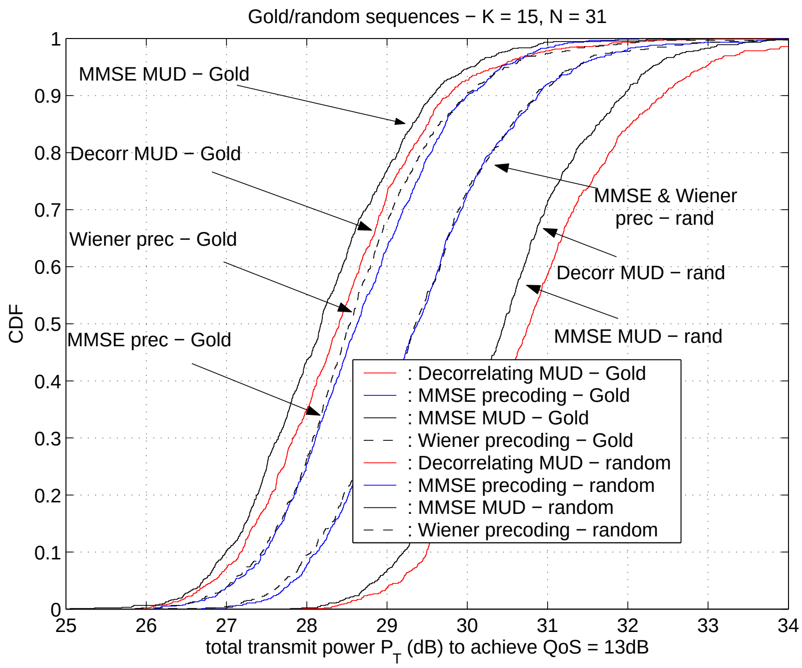


Figure 5.10: Linear precoding vs. linear MUD: CDF of the required power $P_T$ at the transmitter to achieve $\gamma_k = 13$dB, $\forall k$. Spreading gain $N = 31$, $K = 15$ users.

$$\underbrace{\begin{bmatrix} \boldsymbol{s}_1^H \boldsymbol{D}_1^H \boldsymbol{r}_1[i] \\ \boldsymbol{s}_2^H \boldsymbol{D}_2^H \boldsymbol{r}_2[i] \\ \vdots \\ \boldsymbol{s}_K^H \boldsymbol{D}_K^H \boldsymbol{r}_K[i] \end{bmatrix}}_{\boldsymbol{y}[i]} = \underbrace{\begin{bmatrix} \boldsymbol{s}_1^H \boldsymbol{D}_1^H \boldsymbol{D}_1 \boldsymbol{S} \\ \boldsymbol{s}_1^H \boldsymbol{D}_2^H \boldsymbol{D}_2 \boldsymbol{S} \\ \vdots \\ \boldsymbol{s}_K^H \boldsymbol{D}_K^H \boldsymbol{D}_K \boldsymbol{S} \end{bmatrix}}_{\boldsymbol{H}_b} \boldsymbol{M}_b \boldsymbol{A} \boldsymbol{b}[i] + \underbrace{\begin{bmatrix} \boldsymbol{s}_1^H \boldsymbol{D}_1^H \boldsymbol{n}_1[i] \\ \boldsymbol{s}_2^H \boldsymbol{D}_2^H \boldsymbol{n}_2[i] \\ \vdots \\ \boldsymbol{s}_K^H \boldsymbol{D}_K^H \boldsymbol{n}_K[i] \end{bmatrix}}_{\boldsymbol{v}[i]} . \tag{5.44}$$

It is easily seen that the linear MMSE precoding solution still yields $\boldsymbol{M}_b = \boldsymbol{H}_b^{-1}$, where $\boldsymbol{H}_b$ is defined in (5.44). The signal to noise ratio for user $k$ is

$$\mathrm{SINR}_k = \frac{A_k^2}{\sigma^2 \|\boldsymbol{D}_k \boldsymbol{s}_k\|^2}, \quad k = 1, \ldots, K, \tag{5.45}$$

and the required power to achieve an SINR value $\gamma_k$ becomes $A_k^2 = \sigma^2 \gamma_k \boldsymbol{s}_k^H \boldsymbol{D}_k^H \boldsymbol{F}_k \boldsymbol{s}_k$. Therefore, the total transmitted power is given by

$$P_T = E\{\|\boldsymbol{S}\boldsymbol{H}_b^{-1}\boldsymbol{A}\boldsymbol{b}[i]\|^2\} = \mathrm{tr}(\boldsymbol{S}\boldsymbol{H}_b^{-1}\boldsymbol{A}^2\boldsymbol{H}_b^{-H}\boldsymbol{S}^H). \tag{5.46}$$

Notice that the Wiener precoding solution can also be applied to the system in (5.44).

Next we compare the chip-wise linear MMSE precoder given in Section 5.3.2 (which is equivalent to the optimal bit-wise linear MMSE precoder) with the above bit-wise precoder with a RAKE receiver. The results are shown in Fig. 5.9. With Gold sequences the RAKE receiver brings less than 0.5dB gain on average compared with the simple chip-wise precoder with matched-filter receiver. Note that the performance of a communication system is dominated by the outage events. Given an outage probability $p_{out}$, we define the corresponding outage power $P_{out}$ as $p_{out} = Pr\{P_T \geq P_{out}\}$. It is seen that although on average the RAKE receiver is slightly better, it is more prone to outage. For instance, consider in the plot the 5% outage probability for which the chip-wise precoder requires around 34.5 dB whereas the RAKE receiver requires around 35.5dB. When considering the 1% outage probability, this effect is more pronounced and the RAKE receiver requires 5 dB more than the chip-wise precoder to achieve the same performance. This effect will be more clear in the BER simulation results [cf. Fig. 12 and Fig. 13]. Interestingly, the performance of the precoder with RAKE receiver decays considerably when random sequences are used. Therefore, the chip-wise precoder is not only simpler (and it makes the receiver simpler since no CSI is required at the receiver) but it also has excellent performance. From the above simulation results we can conclude that: (a) The original bit-wise precoder with the matched filter at the receiver is far from optimal in multipath channels; (b) The bit-wise precoder with RAKE receiver makes the mobile units more complex and does not bring much improvements with Gold sequences and it can be very detrimental with random spreading sequences; (c) Therefore the proposed chip-wise precoding method offers both low complexity and high performance.

***Linear precoding vs. linear MUD – total transmit power:*** Next we compare linear MUD with linear precoding assuming the same simulations parameters. We compare the CDF of the required total power $P_T$ at the transmitter to achieve a target SINR $\gamma_k = 13$dB, $\forall k$, in each of the four following schemes: (a) linear decorrelating MUD [cf. Eq.(5.26)]; (b) linear MMSE MUD [cf. Alg. 6]; (c) chip-wise linear MMSE precoder, [cf. Eq.(5.41)]; and (d) chip-wise Wiener precoder [cf. Alg. 7]. Simulations are performed for spreading gain $N = 31$, with Gold and random spreading sequences. Fig. 5.10 shows the results with $K = 15$ users and Fig. 5.11 shows the results with $K = 27$ users. It is seen that with Gold codes, MUD is slightly better (although only 0.5dB of difference with linear precoding when 15 users are considered), whereas with random codes linear precoding largely outperforms MUD. Notice that the Wiener precoder is slightly better than the MMSE precoder. It is also seen that the total power required in the precoding solutions

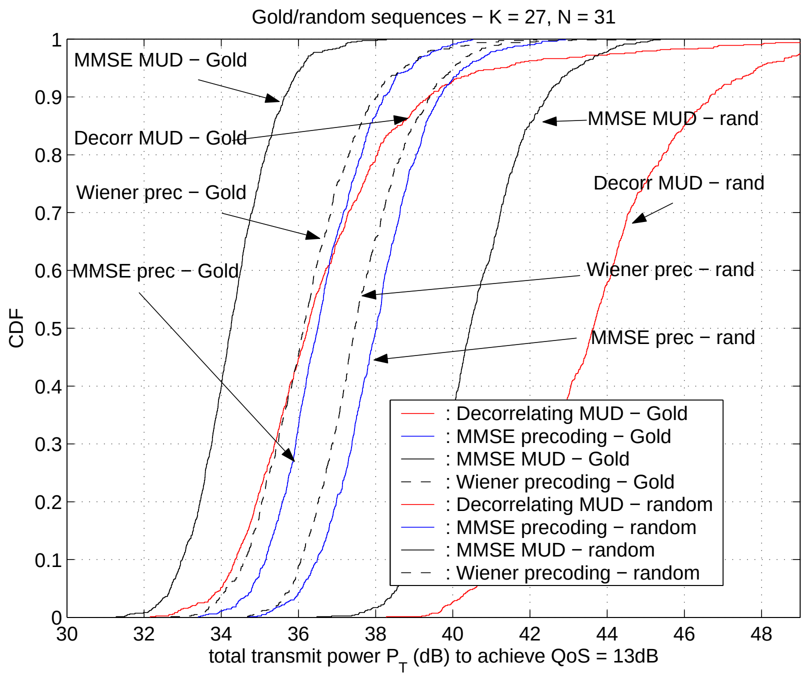


Figure 5.11: Linear precoding vs. linear MUD: CDF of the required power $P_T$ at the transmitter to achieve $\gamma_k = 10$dB, $\forall k$. Spreading gain $N = 31$, $K = 27$ users.

is almost independent of the chosen spreading sequences and therefore, an outage event is less likely to occur. Although the linear MMSE MUD solution seems to be quite effective with Gold codes, we recall that it is unlikely to be implemented in the downlinks of most wireless systems due to the amount of required feedback information to implement perfect power control and other issues discussed in Section 1. Also notice that the linear decorrelator offers very poor performance in heavily loaded systems, which does not occur to the linear MMSE linear precoder.

***Linear precoding vs. linear MUD – BER performance:*** Fig. 5.12 and Fig. 5.13 show the BER performance of the various linear MUD and linear precoding methods. The results are averaged over 100 channel realization and QPSK modulation is employed. Recall that the linear MMSE precoder is equivalent to the transmitter counterpart of the decorrelator. For the decorrelating MUD we consider perfect power loading to achieve the same SNR across the users. It is seen that the linear MMSE precoder with RAKE only performs slightly better with Gold sequences in the very low SNR region. In all the other cases, the chip-wise linear MMSE precoder obtains much better results. On the other hand, the chip-wise MMSE precoder obtains much better results than the decorrelating MUD, especially in heavily loaded systems. These results are due to the outage events of the decor-

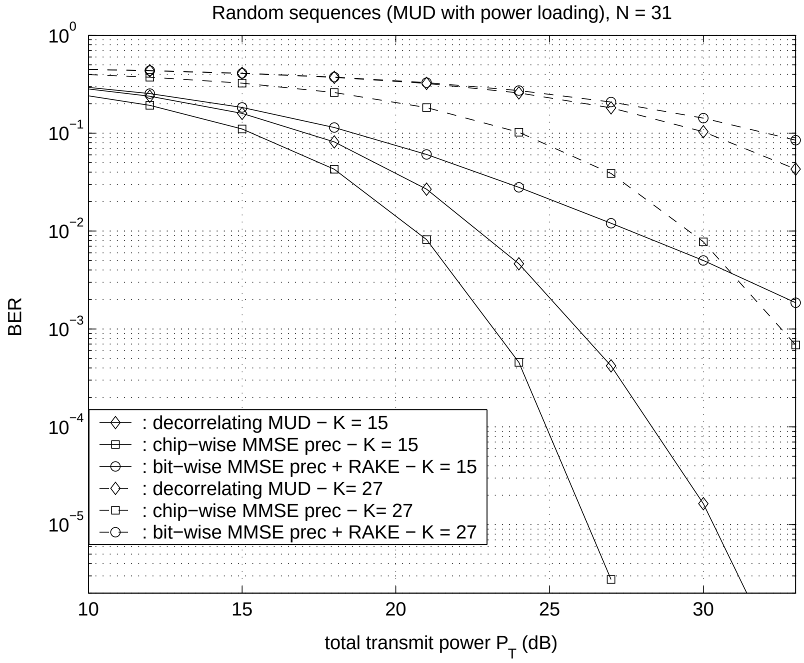


Figure 5.12: Linear precoding vs. linear MUD: BER performance with random spreading sequences. Spreading gain $N = 31$, $K = 15$ and $K = 27$ users.

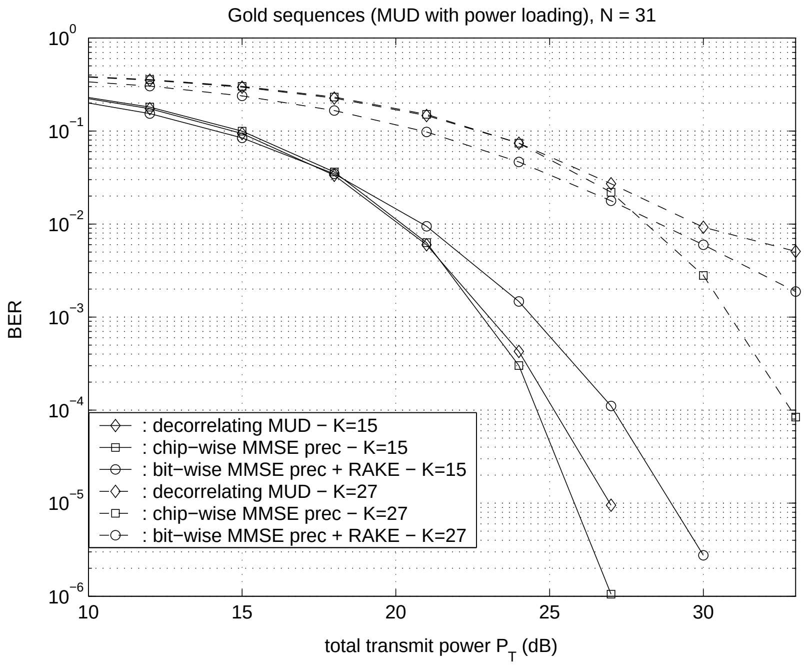


Figure 5.13: Linear precoding vs. linear MUD: BER performance with Gold spreading sequences. Spreading gain $N = 31$, $K = 15$ and $K = 27$ users.

relating MUD observed in Fig. 5.10 and Fig. 5.11. Again, it is seen that the BER performance of the chip-wise precoding solution is almost independent of the chosen spreading sequence.

## 5.4 TH Precoding in Downlink CDMA

In this section we consider nonlinear precoding solutions based on TH precoding that outperform linear precoding.

### 5.4.1 Downlink CDMA System Model with ISI

We consider a $K$-user discrete-time downlink CDMA system signaling over multipath channels. Denote $b_k[i] \in \mathcal{A}$ as the information symbol of the $k$-th user transmitted during the $i$-th symbol interval, where $\mathcal{A}$ is a finite constellation set; and $\boldsymbol{b}[i] = [b_1[i], ..., b_K[i]]^T$. Denote the symbol by symbol precoding operation as $\boldsymbol{x}[i] = \Psi(\boldsymbol{b}[i], ..., \boldsymbol{b}[i-\nu+1])$, where $\boldsymbol{x}[i]$ is the $K \times 1$ precoded symbol vector based on $\nu$ information symbol vectors. Denote $N$ as the spreading factor and $\boldsymbol{s}_k = [s_{k,1}, ..., s_{k,N}]^T$ as the spreading waveform of the $k$-th user. Then the signal transmitted from the base station during the $i$-th symbol interval can be written as $\boldsymbol{p}[i] = \boldsymbol{S}\boldsymbol{x}[i]$, where $\boldsymbol{S} = [\boldsymbol{s}_1, \boldsymbol{s}_2, ..., \boldsymbol{s}_K]$ . The vector $\boldsymbol{p}[i]$ is passed through a parallel-to-serial converter and transmitted over the wireless channel. The path delays are assumed to be integral multiples of the chip interval. Denote the multipath channel seen by the $k$-th user as $\boldsymbol{f}_k = [f_{k,1}, f_{k,2}, ..., f_{k,L}]^T$ , where $L$ is the number of resolvable paths and $f_{k,l}$ is the complex fading gain corresponding to the $l$-th path of the $k$-th user. We assume that $L \leq N$ so that the delay spread is at most one symbol interval.

Different from the previous section, here we also consider intersymbol interference (ISI). Denote $\boldsymbol{r}_k[i]$ as the $N \times 1$ received signal vector by the $k$-th user during the $i$-th symbol interval (i.e., $N$ consecutive chip intervals). Then

$$\boldsymbol{r}_k[i] = \boldsymbol{D}_k\boldsymbol{S}\boldsymbol{x}[i] + \bar{\boldsymbol{D}}_k\boldsymbol{S}\boldsymbol{x}[i-1] + \boldsymbol{n}_k[i], \tag{5.47}$$

where $\boldsymbol{n}_k[i] \sim \mathcal{N}_c\left(\boldsymbol{0}, \sigma_n^2\boldsymbol{I}_N\right)$ is the complex white Gaussian noise vector at the

$k$-th receiver, and

$$\boldsymbol{D}_k = \begin{bmatrix} f_{k,1} & 0 & & \cdots & 0 \\ f_{k,2} & f_{k,1} & 0 & \ddots & \vdots \\ \vdots & \ddots & & \ddots & 0 \\ 0 & \cdots & f_{k,L} & \cdots & f_{k,1} \end{bmatrix}_{N \times N}, \quad \text{and } \bar{\boldsymbol{D}}_k = \begin{bmatrix} 0 & \cdots & f_{k,L} & \cdots & f_{k,2} \\ 0 & \cdots & \ddots & \ddots & \vdots \\ \vdots & \ddots & \ddots & 0 & f_{k,L} \\ 0 & \cdots & & \cdots & 0 \end{bmatrix}_{N \times N}. \tag{5.48}$$

At the $k$-th mobile receiver, a matched-filter is applied to the received signal $\boldsymbol{r}_k[i]$ with this user's signature waveform, i.e., $y_k[i] = \boldsymbol{s}_k^H \boldsymbol{r}_k[i]$. By stacking the matched-filter output from all users into a single vector we have

$$\underbrace{\begin{bmatrix} \boldsymbol{s}_1^H \boldsymbol{r}_1[i] \\ \boldsymbol{s}_2^H \boldsymbol{r}_2[i] \\ \vdots \\ \boldsymbol{s}_K^H \boldsymbol{r}_K[i] \end{bmatrix}}_{\boldsymbol{y}[i]} = \underbrace{\begin{bmatrix} \boldsymbol{s}_1^H \boldsymbol{D}_1 \boldsymbol{S} \\ \boldsymbol{s}_2^H \boldsymbol{D}_2 \boldsymbol{S} \\ \vdots \\ \boldsymbol{s}_K^H \boldsymbol{D}_K \boldsymbol{S} \end{bmatrix}}_{\boldsymbol{H}} \boldsymbol{x}[i] + \underbrace{\begin{bmatrix} \boldsymbol{s}_1^H \bar{\boldsymbol{D}}_1 \boldsymbol{S} \\ \boldsymbol{s}_2^H \bar{\boldsymbol{D}}_2 \boldsymbol{S} \\ \vdots \\ \boldsymbol{s}_K^H \bar{\boldsymbol{D}}_K \boldsymbol{S} \end{bmatrix}}_{\bar{\boldsymbol{H}}} \boldsymbol{x}[i-1] + \underbrace{\begin{bmatrix} \boldsymbol{s}_1^H \boldsymbol{n}_1[i] \\ \boldsymbol{s}_2^H \boldsymbol{n}_2[i] \\ \vdots \\ \boldsymbol{s}_K^H \boldsymbol{n}_K[i] \end{bmatrix}}_{\boldsymbol{v}[i]}. \tag{5.49}$$

A different situation is when instead of applying a fixed matched filter, the receiver implements a RAKE receiver as proposed in [39]. The main difference is that each receiver must also estimate the channel to apply the RAKE receiver, consequently, increasing the number of pilot symbols and the complexity of the receiver. We discuss this method only for comparison since we seek precoding solutions with simple receivers without receiver CSI. The RAKE receiver can be implemented with a matched filter using the normalized effective spreading sequence (i.e., the $k$-th effective spreading sequence is $\bar{\boldsymbol{s}}_k = \boldsymbol{f}_k \star \boldsymbol{s}_k$) instead of the original spreading sequence. With our notation, the normalized $k$-th effective spreading sequence is given by the convolution $\bar{\boldsymbol{s}}_k = \frac{1}{\|\boldsymbol{D}_k \boldsymbol{s}_k\|} \boldsymbol{D}_k \boldsymbol{s}_k$, where we have limited the convolution to $N$ chip samples.

The problem of the precoder design is to choose an appropriate precoding function $\Psi(\cdot)$ so that the output vector $\boldsymbol{y}[i]$ of the matched-filters is as close as possible to the transmitted data vector $\boldsymbol{b}[i]$.

### 5.4.2 Bit-wise Multiuser TH Precoding

If the ISI term $\bar{\boldsymbol{H}}\boldsymbol{x}[i-1]$ were not present in (5.49) (this is the case when a guard interval is inserted between consecutive symbols as considered in section 5.3), then the TH precoding scheme in [130] for multiple-input multiple-output (MIMO) systems can be directly applied here. In such a case the TH precoder consists of a

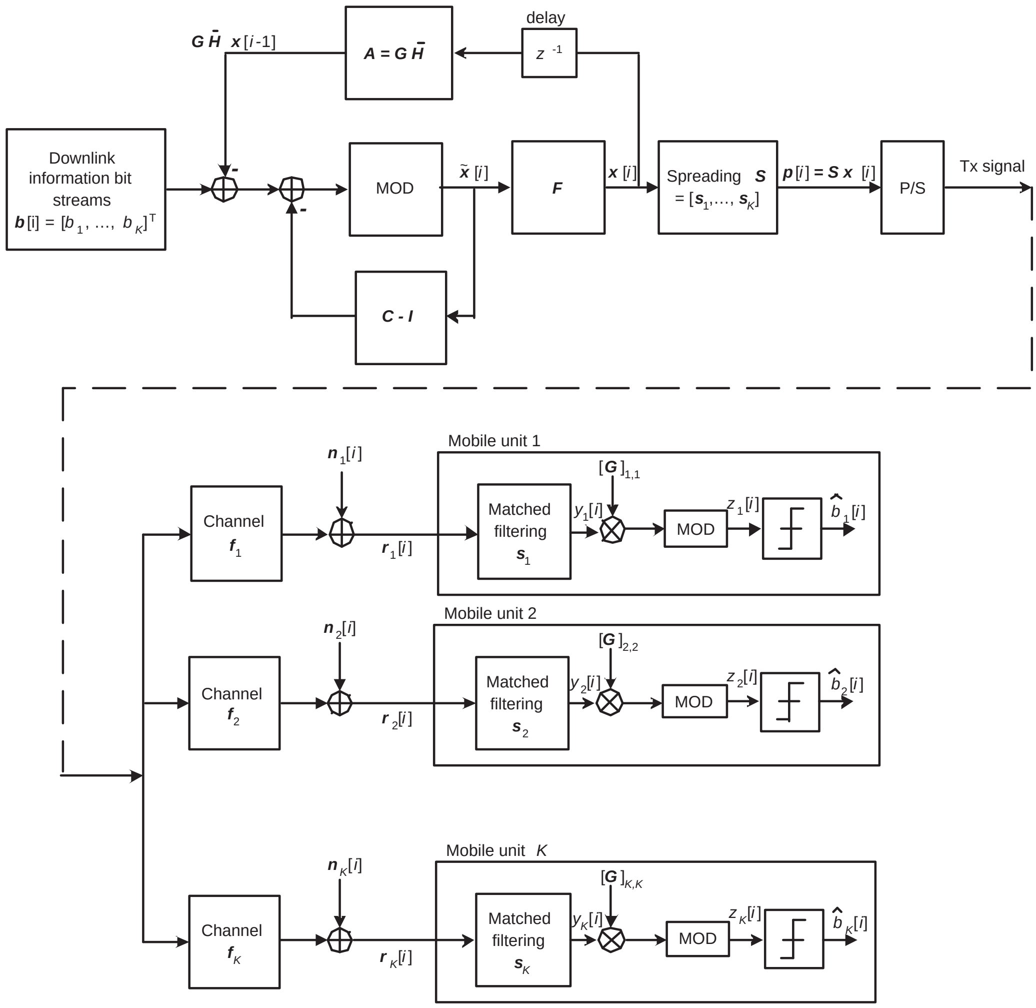


Figure 5.14: Bit-wise TH-precoded downlink CDMA system over multipath channels.

feedforward (FF) filter matrix $\boldsymbol{F}$ and a feedback (FB) filter matrix $(\boldsymbol{C}-\boldsymbol{I})$, which are obtained in the following way. Denote the LQ factorization of the matrix $\boldsymbol{H}$ as $\boldsymbol{H} = \boldsymbol{W}\boldsymbol{F}^H$, where $\boldsymbol{F}$ is unitary and $\boldsymbol{W}$ is lower triangular. The purpose of the FF matrix $\boldsymbol{F}$ is to convert the interference into a causal form without increasing the transmit power. This permits the cancellation of the causal interference using the FB filter matrix $(\boldsymbol{C}-\boldsymbol{I})$. For the interference cancellation to be possible, $\boldsymbol{C}$ needs to be monic lower triangular. To obtain $\boldsymbol{C}$, decompose $\boldsymbol{W} = \boldsymbol{G}^{-1}\boldsymbol{C}$ where $\boldsymbol{G}$ is the diagonal matrix that makes $\boldsymbol{C}$ monic, i.e., $\boldsymbol{G} = \mathrm{diag}(w_{1,1}^{-1}, ..., w_{K,K}^{-1})$ where $w_{i,i}$ denotes the $i$-th diagonal element in $\boldsymbol{W}$. Denote $\tilde{\boldsymbol{x}}[i]$ as the output of the FB filter. Then we have $\tilde{\boldsymbol{x}}[i] = \boldsymbol{b}[i] - (\boldsymbol{C}-\boldsymbol{I})\tilde{\boldsymbol{x}}[i]$, and consequently, the equivalent FB operation is $\tilde{\boldsymbol{x}}[i] = \boldsymbol{C}^{-1}\boldsymbol{b}[i]$. Thus, the input data symbols $\boldsymbol{b}[i]$ are first passed through the FB filter $\boldsymbol{C}^{-1}$ and then through the FF filter $\boldsymbol{F}$, i.e., $\boldsymbol{x}[i] = \boldsymbol{F}\boldsymbol{C}^{-1}\boldsymbol{b}[i]$, followed by spreading (cf. Fig. 5.14).

*Feedback and Modulo Operations:* Due to the lower triangular structure of the matrix $\boldsymbol{C}$, the output of the FB filter $\tilde{x}_k, k = 1, ..., K$, is successively generated from the input data symbols $b_k[i] \in \mathcal{A}$, and the previous output of the FB filter, $\tilde{x}_\ell[i], \ell = 1, ..., k-1$, as $\tilde{x}_k[i] = b_k[i] - \sum_{\ell=1}^{k-1} c_{k,\ell}\tilde{x}_\ell[i],\ k = 1, ..., K$. To prevent an increase in transmit power, a modulo operation with respect to $\mathcal{A}$ is applied. For example, for $M$-QAM constellations, the modulo operation corresponds to adding integer multiples of $2\sqrt{M}$ to the real and the imaginary parts of $b_k[i]$, so that the resulting output signal falls in the range of $\mathcal{A}$. Then the output of the FB filter becomes

$$\tilde{x}_k[i] = b_k[i] + d_k[i] - \sum_{\ell=1}^{k-1} c_{k,\ell}\tilde{x}_\ell[i], \quad k = 1, ..., K, \tag{5.50}$$

where $d_k[i] \in \{2\sqrt{M}(d_I + jd_Q) | d_I, d_Q \in \mathbb{Z}\}$. That is, instead of feeding back $b_k[i]$, the symbols $v_k[i] = b_k[i] + d_k[i]$ are passed through $\boldsymbol{C}^{-1}$. If the receiver applies the same modulo operation, then the effect is cancelled.

*Cascade of Operations:* At the $k$-th user's receiver, a matched-filter $\boldsymbol{s}_k$, a scalar operation $g_k = \boldsymbol{G}[k,k] = w_{k,k}^{-1}$ and the same modulo operation as applied at the transmitter are applied to the received signal $\boldsymbol{r}_k[i]$. Therefore, without considering the modulo operation, the end-to-end operation for all $K$ users is given by

$$\boldsymbol{z}[i] = \boldsymbol{G}\left(\boldsymbol{H}\boldsymbol{F}\boldsymbol{C}^{-1}\boldsymbol{b}[i] + \boldsymbol{v}[i]\right) = \boldsymbol{b}[i] + \boldsymbol{G}\boldsymbol{v}[i]. \tag{5.51}$$

and the $k$-th user makes a decision on $b_k[i]$ based on the decision statistic $z_k[i]$. Note that the scalar gains $g_k, k = 1, ..., K$, can be either estimated at the mobile receiver (automatic gain control) or broadcast by the base station.

*TH-Precoding with ISI:* Consider now (5.49) without dropping the ISI term. In

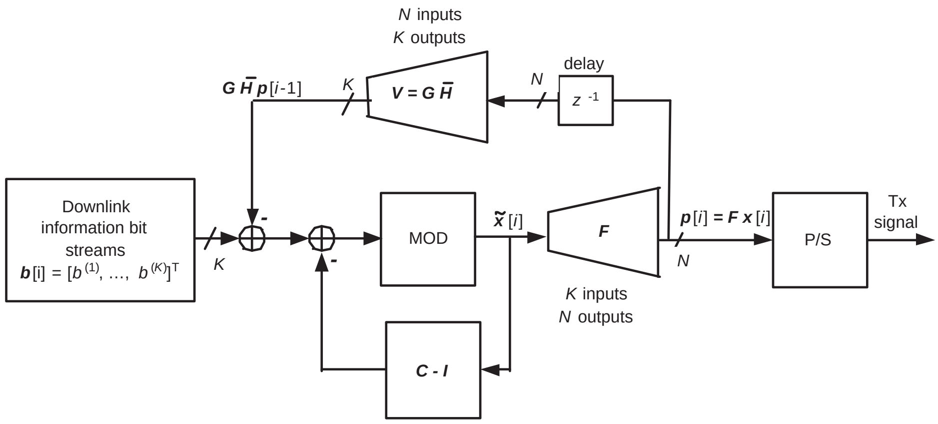


Figure 5.15: Chip-wise TH-precoded downlink CDMA system over multipath channels.

addition to the FF and FB filters discussed above based on the decomposition $\boldsymbol{H} = \boldsymbol{G}^{-1}\boldsymbol{C}\boldsymbol{F}^H$, another FB filter is employed to cancel the ISI term $\bar{\boldsymbol{H}}\boldsymbol{x}[i-1]$. Suppose that the previously precoded symbol $\boldsymbol{x}[i-1]$ is first filtered by a filter $\boldsymbol{V}$ and then substracted from the current data symbol $\boldsymbol{b}[i]$, as shown in Fig. 5.14. To find the matrix $\boldsymbol{V}$ that minimizes the mean-square error (MSE) consider the error signal at the decision device

$$\boldsymbol{e}[i] = \underbrace{\Big(\boldsymbol{G}\boldsymbol{H}\boldsymbol{F}\boldsymbol{C}^{-1}(\boldsymbol{b}[i] - \boldsymbol{V}\boldsymbol{x}[i-1]) + \boldsymbol{G}\boldsymbol{v}[i] + \boldsymbol{G}\bar{\boldsymbol{H}}\boldsymbol{x}[i-1]\Big)}_{\boldsymbol{z}[i]} - \boldsymbol{b}[i]. \quad (5.52)$$

By the orthogonality principle, $E\{\boldsymbol{e}\boldsymbol{z}^H\} = \mathbf{0}$, which leads to $(\boldsymbol{G}\bar{\boldsymbol{H}} - \boldsymbol{G}\boldsymbol{H}\boldsymbol{F}\boldsymbol{C}^{-1}\boldsymbol{V}) = \mathbf{0}$, i.e., $\boldsymbol{V} = \boldsymbol{G}\bar{\boldsymbol{H}}$. Hence the end-to-end cascade of operations is given by

$$\begin{aligned}\boldsymbol{z}[i] &= \underbrace{\boldsymbol{G}}_{\text{rx}}\Big(\underbrace{\boldsymbol{G}^{-1}\boldsymbol{C}\boldsymbol{F}^H}_{\text{channel}}\Big(\underbrace{\boldsymbol{F}}_{\text{FF}}\ \underbrace{\boldsymbol{C}^{-1}}_{\text{cancel,FB}}\ \Big(\boldsymbol{b}[i] - \underbrace{\boldsymbol{G}\bar{\boldsymbol{H}}\boldsymbol{x}[i-1]}_{\text{cancel ISI}}\Big)\Big) + \underbrace{\bar{\boldsymbol{H}}\boldsymbol{x}[i-1]}_{\text{ISI channel}} + \boldsymbol{v}[i]\Big) \\ &= \boldsymbol{b}[i] + \boldsymbol{G}\boldsymbol{v}[i], \end{aligned} \quad (5.53)$$

where the modulo operation is not included for clarity. The transmitter and receiver diagram for the bit-wise TH-precoded downlink CDMA system is shown in Fig. 5.14.

### 5.4.3 Chip-wise Multiuser TH Precoding

In a similar manner to the chip-wise linear precoder scheme in Section 5.3.2, we next propose a chip-wise TH precoding scheme that effectively combines precoding and spreading. The diagram for this scheme is shown in Fig. 5.15. It is seen that the precoder takes as input the $K \times 1$ symbol vectors $\boldsymbol{b}[i]$ and produces as output the $N \times 1$ chip vector $\boldsymbol{p}[i]$ that is transmitted through the channel. At the $k$-th user's receiver, the $N \times 1$ received signal vector corresponding to $\boldsymbol{p}[i]$ is given by

$$\boldsymbol{r}_k[i] = \boldsymbol{D}_k \boldsymbol{p}[i] + \bar{\boldsymbol{D}}_k \boldsymbol{p}[i-1] + \boldsymbol{n}_k[i]. \tag{5.54}$$

At each receiver $k$, the matched-filter $\boldsymbol{s}_k$ is applied to $\boldsymbol{r}_k[i]$. By stacking the outputs of all $K$ matched-filters we obtain

$$\underbrace{\begin{bmatrix} \boldsymbol{s}_1^H \boldsymbol{r}_1[i] \\ \boldsymbol{s}_2^H \boldsymbol{r}_2[i] \\ \vdots \\ \boldsymbol{s}_K^H \boldsymbol{r}_K[i] \end{bmatrix}}_{\boldsymbol{y}[i]} = \underbrace{\begin{bmatrix} \boldsymbol{s}_1^H \boldsymbol{D}_1 \\ \boldsymbol{s}_2^H \boldsymbol{D}_2 \\ \vdots \\ \boldsymbol{s}_K^H \boldsymbol{D}_K \end{bmatrix}}_{\boldsymbol{H}} \boldsymbol{p}[i] + \underbrace{\begin{bmatrix} \boldsymbol{s}_1^H \bar{\boldsymbol{D}}_1 \\ \boldsymbol{s}_2^H \bar{\boldsymbol{D}}_2 \\ \vdots \\ \boldsymbol{s}_K^H \bar{\boldsymbol{D}}_K \end{bmatrix}}_{\bar{\boldsymbol{H}}} \boldsymbol{p}[i-1] + \underbrace{\begin{bmatrix} \boldsymbol{s}_1^H \boldsymbol{n}_1[i] \\ \boldsymbol{s}_2^H \boldsymbol{n}_2[i] \\ \vdots \\ \boldsymbol{s}_K^H \boldsymbol{n}_K[i] \end{bmatrix}}_{\boldsymbol{v}[i]} \tag{5.55}$$

Note that different to Section 5.4.2, here $\boldsymbol{H}$ is not a square matrix but has dimension $K \times N$ with $N \geq K$. Similarly as before, to apply TH-precoding we perform the LQ decomposition on $\boldsymbol{H} = \boldsymbol{W}\boldsymbol{F}^H = \boldsymbol{G}^{-1}\boldsymbol{C}\boldsymbol{F}$. The decomposition is easily obtained applying the Gram-Schmidt orthogonalization procedure on the rows of $\boldsymbol{H}$, where the resulting orthonormal vectors form the columns of $\boldsymbol{F}$ of dimension $N \times K$ with $\boldsymbol{F}^H\boldsymbol{F} = \boldsymbol{I}_K$. The Gram-Schmidt coefficients define the $K \times K$ lower triangular matrix $\boldsymbol{W}$. The diagonal matrix $\boldsymbol{G} = \mathrm{diag}(w_{1,1}^{-1}, ..., w_{K,K}^{-1})$ converts $\boldsymbol{W}$ into the monic lower triangular matrix $\boldsymbol{C}$. In this way, $\boldsymbol{F}$ and $\boldsymbol{C} - \boldsymbol{I}$ are the FF and FB filter matrices respectively, and the FB matrix $\boldsymbol{V} = \boldsymbol{G}\bar{\boldsymbol{H}}$ cancels the inter-symbol interference, as shown in Fig. 5.15. The $k$-th diagonal element in $\boldsymbol{G}$ corresponds to the scalar gain applied at the $k$-th user's receiver.

### 5.4.4 Power Loading and Ordering

#### Power Loading

It is seen from (5.51) that the noise at each user's receiver is amplified by the corresponding diagonal element of $\boldsymbol{G} = \mathrm{diag}(w_{1,1}^{-1}, ..., w_{K,K}^{-1})$ resulting in different SNR (hence BER) performance among users. Power loading can be employed to enforce the same performance across users. That is, the symbol vector $\boldsymbol{b}[i]$ is first multiplied by a diagonal matrix $\boldsymbol{A} = \mathrm{diag}(A_1, \cdots, A_K)$ with $A_k^2$ denoting the power assigned to user $k$. The modulo operation for each user then needs to take the loading value into account since the distance between the constellation points is scaled by it. Given the total transmit power $P_T$, we then need to solve for $A_1, \cdots, A_K$ such that $\sum_{k=1}^{K} A_k^2 = P_T$, and $A_k^2 w_{k,k}^2 = \eta, \forall k$. The solution is

$$A_k^2 = \frac{w_{k,k}^{-2}}{\sum_{k=1}^{K} w_{k,k}^{-2}} P_T, \quad k = 1, ..., K, \text{ and } \eta = \frac{P_T}{\sum_{k=1}^{K} w_{k,k}^{-2}}. \tag{5.56}$$

The base station can broadcast the common constant value $\eta$ to all mobile receivers and then the receivers can adjust their respective $w_{k,k}$ to obtain the required $A_k$ value in the modulo operator. Therefore, the loading operation only requires the transmission of a constant value $\eta$ common to all mobile users.

Assuming that $E\{|b_k[i]|^2\} = 1$, then the bit error probability of each user can be well approximated by $P_e = \alpha Q\left(\sqrt{\eta/\sigma_n^2}\right)$, where $\alpha$ accounts for the increase in number of nearest neighbors due to the modulo operation (e.g., in QPSK $\alpha = 2$) [57, 121]. Note that as in traditional TH-precoding with $M$-QAM constellations, TH-precoding in ISI channels enhances the transmit power by a factor of $\beta = \frac{M}{M-1}$ [57, 121].

We next show that when orthogonal spreading sequences are employed, i.e., when $\boldsymbol{S}^T\boldsymbol{S} = \boldsymbol{I}_K$, then we have $w_{k,k}^{(b)} \leq w_{k,k}^{(c)}$, for $k = 1, ..., K$, and therefore $\eta^{(b)} \leq \eta^{(c)}$, where the superscripts $b$ and $c$ denote bit-wise and chip-wise precoders, respectively. First, comparing (5.49) and (5.55) we have $\boldsymbol{H}^{(b)} = \boldsymbol{H}^{(c)}\boldsymbol{S}$. Let $\boldsymbol{u}_{K+1}, ..., \boldsymbol{u}_N$ be $(N-K)$ orthonormal vectors in $\mathcal{V}^{\perp} \triangleq \mathbb{R}^N \backslash \mathrm{span}(\boldsymbol{S})$. Define the unitary matrix $\boldsymbol{S}' = [\boldsymbol{s}_1, .., \boldsymbol{s}_K, \boldsymbol{u}_{K+1}, ..., \boldsymbol{u}_N] = [\boldsymbol{S}, \boldsymbol{U}]$ and let

$$\boldsymbol{X} \;=\; [\boldsymbol{H}^{(b)}, \boldsymbol{H}^{(c)}\boldsymbol{U}] \;=\; \boldsymbol{H}^{(c)}\boldsymbol{S}'. \tag{5.57}$$

Since $\boldsymbol{S}'$ is a unitary transformation, the rows in $\boldsymbol{X}$ and $\boldsymbol{H}^{(c)}$ maintain the norm and the angles. Therefore, if the $K \times (N-K)$ block matrix $\boldsymbol{H}_c\boldsymbol{U}$ has any non-zero row (i.e., the projection of the rows of $\boldsymbol{H}_c$ onto $\mathrm{span}(\boldsymbol{U})$ is non-zero), the norm of the corresponding row in $\boldsymbol{H}^{(b)}$ will be smaller than in $\boldsymbol{H}^{(c)}$. Now consider the LQ factorization $\boldsymbol{H}^{(c)} = \boldsymbol{W}^{(c)}\boldsymbol{F}^{(c)H}$, obtained using Gram-Schmidt on the rows of $\boldsymbol{H}^{(c)}$, i.e., $\{\boldsymbol{h}_k^{(c)T}\}_{k=1}^{K}$. Each value $w_{k,k}^{(c)}$ can be obtained as follows. Assume that at the $k$-th step of the Gram-Schmidt algorithm the orthonormal vectors $\boldsymbol{f}_1^{(c)}, ..., \boldsymbol{f}_{k-1}^{(c)}$ (i.e., first $k$ columns in $\boldsymbol{F}^{(c)}$) have been obtained from $\boldsymbol{h}_1^{(c)}, ..., \boldsymbol{h}_{k-1}^{(c)}$, and denote $\mathcal{U}_{k-1} = \mathrm{span}\{\boldsymbol{f}_1^{(c)}, ..., \boldsymbol{f}_{k-1}^{(c)}\}$. Then, by simple inspection of the structure of the LQ factorization $w_{k,k}^{(c)}$ is the norm of $\tilde{\boldsymbol{f}}_k^{(c)} = \mathrm{proj}_{\mathcal{U}_{k-1}^{\perp}}\{\boldsymbol{h}_k^{(c)}\}$ where

$\mathcal{U}_{k-1}^{\perp} = \mathbb{R}^N \backslash \mathcal{U}_{k-1}$ and $\boldsymbol{f}_k^{(c)} = \tilde{\boldsymbol{f}}_k^{(c)} / w_{k,k}^{(c)}$. That is

$$w_{k,k}^{(c)} = \|\boldsymbol{h}_k^{(c)} - \mathrm{proj}_{\mathcal{U}_{k-1}}\{\boldsymbol{h}_k^{(c)}\}\| = \|\tilde{\boldsymbol{f}}_k^{(c)}\|. \tag{5.58}$$

On the other hand, the diagonal elements of $\boldsymbol{W}^{(b)}$ are similarly obtained from $[\boldsymbol{H}^{(b)}, \mathbf{0}_{K,N-K}]$. Then, using (5.57) and (5.58) we obtain

$$w_{k,k}^{(b)} = w_{k,k}^{(c)} - \|\mathrm{proj}_{\mathcal{V}^{\perp}}\{\tilde{\boldsymbol{f}}_k^{(c)}\}\|, \tag{5.59}$$

and hence $w_{k,k}^{(b)} \leq w_{k,k}^{(c)}$. Note that when $N = K$ and orthogonal spreading sequences are employed, $\boldsymbol{S}$ is unitary and $w_{k,k}^{(b)} = w_{k,k}^{(c)}$ for all $k$, and hence $\eta^{(b)} = \eta^{(c)}$ [cf. Fig. 9].

On the other hand, when the spreading sequences $\boldsymbol{S}$ are non-orthogonal, it is *not* true that $w_{k,k}^{(b)} \leq w_{k,k}^{(c)}$. However, we conjecture that $\eta^{(b)} \leq \eta^{(c)}$ still holds.

### User Ordering

We can optimize the system BER performance by optimizing the diagonal elements of the matrix $\boldsymbol{W}$ such that the common SNR of all users $\eta$ is maximized. Notice that $\boldsymbol{W}$ is obtained from the LQ decomposition of $\boldsymbol{H}$. The LQ decomposition is essentially the Gram-Schmidt orthogonalization of the rows of $\boldsymbol{H}$. The $k$-th diagonal element of $\boldsymbol{W}$ is the length of the projection of the $k$-th row vector of $\boldsymbol{H}$ onto the orthogonal complement of the space spanned by the first $(k-1)$ row vectors already orthogonalized. Different ordering in the orthogonalization process resulting in different diagonal values of $\boldsymbol{W}$, and hence different values of $\eta$. Let $\mathcal{P}$ be the set of the $K!$ possible $K \times K$ row permutation matrices. Then for any $\boldsymbol{P} \in \mathcal{P}$, $\boldsymbol{PH}$ is a row-permuted version of $\boldsymbol{H}$, which corresponds to a particular ordering of the $K$ users in TH-precoding. Denote $w_{k,k}(\boldsymbol{P})$ as the $k$-th diagonal element of $\boldsymbol{W}$ resulting from the LQ decomposition of $\boldsymbol{PH}$. Then the optimal row permutation matrix is given by

$$\boldsymbol{P}_{opt} = \arg\max_{\boldsymbol{P}\in\mathcal{P}} \frac{P_T}{\sum_{k=1}^{K} w_{k,k}^{-2}(\boldsymbol{P})} = \arg\min_{\boldsymbol{P}\in\mathcal{P}} \sum_{k=1}^{K} w_{k,k}^{-2}(\boldsymbol{P}). \tag{5.60}$$

With the optimal permutation $\boldsymbol{P}_{opt}$, the following modifications are needed at the transmitter and receiver: (1) Perform the LQ decomposition as $\boldsymbol{PH} = \boldsymbol{WF}^H$, or $\boldsymbol{H} = \boldsymbol{P}^T\boldsymbol{G}^{-1}\boldsymbol{CF}$; (2) Apply $\boldsymbol{GP}$ at the receiver (i.e., apply the scalar gains according to the optimal order); (3) The feedback matrix for removing the ISI becomes $\boldsymbol{V} = \boldsymbol{GP}\bar{\boldsymbol{H}}$. With these modifications, the cascade of operations becomes

$$\begin{aligned}
\boldsymbol{z}[i] &= \underbrace{\boldsymbol{GP}}_{\text{rx}}\Big(\underbrace{\boldsymbol{P}^T\boldsymbol{G}^{-1}\boldsymbol{C}\boldsymbol{F}^H}_{\text{channel}}\Big(\underbrace{\boldsymbol{F}}_{\text{FF}}\ \underbrace{\boldsymbol{C}^{-1}}_{\text{cancel,FB}}\ \Big(\boldsymbol{Ab}[i] - \underbrace{\boldsymbol{GP}\bar{\boldsymbol{H}}\boldsymbol{x}[i-1]}_{\text{cancel}\quad\text{ISI}}\Big)\Big) \\
&\quad + \underbrace{\bar{\boldsymbol{H}}\boldsymbol{x}[i-1]}_{\text{ISI}\quad\text{channel}} + \boldsymbol{v}[i]\Big) \\
&= \boldsymbol{Ab}[i] + \boldsymbol{GPv}[i].
\end{aligned} \tag{5.61}$$

Note that the matrices $\boldsymbol{G}, \boldsymbol{F}$ and $\boldsymbol{C}$ above are obtained from $\boldsymbol{PH}$.

Clearly an exhaustive search solution to (5.60) is computationally prohibitive. We next propose a suboptimal algorithm for an approximate solution to (5.60) that performs especially well in the chip-wise precoder when $N > K$. First note that $\prod_{k=1}^{K} w_{kk}^2$ is invariant to the permutation matrix $\boldsymbol{P}$. This result is easily proved recalling that $\boldsymbol{PH} = \boldsymbol{WF}^H$, with orthonormal columns in $\boldsymbol{F}$, then

$$\det(\boldsymbol{HH}^H) \;=\; \det(\boldsymbol{P}^T)\det(\boldsymbol{W})\det(\boldsymbol{W}^H)\det(\boldsymbol{P}) \;=\; \textstyle\prod_{k=1}^{K} w_{k,k}^2. \tag{5.62}$$

We first consider the simplest case with $K = 2$ users, then $\boldsymbol{H}$ contains two rows denoted by $\boldsymbol{h}_1^T$ and $\boldsymbol{h}_2^T$. Without loss of generality, assume that $\|\boldsymbol{h}_2\| < \|\boldsymbol{h}_1\|$. Next we show that to maximize the objective function in (5.60), we should start with $\boldsymbol{h}_2^T$, i.e., start by orthogonalizing the row with minimum $w_{k,k}$. Recall that $w_{k,k}$ is the length of the projection of the $k$-th row of $\boldsymbol{H}$ onto the orthogonal complement of the subspace spanned by the previous $(k-1)$ rows already orthogonalized. Then we need to show that

$$\frac{1}{\|\boldsymbol{h}_2\|^2} + \frac{1}{\|\boldsymbol{h}_1 - \frac{\boldsymbol{h}_2^H\boldsymbol{h}_1}{\|\boldsymbol{h}_2\|^2}\boldsymbol{h}_2\|^2} < \frac{1}{\|\boldsymbol{h}_1\|^2} + \frac{1}{\|\boldsymbol{h}_2 - \frac{\boldsymbol{h}_1^H\boldsymbol{h}_2}{\|\boldsymbol{h}_1\|^2}\boldsymbol{h}_1\|^2}. \tag{5.63}$$

From (5.62), the products of the denominators on both sides in (5.63) are equal. Therefore, (5.63) is equivalent to

$$\|\boldsymbol{h}_1 - \frac{\boldsymbol{h}_2^H\boldsymbol{h}_1}{\|\boldsymbol{h}_2\|^2}\boldsymbol{h}_2\|^2 + \|\boldsymbol{h}_2\|^2 < \|\boldsymbol{h}_2 - \frac{\boldsymbol{h}_1^H\boldsymbol{h}_2}{\|\boldsymbol{h}_1\|^2}\boldsymbol{h}_1\|^2 + \|\boldsymbol{h}_1\|^2 \tag{5.64}$$

which yields

$$\frac{|\boldsymbol{h}_2^H\boldsymbol{h}_1|^2}{\|\boldsymbol{h}_2\|^2} > \frac{|\boldsymbol{h}_2^H\boldsymbol{h}_1|^2}{\|\boldsymbol{h}_1\|^2}, \tag{5.65}$$

which is true by the assumption that $\|\boldsymbol{h}_2\| < \|\boldsymbol{h}_1\|$.

When $K > 2$, we adopt the greedy solution given in Algorithm 8 that at the $k$-th iteration, orthogonalizes the row with minimum $w_{k,k}$. In other words, the algorithm selects the row that is the closest to the subspace spanned by the rows already chosen. In the algorithm, $\mu_{p,j} = \hat{\boldsymbol{h}}_p^H \boldsymbol{h}_j$ and $\Theta_i$ represents the subset of rows already orthogonalized up to the $i$-th step. Note that besides finding the ordering $\boldsymbol{P}$, the algorithm also provides the LQ decomposition $\boldsymbol{PH} = \boldsymbol{WF}^H$, since $\boldsymbol{W}$ is given by the GS coefficients $\mu_{ij}$ and the $i$-th row of $\boldsymbol{F}$ is given by $\hat{\boldsymbol{h}}_i$. Clearly the complexity of the above search algorithm is $\mathcal{O}(K^2)$, which is significantly lower than the $\mathcal{O}(K!)$ complexity of the exhaustive search method.

**Algorithm 8** Greedy ordering and LQ decomposition

INPUT: row vectors $\boldsymbol{h}_1^T, ..., \boldsymbol{h}_K^T$ in $\boldsymbol{H}$
$\boldsymbol{P} = \boldsymbol{0}_{K\times K}$
$k_1 = \arg\min_{i\leq K}\{\|\boldsymbol{h}_i\|\}$;
$\hat{\boldsymbol{h}}_1 = \boldsymbol{h}_{k_1}/\|\boldsymbol{h}_{k_1}\|$; $\boldsymbol{P}(1,k_1) = 1$; $\Theta_1 = \{k_1\}$;
FOR $i = 2 : K$
  FOR EVERY $j \in \{\{1, ..., K\}\backslash\Theta_{i-1}\}$
    $\boldsymbol{u}_j = \boldsymbol{h}_j - \sum_{p=1}^{i-1} \mu_{p,j}\hat{\boldsymbol{h}}_p$;
  END FOR
  $k_i = \arg\min_j\{\|\boldsymbol{u}_j\|\}$;
  $\hat{\boldsymbol{h}}_i = \boldsymbol{u}_{k_i}/\|\boldsymbol{u}_{k_i}\|$; $\Theta_i = \{\Theta_{i-1}\} \cup \{k_i\}$;
  $\boldsymbol{P}(i, k_i) = 1$;
END FOR
OUTPUT: matrix $\boldsymbol{P}$ and LQ decomposition of $\boldsymbol{PH}$.

### 5.4.5 Simulation Results

#### TH-Precoding with Perfect Channel Knowledge

We first provide simulation results to compare the BER performance of different precoding techniques. Each user employs a normalized Hadamard sequences of length $N = 8$ as its spreading signature. The number of users is $K = 3$. All users employ QPSK modulation. We assume that each mobile user experiences an independent multipath channel $\boldsymbol{f}_k = [f_{k,1}, ..., f_{k,L}]^T$ with $L = 3$ resolvable paths and the transmitter has perfect channel state information of all users. The path gains are generated according to $f_{k,i} \sim \mathcal{N}_c(0, \frac{1}{L})$. For each data block, independent channel realizations are simulated for each user and the results are averaged over 1000 blocks.

Figure 5.16 shows the BER performance of the bit-wise TH-precoder proposed in Section 5.4.2 and the chip-wise TH-precoder proposed Section 5.4.3. Loading

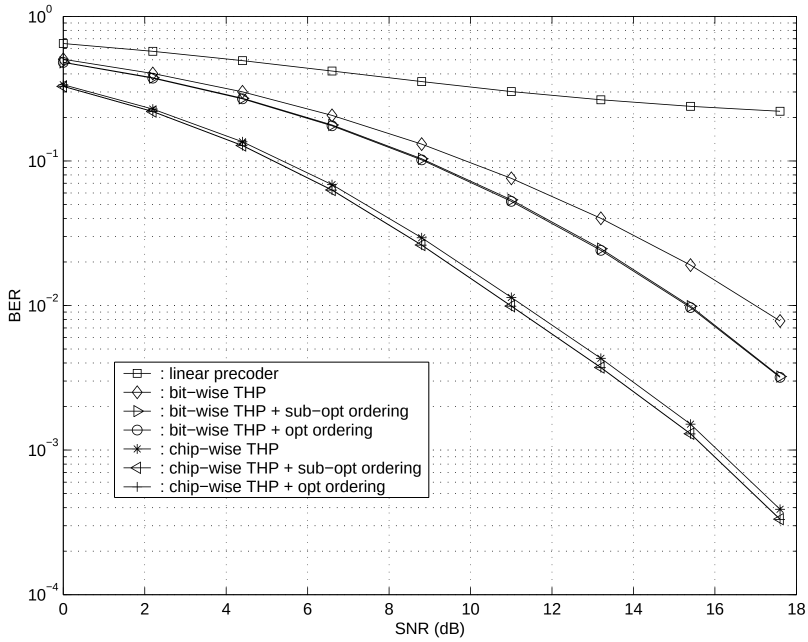


Figure 5.16: BER performance of different precoding schemes with $K = 3$ users, spreading gain $N = 8$, number of paths $L = 3$.

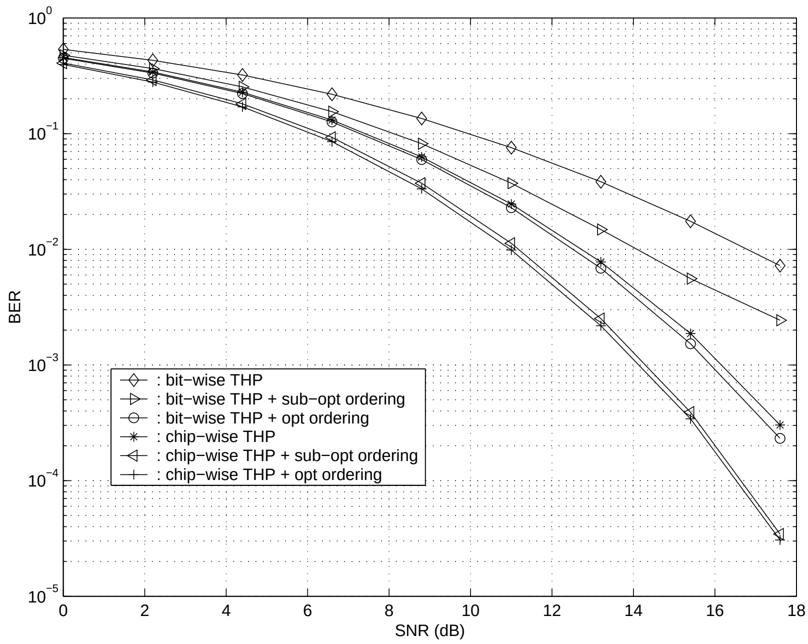


Figure 5.17: BER performance of different precoding schemes with $K = 7$ users, spreading gain $N = 8$, number of paths $L = 3$.

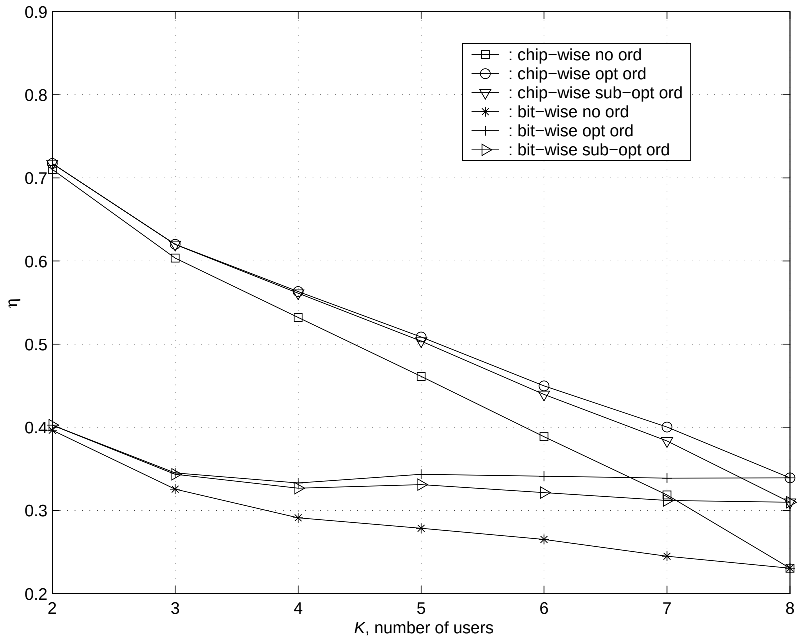


Figure 5.18: The received SNR value $\eta$ after loading as a function of the number of users $K$, spreading gain $N = 8$.

is employed in both schemes. For both methods, we consider the cases of no-ordering, optimal ordering (i.e., exhaustive search) and the suboptimal ordering method given in Algorithm 8. For comparison purposes, we also show the performance of the linear block-wise precoding method given in [126]. In the figure, the solid lines correspond to the approximate BER formula $P_e = \alpha Q(\sqrt{\eta/\sigma_n^2})$, and the symbol marks correspond to the simulated results. It is seen that the analytical BER expression matches very well with simulation results. Both nonlinear TH-precoders significantly outperform the linear precoder. Comparing bit-wise and chip-wise precoding schemes, the chip-wise precoder offers better performance. Moreover, ordering has a significant effect on the bit-wise TH-precoder; whereas it does not make a notable difference to the chip-wise TH-precoder (for small number of users $K$). Therefore, the chip-wise TH-precoder not only offers superior performance but is also computationally less complex since ordering is not required. Furthermore, the greedy ordering algorithm provides performance close to that of the exhaustive search method.

We repeat the simulations with the same parameters except that the number of users is increased to $K = 7$. Figure 5.17 shows that both TH-precoding schemes perform very well even in such highly loaded systems. When the number of users is high, ordering brings a significant improvement for both bit-wise and chip-wise precoders, although the complexity of the exhaustive search method becomes prohibitive (i.e., it involves computing $K! = 5040$ LQ decompositions of $7 \times 7$ matrices). The suboptimal ordering algorithm performs especially well in the chip-wise precoder and it requires less than 7 LQ decompositions. Comparing Fig. 5.16 and Fig. 5.17, we observe that the performance difference between the two precoders is reduced as the number of users increases.

Next we illustrate $\eta$ in (5.56) obtained by the two TH-precoding solutions for different number of users when $L = 3$ and $N = 8$. For both methods we show the $\eta$ value for cases of no-ordering, optimal ordering and suboptimal ordering, averaged over 100 different channel realizations. In the simulations, we keep $P_T/K$ fixed to unit. Figure 5.18 shows that as the difference between $N$ and $K$ is reduced, the chip-wise solution decreases its performance, and eventually, when $N = K$, both the bit-wise and the chip-wise solutions are equivalent. When the number of users $K$ is large, ordering improves the performance considerably. As mentioned before, the greedy ordering algorithm performs especially well when $N > K$.

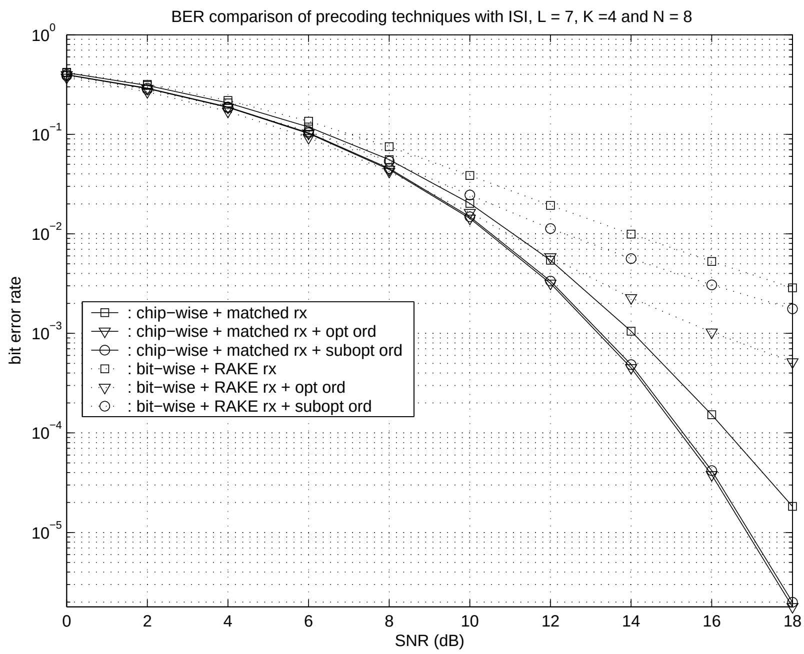


Figure 5.19: chip-wise TH precoding with fixed matched filter at the receiver vs. bit-wise TH precoding with RAKE receiver. Spreading gain $N = 8$ and $K = 4$ users.

Next we compare our chip-wise TH-precoder proposed in Section 5.4.3, which does not require CSI at the receiver, with the bit-wise TH-precoder proposed in

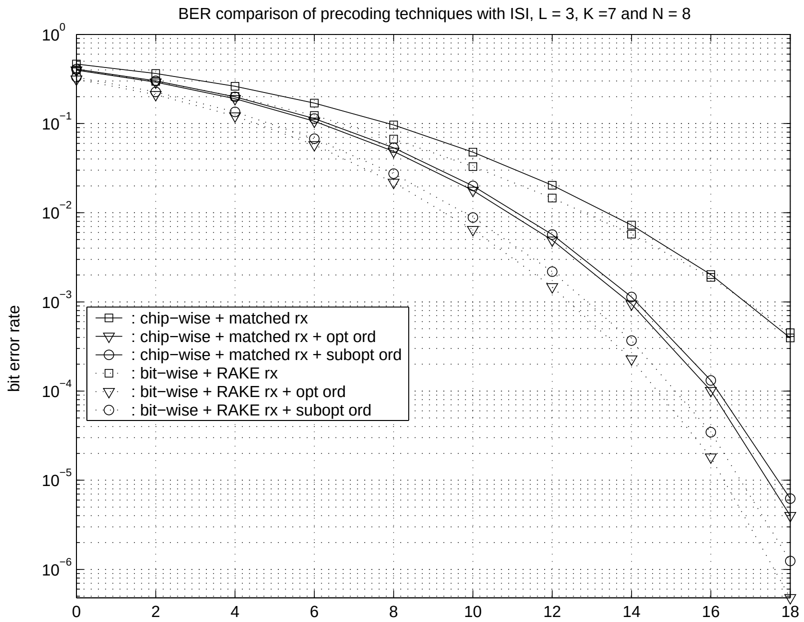


Figure 5.20: chip-wise TH precoding with fixed matched filter at the receiver vs. bit-wise TH precoding with RAKE receiver. Spreading gain $N = 8$ and $K = 7$ users.

[130], which implements a RAKE receiver at each mobile user (i.e., mobile users must estimate the channel). The results are shown in Figure 5.19 and Figure 5.20 for $K = 4$ and $K = 7$, respectively. It is seen that the TH-precoder with a RAKE receiver only performs slightly better in heavily loaded systems. For fewer users, our chip-wise TH precoder obtains better results. Therefore, the chip-wise TH precoder is not only simpler but it also has excellent performance.

**TH-Precoding with Channel Prediction**

A crucial assumption in the development of the precoding techniques in the previous section is that the transmitter has perfect knowledge about the multipath channel states of all mobile users. In TDD wireless systems, the downlink channel state information is available at the transmitter (which is estimated from the uplink transmission) as long as the coherence time of the channel is larger than the time difference between the uplink and downlink slots. On the other hand, in fast fading channels, the channel state that has been estimated during an uplink slot may have changed and the estimate may no longer be accurate for precoding in the next downlink slot. In this case, channel prediction techniques can be used to estimate the future downlink channel state from the current and previous uplink channel estimates, by exploiting the second-order statistics of the fading channel [31]. Assume that the complex Gaussian fading process of each channel path $f_{k,i}(t)$ follows the Jakes' model [68] with the maximum Doppler spread $f_d$, that is, we have $E\{f_{k,i}(t_1)f_{k,i}(t_2)\} = \nu_{k,i}^2 J_0(2\pi f_d|t_1 - t_2|)$, $k = 1,\ldots,K; i = 1,\ldots,L$, where $J_0(\cdot)$ is the zeroth-order Bessel function of the first kind.

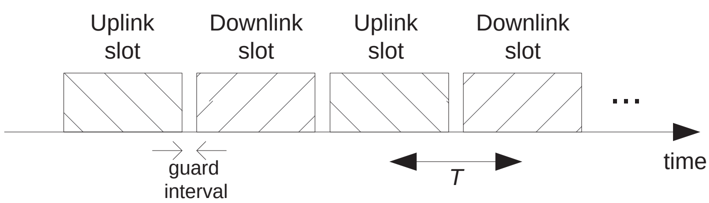


Figure 5.21: Time division duplexing.

Assume that in the TDD system the uplink and downlink slots are separated by $T$ seconds; and the base station estimates the multipath channel of each user every uplink slot. We set the time of the latest channel estimation as the reference $t = 0$. Then the base station will estimate the channel state at times $t \in \{0, -2T, -4T, ...\}$. We consider channel estimation based on pilot symbols and the channel estimate has the form $\hat{f}_{k,i}(t) = f_{k,i}(t) + \xi_{k,i}(t)$, where $\xi_{k,i}(t) \sim \mathcal{N}_c(0, \gamma_{k,i}^2)$. We assume that the base station estimates the channel once per slot and these estimates will be used to predict the channel for data precoding in the next downlink slot.

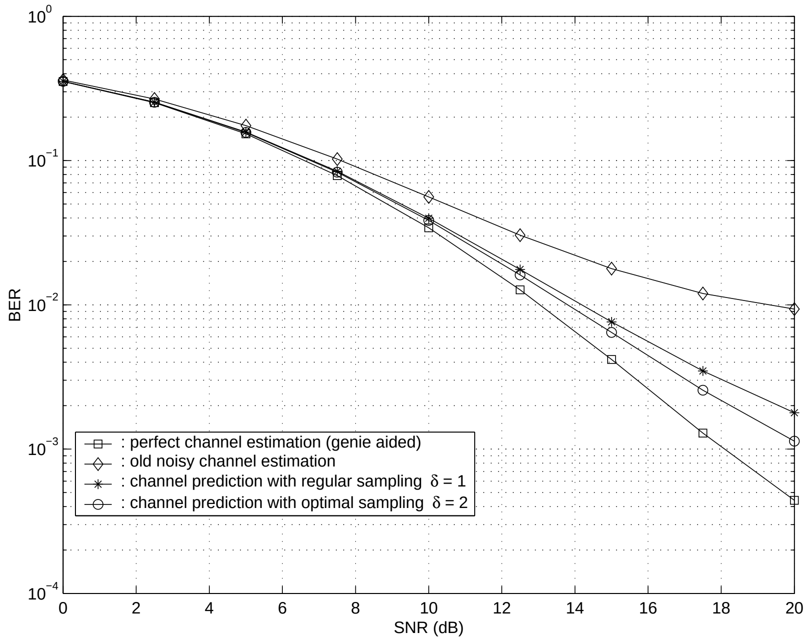


Figure 5.22: BER performance of chip-wise TH-precoding in time-varying channels.

Assume that after the current channel estimate at time $t = 0$ the base station predicts each channel path at time $\tau$ which is called the prediction depth (e.g., $\tau = T$ where $T$ is the slot duration). The prediction is implemented using a $P$-th order finite impulse response (FIR) filter

$$\tilde{f}_{k,i}(\tau) = \sum_{p=0}^{P} w_{k,i}(p)^* \hat{f}_{k,i}(-p2T) = \boldsymbol{w}_{k,i}^H \hat{\boldsymbol{f}}_{k,i}, \tag{5.66}$$

where $\boldsymbol{w}_{k,i} \triangleq [w_{k,i}(0), w_{k,i}(1), \ldots, w_{k,i}(P)]^T$, $\hat{\boldsymbol{f}}_{k,i} \triangleq [\hat{f}_{k,i}(0), \hat{f}_{k,i}(-2T), ..., \hat{f}_{k,i}(-P2T)]^T$. The optimal filter that minimizes the mean square error $\zeta_{\text{pred}} \triangleq E\{|f_{k,i}(\tau) - \tilde{f}_{k,i}(\tau)|^2\}$ is given by $\boldsymbol{w}_{k,i} = \boldsymbol{R}_{k,i}^{-1}\boldsymbol{r}_{k,i}$, where the entries of $\boldsymbol{R}_{k,i}$ and $\boldsymbol{r}_{k,i}$ are given respectively by $[\boldsymbol{R}_{k,i}]_{p,q} = \nu_{k,i}^2 J_0(2\pi f_d|p-q|2T) + \gamma_{k,i}^2\delta_{p,q}$, and $[\boldsymbol{r}_{k,i}]_p = \nu_{k,i}^2 J_0(2\pi f_d(\tau + p2T)),\ p, q = 0, 1, \ldots, P.$

In the prediction filter described above, we use estimates of the channel that have been sampled every $2T$ seconds. This sampling rate is in general much higher than the required minimum Nyquist sampling rate equal to twice the Doppler frequency $2f_d$. It has been shown in [31] that such oversampling could be unfavorable when the order of the filter $P$ is fixed. Assume that the base station is able to estimate the channel every $2T$ seconds. Define the optimal sampling period as $\delta 2T$, where $\delta$ is a positive integer. Then for fixed values of the prediction depth, noise variance, Doppler frequency and filter order, we can compute the MSE of the prediction filter $\zeta_{\text{pred}}$ for different integer values of $\delta$ and select the one that minimizes $\zeta_{\text{pred}}$. On the other hand, it has been observed that when the system parameters are fixed, $\zeta_{\text{pred}}$ decreases with the order of the prediction filter $P$. However, after a certain filter order, $\zeta_{\text{pred}}$ saturates since the noise in the previous channel estimates dominates in the MSE of the prediction error. Therefore, it is convenient to evaluate the MSE expression for different values of $P$ and choose the shortest one that gets $\zeta_{\text{pred}}$ close to the saturation level.

As in the WCDMA TDD mode, we assume that the uplink and downlink are time multiplexed into a carrier centered at $f_c = $ 2GHz. The frame length is 10ms, which is subdivided into 15 slots that can be allocated for either uplink or downlink. Therefore the uplink and downlink transmission can be interleaved in bursts of $T = 666.7\mu$s. As in Section 5.4.5, we consider $N = 8$, $L = 3$ and $\nu_{k,i}^2 = 1/L$. The fading process of each channel path is formed by samples of a stationary zero-mean complex Gaussian process with autocorrelation function $J_0(2\pi f_d t)$ [68] and is generated according to the method described in [29]. We consider the performance of the chip-wise TH-precoding technique with loading and ordering. We assume that all the mobile users are moving at $v = 36$Km/h. The previous channel estimates $\{\hat{f}_{k,i}(t), t = 0, -2T, ...\}$ are given by the true channel values corrupted by complex Gaussian noise with variance $\gamma_{k,i}^2 = 0.001$. Evaluating the MSE expression $\zeta_{\text{pred}}$ for different orders of the prediction filter we find that a very short prediction filter with $P = 2$ obtains good results. Evaluating $\zeta_{\text{pred}}$ we find that slightly better results can be obtained if the channel is sampled with $\delta = 2$. We evaluate the results over 10 different initial channel realizations. For each channel realization, we consider 200 slots of length $T = 666\mu$s (i.e., 200 channel variations) and in each slot we send 1000 QPSK symbols per mobile user. In the results we consider perfect channel estimation (genie aided), old channel estimation $\tau$ seconds before, and channel prediction with the optimal sampling ($\delta = 2$) and with the regular sampling ($\delta = 1$). Figure 5.22 shows that the prediction algorithm gives very good results even considering that all the users are moving at $v = 36$Km/h and the prediction is based on noisy channel estimates. Notice that without channel prediction and only using old channel estimates, the performance would decrease considerably in these scenarios representing very high mobility.

## 5.5 Downlink User Scheduling for Linear Precoding

Scheduling is a technique to increase the utilization of the wireless medium. For example, in the recently proposed multiuser opportunistic scheduling scheme [85] the schedulers opportunistically exploit channel variations of multiple users to select the *best* set of users to transmit data subject to fairness (e.g., maximum delay), QoS (e.g., minimum SNR), and resource constraints (e.g., maximum power available at the transmitter) [84], to obtain a significant increase of total system throughput. In general the number of users that can be simultaneously supported by the system is small and thus, there are a large number of possible user subset selections when the number of users in the system in large. Straightforward implementation of the user subset selection by simple exhaustive enumeration suffers from high computational complexity.

In this section, we propose user subset selection algorithms that can be naturally implemented in precoded systems. We assume that the satisfaction that a user receives in a system (i.e., the utilitiy) is a binary function that takes zero value when the SINR is below a threshold and takes unit value when the SINR is above the threshold. This is appropriate for voice or video-on-demand applications in which the SINR above a threshold will not provide additional benefit and the SINR below the threshold leads to unintelligible speech or video. In this section we restrict ourselves to the linear MMSE precoder. One important property of the chip-wise linear precoder is that in the channel matrix $\boldsymbol{H}_c$, each row depends only on the spreading sequence and channel of one particular user (actually, each row in $\boldsymbol{H}_c$ is the effective spreading sequence, i.e., the convolution between the channel response and the spreading sequence of that particular user). Note that in the bit-wise solution this is not the case and each row depends on the spreading sequence of all the active users. This property will allow us to propose low-complexity algorithms for the chip-wise precoder.

#### Maximum User Allocation – Optimal Solution

Our objective is to accommodate as many users as possible such that if user $k$ is active, $\mathrm{SINR}_k \geq \gamma$, assuming that the base station is constrained to a maximum power budget $P_T$. Recall that in the chip-wise solution, for a fixed power budget $P_T$, the SINR for the $k$-th user is given by

$$\mathrm{SINR}_k = \frac{\beta^2 A_k^2}{\sigma_n^2}, \;\; \text{with} \;\; \beta = \sqrt{\frac{P_T}{\mathrm{tr}(\boldsymbol{A}^2(\boldsymbol{H}_c\boldsymbol{H}_c^H)^{-1})}}. \tag{5.67}$$

Since a same target SINR value $\gamma$ is assumed for all users, the users should have the same transmit power and hence can assume $A_k = 1, \forall k$. Therefore, the QoS constraint $\mathrm{SINR}_k \geq \gamma$ translates into the following condition on $\boldsymbol{H}_c$:

$$\mathrm{tr}((\boldsymbol{H}_c\boldsymbol{H}_c^H)^{-1}) \leq \frac{P_T}{\sigma^2\gamma}. \tag{5.68}$$

Denote $U$ as the total number of users in the network, $\theta$ as the user subset selected, and $|\theta|$ as the number of users in $\theta$ (e.g., selecting the first and third users corresponds to $\theta = \{1,3\}$ and $|\theta| = 2$). The channel matrix corresponding to the active users is $\boldsymbol{H}_\theta$ where $\boldsymbol{H}_\theta$ is the submatrix of $\boldsymbol{H}_c$ (where $\boldsymbol{H}_c$ has $U$ rows) obtained from the rows indicated in $\theta$. Let $\Theta$ be the set of all possible user subsets. Therefore, the total number of possible user subsets is $|\Theta| = \sum_{k=0}^{U}\binom{U}{k}$. Denote $\Omega$ as the set of feasible user selections in $\Theta$, i.e.,

$$\Omega = \{\theta \in \Theta : \mathrm{SINR}_k \geq \gamma,\ \forall k \in \theta\} = \{\theta \in \Theta : \mathrm{tr}((\boldsymbol{H}_\theta\boldsymbol{H}_\theta^H)^{-1}) \leq P_T/(\sigma^2\gamma)\}. \tag{5.69}$$

Then the optimization problem becomes finding $\theta \in \Omega$ such that $|\theta|$ is maximized. This is a highly complex combinatorial problem since for each possible solution in $\Theta$, a matrix pseudoinverse needs to be computed. Thus the total number of complex multiplications required is $\sum_{k=1}^{|\theta|+1}\binom{U}{k}\left(k^3 + Nk^2\right)$.

### Low Complexity Algorithms

Next we propose low-complexity algorithms that employ a greedy approach to add or remove one user at a time. As mentioned before, in addition to being the optimal linear precoder, the advantage of using the chip-wise linear precoding method is that adding or removing one user corresponds to adding or removing a row to the channel matrix $\boldsymbol{H}_c$ and the rest of the rows remain unchanged. Note that the performance only depends on the selected users and not on the order in which the users are selected. This is, for any reordering in rows of $\boldsymbol{H}_c$, the required power is equivalent. Any reordering of the rows can be expressed as $\boldsymbol{H}_c' = \boldsymbol{P}\boldsymbol{H}_c$ where $\boldsymbol{P}$ is a permutation matrix and hence $\boldsymbol{P}^{-1} = \boldsymbol{P}^H$. Therefore, $\mathrm{tr}\left((\boldsymbol{H}_c'\boldsymbol{H}_c'^H)^{-1}\right) = \mathrm{tr}\left((\boldsymbol{P}\boldsymbol{H}_c\boldsymbol{H}_c^H\boldsymbol{P}^H)^{-1}\right) = \mathrm{tr}\left((\boldsymbol{H}_c\boldsymbol{H}_c^H)^{-1}\right)$.

***Maximum Frobenius Norm Criterion:*** An intuitive and classical approach in user allocation is to activate the users that see the best propagation channel. Two approaches can be taken: incremental allocation and decremental allocation. In the incremental allocation algorithm, the base station starts without selecting any user. At each step of the algorithm, it selects the user with maximum channel gain (i.e., maximum norm of the corresponding row of the chip-wise matrix). Then, the algorithm checks if (5.68) holds. If it does, the corresponding user is allocated. This is repeated until no more users can be allocated, i.e., until (5.68) no longer holds, or $|\theta| = \min(U, N)$. On the other hand, the decremental algorithm starts by assuming that all $|\theta| = \min(U, N)$ users with best channels are active. And it removes one user at a time until (5.68) is satisfied. The removed user is the one with the worst channel quality, i.e., with the lowest channel gain. Obviously if the number of active users is expected to be small, it is better to use the incremental algorithm. The main disadvantage of the user allocation approaches described above is that for every new user added, the matrix inverse in (5.68) cannot be reused.

***Geometrical Criterion - Incremental Selection:*** We have already mentioned that users with good channel qualities (i.e., large path gains) are in general good candidates to be allocated. However, due to the precoding operation, a matrix inverse needs to be computed. Therefore, users with very large path gains but with highly correlated effective signature sequences (i.e., rows in the matrix $\boldsymbol{H}_c$ close to parallel) can have a very negative effect in the required power at the transmitter. Therefore here we propose to select users based not only on the gains but also on the correlations (i.e., angles) between the respective effective signature sequences.

Assume that $K = |\theta|$ users have already been allocated, i.e., $\boldsymbol{H}_\theta$ with rows $\boldsymbol{h}_1, ..., \boldsymbol{h}_K$. Then we propose to select a new row $\boldsymbol{h}_i$ from the $(U - K)$ remaining ones (i.e., users not allocated yet) such that the projection onto the orthogonal complement of the already selected rows is maximum, i.e.,

$$\max_i \|\pi^\perp(\boldsymbol{h}_i)\|, \quad i \in \{\text{non-selected users}\}, \tag{5.70}$$

where $\pi^\perp(\boldsymbol{h}_i)$ denotes the projection of $\boldsymbol{h}_i$ on span$(\boldsymbol{h}_1, ..., \boldsymbol{h}_K)^\perp$ and $(\cdot)^\perp$ denotes the orthogonal complement. We consider a greedy incremental approach. The algorithm starts by selecting one row with the maximum norm and at every iteration the algorithm adds the row with the largest projection onto the orthogonal complement of the subspace spanned by the rows already selected. This selection can be implemented with the help of the Gram-Schmidt procedure. At every step of the algorithm, (5.68) needs to be checked to see if a new user can be allocated given the total power budget $P_T$. For every new user added, (5.68) requires a matrix inverse. Next, we propose a method to compute the matrix inverse recursively.

Denote the LQ decomposition of a $K \times N$ matrix as $\boldsymbol{H} = \boldsymbol{L}\boldsymbol{Q}$ where $\boldsymbol{L}$ is $K \times K$ lower left triangular and $\boldsymbol{Q}$ has dimension $K \times N$ with $\boldsymbol{Q}\boldsymbol{Q}^H = \boldsymbol{I}_K$. The LQ decomposition can be obtained using Gram-Schmidt where the row vectors in $\boldsymbol{Q}$, i.e., $\boldsymbol{q}_1, ..., \boldsymbol{q}_K$ are given by the recursion

$$\boldsymbol{q}_1 = \boldsymbol{h}_1/\|\boldsymbol{h}_1\|, \text{ and } \boldsymbol{q}_i = \frac{\boldsymbol{h}_i - \sum_{j=1}^{i-1} \mu_{ij}\boldsymbol{q}_j}{\|\boldsymbol{h}_i - \sum_{j=1}^{i-1} \mu_{ij}\boldsymbol{q}_j\|}, \quad \text{for} \quad i = 2, ..., K, \tag{5.71}$$

where the Gram-Schmidt coefficients form the lower triangular matrix $\boldsymbol{L}$ and are given by

$$\mu_{ij} = \langle \boldsymbol{h}_i, \boldsymbol{q}_j \rangle, \quad j < i, \text{ and } \mu_{ii} = \|\boldsymbol{h}_i - \sum_{j=1}^{i-1} \mu_{ij} \boldsymbol{q}_j\|. \tag{5.72}$$

By simple inspection, we have that $[\boldsymbol{L}]_{ij} = \mu_{ij}$, and $\mu_{jj}$ is the value required in (5.70). Therefore, the LQ decomposition does not require any extra computations if we use the greedy geometrical user allocation.

Assume that one knows the LQ decomposition of $\boldsymbol{H}$. Then, (5.68) can be evaluated using

$$\text{tr}\left((\boldsymbol{H}\boldsymbol{H}^H)^{-1}\right) = \text{tr}\left((\boldsymbol{L}\boldsymbol{Q}\boldsymbol{Q}^H\boldsymbol{L}^H)^{-1}\right) = \|\boldsymbol{L}^{-1}\|_F^2. \tag{5.73}$$

Note that (5.73) can be computed recursively as follows. Assume that we have computed $\boldsymbol{L}_{i-1}^{-1}$ of size $(i-1) \times (i-1)$. Then, after selecting the new user (i.e., add one row to $\boldsymbol{H}$), the $(i-1)$-th leading submatrix of $\boldsymbol{L}_i^{-1}$ is given by $\boldsymbol{L}_{i-1}^{-1}$ available from the previous iteration and the last row in $\boldsymbol{L}_i^{-1}$ is given by

$$\boldsymbol{l}_i^{-1} = \frac{1}{\mu_{i,i}}(\boldsymbol{e}_i - \sum_{j=1}^{i-1} \mu_{ij} \boldsymbol{l}_j^{-1}), \tag{5.74}$$

which follows from the Gauss-Jordan elimination and the relationship between the Gram-Schmidt coefficients and the triangular matrix $\boldsymbol{L}$. Hence (5.73) is computed recursively as

$$\|\boldsymbol{L}_i^{-1}\|_F^2 = \|\boldsymbol{L}_{i-1}^{-1}\|_F^2 + \|\boldsymbol{l}_i^{-1}\|_2^2. \tag{5.75}$$

Finally a low-complexity incremental selection algorithm for user allocation is summarized in Algorithm 3. Clearly, the complexity is dominated by the computation of all the Gram-Schmidt coefficients in step ($\diamondsuit$) computed using (5.72), which requires $\sum_{i=1}^{|\theta|} N(U-i)i$ complex multiplications. The total complexity of the algorithm is upper bounded by $NU|\theta|^2$ complex multiplications.

### Simulation Results

Next we give some simulation results to illustrate the performance of the different user allocation algorithms when the chip-wise linear precoder is employed.

We first consider the average number of users that each algorithm is able to allocate with respect to the total available power at the transmitter $P_T$. We set $\gamma = 12$dB. We assume that each mobile user experiences an independent multipath channel $\boldsymbol{f}_k = [f_{k,1}, ..., f_{k,L}]^T$ with $L = 3$ resolvable paths and the transmitter has perfect CSI of all users. The path gains are generated according to $f_{k,i} \sim$

**Algorithm 9** Low-complexity user allocation based on geometrical criterion

```
INPUT: all row vectors h_1,...,h_U, γ, P_T, σ.
θ = ∅; P_r = 0; %start without any user selected
FOR i = 1,2,...,
  FOR EVERY j ∈ {{1,...,U}\θ} DO % every user not selected yet
    b_j = h_j − Σ_{p=1}^{i−1} μ_{j,p} q_p                          (◇)
  END FOR
  k_i = arg max_j{b_j b_j^H}; %user with max projection onto orthogonal complement
  q_i = b_{k_i}/||b_{k_i}|| ; %the new Gram-Schmidt vector
  l_i^{-1} = 1/μ_{i,i} (e_i − Σ_{t=1}^{i−1} μ_{i,t} l_t^{-1}); %last row in the new L^{-1}
  P_r = P_r + σ^2 γ ||l_i^{-1}||^2; %power required if we allocate this user k_i
  IF P_r < P_T
    θ = θ ∪ k_i; %allocate this user and continue
    IF |θ| = min(U,N) THEN BREAK;   %finish the algorithm
  ELSE
    P_r = P_r − σ^2 γ ||l_i^{-1}||^2;
    BREAK;   % finish the algorithm
  END IF
END FOR
OUTPUT: selected users θ, required power P_r, selected submatrix H_θ and H_θ^† = Q^H L^{-1}.
```

$\mathcal{N}_c(0, \frac{1}{L})$. We consider random spreading sequences with spreading gain $N = 8$, and $U = 12$ available users in the region. Fig. 5.23 illustrates the average number of users allocated, i.e., $|\theta|$ with respect to $P_T$ by different algorithms. It is seen that the low-complexity geometrical incremental algorithm achieves almost the optimal performance. Note that for instance, with $P_T = 26$dB, the optimal algorithm allocates around 7 users and it would require $\sum_{i=0}^{8} \binom{12}{i}(i^3 + Ni^2) = 1931664$ complex multiplications, whereas the complexity for the proposed low-complexity algorithm is upper bounded by $NU|\theta|^2 = 6144$ complex multiplications. As the number of users increases, the optimal solution becomes intractable. It is seen that under this scenario, the maximum Frobenius norm selection criterion incurs a loss of between 2-4dB.

Next, to illustrate the effectiveness of the different algorithms, we consider a hypothetical scenario in which $K$ users need to be allocated. The $K$ users are chosen among the $U$ available users in the network using either optimal selection, maximum gain selection, or low-complexity geometrical selection. We look at the total power required at the transmitter $P_T$ to obtain $\gamma = 12$dB across the

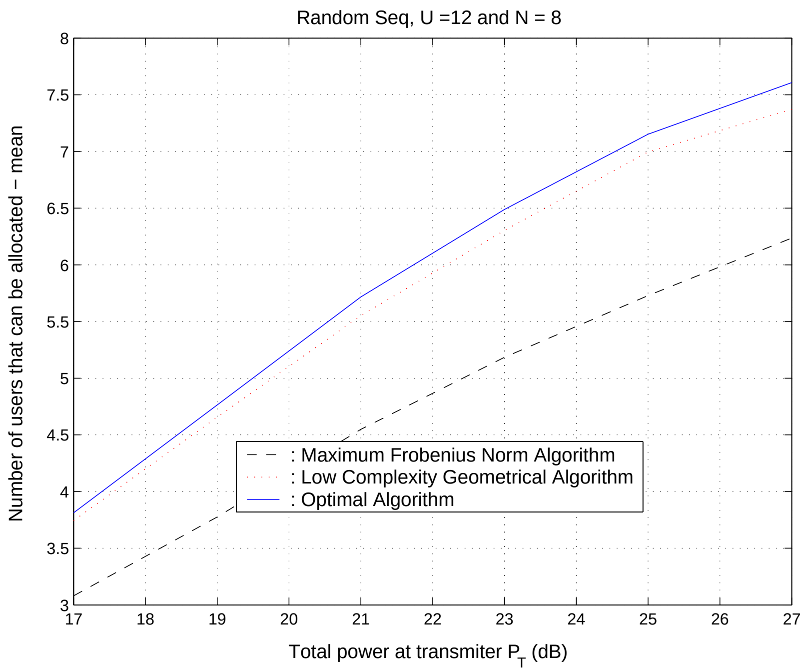


Figure 5.23: Average number of users allocated with respect to the total transmit power. Random codes, spreading gain $N = 8$, $U = 12$ available users in the network, and target SINR $\gamma = 12$dB.

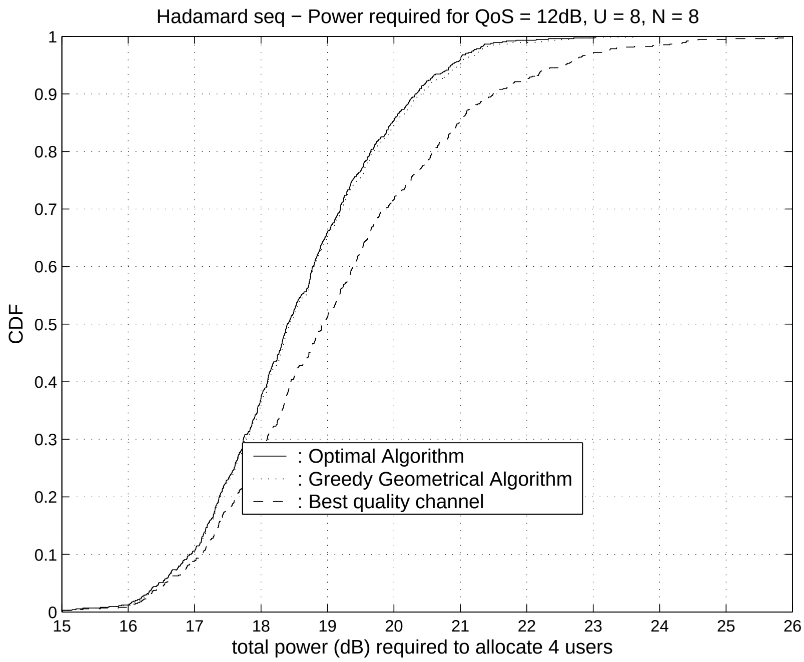


Figure 5.24: CDF of the required total power at the transmitter to allocate the best $K = 4$ users with target SINR per user $\gamma = 12$dB. Hadamard codes, spreading gain $N = 8$, $U = 8$ available users.

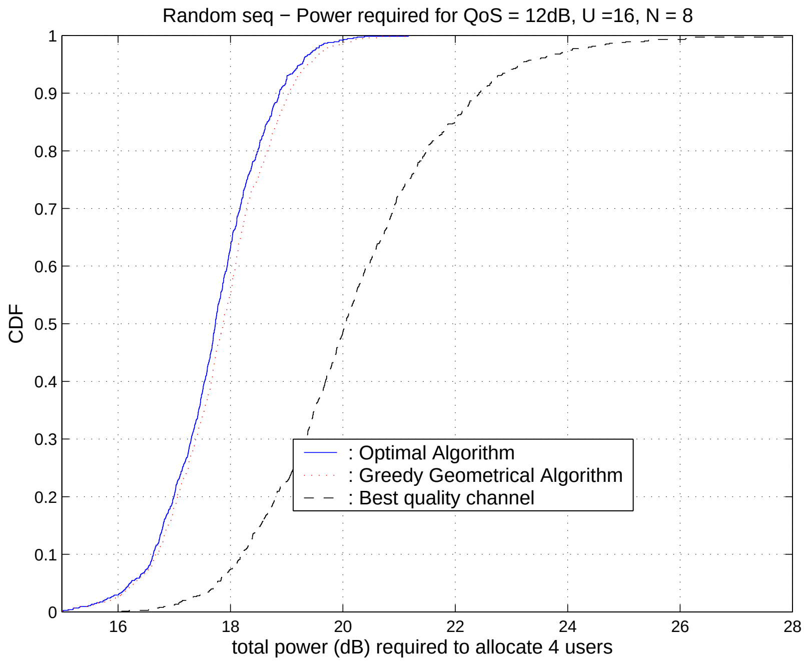


Figure 5.25: CDF of the required total power at the transmitter to allocate the best $K = 4$ users with target SINR per user $\gamma = 12$dB. Random codes, spreading gain $N = 8$, $U = 16$ available users.

$K$ selected users. Fig. 5.24 shows the results with $U = 8$ available users, and Hadamard spreading sequences with $N = 8$. It is seen that the geometrical algorithm again achieves almost the optimal performance. Fig. 5.25 shows the results with $U = 16$ available users, spreading gain $N = 8$ and $K = 4$. It is seen that as the number of possible combinations increases, the maximum Frobenius norm criterion incurs performance loss whereas the the geometrical algorithm is quite robust. Note that with $U = 16$ and $K = 4$, the optimal algorithm would compute $\binom{U}{K}(NK^2 + K^3)$= 349440 complex multiplications, whereas the low complexity algorithm would require less than $K^2NU = 2048$ complex multiplications.

## 5.6 Conclusions

In this chapter, we have first obtained the capacity results for downlink CDMA systems employing either multiuser detection or transmitter precoding. It is seen from numerical examples that these two techniques offer comparable capacity regions. However, multiuser detection at the downlink mobile receiver may not be practical due to the requirement that each mobile receiver should have the knowledge of all users'spreading sequences and channel states, as well as the limited signal processing capability of the mobile receiver. On the other hand, transmitter precoding is an attractive solution for systems employing time-division multiplexing, where uplink and downlink channels are reciprocal. Then we have compared the performance of linear precoding and linear MUD in the downlink of frequency selective TDD-CDMA systems. We have proposed different linear precoding schemes and our results reveal that in general precoding can outperform the more complex MUD. Moreover, we have shown that the proposed chip-wise linear MMSE precoding method is optimal in the sense that it requires the minimum total transmitted power to meet a certain receiver QoS performance. Later, we have developed nonlinear multiuser precoding algorithms based on the Tomlinson-Harashima precoding technique. Our precoding algorithms effectively remove multi-user interference, inter-chip interference and inter-symbol interference in the downlink of CDMA systems. The main property of the proposed algorithms is that they can be implemented at either bit level or chip level, and they are considerably less complex compared with the block-wise linear precoders in the literature. We have also proposed a suboptimal user ordering algorithm for power loading which further optimizes the system performance. Channel prediction for precoding has also been discussed. Simulations results have shown that the proposed precoding techniques offer excellent performance even in heavily loaded systems or time-varying scenarios. These results strongly motivate the use of transmit precoding in the downlink of TDD-CDMA systems due to the multiple advantages over MUD, including the simple implementation of power control and user scheduling, and the reduction of the power consumption and complexity at the mobile unit. Finally, in conjunction with the precoding techniques we have proposed very low-complexity opportunistic user scheduling algorithms to maximize the utilization of the wireless resources. Simulations results have shown that the proposed algorithms obtain nearly optimal performance.

# Chapter 6

# Conclusions and Future Work

This dissertation has considered communications through MIMO channels which encompasses many different scenarios including multiple antenna systems and multiple-user communications.

For the multiple antenna scenarios presented in Chapter 3, we have developed adaptive antenna selection algorithms that converge to optimal solutions based on various performance criteria in situations where only noisy estimates of the channels are available. We have also developed antenna selection algorithms for time-varying channels where the optimal antenna subset will change only gradually. Furthermore, we have considered new selection criteria which permit suboptimal algorithms to be developed that yield a considerable reduction in complexity with only a small loss in performance.

Chapter 4 has proposed a systematic method to design LAttice Space-Time (LAST) codes that minimize the error rate when the structure of the receiver and the statistics of the channel are known a priori. It has been shown that our LAST codes outperform other LAST codes proposed in the literature and also that the LAST code optimization method is flexible enough to be applied in different detector schemes and for different channel statistics.

For the multiple user scenario, Chapter 5 has shown that precoding schemes are an effective technique for the downlink of TDD-CDMA systems. In particular, we have considered precoding schemes with very simple receivers, i.e., having only a fixed matched-filter corresponding to the *own* spreading sequence and without employing CSI. This translates into a power consumption reduction and a decrease in cost of terminals since they do not have to perform sophisticated signal processing for channel estimation and interference mitigation. Note that variations in channel conditions and the number of active users in the network do not affect the receiver operations. Power control is also easy to implement with precoding since the base station has information about the quality of each link and so additional feedback information from the terminals is not required in order to control the transmit power from the base station.

## Future Work

The work presented in this thesis can be extended in many ways.

In Chapter 3, antenna selection algorithms to reduce the cost of multiple antenna systems while improving the performance has been considered. Different antenna selection criteria (e.g., minimum error rate, maximum SNR, etc.) might be required for each of the different space-time schemes proposed in the literature. Moreover, fast selection algorithms for each of these criteria would be valuable since they would permit antenna selection to be implemented in practical systems when there are a large number of antenna subsets available.

In Chapter 4, a new systematic stochastic optimization method has been presented to minimize the error rate of LAST codes. This method departs from the typical optimization approach to design space-time codes based on number theoretic tools. It is possible that our powerful optimization method and others employing a similar rationale could be used to optimize other codes that do not need to be designed in real time (just like the LAST codes considered). On the other hand, in cooperative diversity scenarios we have assumed that the power assigned to the source and to the cooperative relays is fixed. An interesting topic of research would be to incorporate the optimization of the power allocated to each node into a joint optimization problem (i.e., optimize jointly the LAST code and the allocated powers). Extensions to nodes with more than one antenna are also worth investigating.

In Chapter 5 we have proposed different precoding techniques in the downlink of CDMA systems when the base station has CSI of all the users. In this situation, it is natural to combine precoding, power control, and opportunistic scheduling with fairness in the form of cross-layer optimization. In multiuser opportunistic scheduling schemes, the schedulers opportunistically exploit the channel variations experienced by the multiple users. That is, the schedulers select the *best* set of users to transmit data subject to fairness (e.g., maximum delay), QoS (e.g., minimum SNR), and resource constraints (e.g., maximum power available at the transmitter), to obtain a significant increase in the total system throughput. A complete framework and solution based on our precoding schemes needs to be investigated.

# Appendix A

# Unbiased estimate of $\det(\cdot)$ in (3.30)

Obtain an estimate of

$$\det\left(\boldsymbol{I}_{n_T} + \frac{\rho}{n_T}\boldsymbol{H}^H[\omega]\boldsymbol{H}[\omega]\right) \tag{A.1}$$

using

$$\phi[n,\omega] = \det\left(\boldsymbol{I}_{n_T} + \frac{\rho}{n_T}\hat{\boldsymbol{H}}_1^H[n,\omega]\hat{\boldsymbol{H}}_2[n,\omega]\right), \tag{A.2}$$

where the channel estimates $\hat{\boldsymbol{H}}_1[n,\omega]$ and $\hat{\boldsymbol{H}}_2[n,\omega]$ are obtained from independent training blocks. We consider the case in which $\hat{\boldsymbol{H}}_1[n,\omega]$ and $\hat{\boldsymbol{H}}_2[n,\omega]$ satisfy (3.5).

**Theorem 5** *With $\phi[n,\omega]$ computed according to (A.2), the estimate of the determinant in (A.1) is unbiased.*

**Proof**: For convenience define

$$\begin{aligned} \boldsymbol{M}[\omega] &= \boldsymbol{I}_{n_T} + \frac{\rho}{n_T}\boldsymbol{H}^H[\omega]\boldsymbol{H}[\omega], \\ \hat{\boldsymbol{M}}[n,\omega] &= \boldsymbol{I}_{n_T} + \frac{\rho}{n_T}\hat{\boldsymbol{H}}_1^H[n,\omega]\hat{\boldsymbol{H}}_2[n,\omega] \end{aligned} \tag{A.3}$$

and denote the elements of $\hat{\boldsymbol{M}}[n,\omega]$ as $\hat{m}_{i,j}$.

Consider (A.3). Since $\hat{\boldsymbol{H}}_1[n,\omega]$ and $\hat{\boldsymbol{H}}_2[n,\omega]$ are statistically independent samples, clearly $\hat{\boldsymbol{M}}[n,\omega]$ is an unbiased estimator of $\boldsymbol{M}[\omega]$. Now consider $\det(\hat{\boldsymbol{M}}[n,\omega])$.

From [65, p.8]

$$\det(\hat{\boldsymbol{M}}[n,\omega]) = \sum_{\sigma} \operatorname{sign}(\sigma) \prod_{i=1}^{n_T} \hat{m}_{i,\sigma(i)}, \tag{A.4}$$

where the sum runs over all $n_T!$ permutations $\sigma$ of the $n_T$ items $\{1, ..., n_T\}$ and $\operatorname{sign}(\sigma)$ is $+1$ or $-1$. Omitting the sign, each term in the summation is of the form

$$\hat{m}_{1,\sigma(1)}\hat{m}_{2,\sigma(2)}...\hat{m}_{n_T,\sigma(n_T)}. \tag{A.5}$$

Thus, each term in the summation involves the product of elements of $\hat{\boldsymbol{M}}[n,\omega]$ from different rows and columns.

Next, due to the independence assumption in (3.5), it follows that for the matrix $\hat{\boldsymbol{M}}[n,\omega]$, the elements $\hat{m}_{i,j}$ and $\hat{m}_{p,q}$ are independent for $i \neq p$ and $j \neq q$, i.e., elements of $\hat{\boldsymbol{M}}[n,\omega]$ from distinct rows and columns are statistically independent. Hence $\hat{m}_{1,\sigma(1)}, \hat{m}_{1,\sigma(1)}, ..., \hat{m}_{n_T,\sigma(n_T)}$ are statistically independent with zero mean which implies that $\det(\hat{\boldsymbol{M}}[n,\omega])$ is an unbiased sample of $\det(\boldsymbol{M}[\omega])$ and satisfies

$$\det(\hat{\boldsymbol{M}}[n,\omega]) = \det(\boldsymbol{M}[\omega]) + v[n,\omega] \tag{A.6}$$

where $v[n,\omega]$ is a zero mean random variable. ■

# Appendix B

# Enumeration of all the lattice points in a sphere

In this appendix we show how to enumerate the coordinates of all the points belonging to a $n$ dimensional lattice $\boldsymbol{G}$ (i.e., defined by the basis $\{\boldsymbol{g}_1, ..., \boldsymbol{g}_n\}$) that fall inside a sphere $\mathcal{S}$ of radius $r$ centered at $-\boldsymbol{u}$. That is, enumerate all the points $(\Lambda + \boldsymbol{u}) \cap \mathcal{S}$. Following the derivation and geometric meaning in [94] let $\boldsymbol{u}$ be the optimal translation vector which can be written as a function of the basis vector of the lattice, i.e., $\boldsymbol{u} = \nu_1 \boldsymbol{g}_1 + \nu_2 \boldsymbol{g}_2 + ... + \nu_n \boldsymbol{g}_n \in \mathbb{R}^n$ (where $n = 2MT$), or in matrix form $\boldsymbol{u} = \boldsymbol{G}\nu$ (and therefore, $\nu = \boldsymbol{G}^{-1}\boldsymbol{u}$). If a lattice point $\boldsymbol{x} = z_1 \boldsymbol{g}_1 + ... + z_n \boldsymbol{g}_n \in \Lambda$ is inside the sphere of radius $r$ centered at $-\boldsymbol{u}$, it satisfies the sphere constraint $\|\boldsymbol{x} + \boldsymbol{u}\| \leq r$. The enumeration problem is to determine all valid combinations of $\boldsymbol{z} = [z_1, ..., z_n] \in \mathbb{Z}^n$ under the sphere constraint which can also be expressed in terms of the Gram-Schmidt vectors. Recall that the Gram-Schmidt vectors can be obtained as

$$\begin{aligned} \boldsymbol{g}_k^* &= \boldsymbol{g}_k - \sum_{i=1}^{k-1} \mu_{ki} \boldsymbol{g}_i^*, \\ \mu_{ki} &= \frac{\boldsymbol{g}_i^{*T} \boldsymbol{g}_k}{\|\boldsymbol{g}_i^*\|^2}, \end{aligned} \tag{B.1}$$

which can be expressed as

$$\begin{aligned} [\boldsymbol{G}]^T &= \boldsymbol{U}[\boldsymbol{G}^*]^T \\ \boldsymbol{G} &= \boldsymbol{G}^* \boldsymbol{U}^T, \end{aligned} \tag{B.2}$$

where $[\boldsymbol{U}]_{ki} = 1$, if $k = i$, $\mu_{k,i}$ if $k > i$, and 0 otherwise. That is $\boldsymbol{g}_k = \boldsymbol{g}_k^* + \sum_{i=1}^{k-1} \mu_{ki} \boldsymbol{g}_i^*$. Denote $\boldsymbol{h} = \boldsymbol{x} + \boldsymbol{u} = \boldsymbol{G}[\boldsymbol{z} + \nu] = \boldsymbol{G}^* \boldsymbol{U}^T [\boldsymbol{z} + \nu]$. And the constraint $\|\boldsymbol{h}\|^2 \leq r^2$ becomes

$$\begin{aligned}
\|\boldsymbol{h}\|^2 &= \operatorname{tr}\left\{ \left[\boldsymbol{G}^* \boldsymbol{U}^T [\boldsymbol{z} + \nu]\right] \left[\boldsymbol{G}^* \boldsymbol{U}^T [\boldsymbol{z} + \nu]\right]^T \right\} \\
&= \operatorname{tr}\left\{ \boldsymbol{G}^{*T} \boldsymbol{G}^* \boldsymbol{U}^T [\boldsymbol{z} + \nu][\boldsymbol{z} + \nu]^T \boldsymbol{U} \right\} \\
&= \sum_{i=1}^{n} \left( \sum_{k=1}^{n} \mu_{ki}(z_k + \nu_k) \right)^2 \|\boldsymbol{g}_i^*\|^2 \\
&= \sum_{i=1}^{n} \left( \sum_{k=i}^{n} \mu_{ki}(z_k + \nu_k) \right)^2 \|\boldsymbol{g}_i^*\|^2 \leq r^2 \qquad \text{(B.3)}
\end{aligned}$$

where in the last equation we have applied that $\mu_{ki} = 0$ if $k < i$. Recall that $\mu_{ii} = 1, \forall i$. Start by $i = n$, i.e., $(z_n + \nu_n)^2 \|\boldsymbol{g}_n^*\|^2 \leq r^2$

$$-\frac{r}{\|\boldsymbol{g}_n^*\|} - \nu_n \leq z_n \leq +\frac{r}{\|\boldsymbol{g}_n^*\|} - \nu_n \qquad \text{(B.4)}$$

and since $z_n \in \mathbb{Z}$

$$\left\lceil -\frac{r}{\|\boldsymbol{g}_n^*\|} - \nu_n \right\rceil \leq z_n \leq + \left\lfloor \frac{r}{\|\boldsymbol{g}_n^*\|} - \nu_n \right\rfloor . \qquad \text{(B.5)}$$

Note that there are $\left\lfloor \frac{2r_n}{\|\boldsymbol{g}_n^*\|} \right\rfloor + 1$ possible choices of $z_n$. For each of these choices, we recursively do the same but updating a new radius (similarly to a tree search). For example, with $i = n - 1$

$$\begin{aligned}
\sum_{i=n-1}^{n} \left( \sum_{k=n-1}^{n} (z_k + \nu_k)\mu_{ki} \right)^2 \|\boldsymbol{g}_i^*\|^2 &\leq r^2 \\
\left[(z_{n-1} + \nu_{n-1}) + (z_n + \nu_n)\mu_{n,n-1}\right] \|\boldsymbol{g}_{n-1}^*\| &\leq \underbrace{\sqrt{r^2 - (z_n + \nu_n)^2 \|\boldsymbol{g}_n^*\|^2}}_{r_{n-1}} .
\end{aligned}$$

That is, for $i = n-1, n-2, ..., 1,$

$$
\begin{aligned}
r_i &= \sqrt{\left( r_{i+1}^2 - \left| \sum_{k=i+1}^{n} (z_k + \nu_k)\mu_{k,i+1} \right|^2 \|\boldsymbol{g}_{i+1}^*\|^2 \right)} \\
|(z_i + \nu_i) + (\sum_{k=i+1}^{n} (z_k + \nu_k)\mu_{k,i})| &\le \frac{r_i}{\|\boldsymbol{g}_i^*\|}, \qquad \text{(B.6)}
\end{aligned}
$$

or making use of the granularity of $z_k$ we have

$$
\left\lceil -\frac{r_i}{\|\boldsymbol{g}_i^*\|} - \left( \sum_{k=i+1}^{n} (z_k + \nu_k)\mu_{k,i} \right) - \nu_i \right\rceil \le z_i \le \left\lfloor +\frac{r_i}{\|\boldsymbol{g}_i^*\|} - \left( \sum_{k=i+1}^{n} (z_k + \nu_k)\mu_{k,i} \right) - \nu_i \right\rfloor . \qquad \text{(B.7)}
$$

Note that there are $\left\lfloor \frac{2r_i}{\|\boldsymbol{g}_i^*\|} \right\rfloor + 1$ possible choices of $z_i$. One way to speed up the enumeration by reducing the width of the stages of the tree (i.e., number of possible choices of $z_i$) is to apply a preprocessing step applying lattice reduction to the rows of $\boldsymbol{G}^{-1}$ [38, 94]. Note that the lattice reduction change of basis also needs to be applied to the translation vector.

# Appendix C

# MMSE unconstrained linear precoding solution

For both the chip-wise and bit-wise system models, the total received vector can be written as

$$\boldsymbol{y} = \boldsymbol{HMb} + \boldsymbol{v}, \tag{C.1}$$

where $\boldsymbol{H} \in \mathbb{C}^{K \times N}$ for the chip-wise solution and $\boldsymbol{H} \in \mathbb{C}^{K \times K}$ for the bit-wise solution. We restrict ourselves to the chip-wise solution since the bit-wise solution (square matrices) is a special case of it. When the mobile units are constrained to the matched filter receiver, the MMSE optimization function becomes

$$J = E\{\|\boldsymbol{b} - \boldsymbol{y}\|^2\} = E\{\|\boldsymbol{b} - \boldsymbol{HMb} - \boldsymbol{v}\|^2\}. \tag{C.2}$$

**Proposition 5** *The choice of* $\boldsymbol{M} \in \mathbb{C}^{N \times K}$ *that minimizes* $J$ *is* $\boldsymbol{M} = \boldsymbol{H}^H(\boldsymbol{HH}^H)^{-1}$.
**Proof** In a similar manner to [99] we offer the following proof by contradiction. Suppose there exists a matrix $\boldsymbol{M}_0$ that results in a smaller $J$ than $\boldsymbol{M} = \boldsymbol{H}^H(\boldsymbol{HH}^H)^{-1}$. Then,

$$E\{\|\boldsymbol{b} - \boldsymbol{HM}_0\boldsymbol{b} - \boldsymbol{v}\|^2\} < E\{\|\boldsymbol{v}\|^2\}. \tag{C.3}$$

The left hand side of (C.3) can be rewritten as

$$\begin{aligned} E\{\|\boldsymbol{b} - \boldsymbol{HM}_0\boldsymbol{b} - \boldsymbol{v}\|^2\} &= E\{\boldsymbol{b}^H\boldsymbol{b}\} - 2E\{\Re[\boldsymbol{b}^H\boldsymbol{HM}_0\boldsymbol{b}]\} \\ &\quad + E\{\boldsymbol{b}^H\boldsymbol{M}_0^H\boldsymbol{H}^H\boldsymbol{HM}_0\boldsymbol{b}\} + E\{\boldsymbol{n}^H\boldsymbol{v}\}, \end{aligned}$$

which combined with (C.3) implies

$$E\{\boldsymbol{b}^H\boldsymbol{b}\} - 2E\{\Re[\boldsymbol{b}^H\boldsymbol{H}\boldsymbol{M}_0\boldsymbol{b}]\} + E\{\boldsymbol{b}^H\boldsymbol{M}_0^H\boldsymbol{H}^H\boldsymbol{H}\boldsymbol{M}_0\boldsymbol{b}\} < 0 \tag{C.4}$$

However, the left hand side of (C.4) is equal to $E\{\|\boldsymbol{b} - \boldsymbol{H}\boldsymbol{M}_0\boldsymbol{b}\|^2\}$ which can never be less than zero, which leaves a contradiction. This completes the proof. ■

# References


[1] L. Afflerback and H. Grothe. Calculation of Minkowski-reduced lattice bases. *Comput.*, 35:269276, 1985.

[2] E. Agrell, T. Eriksson, A. Vardy, and K. Zeger. Closest point search in lattices. *IEEE Trans. Inform. Theory*, 48(8):2201–2214, Aug. 2002.

[3] S.M. Alamouti. A simple transmit diversity technique for wireless communications. *IEEE J. Select. Areas Commun.*, 16(8):1451–1458, Oct. 1998.

[4] M. Alrefaei and S. Andradottir. A simulated annealing algorithm with constant temperature for discrete stochastic optimization. *Management Science*, 45(5):748–764, 1999.

[5] S. Andradottir. A global search method for discrete stochastic optimization. *SIAM J. Optim.*, 6(2):513–530, May 1996.

[6] S. Andradottir. Accelerating the convergence of random search methods for discrete stochastic optimization. *ACM Trans. on Modelling and Computer Simulation*, 9(4):349–380, Oct. 1999.

[7] D. Asztely. On antenna arrays in mobile communications systems: Fast fading and GSM base station receiver algorithms. Technical Report S3-SB-9611, KTH, March 1996.

[8] C. R. N. Athaudage and V. Krishnamurthy. A low complexity timing and frequency synchronization algorithm for OFDM systems. In *Proc. IEEE Globecom*, Taipei, Taiwan, Nov. 2002.

[9] I. Bahceci, T.M. Duman, and Y. Altunbasak. Antenna selection for multiple-antenna transmission systems: performance analysis and code construction. *IEEE Trans. Inform. Theory*, 49(10):2669–2681, Oct. 2003.

[10] A. H. Banihashemi and A. K. Khandani. On the complexity of decoding lattices using the KorkinZolotarev reduced basis. *IEEE Trans. Inform. Theory*, 44:162171, Jan. 1998.

[11] S. Baro, G. Bauch, and A. Hansmann. Improved codes for space-time trellis-coded modulation. *IEEE Commun. Lett.*, 4(1):20–22, Jan. 2000.

[12] G. Bauch. Concatenation of space-time block codes and Turbo-TCM. In *Proc. IEEE Int. Conf. Commun. (ICC)*, Vancouver, BC, Canada, June 1999.

[13] J-C. Belfiore, G. Rekaya, and E. Viterbo. The golden code: a $2 \times 2$ full-rate space-time code with non-vanishing determinants. In *Proc. Int. Symp. Inform. Theory (ISIT'04)*, Chicago, IL, July 2004.

[14] A. Benveniste, M. Metivier, and P. Priouret. *Adaptive Algorithms and Stochastic Approximation*. Springer Verlag, Berlin and New York, 1990.

[15] E. Biglieri, D.Divsalar, P.J. McLane, and M.K.Simon. *Introduction to Trellis-Coded Modulation with Applications*. New York: Macmillan, 3rd edition, 1991.

[16] H. Boche and M. Schubert. A general duality theory for uplink and downlink beamforming. In *Proc. IEEE Vehicular Technol. Conf. (VTC)*, Vancouver, Canada, Sep. 2002.

[17] H. Bolcskei, D. Gesbert, and A.J. Paulraj. On the capacity of OFDM-based multi-antenna systems. In *Proc. IEEE Int. Conf. Acoust., Speech, Sig. Proc. (ICASSP)*, Istanbul, Turkey, Jun. 2000.

[18] H. Bolcskei and A. J. Paulraj. Space-frequency codes for broadband fading channels. In *Proc. IEEE Int. Symp. on Inform. Theory (ISIT)*, Washington, D.C., June 2001.

[19] G. Caire and S. Shamai. On the achievable throughput of a multiantenna Gaussian broadcast channel. *IEEE Trans. Inform. Theory*, 49(7):1691–1706, July 2003.

[20] C.N. Chuah, D.N.C. Tse, J.M. Kahn, and R.A. Valenzuela. Capacity scaling in MIMO wireless systems under correlated fading. *IEEE Trans. Inform. Theory*, 48(3):637–650, Mar. 2002.

[21] A. Cohen and A. Lapidoth. The Gaussian watermarking game. *IEEE Trans. Inform. Theory*, 48:1639–1667, June 2002.

[22] J.H. Conway and N.J.A.Sloane. *Sphere Packings, Lattices and Groups*. Springer Verlag, New York, 1992.

[23] J.H. Conway and N.J.A. Sloane. A fast encoding method for lattice codes and quantizers. *IEEE Trans. Inform. Theory*, 29(6):820–824, Nov. 1983.

[24] M. Costa. Writing on dirty paper. *IEEE Trans. Inform. Theory*, 29:439–441, May 1983.

[25] T. M. Cover and J. A. Thomas. *Elements of Information Theory*. Wiley, 1991.

[26] M.O. Damen, A. Chkeif, and J.-C. Belfiore. Lattice code decoder for space-time codes. *IEEE Commun. Lett.*, pages 161–163, May 2000.

[27] P. Dayal and M.K. Varanasi. An optimal two transmit antenna space-time code and its stacked extensions. In *Proc. IEEE Asilomar Conf. Sig., Systems and Comp.*, Monterey, CA, Nov. 2003.

[28] T. Homem de Mello. Variable-sample methods for stochastic optimization. *ACM Trans. Modeling and Computer Simulation*, 13(2):108–133, Apr. 2003.

[29] P. Dent, G.E. Bottomley, and T. Croft. Jakes fading model revisited. *IEE Electron. Lett.*, 29(13):1162–1963, June 1993.

[30] B. Dong, X. Wang, and A. Doucet. A new class of soft MIMO demodulation algorithms. *IEEE Trans. Sig. Proc.*, 51(10):2752–2763, Nov. 2003.

[31] A. Duel-Hallen, S. Hu, and H. Hallen. Long-range prediction of fading signals: enabling adapting transmission for mobile radio channels. *IEEE Sig. Proc. Magazine*, 17(3):62–75, May 2000.

[32] P. Elia, R. Kumar, S. Pawar, P.V.Kumar, and H-F. Liu. Explict construction of space-time block codes: achieving the diversity-multiplexing gain tradeoff. *IEEE Trans. Inform. Theory*, submitted 2004.

[33] U. Erez, S. Litsyn, and R. Zamir. Lattices which are good for (almost) everything. *IEEE Trans. Inform. Theory*, submitted 2004.

[34] U. Erez, S. Shamai, and R. Zamir. Capacity and lattice-strategies for cancelling known interference. In *Proc. ISITA*, Honolulu, Hawai, Nov. 2000.

[35] U. Erez and R. Zamir. Achieving 1/2 log (1+SNR) on the AWGN channel with lattice encoding and decoding. *IEEE Trans. Inform. Theory*, 50(10):2293–2314, Oct. 2004.

[36] R.B. Ertel, P.Cardieri, K.W. Sowerby, T.S. Rappaport, and J.H.Reed. Overview of spatial channel models for antenna array communication systems. *IEEE Personal Commun.*, 5(1):10–22, Feb. 1998.

[37] R. Esmailzadeh, E. Sourour, and M. Nakagawa. Pre-rake diversity combining in time-division duplex CDMA mobile communications. *IEEE Trans. Veh. Tech.*, 48:795–801, May 1999.

[38] U. Fincke and M. Pohst. Improved methods for calculating vectors of short length in a lattice, including a computational complexity. *Mathematics for Computation*, 44:463–471, Apr. 1995.

[39] R.F.H. Fischer, C. Windpassinger, A. Lampe, and J.B. Huber. MIMO precoding for decentralized receivers. In *Proc. Int. Symp. Inform. Theory (ISIT)*, Lausanne, Switzerland, June 2002.

[40] G. J. Foschini and M. J. Gans. On the limits of wireless communications in a fading environment when using multiple antennas. *Wireless Personal Commun.*, 6(3):311–335, 1998.

[41] G. J. Foschini, G. D. Golden, R. A. Valenzuela, and P. W. Wolniansky. Simplified processing for high spectral efficiency wireless communication employing multi-antenna arrays. *IEEE J. Select. Areas Commun.*, 17(11):1841–1852, Nov. 1999.

[42] G.J. Foschini. Layed space-time architecture for wireless communication in a fading environment when using multi-element antennas. *Bell Labs. Tech. J.*, 1(2):41–59, 1996.

[43] H. El Gamal, G. Caire, and M.O. Damen. Lattice coding and decoding achieve the optimal diversity-multiplexing tradeoff of MIMO channels. *IEEE Trans. Inform. Theory*, 50(6):968–985, June 2004.

[44] H. El Gamal and B. M. Hochwald. A new approach to layered space-time coding and signal processing. *IEEE Trans. Inform. Theory*, 47(6):2321–2334, Sep. 2001.

[45] S.L. Georgoulis and D.G.M. Cruickshank. Transmitter-based inverse filters for reducing MAI and ISI mitigation in a CDMA-TDD downlink. *IEEE Trans. Wireless Commun.*, 3(2):353–358, Mar. 2004.

[46] M. Gharavi-Alkhansari and A.B. Gershman. Fast antenna subset selection in MIMO systems. *IEEE Trans. Sig. Proc.*, 52(2):339–347, Feb. 2004.

[47] G. Ginis and J. M. Cioffi. Vectored transmission for digital subscriber line systems. *IEEE J. Sel. Areas Commun.*, 20(5):1085–1104, June 2002.

[48] G.D. Golden, G.J. Foschini, R.A. Valenzuela, and P.W. Wolniansky. Detection algorithm and initial laboratory results using the V-BLAST space-time communication architecture. *IEE Electron. Lett.*, 35(1):14–15, Jan. 1999.

[49] D. Gore and A. Paulraj. Statistical MIMO antenna sub-set selection with space-time coding. In *Proc. IEEE Int. Conf. Commun. (ICC)*, New York, NY, Apr. 2002.

[50] D.A. Gore and R.W. Heath Jr. Transmit selection in spatial multiplexing systems. *IEEE Commun. Lett.*, 6(11):491–493, Nov. 2002.

[51] D.A. Gore and A.J. Paulraj. MIMO antenna subset selection with space-time coding. *IEEE Trans. Sig. Proc.*, 50(10):2580–2588, Oct. 2002.

[52] A. Gorokhov. Antenna selection algorithms for MEA transmission systems. In *Proc. IEEE Int. Conf. Acoust. Speech, Sig. Processing (ICASSP)*, Orlando, FL, May 2002.

[53] A. Gorokhov, D.A. Gore, and A.J. Paulraj. Receive antenna selection for MIMO spatial multplexing: theory and algorithms. *IEEE Trans. Sig. Proc.*, 51(11):2796–2807, Nov. 2003.

[54] I.S. Gradshteyn and I.M. Ryzhik. *Table of Integrals, Series, and Products*. 5th ed., Academic Press, Orlando, FL, 1994.

[55] D. Guo and X. Wang. Blind detection in MIMO systems via sequential Monte Carlo. *IEEE J. Select. Areas Commun.*, 21(3):453–464, Apr. 2003.

[56] I. Hammerstroem, M. Kuhn, B. Rankov, and A. Wittneben. Space-time processing for cooperative relay networks. In *Proc. IEEE Veh. Technol. Conf., VTC Fall*, Orlando, FL, Oct. 2003.

[57] H. Harashima and H. Miyakawa. Matched transmission technique for channels with intersymbol interference. *IEEE Trans. Commun.*, 20:774–780, 1972.

[58] B. Hassibi and B.M. Hochwald. High-rate codes that are linear in space and time. *IEEE Trans. Inform. Theory*, 48(7):1804–1824, July 2002.

[59] R. Heath and A. Paulraj. Antenna selection for spatial multiplexing systems based on minimum error rate. In *Proc. IEEE Int. Conf. Commun. (ICC)*, Helsinki, Finland, June 2001.

[60] R. W. Heath and A. Paulraj. Switching between spatial multiplexing and transmit diversity based on constellation distance. In *Proc. of Annual Allerton Conf. Commun., Comput. & Control*, Monticello, IL, Oct. 2000.

[61] A. S. Hedayat, N. J. A. Sloane, and John Stufken. *Orthogonal Arrays: Theory and Applications*. Springer-Verlag, New York, 1991.

[62] B. Helfrich. Algorithms to construct Minkowski-reduced lattice bases. *Theor. Comput. Sci.*, 41:125–139, 1985.

[63] Y. Hochberg and A.C. Tamhane. *Multiple Comparison Procedures*. Wiley, New York, 1987.

[64] B. Hochwald, T.L. Marzetta, and C.B. Papadias. A transmitter diversity scheme for wideband CDMA systems. *IEEE J. Select. Areas Commun.*, 19(1):48–60, Jan. 2001.

[65] R. A. Horn and C. R. Johnson. *Matrix Analysis*. Cambridge University Press, Cambridge, U.K., 1985.

[66] B.L. Hughes. Differential space-time modulation. *IEEE Trans. Inform. Theory*, 46(7):2567–2578, Nov. 2000.

[67] H. Jafarkhami and V. Tarokh. Multiple transmit antenna differential detection from generalized orthogonal designs. *IEEE Trans. Inform. Theory*, 47(6):2626–2631, Sep. 2001.

[68] W. C. Jakes. *Microwave Mobile Communications*. Wiley, 1974.

[69] M. Joham, K. Kusume, M.H. Gzara, and W. Utschick. Transmit wiener filter for the downlink of TDD DS-CDMA systems. In *Proc. 7th Int. Symp. on Spread-Spectrum Tech. & Appli.*, Prague, Czech Replubic, Sep. 2002.

[70] M. Joham, W. Utschick, and J.A. Nossek. Linear transmit processing in MIMO communications systems. *IEEE Trans. Sig. Proc.*, to be published.

[71] M. Kang and M.S. Alouini. Capacity of MIMO Rician channels. *Submitted to IEEE Trans. Wireless Commun.*, 2004.

[72] N. Kong and L. B. Milstein. Average SNR of a generalized diversity selection combining scheme. *IEEE Commun. Lett.*, 3(3):57–59, Mar. 1999.

[73] A. Korkin and G. Zolotarev. Sur les formes quadratiques. *Math. Ann.*, 6:366389, Jan. 1873.

[74] V. Krishnamurthy, X. Wang, and G. Yin. Spreading code optimization and adaptation in CDMA via discrete stochastic approximation. *IEEE Trans. Inform. Theory*, 50(9):1927–1949, Aug. 2004.

[75] V. Krishnamurthy, G. Yin, and S. Singh. Adaptive step size algorithms for blind interference suppression in DS/CDMA systems. *IEEE Trans. Sig. Proc.*, 49(1):190–201, Jan. 2001.

[76] H. J. Kushner and G. Yin. *Stochastic Approximation Algorithms and Applications*. Springer Verlag, New York, 1997.

[77] H.J. Kushner and J. Yang. Analysis of adaptive step-size SA algorithms for parameter tracking. *IEEE Trans. Automatic Control*, 40(8):1403–1410, Aug. 1995.

[78] H.J. Kushner and G. Yin. *Stochastic approximation and recursive algorithms and applications*. Springer, New York, 2003.

[79] J.C. Lagarias, H.W. Lenstra, and C.P. Schnorr. Korkin-Zolotarev bases and successive minima of a lattice and its reciprocal. *Combinatorica*, 10:333–348, 1990.

[80] B.A. LaMacchia. *Basis reduction algorithms and subset sum problems*. SM Thesis, Massachusetts Inst. Technol., Cambridge, MA, 1991.

[81] J.N. Laneman and G.W. Wornell. Distributed space-time coded protocols for exploiting cooperative diversity in wireless networks. *IEEE Trans. Inform. Theory*, 49:2415–2425, Oct. 2003.

[82] E.A. Lee and D.G. Messerschmitt. *Digital Communications*. Kluwer Academic Publishers, 2nd Ed., 1974.

[83] W.C.Y. Lee. *Mobile Communications Design Fundamentals*. Wiley, 2nd edition, 1992.

[84] X. Liu, E.K.P. Chong, and N.B. Shroff. A framework for opportunistic scheduling in wireless networks. *Computer Networks: International J. of Computer and Telecommun. Networking*, 41(4):451–474, Mar. 2003.

[85] Y. Liu and E. Khightly. Opportunistic fair scheduling over multiple wireless channels. In *Proc. IEEE INFOCOM*, San Francisco, CA, Mar. 2003.

[86] H.A. Loeliger. Averaging bounds for lattices and linear codes. *IEEE Trans. Inform. Theory*, 43(6):1767–1773, No. 1997.

[87] L. Lovasz. *An Algorithmic Theory of Numbers, Graphs, and Convexity*. Philadelphia, PA: SIAM, 1986.

[88] B. Lu and X. Wang. Iterative receivers for multiuser space-time coding systems. *IEEE J. Select. Areas Commun.*, 18(11):2322–2335, Nov. 2000.

[89] B. Lu and X. Wang. A space-time trellis code design method for OFDM systems. *Wireless Personal Commun.*, 24(3):403–418, Feb. 2003.

[90] B. Lu, G. Yue, and X. Wang. Performance analysis and design optimization of LDPC-coded MIMO OFDM systems. *IEEE Trans. Sig. Proc.*, 52(2):348–361, Feb. 2004.

[91] T. L. Marzetta. BLAST training: estimation channel characteristics for high-capacity space-time wireless. In *Proc. 37th Annual Allerton Conf. Commun., Comput. & Control*, Monticello, IL, Sep. 1999.

[92] A.F. Molisch and M.Z. Win. MIMO systems with antenna selection. *IEEE Microwave Magazine*, 5(1):46 – 56, Mar 2004.

[93] A.F. Molisch, M.Z. Win, and J.H. Winters. Capacity of MIMO systems with antenna selection. In *Proc. IEEE Int. Conf. Commun. (ICC)*, Helsinki, Finland, June 2001.

[94] W.H. Mow. Universal lattice decoding: a review and some recent results. In *Proc. IEEE Int. Conf. Commun. (ICC'04)*, Paris, France, June 2004.

[95] R. Nabar, D. Gore, and A. Paulraj. Optimal selection and use of transmit antennas in wireless systems. In *Proc. Int. Conf. Telecommun. (ICT)*, Acapulco, Mexico, May 2000.

[96] R.U. Nabar, H. Bolcskei, and F.W. Kneubuhler. Fading relay channels: performance limits and space-time signal design. *IEEE J. Select. Areas Commun.*, 22(6):1099–1109, Aug. 2004.

[97] C. Peel, B. Hochwald, and L. Swindlehurst. A vector-perturbation technique for near-capacity multi-antenna multi-user communication - part 2. *IEEE Trans. Commun.*, submitted.

[98] A. Peled and A. Ruiz. Frequency domain data transmission using reduced computational complexity algorithms. In *Proc. IEEE Int. Conf. Acoust., Speech, Sig. Processing (ICASSP)*, Denver, CO, Apr. 1980.

[99] D. Reynolds, A. Host-Madsen, and X. Wang. Adaptive transmitter precoding for time division duplex CDMA in fading multipath channels: strategy

and analysis. *EURASIP J. Applied Sig. Proc.*, 2002(12):1325–1334, Dec. 2002.

[100] D. Reynolds, X. Wang, and H.V. Poor. Blind adaptive space-time multiuser detection with multiple transmitter and receiver antennas. *IEEE Trans. Sig. Proc.*, 50(6):1261–1276, June 2002.

[101] H. Robbins and S. Munro. A stochastic approximation method. *Ann. Math. Stat.*, 22:400–407, 1951.

[102] H. Sampath, P. Stoica, and A.J. Paulraj. Generalized linear precoder and decoder design for MIMO channels using the weighted MMSE criterion. *IEEE Trans. Commun.*, 49(12):2198–2206, Dec. 2001.

[103] S. Sanayei and A. Nosratinia. Antenna selection in MIMO systems. *IEEE Commun. Magazine*, 42(10):68–73, Oct. 2004.

[104] C. P. Schnorr. A hierarchy of polynomial time lattice basis reduction algorithms. *Theory Comput. Sci.*, 53:201224, 1987.

[105] C. P. Schnorr. A more efficient algorithm for lattice basis reduction. *J. Algorithms*, 9:47–62, 1988.

[106] C. P. Schnorr and M. Euchner. Lattice basis reduction: improved practical algorithms and solving subset sum problems. *Math. Program.*, 66:181–191, 1994.

[107] M. Sellathurai and S. Haykin. Turbo-BLAST for wireless communications: Theory and experiments. *IEEE Trans. Sig. Proc.*, 50(10):2538–2546, Oct. 2002.

[108] B.A. Sethuraman, B. Sundar Rajan, and V. Shashidhar. Full diversity, high rate, space-time block codes from division algebras. *IEEE Trans. Inform. Theory*, 49(10):2596–2616, Oct. 2003.

[109] M. Seysen. Simultaneous reduction of a lattice basis basis. *Combinatorica*, 13:363376, 1985.

[110] L. Shi and S. Olafsson. An integrated framework for deterministic and stochastic optimization. In *Proc. Winter Simulation Conf.*, pages 395–401, 1997.

[111] J.C. Spall. *Introduction to stochastic search and optimization*. Wiley, 2003.

[112] M. Stege, M. Bronzel, and F. Fettweis. MIMO-Capacities for COST 259 scenarios. In *Proc. Int. Zurich Seminar on Broadband Commun.*, ETH Zurich, Switzerland, Feb. 2002.

[113] V. Tarokh and H. Jafarkhami. A differential detection scheme for transmit diversity. *IEEE J. Select. Areas Commun.*, 18(7):1169–1174, July 2000.

[114] V. Tarokh, H. Jafarkhami, and A.R. Calderbank. Space-time block codes from orthogonal designs. *IEEE Trans. Inform. Theory.*, 45(5):1456–1467, July 1999.

[115] V. Tarokh, H. Jafarkhami, and A.R. Calderbank. Space-time block coding for wireless communications: Performance results. *IEEE J. Select. Areas Commun.*, 17(3):451–460, Mar. 1999.

[116] V. Tarokh, A. Naguib, N. Seshadri, and A. R. Calderbank. Combined array processing and space-time coding. *IEEE Trans. Inform. Theory*, 45(4):1121–1128, May 1999.

[117] V. Tarokh, A. Naguib, N. Seshadri, and A. R. Calderbank. Space-time codes for high data rate wireless communication: performance criteria in the presence of channel estimation error, mobility and multiple paths. *IEEE Trans. Commun.*, 47(2):199–207, Feb. 1999.

[118] V. Tarokh, N. Seshadri, and A.R. Calderbank. Space-time codes for high data rate wireless communications: Performance criterion and code construction. *IEEE Trans. Inform. Theory*, 44(2):744–765, Mar. 1998.

[119] I. E. Telatar. Capacity of multi-antenna Gaussian channels. *Euro. Trans. Telecommun.*, 10(6):585–595, Nov. 1999.

[120] S. ten Brink, G. Kramer, and A. Ashikhmin. Design of low-density parity-check codes for multi-antenna modulation and detection. *IEEE Trans. Commun.*, 52(4):670–678, April 2004.

[121] M. Tomlinson. New automatic equaliser employing modulo arithmetic. *IEE Electron. Lett.*, pages 138–139, Mar. 1971.

[122] S. Ulukus and R. Yates. Adaptive power control and MMSE interference suppression. *Wireless Networks*, 4(6):489–496, Nov. 1998.

[123] Sergio Verdu. *Multiuser Detection*. Cambridge University Press, 1998.

[124] S. Vishwanath, N. Jindal, and A. Goldsmith. Duality, achievable rates, and sum-rate capacity of Gaussian MIMO broadcast channels. *IEEE Trans. Inform. Theory*, 49(10):2658 – 2668, Oct. 2003.

[125] P. Viswanath and D. Tse. Sum capacity of the vector Gaussian channel and uplink-downlink duality. *IEEE Trans. Inform. Theory*, 49(8):1912–1921, Oct. 2003.

[126] B.R. Vojcic and W.M. Jang. Transmitter precoding in synchronous multiuser communications. *IEEE Trans. Commun.*, 46(10):1346–1355, Oct. 1998.

[127] J. Wang, X. Wang, V. Krishnamurthy, and M. Madihian. On the design of high rate space-time codes. *IEEE Trans. Commun.*, submitted.

[128] H. Weingarten, Y. Steinberg, and S. Shamai (Shitz). The capacity region of the gaussian MIMO broadcast channel. In *Proc. 38th Conf. Inform. Sci. and Syst., (CISS)*, Princeton, NJ, Mar. 2004.

[129] M.Z. Win and J.H. Winters. Analysis of hybrid selection/maximal-ratio combining in rayleigh fading. *IEEE Trans. Commun.*, 47(12):1773–1776, Nov. 1999.

[130] C. Windpassinger, R.F.H. Fischer, T.Vencel, and J.B. Huber. Precoding in multi-antenna and multi-user communications. *IEEE Trans. Wireless Commun.*, 3(4):2004, Mar. 2004.

[131] P. W. Wolniansky, G. J. Roschini, G. D. Golden, and R. A. Valenzuela. V-BLAST: an architecture for realizing very high data rates over the rich-scattering wireless channel. In *Proc. 1998 Int. Symp. Sig. Sys. Elect. (ISSSE'98)*, Pisa, Italy, Sep. 1998.

[132] D. Yan and H. Mukai. Stochastic discrete optimization. *SIAM J. Control and Optim.*, 30(3):594–612, Oct. 1992.

[133] H. Yao and G.W. Wornell. Lattice-reduction-aided detectors for MIMO communication systems. In *Proc. IEEE Globecom*, Taipei, Taiwan, Nov. 2002.

[134] H. Yao and G.W. Wornell. Achieving the full MIMO diversity-multiplexing frontier with rotation-based based space-time codes. In *Proc. of Annual Allerton Conf. Commun., Comput. & Control*, Monticello, IL, Oct. 2003.

[135] W. Yu and J. Cioffi. Sum capacity of the Gaussian vector broadcast channels. *IEEE Trans. Inform. Theory*, 50(9):1875–1892, Sep. 2004.

[136] L. Zheng and D. Tse. Diversity and multiplexing: a fundamental tradeoff in multiple antenna channels. *IEEE Trans. Inform. Theory*, 49(5):1073–1096, May 2003.